2000-12-01

An ATM System Model and Wireless Channel Simulation

Karen Dunne
Technological University Dublin

Dublin Institute *of* Technology

Faculty of Applied Arts

DIT Aungier Street, Dublin 2

AN ATM SYSTEM MODEL AND WIRELESS CHANNEL SIMULATION

Karen Dunne B.Sc (Applied Science)

For the award of

Masters of Philosophy

December 2000

Supervised by:

Dr. Brendan O'Sullivan & Dr. Ciaran McDonnaill

DECLARATION PAGE

I certify that this thesis which I now submit for examination for the award of Masters of Philosophy, is entirely my own work and has not been taken from the work of others save and to the extent that such work has been cited and acknowledged within the text of my work.

This thesis was prepared according to the regulations for postgraduate studies by research of the Dublin Institute of Technology and has not been submitted in whole of in part for an award on any other Institute or University.

The Institute has permission to keep, to lend or to copy this thesis in whole or in part, on condition that any such use of the material of the thesis is duly acknowledged.

Signature _____ Date_____

Candidate

ABSTRACT

Congestion in the low frequency regions of the electromagnetic spectrum and demand for support of high bandwidth applications has prompted widespread investigations into networking technologies and communications media. Traditional networking technologies such as Ethernet that are not capable of adequately supporting high bandwidth applications (e.g. videoconferencing) are being replaced by high speed, high bandwidth technologies such as Asynchronous Transfer Mode (ATM). In the communications media market, wireless systems are becoming ubiquitous due to their ease of installation and maintenance costs.

In this research, the networking technology of interest is ATM. ATM uses a cell switching architecture that allows seamless support for all traffic types. It is also capable of providing guaranteed quality of service to different applications. This research seeks to develop a model of an ATM system in order to simulate the processes of file manipulation of an application in an ATM network in which a reliable transmission medium is deployed.

The transmission medium under investigation is a wireless optical communication link (laser). Laser systems offer a number of advantages over microwave systems. They do not require an operating license and they potentially offer larger bandwidth. Similar to microwave systems however, the performance of the laser link is dependent on atmospheric conditions. Scattering and absorption of the signal by atmospheric/weather particles may produce power losses in the transmitted signal. Theoretical models predicting such propagation impairments are widely available for microwave systems. However, there is little information available for optical systems. In this project, a model is developed to predict the effects due to rain on an optical link. This atmospheric channel model is based on the form of the drop size distribution proposed by [Marshall and Palmer, pp.165-166] and the results for the terminal velocity of raindrops found by [Gunn-and-Kinzer, pp. 243-248].

Experimental tests were conducted so that comparison could be made with both theoretical models developed.

ACKNOWLEDGEMENTS

There are a number of people I would like to thank for their assistance through the course of this research. Firstly, to my supervisors, Dr. Brendan O'Sullivan and Dr. Ciaran McDonnaill, for their support, encouragement and inspiration over the last two years. I am indebted to both of you for your patience and help. To all of the staff at the Digital Media Centre, for their ideas on this project. In particular, I would like to thank Eoin Kilfeather for his technical assistance and friendship. To my brother Paul, for his contribution to the editing and ideas for this report. Finally, to my family and friends for their love and support.

TABLE OF CONTENTS

LIST OF FIGURES

LIST OF TABLES

LIST OF GRAPHS

LIST OF ACRONYMS

AAL	ATM Adaptation Layer
AM	Amplitude Modulation
AMI	Alternate Mark Inversion
ANSI	American National Standards Institute
ARP	Address Resolution Protocol
ASK	Amplitude Shift Keying
ATM	Asynchronous Transfer Mode
BER	Bit Error Rate
B-ISDN	Broadband Integrated Digital Services Network
BRI	Basic Rate Interface
CAT3	Category 3 cabling
CAT5	Category 5 Cabling
CBR	Constant Bit Rate
CRC	Cyclic Redundancy Check
CS	Convergence Sublayer
CSMA/CD	Carrier Sense Multiple Access\Collision Detection
DSD	Drop Size Distribution
EMI	Electromagnetic Interference
FDDI	Fibre Distributed Data Interface
FDM	Frequency Division Multiplexing
FM	Frequency Modulation
FTP	File Transfer Protocol
IEEE	Institute of Electrical and Electronic Engineers
IP	Internet Protocol
ISDN	Integrated Services Digital Network
ISO	International Standards Organisation
ITU	International Telecommunications Union
ITU-T	ITU-Telecommunications Standardisation Section
LAN	Local Area Network

LANE	LAN Emulation
LASER	Light Amplification by Stimulated Emission of Radiation
LED	Light Emitting Diode
LF	Low Frequency
MAC	Media Access Control
MAN	Metropolitan Area Network
MF	Medium Frequency
MPOA	Multiprotocol Encapsulation Over ATM
N-ISDN	Narrowband Integrated Services Digital Network
NRZ	Non Return to Zero
OAM	Operations Administration and Maintenance
OC	Optical Carrier
OSI	Open Systems Interconnect
PDU	Protocol Data Unit
PMD	Physical Medium Dependent
PRI	Primary Rate Interface
QoS	Quality of Service
RZ	Return to Zero
SAR	Segmentation And Reassembly
SDH	Synchronous Digital Hierarchy
SONET	Synchronous Optical Network
STP	Shielded Twisted Pair
STS	Synchronous Transport Signal
TC	Transmission Convergence
TCP	Transmission Control Protocol
TDM	Time Division Multiplexing
UDP	User Datagram Protocol
UTP	Unshielded Twisted Pair
VBR	Variable Bit Rate
VCI	Virtual Circuit Identifer
VHF	Very High Frequency
VLF	Very Low Frequency
VPI	Virtual Path Identifier
WAN	Wide Area Network

WDM	Wavelength Division Multiplexing

1 INTRODUCTION

1.1 Introduction

When an electromagnetic wave propagates through the atmosphere, it is affected by interactions with atmospheric particles. Scattering, refraction and absorption of the wave may result from such interactions. If the electromagnetic wave is used to carry digital information across a computer network, the integrity of the data received at the destination may be compromised. In the case of a wireless optical communications system, interactions between the optical beam transferring the data and atmospheric particles will result in temporal reductions in received power. Depending on the sensitivity of the receiving system and the reliability and quality of service required by the application, such losses may compromise the integrity of the data link.

Accounting for any signal loss that may result from the propagation characteristics of an atmospheric channel is an important design task for communication system designers. Due to the complexities involved in accurate representation of the dynamic channel medium (atmosphere), prediction models are widely employed. Many of these models use empirical relations to forecast the effects of particular weather conditions on the reliability of the wireless channel operating at frequencies above 10GHz. Since World War II, the development and refinement of these models has played a vital role in the advancement of broadband wireless communications [Mead, p.1][Pratt and Bostian Ch. 8.3, pp. 327].

1.2 Broadband Applications

The proliferation of broadband applications, such as video conferencing and media streaming, are placing increasing pressure on the capacity and performance of communication systems. Widespread demand for network support for these applications over recent years has prompted communication network designers to upgrade device performance to enable the delivery of these services seamlessly across networks. An upgrading of present infrastructure will be necessary to ensure adequate support for high capacity applications in the years to come. It is not sufficient to solely replace/upgrade technologies and transmission media deployed on local area networks however. Moreover, it is essential that backbone communication links be equipped with state of the art broadband transmission media and devices to ensure that appropriate and consistent support

for applications is maintained throughout an entire metropolitan and wide area network system.

Since the deregulation of the Irish Telecommunications industry in December 1998 there has been increasing evidence of the implementation of these strategies by telecommunications operators. In the chase for competitive advantage, these operators are upgrading and/or replacing their backbone communications systems with new, high-speed technologies so that they may deliver multimedia applications to consumers. The trend has been to upgrade from legacy systems, such as 10BaseT Ethernet (10Mbps) to Cat5 Fast Ethernet (100Mbps) or to replace existing network infrastructure with newer high-speed broadband technologies such as Asynchronous Transfer Mode (ATM).

The technological focus for this research is Asynchronous Transfer Mode, a high-speed cell switching technology. The ATM system environment was chosen for a number of reasons. Asynchronous Transfer Mode was developed as part of the International Telecommunications Union (ITU) standard for the Broadband-Integrated Services Digital Network (B-ISDN) [Washburn and Evans, Ch.10, pp.193]. Since the first test bed implementations of the early 1990's, ATM has become a strong competitor in the local area and backbone network architectures. ATM has become a proven de facto standard in Metropolitan and Wide Area Networking and is the technology of choice of huge international operators in their backbone implementations. The manner in which ATM processes all traffic types is unique: all traffic is segmented into fixed size cells to allow high-speed switching of different applications to be achieved efficiently and seamlessly. Quality of Service (QoS) and bandwidth reservation options provided by the technology ensure efficient application processing and support for broadband networking.

All of these factors provide sufficient justification for the study of ATM in this research. However, the technology is investigated in a particular network setup, one that includes a wireless communication link. The wireless link is provided by a laser communication system operating in the 800nm-wavelength region of the electromagnetic spectrum. There have been considerable advances in wireless communications in recent years, with speeds and performance of these systems fast approaching and often exceeding those supplied by their wired counterparts. Further, wireless solutions are often more cost-effective and timely. Nevertheless, there are a number of additional criteria to consider

where wireless links are implemented. It is these criteria as well as the impact of them on the reliability of the network that this research seeks to address.

1.3 Objectives

The main objectives of this research are briefly presented in this section to give an overview of the project. The objectives are as follows

- Development of an ATM system model in a MATLAB environment to demonstrate the process of file manipulation in an ATM network.
- Development of a theoretical model in MATLAB to predict the effects of rain attenuation on a wireless optical communications link.
- Design and testing of an experimental apparatus in order to obtain results that could be compared with those predicted by the theoretical model.

1.4 Methodology

The methodology followed in order to achieve the objectives outlined above is described in this section. Firstly, there was an investigation into the relevant theory governing ATM and wireless optical communications. This was followed by the experimental work for the project, which entailed the configuration of an ATM network and an investigation into the effects of rain in a wireless channel supporting ATM. The final stage was to compare and conclude from the theoretical and experimental work undertaken. This was achieved by comparing the results obtained in the theoretical and experimental work. The flowchart shown in figure 1.1 illustrates the methodology followed in the project. The purposes of the main theoretical and experimental sections are discussed in following paragraphs.

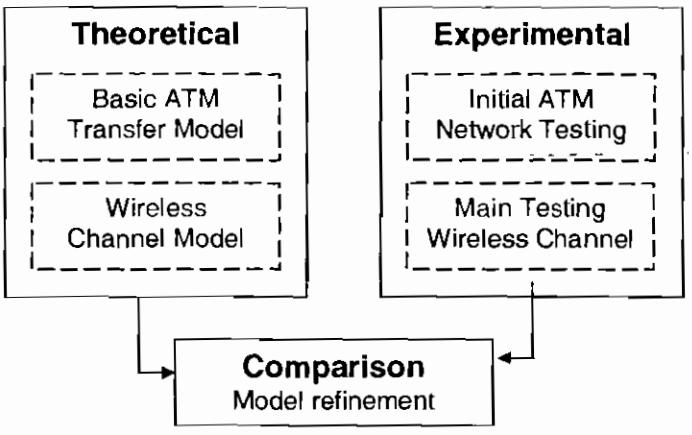

Figure 1.1; *Project Methodology*

1.4.1 Theoretical Model

In order to model the processes of manipulation of a file in an ATM system, it is necessary to develop a basic ATM transfer model. This model comprises two main modules namely the ATM source module and ATM destination module. A data file is chosen for manipulation, is passed through the layers of the ATM source module, and is manipulated according to the network protocol. This involves breaking up the data into fixed size calls, the addition of headers and trailers, and the inclusion of error checks in the form of matrix comparisons. The data then transfers completely to the ATM destination module, the headers and trailers are removed and the data is reverted to its original form. If the channel is ideal, then the transfer process is consistently error free, a performance which is consistently attained using an optical fibre. This was the assumed situation for the basic ATM model and is depicted in figure 1.2 (a).

The next stage in the theoretical model was the development of a channel module to simulate transmission on a channel in which signal degradation may occur (wireless channel subject to adverse weather conditions). The underlying transmission effects are based on the rain attenuation effects on electromagnetic signals propagation through the atmosphere described by a number of authors [Manabe *et al.*, pp.474-477] and [Olsen *et al.*, pp.318-328]. The model employs the negative exponential drop size distribution proposed by Marshall and Palmer in 1948 [Marshall and Palmer, pp.165-166]. The channel module requires user input of rain rate R required by the controlling theoretical equations. The aim of the channel module is to predict the effect of particular rain intensities on the availability of a wireless channel section of an ATM network, a situation depicted in figure 1.2 (b).

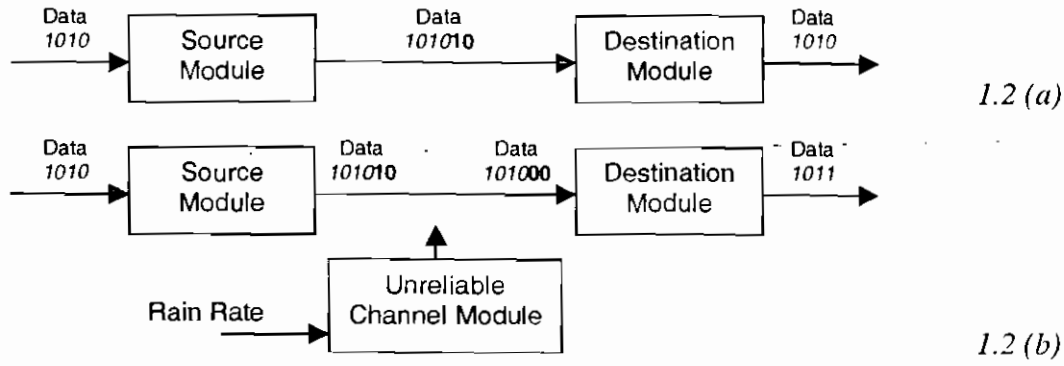

Figure 1.2; *Theoretical Model: (a) ATM system using reliable channel, (b) ATM system using unreliable channel*

Rather than create a highly computationally intensive model based on a propriety system, it was deemed more practical within the context of this research to develop a model to simulate a generic Asynchronous Transfer Mode system process. The objective was to thus take a top-down approach to reflect the manipulation of the application data by the principle layers of the Asynchronous Transfer Mode system. Complex algorithms were avoided in order to achieve a clear and manageable design. The modelling environment (MATLAB) was chosen for its ease of adaptation and flexibility. Further, its reasonably rapid learning period and simple debugging mechanism set it aside for the inexperienced programmer from more traditional programming environments such as C++, where thorough knowledge of object oriented structures would have been required.

1.4.2 Experimental Work

In this section a brief description of the experimental work undertaken is given. The first stage in the experimental work was to show that rain has an adverse effect on the transfer of data over a wireless ATM channel. This was shown by undertaking a series of preliminary tests on a real ATM network. Initially the network was connected entirely using a reliable transmission medium (optical fibre). It was observed that, as expected, connectivity was consistently maintained when fibre was used. When the network configuration was modified to incorporate a wireless link however, it was found that connectivity was dependent on the atmospheric situation in the channel. The most notable cause of disruption to connectivity was due to rain. The initial findings of these tests instigated further experimental work. Consequently, further experimentation was

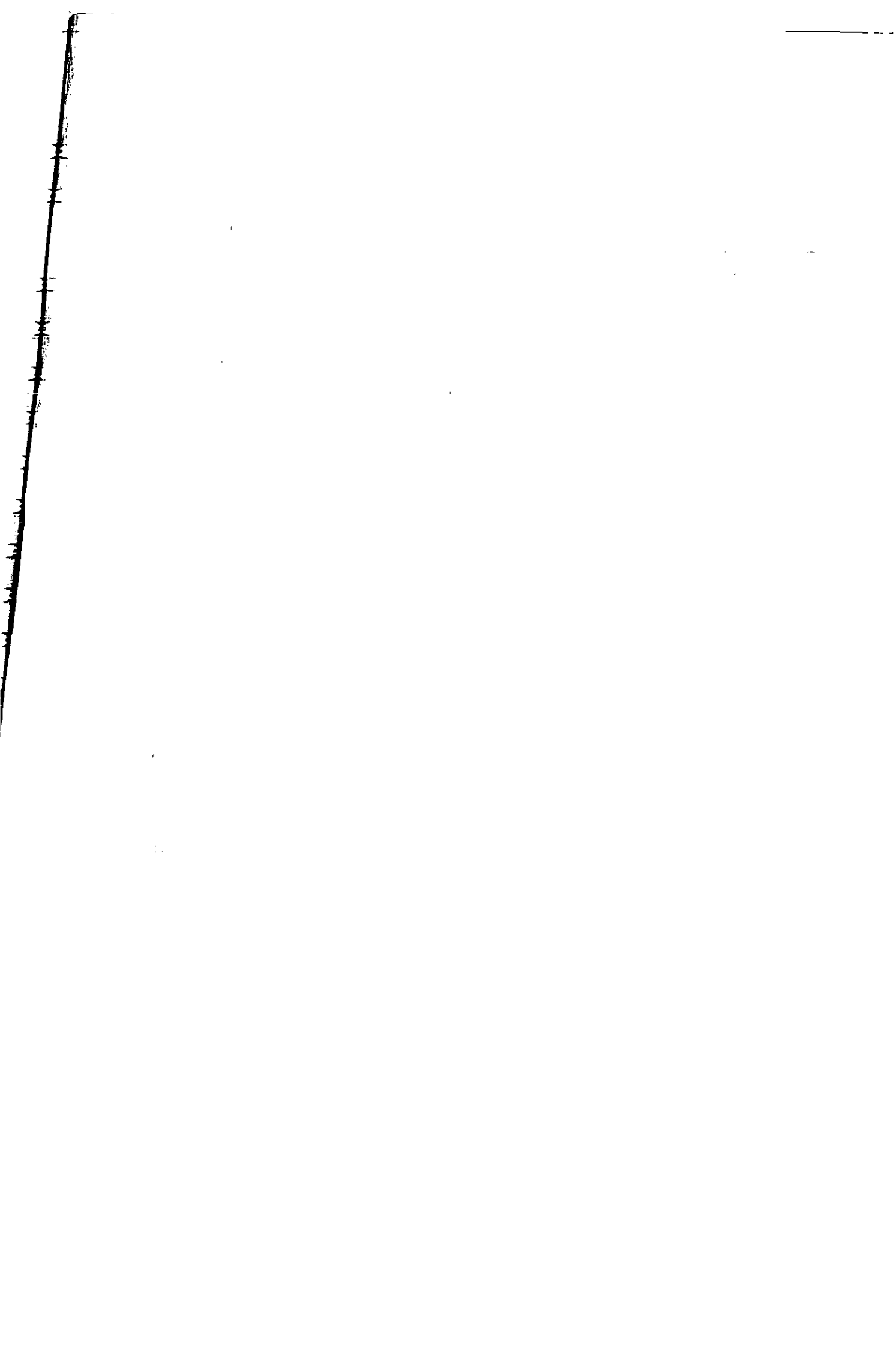

Section 2.3 is dedicated to describing the main transmission media available for communication transfer. These include bounded (wired) and unbounded (wireless) media. The advantages and disadvantages of each media type is outlined and justification for the use of two particular media types in the research of interest is provided. These are optical fibre (a bounded medium) and infrared laser (an unbounded medium).

In section 2.4, the broadband networking technology Asynchronous Transfer Mode (ATM) is examined. The differences between ATM and traditional circuit and packet switched networks are firstly outlined. This is followed by the brief description of the use of ATM as a networking technology for the Internet Protocol.

In order to gain insight into the reliability of the laser communications link under different weather conditions, it was necessary to review the relevant theory and literature on transmission through the atmosphere. The findings are presented in section 2.5. It was particularly the effect of rain on the performance of a wireless laser link that was of concern. Rain has been reported as the principal precipitation process throughout the world and has been noted as having a severe effect on transmission at high frequencies [Rogers Ch.7, pp.87].

The development of the theoretical model, which simulates the process of an ATM system data transfer in a MATLAB environment, is described in chapter 3. The reasons for modelling the system with proprietry or connection specific details are also presented. This is followed by the separate development of a wireless theoretical model, also developed in MATLAB.

In chapter 4, the experimental work undertaken is described. This includes the implementation of the first ATM network in the Dublin Institute of Technology (DIT) as well as an indication of some of the problems that arose in the network configuration. Next, the design and testing of an experimental apparatus in two separate environments (natural rain and simulated rain) is presented.

Chapter 5 is dedicated solely to the results obtained in the experimental and theoretical work and, for each set of results obtained, a discussion on the findings is provided. Finally, the conclusions of the research and recommendations for further study and model refinement are described in Chapter 6.

2 LITERATURE REVIEW

2.1 Layout

The literature review in this chapter is divided into 7 sections. These sections range from a general study of the general aspects of communication systems to specific investigation into particular types of communication systems and communications media. In particular, the broadband networking technology. Asynchronous Transfer Mode (ATM) is examined. The context in which ATM is studied is as a backbone networking solution for in high speed, high capacity computer networks. A further study is made into the impact of deploying a wireless optical link subject to variations in atmospheric conditions in such a network.

In the current section 2.1, a detailed layout of the literature review is provided. A brief description of the topics covered in the different sections is given here.

In section 2.2, an introduction to the area and main aspects of data communication systems is presented. This includes the differences between analog and digital systems and a description of the numerous different classifications of communications systems.

In section 2.3, discussion moves from the general topics of communication systems to a particular type of communication system, the computer network. A brief study of the main components and operations of the computer network is presented here. The simulation model developed during the course of the research seeks to simulate the processes of file manipulation in an ATM system using TCP/IP, hence an examination of the TCP/IP protocol stack is required. In section 2.3.7, a short description of Ethernet is provided. [Washburn and Evans, p.152] reported that Ethernet is possibly the most common medium over which TCP/IP operates. This is true of the particular campus configuration in which the experimental work for this research was undertaken, hence a brief description is appropriate.

Section 2.4 is dedicated to describing the main transmission or physical media that are available for communication. These include bounded (wired) and unbounded (wireless) media. The advantages and disadvantages of each media type are outlined and justification for the use of two particular media types in the research of interest, optical fibre and laser, is also provided.

In section 2.5, the broadband networking technology Asynchronous Transfer Mode (ATM) is described. The differences between ATM and traditional networking technologies are outlined followed by an examination of ATM as a platform for the Internet Protocol.

The final section of the literature review, section 2.6, examines the degradation of a wireless optical signal subject to rain in the atmospheric channel. Although this specific research is concerned with the impact of rain on an optical communications link, it has been necessary to review much of the principles and effects reported for signals operating in the microwave region. The reason for this is that the theoretical principles relating to electromagnetic wave propagation at microwave frequencies are equally relevant in the optical region [Olver, p.1]. Further, considering the fact that there was found to be little information available on rain attenuation at optical frequencies, it was necessary to examine alternative available literature written on the subject. It was found that most of the literature related to rain attenuation at microwave frequencies.

The principal findings and observations of the literature review are discussed in section 2.7. The experimental and theoretical research conducted during the course aims to address some notable gaps in the literature.

2.2 Data Communications Systems

In this section, the main aspects of communication systems are presented. Two forms of information exist, analog and digital. The differences between them are firstly outlined. The way in which information is transferred over analog and digital media is also presented since this an important requirement in a hybrid communication system. The latter sections. 2.2.5 - 2.2.8 are set aside to describe a number of classifications found in the literature for communication systems. These include classifications based on communication direction (simplex or duplex) and based on the number of signals used for communication (baseband or broadband).

2.2.1 Introduction

The aim of any communication system is to convey information between two or more points [Gagliardi and Karp, p.1]. The generic communication system comprises three components, a source where information is generated. a channel over which information is

transferred, and a destination where information is received. The human voice, for example, conveys information in the form of sound waves between two people over an air medium. Radio and microwave signals may be used for communication through the atmosphere [Tanenbaum, pp.97-100].

Information can take two distinct forms, analog or digital. Analog information may be represented by an infinite number of values whereas digital information may be represented by only finite values [Haykin, p.1]. A thermometer for example, provides analog information in the form of a temperature scale with infinite resolution. A Light Emitting Diode (LED) on the other hand is an example of a device that provides digital information. The device is either switched on or off. Analog information is continuously time and amplitude varying whereas digital information is confined to specific amplitude levels and time intervals. The differences between analog and digital information are illustrated in figure 2.1. In the following sections, these information forms are described in more detail.

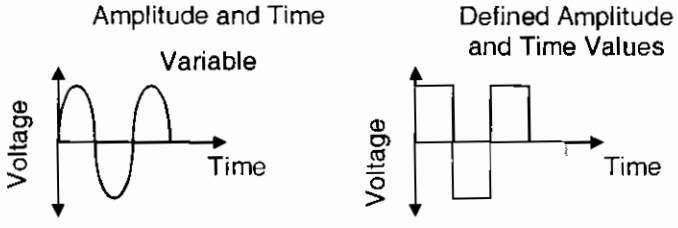

Figure 2.1; *(left to right) Analog and Digital Information*

2.2.2 Analog Systems

In an analog communication system, information is superimposed onto a continuous, time and amplitude-varying electromagnetic carrier wave [Haykin, p.1]. Electromagnetic waves are produced by electric circuits and propagated outwards using transmitting antennae. The term electromagnetic refers to the fact that these waves contain electric and magnetic field components induced in the region around the propagating wave by the movement of electrical charges [Uiga, p.5]. The electric and magnetic field components are perpendicular to one another and perpendicular to the direction of propagation of the wave. A simple illustration of the components of the electromagnetic wave is shown in figure 2.2.

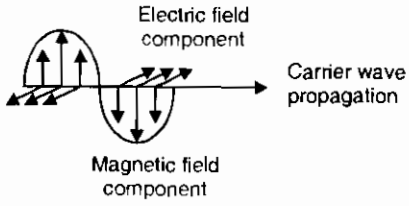

Figure 2.2; *Electromagnetic wave*

Electromagnetic waves are characterised by properties such as wavelength, period, frequency, amplitude and phase. The wavelength (metres) describes the distance between one point on the wave and the corresponding point on the next wave cycle. The period (seconds) describes the time to complete one full oscillation and frequency (Hertz) describes the number of complete oscillations of the wave per unit time. The difference between the highest and lowest value of the carrier wave on a wave cycle determines the amplitude (strength) of the wave.

2.2.3 Digital Systems

In a digital system, amplitude and time values are confined to specific or discrete levels [Haykin, p.2]. Since the information can only take on one of the digital values at a specified time, digital systems are inherently more accurate and robust than analog ones. Amplitude and data rates are typically used to characterise digital signals. The amplitude represents the difference between the highest and lowest value specified for the system. The data rate describes the number of information units that can be represented by the digital signal per time interval [Niedermiller and Heywood, p.148].

A particular type of digital system of specific interest to computer communication is the binary system. Here, only two values are specified to represent information at a defined time. Binary communication is achieved in hardware using mechanical or electrical switches that are switched on or off to represent the information in the form of binary digits (bits) that takes the form of either ones or zeros. All computer information is processed as sequences of bits.

2.2.4 Integration of Analog and Digital Systems

Industry trends in recent years have shown a dramatic growth in demand for digital technology, most notably due to the increase in the use of personal computers. A further demand has been for communication between these computers. This was initially achieved

using existing analog cabling. The replacement/upgrade of all installed analog cabling to digital is not economically feasible for most implementations. Consequently, integration is required to allow seamless communication over hybrid systems. The most common integration requirement is the transfer of digital information over analog carriers, as outlined in the next section. For completeness, the integration of analog information over a digital carrier is also presented.

Transferring digital information over an analog medium

When digital information is to be transferred over an analog medium such as a telephone line, a process known as modulation is employed. A modulation scheme describes the manner by which the digital information is superimposed onto the analog carrier signal. Modulation is achieved by modifying one of the properties of the analog signal e.g. amplitude, frequency or phase to reflect the digital information [Niedermiller and Heywood, p.150].

Amplitude Modulation (AM) or Amplitude Shift Keying (ASK), involves changing the amplitude of the carrier signal between a number of amplitude levels that correspond to the levels defined by the digital system. For example, in a binary system, the amplitude of the carrier would be altered between two defined values to reflect the bits of digital information. The use of amplitude modulation schemes for communication systems is not recommended in electrical environments. The reason for this is that noise interference from adjacent electrical devices may cause the amplitude of the carrier signal to shift to an incorrect amplitude level, resulting in the transfer of an incorrect digital information unit. In such environments, frequency or phase modulation is preferred.

Frequency Modulation (FM) or Frequency Shift Keying (FSK) assigns separate frequencies for the transmission of different digital information units. Alternating among these frequencies allows the digital information to be superimposed onto the analog carrier. Phase Modulation (PM) or Phase Shift Keying (PSK), on the other hand, assigns carrier signals with different cycle start times to the different units of digital information [Niedermiller and Heywood, pp.151-152]. Each of these different modulation schemes is illustrated in figure 2.3.

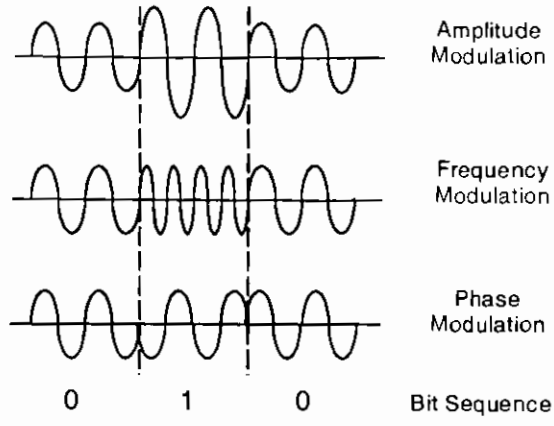

Figure 2.3; *Modulation Schemes*

Once the digital information has been superimposed onto the carrier wave, the modulated signal is transferred to the destination. In order to recover the digital information at the destination, it is necessary to perform a reverse modulation process, known as demodulation, on the received signal [Niedermiller and Heywood, p.161]. The actual devices that allow these conversion processes are called modems; the name derives from the concatenation of the words modulator and demodulator. An illustration of the modulation/demodulation processes is shown in figure 2.4.

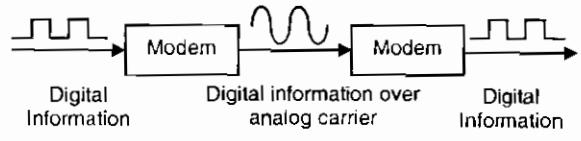

Figure 2.4; *Digital information over analog carrier*

Transferring analog information over a digital medium

When analog information is to be transferred on a digital carrier wave, a different method is employed. There are three processes performed on the analog information namely sampling, quantisation and encoding [Haykin, p.2]. Sampling involves recording the value of the analog information at equally spaced time intervals. Quantisation is the categorisation of the measured sample value into the closest discrete level defined by the digital system. The accuracy of the quantisation also determines the overall accuracy of the representation. Errors may be introduced due to invalid quantisation and sampling rate decisions. The last stage in the conversion is encoding, which is the representation of the

discrete level value by a code word e.g. a binary code containing a certain number of code elements. A reverse decoding process at the destination recovers the original analog information. The devices that achieve this conversion are known as codecs, a concatenation of the words, coder and decoder [Niedermiller and Heywood, p.165]. An illustration of analog to digital conversion is shown in figure 2.5

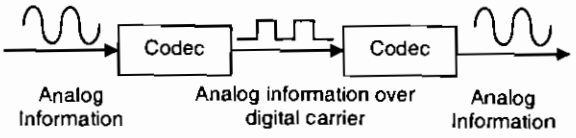

Figure 2.5; *Analog information over digital carrier*

2.2.5 Simplex and Duplex Communication

Communication systems may be defined based on the direction over which information is transferred. Simplex communication is uni-directional; only the source may transmit information and the destination receive information. Duplex communication allows transmission and reception of information at both the source and destination devices. Two types of duplex communication exist: half-duplex and full duplex. In half-duplex mode, only one party may transmit over a specific interval while the other party receives while in full-duplex mode, both parties may transmit and receive at all times [Niedermiller and Heywood, p.183]. These scenarios are depicted in figure 2.6.

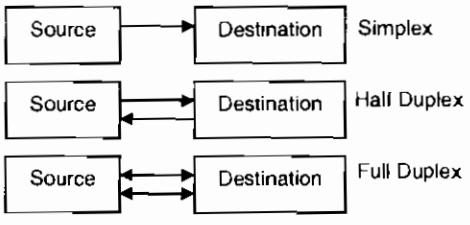

Figure 2.6; *Simplex and duplex communication*

2.2.6 Synchronous and Asynchronous Communication

Communication systems may be described based upon whether they are synchronous or asynchronous. Synchronous communication involves the transfer of information as a series of bits using clocking between source and destination devices to synchronise transmissions. Usually information transferred on a system using synchronous

communication is sent with a sophisticated error check code so that errors caused in transmission may be detected at the destination. The implementation of an accurate clocking mechanism and error-checking algorithm at both the source and destination however is expensive and often unnecessary for some information transfers.

Asynchronous communication is simple and inexpensive by comparison since no clocking or error-checking algorithms are implemented. Rather, the source and destination are synchronised at the start of a transmission and information is transferred at a rate acceptable to the destination for processing. This type of communication operates well when information is in the form of small, irregular chunks, such as is often the case with computer transmissions [Niedermiller and Heywood, pp.185-195].

2.2.7 Baseband and Broadband Communication

The terms baseband and broadband are used to describe the type of transmission deployed in the communication system. Baseband transmission involves the transfer of information via a single carrier wave propagating through the channel of the system. In a computer network, baseband transmission of digital information is achieved through the representation of bits by one of two carrier voltage levels [Tangney, pp.7-9]. Baseband transmission is limited to a low range of frequencies and offers low bandwidth [Kercheval, p.1]. Examples of systems that employ baseband transmission are the telephone network and two types of computer network technologies, Ethernet and Token Ring [Niedermiller and Heywood, pp.186].

In broadband systems, on the other hand, a number of analog carrier waves may be used to simultaneously transfer information over a transmission medium. This is achieved by dividing the bandwidth (range of frequencies available for transmission) into sub-bands of different frequencies. Each carrier wave thus uses a specific frequency for transmission. In this manner, the bandwidth available is used more efficiently than with baseband [Tangney, pp.8]. Cable television uses broadband transmissions as does the Ethernet computer network standard. In the case of television, a number of video signals are carried simultaneously on the cable and transferred to the subscriber's home. A tuner separates out the signals of different frequencies and assigns each to a separate channel on the television. In the Ethernet network, there are two broadband configurations, dual and split configurations. In a dual cable configuration, two separate cables are used for transmit and

received signals. In a "split" configuration, a single cable is used but different frequencies are used for transmitting and received waves [Niedermiller and Heywood, pp.185-186][Tanenbaum, p.85].

2.2.8 Transmission Frequencies

A further way to describe a communication system is based on the location of the carrier wave in the electromagnetic spectrum [Gagliardi and Karp, p.1]. The electromagnetic spectrum is defined as the distribution of electromagnetic radiation according to energy, frequency or wavelength. The spectrum extends from low frequency (kHz) regions used in radio communications to high frequency (GHz and THz) regions used in microwave and optical communications [Gagliardi and Karp, p.1]. Radio systems use frequencies available in the Radio Frequency (RF) region of the electromagnetic spectrum, which extends from 10^4 to 10^8 Hz. Microwave systems use carrier wave frequencies located in the microwave region that lies between approximately 10^8 and 10^{11} Hz. Licensing is required to control the operation of radio and microwave systems [Niedermiller and Heywood, pp.177-179].

Optical systems use carrier frequencies that lie in the optical region of the electromagnetic spectrum, which lies between 10^{11} and 10^{16} Hz. The region extends from the infrared through the visible to the ultraviolet region [Gagliardi and Karp, p.1][Tanenbaum, p.95]. Licensing is not required to operate infrared communication systems since these frequencies are not regulated [Ayanoglu, p.402]. Since regulation can be a lengthy and expensive process, wireless infrared systems are often an attractive and timely solution. Further, as described in more detail later, the bandwidth capacity available at optical frequencies is greater than available in the microwave region. It is with communication in the optical region, in particular in the infrared region, with which this research is concerned.

The choice of transmission frequency for a particular system is dependent on requirements and applications that will be run on the system. In 1948, Claude Shannon proposed a fundamental theorem of communication. The theorem states that the amount of information that can be transferred per unit time i.e. the data rate, is dependent on the bandwidth of the medium deployed in the channel of the system [Tanenbaum, p.82]. The bandwidth describes the frequency range over which there is little loss in signal strength.

By thus choosing a frequency that offers high bandwidth, a higher data rate is achieved and broadband multimedia applications may be effectively supported.

Low carrier frequency links have a correspondingly low capacity. Conversely, high frequency links, such as microwave or optical, have inherently high capacity. Clearly, the potential increase in modulation bandwidth at higher frequencies provides the impetus for their use in systems requiring high capacity. In recent years, the proliferation of broadband applications such as video-conferencing and media streaming has led to an increase in demand for bandwidth. New communication systems are expected to provide seamless support for these applications. Consequently, communications systems operating in the microwave and optical frequency bands of the electromagnetic spectrum have become increasingly attractive [Gagliardi and Karp, p.1].

The gain in capacity at these frequencies is however, offset by a number of unfavorable factors that arise in transmission at these high frequencies. Firstly, in contrast to low frequency signals like radio waves that spread out uniformly in space, high frequency microwave and optical signals propagate in straight lines. Therefore, when high frequency communication takes place through the atmosphere, source and destination antennas must be carefully aligned to ensure communication is reliably achieved [Niedermiller and Heywood, pp.176-181].

In addition, high frequency microwave and optical signals are subject to interference from atmospheric and weather particles, which have less of an effect on low frequency radio signals. This is because it is the relationship between the wavelength of the signal and the diameter of the atmospheric or weather particle encountered that determines the amount of interference experienced. Interference effects become more pronounced as the signal wavelength approaches the magnitude of the particle diameter [Gagliardi and Karp, p.3][McCartney, p.20]. Radio signals have long wavelengths and easily pass through the encountered particles in comparison with microwave and optical signals. Microwave signals have shorter wavelengths and are prone to absorption and scattering by the atmospheric particles. Optical signals have shorter wavelengths again, and suffer worst from such interference effects. The interference may cause interruptions to, or degradation of, the communication link. Often the optical communication link may be rendered unavailable for reliable transmission. Consequently, it is necessary to readily account for

such effects when employing communication systems operating in these regions [Gagliardi and Karp, p.3]. These interference effects are described in more detail in section 2.6 of the literature review.

The principal objective of this section was to outline the main aspects relating to communication systems so as to provide a general introduction to the area in which this research is undertaken. This was initially achieved by describing the generic purpose of any communication system, assessing the different information forms and processes involved in the transfer of information in a communication system. In the following sections of the literature reviews, more detailed descriptions of some of the specific research topics of concern here are presented. Section 2.3 looks at a particular type of ubiquitous communication system, the computer network and outlines the main components of and issues relating to such networks. It may be said that the computer network has been the most influential invention of the modern age by providing global connectivity via the Internet to millions of homes and businesses. In this manner, it has brought many changes to modern life by allowing rapid information dissemination and effective collaboration between people in geographically dispersed and culturally diverse nations.

2.3 Computer Networks

In section 2.2, the general aspects of communication systems were outlined. In this section, the particular communication system under investigation in this research i.e. the computer network is examined. Firstly, the applications of computer networks and their significance to research and commercial advances are highlighted. This is followed by a definition of the computer network and the main network designs, operations and protocols.

2.3.1 Introduction

Innovative research and development relies on the rapid dissemination of information, resource and idea sharing across geographical, academic and professional boundaries. The escalating demand for inter-disciplinary communications has played a significant role in the evolution of computer network designs and technologies and has been responsible for their expansion from principally militaristic and academic domains into the commercial sector.

A number of advantages are to be gained with the implementation of computer networks in academic and corporate sectors. These include the sharing of resources among users, the localisation of maintenance, reliability and, in many cases, substantial cost savings [Tanenbaum, p.3]. With potential benefits across a wide range of disciplines, it is critical to understand how networks physically operate and where primary limitations in their use arise. There are many complex technical issues involved in network design and potential limitations that must be comprehended before a particular implementation is undertaken. In the following sub-section, a basic definition of a computer network is presented.

2.3.2 Network Basics

One of the most common definitions of a computer network is that of a set of interconnected and autonomous nodes. The term node is generally given to any device capable of communication over the network e.g. personal computer or printer. Interconnected implies that all devices are connected either physically by means of a cable or by network devices such as switches and routers. Autonomy ensures that applications may be processed on each node independent of any network involvement [Tanenbaum, p.2]. A basic illustration of a computer network is given in figure 2.7. An internetwork consists of two or more networks connected to one another. The Internet is described as a global collection of nodes that communicate using the Transmission Control Protocol/Internet Protocol (TCP/IP) [Kercheval, p.13]. The TCP/IP protocol is explained in more detail in section 2.3.4.

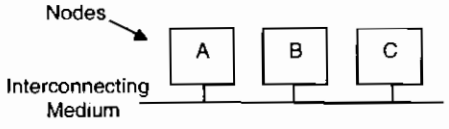

Figure 2.7; *Computer Network*

2.3.3 Network Types

There are many ways of categorising networks, including categorisation by network span, topology (layout) and the types of transmission media and techniques deployed to enable network communication. In terms of network span, three network types exist: Local Area Networks (LANs), Metropolitan Area Networks (MANs) and Wide Area Networks (WANs). Each type is distinguished based on the range over which it extends, it's

ownership and the types of transmission techniques and media that may be deployed within it.

Local Area Networks (LANs) are short-range networks that are used to connect office branches and college faculties at a single site. Metropolitan Area Networks (MANs) are medium range networks that connect different sites in a city. Wide Area Networks (WANs) are long range networks used to connect cities or countries. In general, the more localised a network is, the higher speeds and lower error rates that are achieved [Tanenbaum, pp.9-10]. The characteristics of each network type are outlined in table 2.1.

Network	Range	Application	Typical Ownership
LAN	<10km	Short range interconnects	Private
MAN	City	Medium range interconnects	Private/Public
WAN	Country	Long range interconnects	Government

Table 2.1; *Characteristics of LANs, MANs and WANs*

2.3.4 Network Topologies

Network topology describes the design or layout of a network. Perhaps the most common topologies are the bus, ring and star networks [Tangney, p.16]. On a bus network, all nodes are attached to a single cable on which network traffic is transferred. In this manner, the medium is shared by all nodes connected to the network and transmission must be arbitrated among the nodes. Ethernet is an example of a system that uses a bus topology [Tanenbaum, p.10][Niedermiller and Heywood, p.225].

In a ring network, all nodes are connected in a loop and a token, in the form of a bit string, is passed around the network. When a node wishes to transmit, it removes the token and transmits. The data and token propagate through the network until they reach the destination node. The destination node copies the data and the token is sent back to the transmitting node when all of the data has been received. The transmitting node then outputs a new token onto the network so that the other nodes may be given a chance to transmit. A typical ring network is the IBM Token Ring network, IEEE 802.5. Typical operating speeds range from 4Mbps to 16Mbps [Niedermiller and Heywood, p.227][Tanenbaum, p.11][Schatt, p.33].

In a star network all nodes are connected to a central device called a hub. All network transmissions are transmitted from the nodes to the hub and routed through to their appropriate destination. The implementation of a single central point ensures that fault

location and isolation is possible. In the case of failure of a particular node, the entire network will still operate and the failing node may be isolated from the network for maintenance. If the hub fails however, the entire network ceases to operate [Tangney, p.16][Niedermiller and Heywood, pp.220-224]. An illustration of the bus star and ring topologies is given in figure 2.8.

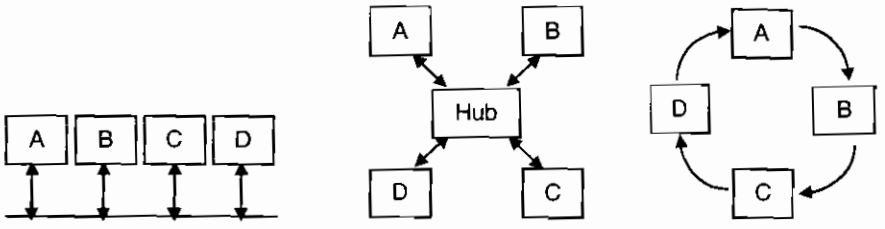

Figure 2.8; *(left to right) Bus, star and ring networking topologies*

2.3.5 Protocol Architecture

Communication over a computer network is achieved through the use of specific rules for communication known as protocols. By conforming to protocols, communication between different types of machines running on different hardware and software platforms is enabled [Zacker, p.5]. The set of protocols for a particular network is called a protocol stack and is typically composed of several layers [Gagliardi and Karp, p.143]. In this section, the main features of the commonly used Transmission Control Protocol / Internet Protocol (TCP/IP) are described. Before discussing TCP/IP however, it is useful to examine one of the first reference protocol stacks developed, the Open Systems Interconnect (OSI) model. Although the OSI model has been superseded in practical implementations by TCP/IP, the design of the protocol layers and functions are similar in both models [Washburn and Evans, p.147].

Open Systems Interconnect (OSI) Protocol Model

The OSI model was developed by the International Standards Organisation (ISO) as a reference model with the primary objective of standardising the functions and services provided at each protocol layer. A number of conventions are usually followed in the design of a protocol stack. These include the creation of a new protocol layer wherever a new function or service is required. Each layer has unique functions to perform and services to deliver so that duplication is avoided. Clean interfaces between protocol layers are defined so that a layer may be replaced or upgraded without any requirements to alter

the services and functions provided by the adjacent layers. The OSI model is a seven-layered model [Washburn and Evans, pp.8-9][Tanenbaum, pp.28-35]. Communication takes place vertically through the protocol stack as depicted in figure 2.9.

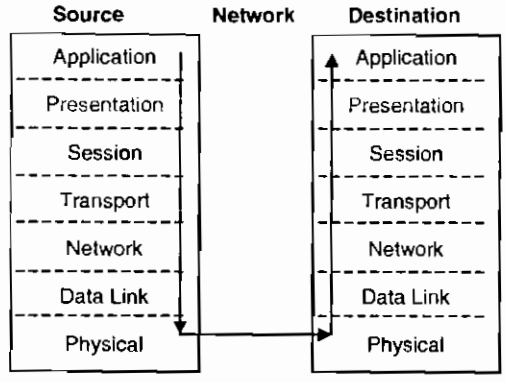

Figure 2.9; *Transmission through the layers of the OSI model*

When a node requests permission to transmit over a network, the message is passed to the top layer of the protocol stack, the application layer. The application layer encapsulates the application into a transmission unit and adds a header field containing additional information to the front of the transmission unit. This header provides information to the equivalent application layer in the destination node's protocol stack about how to process the received transmission unit. Application layer functions allow the application to be read by all nodes on the network.

The application layer then passes the transmission unit to the presentation layer below for further processing. The main function of the presentation layer is to convey the meaning and arrangement of received information to the destination. Data structures at the source presentation layer convert the node specific representation of the application unit into a standard representation for the network. It is the responsibility of the destination presentation layer to convert the standard network representation back into the appropriate representation for the individual node [Tanenbaum, p.33][Zacker, p.20].

Next, the presentation layer passes the unit to the session layer. The session layer initiates and maintains dialog between nodes [Zacker, p.20]. It also provides specific services to specific applications as well as data transport [Tanenbaum, p.32]. This layer is also responsible for placing checkpoints into the data stream to prevent data duplication in the event of a crash of the system so that only data following the last received checkpoint in the stream is retransmitted.

After processing has been completed in the session layer, the unit is transferred to the transport layer, where connection establishment and termination is carried out. The layer also ensures that the required quality of service e.g. reliability or low delay is provided to transmissions. The transport layer subsequently passes the transmission unit to the network layer.

The network layer is responsible for routing the data from source to destination. Routing may be static or dynamic [Tanenbaum, p.31]. Static routing entails the routing of information along defined routes through the network. Dynamic routing entails the routing of data along different links through the network, depending on the network traffic conditions. The network layer may also provide flow control and error detection services [Zacker, p.20]. The network layer transfers the data to the data link layer for further processing.

The data link layer receives the transmission unit from the network layer and converts it into the appropriate format for the network. Access to the physical medium is also arbitrated at this layer [Zacker, p.20]. When the data is in the appropriate form for the network, the data link layer transfers the data to the physical layer.

Actual transmission of the unit over the network is done at the physical layer. If the physical layer medium is copper cable, a varying signal voltage is propagated from the source physical layer to reflect the transmitted information. The physical medium thus deals with electrical and mechanical issues of bit transmission [Tanenbaum, pp.29-30].

In this section, brief outlines of the processes that occur in the OSI model were presented. Although OSI has been superseded in practical implementations by TCP/IP, the protocol outlines the main requirements of a functional protocol stack. It is consequently often used as a reference model for protocol design. In this section, the main processes of the OSI model were described. In the next section, the TCP/IP protocol is examined.

Transmission Control Protocol/Internet Protocol (TCP/IP) Model

In the last section, the OSI reference model was discussed but it was noted that in terms of practical implementations, TCP/IP has been the predominant model used. There are a number of reasons that TCP/IP surpassed OSI in modern day networks. Firstly, the protocols differ in the way in which the standards were developed. The TCP/IP standards were developed openly over the Internet by interested individuals who had implemented the

protocol practically and were keen to develop a reliable and timely standard solution for communication between diverse machines. They were developed by the Internet Engineering Task Force (IETF) in documents called Request for Comments (RFC) documents. On the other hand, the OSI protocol was developed within the International Standards Organisation (ISO). The rapid evolution of TCP/IP standards combined with the physical layer transparency of TCP/IP are key to the explanation of the dominance of TCP/IP in current network implementations throughout the world [Washburn and Evans, pp.8 and 147][Zacker, p.20].

Another difference between OSI and TCP/IP is that TCP/IP was designed to be medium independent whereas specific transmission media are defined for OSI implementations [Washburn and Evans, p.147]. As a result, designers are limited in the physical media they may use if OSI is to be deployed successfully whereas there are no constraints on the physical media types that may be deployed where TCP/IP is implemented. This gave TCP/IP a further advantage over OSI.

The TCP/IP model is a five-layer protocol stack that was devised in the late 1970's by the United States Defense Advanced Research Project Agency (DARPA) as the standard transport mechanism for the ARPANET research network [Mazda, pp.16/19]. TCP/IP was chosen as the standard protocol for the ARPANET in 1982 and it thus became the standard for the Internet [Kecheval, p.15]. The TCP/IP protocol stack is illustrated in figure 2.10.

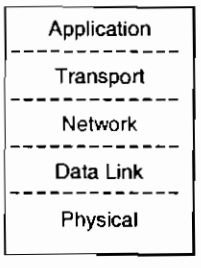

Figure 2.10; *Layers of the TCP/IP Model*

Comparing figure 2.9 and 2.10, the most obvious difference between the OSI and TCP/IP protocols is that, while the OSI stack contains three layers above the transport layer, TCP/IP contains only a single layer, the application layer. By discarding the presentation and the session layers, the TCP/IP stack remained operable and in fact, provided a less complex protocol solution as a result. According to [Kercheval p.2], if a workable networking protocol solution could be found by omitting certain functions and

layers without disrupting efficiency or causing any degradation to transmission, then ultimately, the solution was highly feasible and efficient. Consequently, when the 5 layer TCP/IP stack was standardised, it was widely deployed instead of OSI.

Transmission in the TCP/IP stack takes place vertically although logically communication is between peer layers. The application layer is responsible for providing services to different applications. These applications include the File Transfer Protocol (FTP) that is used for transferring files between one computer and another, the popular electronic messaging service, email and Hyper Text Transfer Protocol (HTTP), that is used to browse web pages on the World Wide Web (WWW) [Tanenbaum, p.37].

In the transport layer of the TCP/IP stack, two options are available, User Datagram Protocol (UDP) and Transmission Control Protocol (TCP). The particular option employed depends on the Type Of Service (TOS) required by the application. UDP is a connectionless and unreliable protocol. The term connectionless means that there is no connection setup between the source and destination nodes prior to transmission. The term unreliable means that there is no guaranteed delivery of the application data. Rather, a best effort service is employed. In this manner, the data is output onto the network and is routed through the network to its destination. The network makes its best effort to deliver the data to the correct destination and in correct form. Clearly, this option is not suitable for critical applications which require a guaranteed Quality Of Service (QOS) and transmission integrity e.g. file transfers. However, it does suffice for time varying applications such as stock exchange values and network management using Simple Network Management Protocol (SNMP) [Washburn and Evans, p.144][Tanenbaum, p.36].

Wherever an application requires a reliable and guaranteed service, then the TCP option is employed at the transport layer. This option provides a connection-oriented and guaranteed delivery of service to the application. Hence, before transmission occurs, a connection is established between the equivalent transport layers on the source and destination nodes. This guarantees a static path over which the application data is transferred. To ensure transmission integrity and delivery of the required level of service to the application, error correction and flow control mechanisms are implemented. As a result of the extra information generated for such transfers, TCP applications consume more bandwidth than UDP applications [Washburn and Evans, p.145].

One of the objectives of this research is to simulate a TCP/IP transfer over an Asynchronous Transfer Mode (ATM) network. The principal aspects of the ATM network will be described in more detail in section 2.5. It is hoped to achieve the objective without the need for implementing connection or vendor specific information in the model. Instead, a generic simulation of the manipulation of an application file by the different layers of the TCP/IP over ATM protocol stacks is developed. As mentioned before, specific layer information is added to the application unit in different layers of the protocol stacks. This is also true of TCP/IP over ATM. Header information is added to the application unit at the transport (TCP) and network (IP) layers. These headers contain address and connection specific information to ensure that the application data reaches the correct destination. Exact details of the contents of the TCP and IP headers may be found in [Washburn and Evans, pp. 204-207 and 270-273].

It must be noted that, in the development of the ATM system model, modelling of the specific header information contained in the TCP and IP headers is not attempted. The sole aim is to create a generic simulation model and to avoid the implementation of complex algorithms. As soon as the relevant information has been appended to the transmission unit in the TCP and IP layers, the datagram (as it is known in the network layer) is passed to the data link layer. This layer converts the datagram into the appropriate format for transmission over the particular network. In an Ethernet network for example, the data link layer assembles the IP datagrams into Ethernet frames for transmission while in an ATM network, the IP datagrams are segmented into fixed size cells for transmission. The data link layer then passes the frame to the physical layer that transfers the application from the source to the destination node by means of a transmission medium. At the destination, the application is removed from the physical medium and stripped to recover the original information. Although ATM is the data link layer technology of interest here, a brief description of the widely used data link layer technology Ethernet is given.

Ethernet

As already stated, Ethernet has been described as possibly the most common medium over which the TCP/IP protocol operates. It was developed jointly by three corporations namely Digital Equipment Corporation, Intel Corporation and Xerox Corporation (DIX)

[Washburn and Evans, p.152][Niedermiller and Heywood, p.412]. There is often confusion between Ethernet and the Institute of Electrical and Electronic Engineers (IEEE) standard IEEE 802.3. [Tanenbaum, p.276] states that the term "Ethernet" describes the type of cabling used in the network. The 802.3 standard on the other hand, relates to the family of systems that use the medium access mechanism Carrier Sense Multiple Access/Collision Detection (CSMA/CD).

Ethernet uses baseband transmission over coaxial cable on a bus topology [Washburn and Evans, p.152]. Two types of coaxial cable may be used for Ethernet transmissions: thick-wire and thin-wire coaxial cable. The IEEE standard for thick net Ethernet is 10Base5. This standard relates to a 10Mbps-network using baseband transmission with a maximum segment length of 500m and a maximum of 100 nodes per segment. The IEEE standard for thin net is 10Base2 and describes a 10Mbps-network using baseband transmission with a maximum segment length of 200m and maximum number of nodes per segment of 30 [Niedermiller and Heywood, pp.416-419]. There is also an Unshielded Twisted Pair (UTP) version of Ethernet called 10Base-T. This allows a maximum segment length of 100m and a maximum of 1,024 nodes per segment. Finally, a fibre option for Ethernet, 10Base-F, allows a maximum segment length of 2000m and a maximum of 1,024 nodes per segment [Tanenbaum, p.277].

In a network that uses Ethernet, the data link layer receives the Internet Protocol datagram from the network layer, encapsulates it into an Ethernet frame and adds on an Ethernet header. The format of the Ethernet frame is illustrated in figure 2.11 [Washburn and Evans, pp.154-155][Niedermiller and Heywood, pp.293-294].

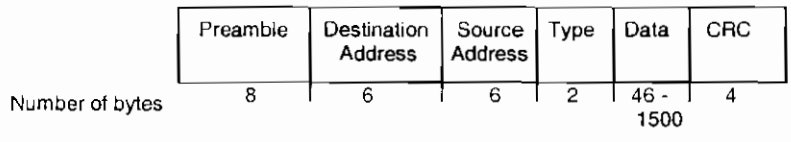

Figure 2.11; *Ethernet frame format*

As with the IP and TCP headers, the Ethernet header contains source and destination addresses. However, in contrast to the 32-bit IP addresses contained in the headers of the former protocols, the addresses contained in the Ethernet header are 48-bit physical hardware addresses of the source and destination nodes. These addresses are the Ethernet or Medium Access Control (MAC) addresses that are uniquely assigned to each network

interface card at manufacture. A mapping address scheme is required to provide to map physical MAC addresses to logical IP addresses to ensure that the data reaches the correct destination. This is achieved through the use of a protocol called Address Resolution Protocol (ARP).

The header contains a number of other fields. These include a preamble field used for synchronisation and type field that allows the communicating nodes to distinguish between different protocols such as IP and ARP. This field ensures that the contents of the frame are directed to the appropriate software for processing at the network layer. Data received from the network layer is encapsulated into the data field of the Ethernet frame. At the end of each Ethernet frame, a 32-bit Cyclic Redundancy Check (CRC) value on all the bits of the Ethernet frame is included. This value is the result of a mathematical computation, which involves the division of the binary representation of the frame contents by a predefined polynomial known to the source and destination nodes. The value is initially computed at the source node and the destination node checks the result of performing the same computation on the received frame with the value contained in the header of the Ethernet frame. If the results of the computation match the CRC value in the Ethernet frame header, the Ethernet frame is uncorrupted and is processed further [Schatt, p.42][Washburn and Evans, pp.154-155].

When a node wishes to transmit over an Ethernet network, it transmits a broadcast message over the network containing the IP address of the destination, requesting the corresponding Ethernet address of the destination node. The broadcast message is received by all nodes on the network but it is processed only by the node whose IP address matches the IP address contained in the broadcast message. The destination node then responds to the source node with a message containing its corresponding Ethernet address so that the source can transmit the data over the network. Once the source node learns of the destination Ethernet address, it inputs the 48-bit Ethernet address into the header of the Ethernet frame containing the application data and outputs the frame onto the network. [Washburn and Evans, p.154].

The minimum size of an Ethernet frame is 64 bytes. Consequently, Ethernet is not particularly efficient for very small transmissions. When the application unit is smaller than 64 bytes, padding must be added in order for the frame to meet the minimum frame

size allowed by the Ethernet network. The maximum size of an Ethernet frame is 1,518 bytes, including the preamble bytes. In a TCP/IP transfer over Ethernet, this leaves 1,460 (1,518-40-18) bytes for application data. The actual amount of data that can be transmitted in a single frame is dependent on the amount of header/overhead information implemented over all of the layers of the protocol stack [Washburn and Evans, p.154-155][Niedermiller and Heywood, p.290-295].

Access to the transmission medium by the network nodes is arbitrated by a mechanism known as Carrier Sense Multiple Access with Collision Detection (CSMA/CD) that allows the system to be used by a wide range of protocols. The nodes listen to the transmission medium and transmit when they do not sense a transmitted signal already on the cable belonging to another node. If two nodes transmit simultaneously and a collision is imminent, a jam signal is generated, indicating to the offending nodes to cease transmission. The nodes then both wait for a random period before attempting to transmit again [Niedermiller and Heywood, p.292][Derfler, p.129][Schatt, p.43].

In this section, the computer network was discussed and the operation of the OSI and TCP/IP protocols was summarised. The importance of the TCP/IP stack cannot be understated. TCP/IP provides a standard to allow nodes from different vendors and possibly operating on different platforms, to communicate seamlessly. Ethernet was described due to its ubiquity in modern computer networks. This section examined only some of the issues related to the higher layers of the TCP/IP protocol stack. Actual transmission is achieved between nodes on a computer network by particular transmission processes and using transmission media such as copper cables, optical fibres and microwave links which are deployed at the physical layer of the network. In the next section, the processes and media used in the physical layer are described.

2.4 Transmission Processes and Media

In the previous sections the main aspects of networks were presented, including an overview of different network types, topologies and protocols. In this section, some of the aspects related to data transmission are given. These include the processes used to represent and transmit digital data, and the media over which the data is transmitted. [Niedermiller and Heywood, p.166] define two classes of transmission media; bounded and unbounded. Bounded media confine data signals to a specific path through a copper wire

or optical fibre. Unbounded media transmit information through the atmosphere. Both electrical and optical bounded and unbounded media are described.

2.4.1 Encoding Processes

The type of communication system of interest is a computer network. Lying at the core of the network is the physical medium that allows communication to take place. It is appropriate to examine the way in which digital information is represented in computer networks. Typically in Ethernet and Token Ring networks, digital information is carried over digital signals. To achieve this, a process known as encoding is required. This process describes the way in which the digital information is represented on the digital carrier wave. There are numerous encoding techniques including unipolar, polar, bipolar, Return-to-Zero (RZ), Non-Return-to-Zero (NRZ) and biphase techniques. The specific technique chosen defines the voltages that represent one and zero bits, as well as the amount of the digital carrier that must be sampled to determine the value of the bit transmitted [Niedermiller and Heywood, p. 152].

Unipolar encoding involves the use of either a positive or negative voltage level to represent a one bit and a zero voltage level to represent a zero bit. Polar encoding uses a positive voltage level to represent a one bit and a negative voltage level to represent a zero bit. Bipolar encoding uses alternate positive and negative voltages to represent one bits and a zero voltage level to represent zero bits. This type of encoding is also known as Alternate Mark Inversion (AMI) encoding. Return-to-Zero encoding uses a voltage transition to represent each bit. The transition from a positive voltage level to a zero voltage represents a one bit whereas a transition from a negative voltage level up to a zero voltage level represents a zero bit. [Niedermiller and Heywood, p.155] describe that transition based encoding schemes are less susceptible to the effects of noise than those that are not based on voltage transitions. Similarly, Non-Return-to-Zero encoding uses voltage transitions to represent each bit. If a voltage transition occurs at the beginning of a bit, a one bit is registered. On the other hand, if there is no voltage transition at the start of the bit, a zero bit is registered.

Biphase encoding uses at least one voltage transition per bit. Two variations of biphase encoding exist, Manchester and Differential Manchester encoding. These encoding techniques are used in Ethernet and Token Ring LAN's respectively. Manchester

encoding uses a mid bit transition to encode data. A negative to positive mid bit voltage transition represents a one bit and a positive to negative mid bit voltage transition represents a zero bit. Differential Manchester encoding, on the other hand, provides clocking by the mid bit transition. A one bit is represented by a voltage transition at the start of the bit whereas a zero bit is encoded when there is no voltage transition at the start of the bit [Niedermiller and Heywood, pp.154-155].

2.4.2 Multiplexing Processes

In many cases, the full bandwidth of the transmission medium is not used. This fact may be exploited and the remaining bandwidth used to transmit extra signals. Multiplexing is the process of combining a number of messages together for transmission on the remaining bandwidth of the medium.

Multiplexing is described as the process of combining several low bandwidth (baseband) signals for simultaneous transmission on a high bandwidth medium. A device known as a multiplexer combines several signals at the transmitter and a demultiplexer separates and recovers the individual signals. In the following section, different types of multiplexing techniques are presented [Niedermiller and Heywood, p.187][Zacker, p.178].

Frequency Division Multiplexing (FDM)

In frequency division multiplexed communication, the entire bandwidth of the transmission medium is divided into sub-bands. Each of these sub-bands is assigned a different carrier frequency. Numerous signals may be transferred over the transmission medium simultaneously by assigning each signal to a separate carrier frequency and modulating the signal onto the carrier signal at that frequency. The advantage of FDM systems is that both analog and digital signals may be carried simultaneously over the same transmission medium [Tanenbaum, p.118].

Time Division Multiplexing (TDM)

[Shtainhart et al., p.2] describe TDM as the multiplexing together of several lower speed channels in time onto a single higher speed channel. TDM may be achieved in electrical and optical systems. Each node is allocated a time slot during which time it is allocated the entire bandwidth of the channel to transmit information e.g. a bit or group of bits. Once the time slot is over, the bandwidth of the channel is allocated to a different

node [Niedermiller and Heywood, pp.188-189]. All other nodes must wait their turn to transmit within their allocated time slot. TDM is suitable for channel speeds up to approximately 100Gbps. Beyond this range, the time of the multiplexing and demultiplexing processes limit the success of the mechanism in using the available bandwidth effectively. An optical carrier on a single fibre may be baseband modulated to offer much more bandwidth, as much as 25,000Gbps before transmission losses begin to inhibit transmission. Consequently TDM techniques do not use bandwidth effectively and the necessity for alternative multiplexing techniques arises. An alternative solution is found in Wavelength Division Multiplexing, where the bandwidth of the channel is divided into wavelength bands.

Wavelength Division Multiplexing (WDM)

In WDM, several optical carriers are baseband modulated at different wavelength locations in the fibre. Each carrier is then used to transmit information over the fibre. A separation in wavelength ensures that cross talk is avoided between channels. The total data rate of the fibre is given by the product of the number of sources and the rate at which they transmit. Each fibre may simultaneously support lower speed TDM channels. The combination of WDM systems and high-speed sources ensures a more effective use of available fibre bandwidth. Other multiplexing techniques include Subcarrier Multiplexing (SCM), Code-Division Multiplexing (CDM) and Space-Division Multiplexing (SDM). These techniques are further discussed in [Shtainhart et al., p.2][Tanenbaum, pp.119-120].

2.4.3 Bounded Media

In the previous sub-section, the processes of representing digital information on physical media were described. The different types of physical media are now outlined. As previously noted, physical media may be classified as either bounded (wired or guided) or unbounded (wireless or unguided) media. In this section, the main aspects relating to bounded media are outlined.

Bounded media are categorised into electrical conductors and optical fibres [Niedermiller and Heywood, p.166]. Within each category, various types and grades are available [Schatt, p. 25]. Copper transmission media are presented first; these include twisted pair and coaxial cable types. The main features of bounded optical transmission media (fibre) are then presented.

Twisted Pair

Twisted pair consists of two copper wires wrapped around one another. The twists enable the sensitivity of the cable to ElectroMagnetic Interference (EMI) to be reduced. They also prevent the wires acting as radiating antennas for radio signals. A further classification of twisted pair cable may be made, based on whether the twisted pair cable is unshielded or shielded [Tanenbaum, pp.82-83][Niedermiller and Heywood, pp.170-171].

Unshielded Twisted Pair (UTP) consists of two wires wrapped around one another surrounded by a plastic sheath for protection. UTP is both inexpensive and robust [Kercheval, p.49]. This type of cabling is also ubiquitous; it constitutes much of the cabling installed by telephone companies to offer telephony services to subscribers. It's dominance in worldwide telephone networks has played and continues to play a vital role in its deployment in computer networks. Typical UTP grades for computer networks include Category3 (CAT3) and Category5 (CAT5). CAT3 consists of two insulated wires that are gently twisted together, whereas CAT5 has a larger number of twists per centimetre than CAT3, offering a better quality signal. CAT5 is thus more suitable for data transmission than CAT3 [Tanenbaum, pp.83-84]. UTP provides the standard cabling for 10BaseT Ethernet [Niedermiller and Heywood, p.171].

The cable is unshielded i.e. it is not electrically insulated from its surroundings. Therefore, stray fields from nearby machinery and adjacent electrical cables may interfere with propagating signals and degrade the signal before it reaches the destination node. The quality of signal transmission is affected by the amount of electrical interference experienced, the length of the cable and on the quality of cable terminations [Kercheval, p.49]. An inverse relationship between signal strength and distance imposes a limit on the maximum distance over which a signal may be carried reliably.

In Shielded Twisted Pair (STP) or data-grade twisted pair, the twisted pair cable is shielded by a metal braid or mesh, which reduces the cable's electrical noise absorption [Derfler, p.111]. A layer of insulation separates the metal conductor at the core from the metal shield. STP is bulkier, more expensive and less flexible than UTP [Tanenbaum, p.84].

Coaxial Cable

Coaxial cable consists of four layers and two conductors. At the core of the cable lies a copper conductor that may be solid or stranded, depending on the degree of flexibility required. An insulating layer that separates the inner and outer conductors surrounds the core. The second conductor, either a layer of metal foil or a braided wire encases the insulating layer. This provides an electrical shield to protect signals in the inner conductor from outside electrical interference. The outermost layer consists of a plastic or Teflon jacket. This provides a protective sheath for the entire cable. Coaxial cabling has better shielding than twisted pair cabling [Tanenbaum, p.84]. Different grades of coaxial cable types are available and are tabulated in table 2.2. The impedance of the cable provides a comparative indication of the level of resistance of the cable to current flow and is determined by the type of materials used in the construction of the cable [Niedermiller and Heywood, pp.168-169].

Coaxial Type	Impedence Ω	Application	LAN standard
RG-8, RG-11	50	Thickwire Ethernet	10Base5
RG-58	50	Thinwire Ethernet	10Base2
RG-59	75	Cable TV, Ethernet	IEEE 802.3

Table 2.2; *Coaxial cable types and applications*

It must be noted however, that although coaxial cable is highly insensitive to EMI, it is not immune to the effects of EMI and therefore is not recommended for use in electrical environments. In these environments, it is recommended to use a transmission medium that is completely insensitive to EMI. This solution is found in optical fibres [Niedermiller and Heywood, p.170 and 174].

Optical Fibres

In optical fibres, light waves are used to transmit information. The fibre consists of a conductor core surrounded by a layer of cladding. This core is usually glass but may be plastic. Glass cores are more common since the material used to fabricate them, silica, is widely available. Glass fibres are also capable of reliably supporting the transfer of information over a longer propagation distance than plastic ones [Niedermiller and Heywood, p.173]. When light signals are coupled into the fibre at sufficiently small angles, the signal is continually reflected off the internal walls of the core, allowing the signal to propagate from one end of the fibre to the other. This is known as total internal reflection

and requires that the core and cladding material have different refractive indices [Gloge, p.250][Gagliardi and Karp, p.21].

Two types of fibre are available, monomode and multimode [Kercheval, p.39]. Conventionally, fibre sizes are given in terms of their core/cladding diameters (in μm). Monomode fibre is narrow (9/125μm) and contains one mode or path for light pulses to propagate. Multimode fibre is wider than monomode (62.5/125μm) and contains several modes for propagation [Smith, p.349] [Al-Salameh et al., p.46]. Monomode fibres are expensive but are capable of supporting high transmission speeds over long distances, of the order of several Gigabits per second over 30km. Multimode fibres are less expensive than monomode fibres and they easier to splice [Schatt, p.30]. An illustration of both fibre types is shown in figure 2.12.

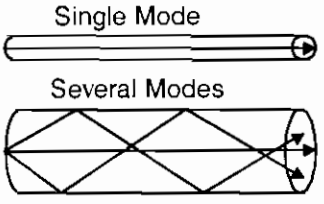

Figure 2.12; *Monomode Fibre (upper) Multimode Fibre (lower)*

The transmission rate achievable over a fibre is dependent on the maximum bandwidth that is given by

$$B = 2\Delta f \tag{2.1}$$

where B is the bandwidth in bps and Δf is the maximum signal bandwidth in Hz [Uiga, p.317]. The bandwidth is limited by the power loss in the signal as it propagates through the fibre. This loss is proportional to the fibre length and the amount of distortion in fibres. There are two sources of distortion; attenuation and dispersion [Smith, p.345].

Attenuation is the reduction of power in the light signal while dispersion is the spreading out of the light signal [Tanenbaum, p.89]. The attenuation is related exponentially to the fibre length by the formula

$$A = e^{-\alpha l} \tag{2.2}$$

where A is the attenuation in dB/km, α is the attenuation coefficient, which is dependent on fibre length l in meters, fibre material and the wavelength of the light used for transmission. One of the principal causes of attenuation is Rayleigh scattering that arises due to

interactions between the signal photons and the fibres crystal structure. This produces an attenuation that is proportional to the fourth power of the wavelength. At wavelengths greater than 1.7μm, the primary cause of attenuation is due to vibrations in the crystal structure of the fibre material [Uiga, p.321]. At 1.2μm and 1.4μm, the peak attenuation is due to vibrations of Oxygen and Hydrogen (OH^-) ions. There are minimum attenuation troughs at 0.85μm, 1.30μm and 1.55um of 0.85dB/km, 0.4dB/km and 0.25dB/km respectively. The regions around these wavelengths offer large amounts of bandwidth and are known as optical transmission windows [Tanenbaum, p.89] [Gagliardi and Karp, p.26][Smith, p.46].

There are two types of dispersion, modal and chromatic [Uiga, pp. 316-317]. Modal dispersion arises when complex mode patterns develop in the fibre and light signals reach the far end of the fibre slightly out of phase with one another. The quality of the received signal is degraded depending on the amount of dispersion. In long, wide fibres the amount of modal dispersion is accentuated. Multimode fibres thus suffer more from the effects of modal dispersion than monomode types. Increasing the rate at which signals are coupled into the fibre further increases the amount of modal dispersion generated [Kercheval, p.39]. Higher signaling rates and longer transmission path lengths may be achieved using monomode fibre. Chromatic dispersion arises when light rays of different wavelengths enter the fibre, causing the propagation velocity of the light rays to differ and introducing pulse dispersion effects at the far end of the fibre [Smith, p.347][Uiga, p.317].

The most important characteristics of optical fibres are high bandwidth capacity and low loss [Uiga, p.316]. A single fibre may offer the same bandwidth capacity as a number of copper cables, making fibre an attractive option for broadband networks. Low loss means that it can support data transmission over a long distance without the need for repeaters to regenerate the signal at intermediate points. Fibres are also thinner than copper cables making them ideal in situations where space is limited. As signal transmission through optical fibre is not electrical, fibres may be installed for transmission through areas where fire safety regulations prohibit the installation of electrical cables. Two further associated benefits arise. Firstly, the fibre is immune to EMI and may be the preferred option in electrical environments. Secondly, optical signals are very difficult for

unauthorised users to detect without physically cutting through the fibre. This provides a high degree of security [Niedermiller and Heywood, p.174].

In comparison to copper, fibre is a relatively new and expensive transmission medium. While copper is robust and equipment for its installation and maintenance is inexpensive and widely understood, optical fibre is less robust and installation equipment is more expensive [Schatt, p.31]. These disadvantages are however, offset by the demand for increased bandwidth and recognition of the potential long-term benefits offered by fibre. These factors are increasing the popularity of fibre in the marketplace and increased sales are driving the cost of the cabling and the interface connectors down. The traditional view of fibre representing a high-cost, high-risk transmission medium investment has diminished in recent years. Fibre has dramatically reduced the cost of fixed line bandwidth. Given the escalating demand for high-speed broadband capable networks, fibre installations in trunk applications are on the increase.

In this sub-section, bounded media were described. In the following sub-section, unbounded media that use transmission through the atmosphere, are discussed.

2.4.4 Unbounded Media

As has been already stated, unbounded media broadcast signals through the air [Niedermiller and Heywood, p.175]. Signals may be directed either to a signal receiver or to multiple receivers. Unbounded media are usually deployed where the implementation of bounded media is neither practically or economically feasible. The main types of unbounded media are radio, microwave, infrared and laser. A brief description of each of these is given in the following sections.

Radio

The radio region of the electromagnetic spectrum is divided into sub-regions defined as the Very Low Frequency (VLF), Low Frequency (LF), Medium Frequency (MF), High Frequency (HF) and Very High Frequency (VHF) bands. VLF, LF and MF radio signals follow the curvature of the earth while HF and VHF radio signals bounce off the ionosphere and may be used for long distance communications. Low and medium frequencies are omni-directional and may thus be intercepted by a wide range of receivers. Communication systems of this type have been in use for over a century and therefore,

equipment is widely available and relatively inexpensive. Radio licenses are required to operate systems in the radio region [Tanenbaum, pp.97-98].

Radio signals penetrate through dense objects such as the walls of buildings, allowing them to be used for indoor and outdoor communications over short or long distances. Higher frequency signals travel in straight lines and careful alignment of transmitter and receiver antennas is required to ensure reliable transmission. Higher frequencies however are easily absorbed and are not suitable for long distance communications. The power of the radio signal decreases as distance increases according to a square inverse law relationship [Niedermiller and Heywood, pp.179-180].

Microwave:

Microwave communication systems operate at higher frequencies than radio systems. By operating at higher frequencies than radio systems, they thus offer larger bandwidth than radio systems and consequently are capable of supporting higher data rates. Like communication systems that operate in the radio region of the EM spectrum, microwave systems also require a license to operate.

Microwave signals are line of sight and are easily absorbed by obstructions and atmospheric particles. As a result, transmitter and receiver antennas must be carefully aligned and must be of sufficient height to allow the signals to overcome the curvature of the earth (earth bulge) and any intermediate terrain and obstructions. The reliability of the microwave system is affected by weather conditions. Signal refraction effects may be manifested in bad weather. This results in waves of the signal arriving at the receiver slightly out of phase with one another, an effect known as multipath fading. Microwave systems are designed to operate with a specific fading margin [Tanenbaum, pp.98-99]. If this power of the received signals falls below a minimum value as defined by the system margin, the link is rendered inoperable. The link remains inoperable until the received power level exceeds the minimum power level. The results of many experimental and theoretical studies at microwave frequencies have been employed to produce propagation models and prediction formula to estimate the reliability of microwave systems under various weather conditions. These are used as guidelines for microwave system designers [Pratt and Bostian, p.327].

Microwave communication has applications in a wide number of areas. For example, geostationary orbiting satellites employ microwave signalling for communications. A further application of microwave systems has been in the telephony sector. Recently, many telephone companies have deployed microwave systems to transfer several voice signals simultaneously using multiplexing techniques [Niedermiller and Heywood, pp.176-179].

Laser Links

Laser links operate at optical frequencies and offer even higher bandwidth than microwave communication systems. Laser signals are coherent light waves of a single frequency (monochromatic) [Niedermiller and Heywood, p.180]. The coherency of the signal implies that signal divergence (spread out) is minimal and consequently laser signals are difficult to intercept undetected. Laser communication thus provides high security for data networks. Similar to high frequency radio and microwave signals, laser signals are line-of-sight and alignment of the transmitters and receivers is required to ensure reliable transmission. In contrast to microwave and radio systems however, laser systems do not require an operating license since the optical frequencies at which they operate, are not regulated [Ayanoglu, p.402][Tanenbaum, p.100].

Transmission in the optical region is affected by atmospheric and weather conditions. Scattering, absorption and refractions may reduce the power of the transmitted signal in the channel and may cause a signal of decreased power to be received at the destination. Clear air conditions do not produce significant power loss or attenuation of these signals. Turbulence effects however, that manifest in such conditions may cause a slight redirection of the signal. Cloudy conditions are characterised by higher particle densities and an increase in signal attenuation due to increased interactions between the signal particles and the atmospheric particles. Finally, rain conditions cause the maximum attenuation to the signal since numerous particles of varying sizes are present in the atmosphere and cause increased scattering and absorption of the optical signal. The attenuation increases with increasing rain rate [Gagliardi and Karp, pp.287-288].

Increased attenuation may lead to an insufficient amount of power transferred to the destination receiver. Depending on the sensitivity of the receiver, the transmitted information may or may not be reliably detected. Further, interference in the channel may cause corruption of the information in the form of bit errors or data losses.

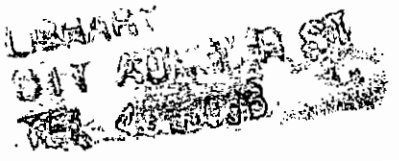

When the rain in the channel completely blocks the signal from reaching the receiver, the bit error rate may be regarded as irrelevant, since all of the data is effectively obliterated. In this case the link is unreliable for transmission and is said to be unavailable. The sensitivity of the receiver as well as the amount of scattering and absorption of the signal by rain in the channel determines the length of time for which the signal is blocked. In the context of a high-speed network such as an Asynchronous Transfer Mode (ATM) network, a shower of a short duration may result in the disruption or even loss of enormous amounts of information. Thus, it is more important to examine the length of time for which transmission is not possible. This length of time is characterised by a parameter known as availability. The availability is often used to describe the performance of wireless links. It is expressed as a percentage and is based on the ratio between the total "uptime" of the link to the total length of time that the link is switched on. Disruptions to link availability are typically due to weather effects and passing objects.

In this chapter, the main processes and media used in the physical layer of a computer network were presented. In the following section Asynchronous Transfer Mode (ATM), the specific technology of interest to this project, is described.

2.5 Asynchronous Transfer Mode

This section is devoted to the presentation of some of the main functions and operations of the Asynchronous Transfer Mode (ATM) networking technology, which is the standard networking technology of the Broadband Integrated Services Digital Network (B-ISDN). Many of the benefits offered by ATM over alternative networking technologies are also highlighted.

2.5.1 Integrated Services Digital Network

An Integrated Services Digital Network (ISDN) is one in which different traffic types e.g. data, voice and video are integrated onto a single network [Kercheval, p.1]. A simple illustration of the ISDN network is shown in figure 2.13. The basic form of ISDN, known as Narrowband ISDN (N-ISDN) was chosen for the digital transmission of voice. Each ISDN voice channel has a bandwidth of 64kbps. A number of versions of N-ISDN are available including Basic Rate Interface (BRI) and Primary Rate Interface (PRI) [Tanenbaum, p.142]. A BRI connection provides two 64kbps channels for voice and video

and a single 16kbps channel for data transfer while a European PRI connection consists of 30 64kbps channels for voice and one 16kbps channel for data. The voice and data channels are referred to as the B and D channels respectively. Basic rate interface connections are primarily aimed at small business users while primary rate interface connections are deployed in large corporations [Washburn and Evans, p.182][Niedermiller and Heywood, p.209].

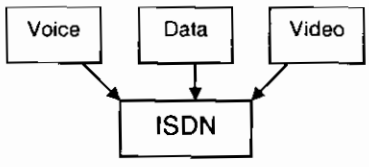

Figure 2.13; *Integrated Services Digital Network*

From a financial perspective, integrating traffic types is beneficial as it alleviates the need for separate network implementations and individual maintenance of separate networks for each traffic type. Despite the fact that N-ISDN met the needs of many users, others were unsatisfied with the marginal increase in bandwidth provided by this version of ISDN. This prompted the development of a broadband version of the technology called Broadband ISDN (B-ISDN), the standard technology for which would be provided by a cell-switching architecture known as Asynchronous Transfer Mode (ATM). ATM parallels the functionality of N-ISDN by facilitating the integration of numerous traffic types over a single network but offers greater bandwidth. Promising results from test bed implementations in the early 1990's stimulated interest in ATM throughout the telecommunications industry and led to the deployment of ATM on many national and international backbone links.

Initially ATM equipment was beyond the financial means of many businesses, this combined with interoperability issues between different vendor products led to limited applications of ATM. Standardisation and proven results from ATM test bed implementations have however, propelled ATM from a high-risk, relatively unknown networking solution, to a feasible and even cost-effective networking solution. Currently ATM is at the forefront of the broadband networking race, competing with other broadband networking technologies such as Gigabit Ethernet for the backbone networks [Kapoor and Ryan, p. 49].

2.5.2 Cell Switching Architectures

There are a number of different types of network switching architectures. These include circuit switching, message switching, packet switching and cell switching [Niedermiller and Heywood, pp.198-201]. In circuit switched networks, a circuit is set up between the source and destination nodes before transmission so that voice signals may be relayed between the nodes. Circuits are terminated as soon as the call is terminated at each node. Circuit switching is often regarded as inefficient as the bandwidth of the circuit may be wasted if it is not used all of the time. The most common example of a circuit switched network is the telephone network [Tanenbaum, p.130].

Message switched networks transfer variable-sized messages between source and destination nodes without a direct connection between the nodes. All network nodes are assigned a unique address. When a node has a message to transmit, it simply outputs the message onto the network with an additional data stream at the beginning of the message to indicate the message origin and destination. Message switching makes effective use of the available channel bandwidth, allowing multiple messages to be routed simultaneously through the network [Niedermiller and Heywood, pp.199-201].

Packet switched networks operate in a similar manner except that they impose a limit on the maximum size of the packets that can be transferred. If a message larger than a predefined maximum transmission unit size is to be transmitted, the message must be broken into a number of smaller units called packets before transmission can take place. Each packet contains source and destination node addresses and a sequence number to indicate the location of the current packet in a message. Packet switching has facilitated data transmission over computer networks in the latter part of the 20^{th} century. Most LANs employ packet switching techniques to route messages [Niedermiller and Heywood, pp.201-204][Tanenbaum, p.133].

As an appropriate switching technology to provide the broadband integrated services digital network, circuit and packet switched networks were inefficient and ineffective. Neither is capable of efficiently supporting applications other than those for which they were originally designed. For example, circuit switched networks are designed to transmit time critical Constant Bit Rate (CBR) voice messages at specified intervals. They are unsatisfactory in supporting "bursty" data traffic. On the other hand, packets switched

networks, designed to handle Variable Bit Rate (VBR) data transmissions, are not sufficiently capable of supporting time-critical constant bit rate applications such as voice and video. For these reasons, an alternative architecture was chosen to provide the B-ISDN service. This alternative architecture was known as cell switching.

Cell switched networks enable the integration of traffic types by converting all traffic from these applications into transmission units of fixed size called cells before transmission [Washburn and Evans, p.194]. The size of the cell chosen for transmission is key to the efficiency of the technology. Choosing a small cell size reduces the length of time to output data bits onto a transmission link, a time which is referred to as serialisation delay. Minimisation of this delay is vital to guarantee that time-critical applications like voice messages are not caught behind large non time-critical data applications. This situation is known as head of line blocking and is illustrated in figure 2.14 [Kercheval, p.55][Tanenbaum, p.149]. By converting all application data, no matter what traffic type, into fixed size cells, this situation is effectively eliminated.

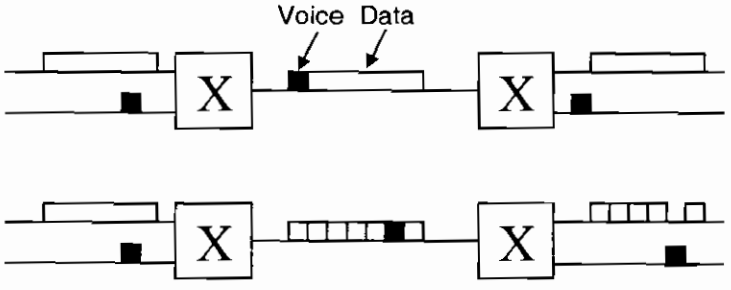

Figure 2.14; *Head of line blocking (upper) Elimination of head of line blocking situations in a cell network (lower)*

The standard cell size agreed for ATM is 53 bytes. This includes 5 bytes of control information (header) and 48 bytes of application data (payload) [Washburn and Evans, p.194]. The efficiency achieved by cell switching architectures cannot be understated. The fixed cell size enables cell switched networks to transmit high priority traffic such as voice and video alongside low priority traffic such as data. Use of a fixed cell size also simplifies hardware and software design. Internetworking devices and processors may be designed to switch cells of a specified size relatively easily [Kercheval, p.55-56].

2.5.3 Asynchronous Transfer Mode Model

The ATM reference model comprises three layers and three planes. The layers of the model are the ATM Adaptation Layer (AAL), ATM layer and the Physical Layer. The first two correspond to the data link layer in the OSI and TCP/IP protocol while the physical layer corresponds to the physical layer in both protocols. Layers are responsible for accepting applications and converting them into the format required for transmission over the ATM network. Each layer has a unique set of defined services to offer and operations to perform. The planes of the model are the user plane, control plane and management plane. The user plane manages and transfers user data, the control plane generates signalling requests and the management plane manages both the layers and the plane functions, detecting problems in the network and controlling the functionality of the entire system [Kercheval, pp.52-53][Tanenbaum, p.63-64]. The layers and planes of the ATM model are illustrated in figure 2.15.

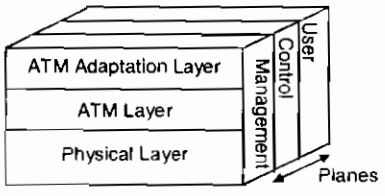

Figure 2.15; *ATM protocol stack*

ATM Adaptation Layer (AAL)

When an application requires transmission over an ATM network, the application data is passed to the ATM Adaptation Layer (AAL). One of the main functions of the AAL is to map user data into cell streams i.e. segment application data into 48-byte blocks that will be inserted into the payload of the ATM cells [Kercheval, p.59]. The AAL is divided into two sublayers; the Convergence Sublayer (CS) and the Segmentation and Reassembly (SAR) sublayer. The convergence sublayer provides the interface between the ATM protocol stack and the application layer and controls the data flow to and from the SAR sublayer [Tanenbaum, pp.546-547]. It is within this sublayer that a variable length pad and an 8-byte trailer are added to the application data to ensure that the data will fit evenly into a number of cells. The trailer contains a length field and a 32-bit CRC check computed on the entire Protocol Data Unit (PDU). The segmentation and reassembly sublayer deals with

the actual breakup of the application data into the 48-byte blocks at the source and the reassembly of the blocks into application data at the destination.

There are different types of AAL available, each offer different services and support to different applications [Gupta, p.1]. AAL1 for example. provides a connection-oriented service and supports constant bit rate applications like video and voice. When AAL1 is used, an application sample is inserted into the payload at defined intervals e.g. one byte every 125μs. A sequence number and a sequence number protection field arc inserted to ensure cells are delivered in order.

Other AALs include AAL2, AAL¾ and AAL5. AAL2 is an ATM protocol standard for supporting variable bit rate connection-oriented traffic while AAL¾ is a protocol standard for supporting connection and connectionless VBR traffic. Possibly, the most commonly used AAL type is AAL5. The reason for this is that AAL5 is the standard AAL for the transfer of data over an ATM network. By providing either a connection or a connectionless service and is used to transfer classical IP packets over ATM networks and for LAN Emulation (LANE). AAL5 is capable of dealing with IP payloads of up to 65,527 bytes [Washburn and Evans, p.195].

ATM Layer

The ATM layer interfaces with the ATM adaptation layer above and the transmission convergence sublayer of the physical layer below. The ATM layer is primarily concerned with establishing the transmission path for the ATM cell through the network to the destination. When the ATM layer receives the 48-byte unit from the AAL layer, it adds on a four-byte header containing transmission path identifiers to transfer the ATM cell through the network. Since ATM is connection-oriented technology. a connection must bc established between the source and destination nodes before transmission may take place [Tanenbaum, p. 62]. The Virtual Circuit or Channel Identifier (VCI) and the Virtual Path Identifier (VPI) fields in the ATM header define the ATM connection. Thc virtual circuit represents the path through intermediate switches to the destination while the virtual path identifies a number of virtual circuits grouped together [Kercheval, p.59]. An illustration of a number of virtual channels aggregated into a virtual path is given in Figure 2.16.

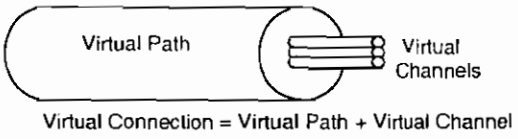

Figure 2.16; *ATM Connection Identifiers*

ATM Connections may be permanent or switched [RFC 1577]. Permanent connections are called Permanent Virtual Circuits (PVCs) while switched connections are called Switched Virtual Circuits (SVCs). PVCs provide a permanent connection between the ATM end nodes. They are manually configured static connections that are used widely in local area networks [Kercheval, p.59]. SVCs on the other hand, are dynamically configured. Signalling protocols between the source and destination nodes negotiate a virtual connection through the ATM network and transmissions are sent over this. SVCs are flexible connections and, since they are setup only when there is traffic to be sent, they use the available bandwidth efficiently. When a connection is set up between nodes a traffic contract is made. This outlines the required Quality of Service (QoS) for the connection.

Two types of network interfaces are defined for ATM networks. These are User Network Interface (UNI) and Network-Network Interface (NNI). UNIs defined the interfaces between ATM nodes and ATM switches while NNIs defined the interface between two ATM switches. Different versions of both interface types exist. These are outlined in table 2.3.

Interface Type	Connecting Devices
Private UNI	Private ATM node - Private ATM switch
Public UNI	Private ATM node - Public ATM switch
Private NNI	Private ATM switch - Private ATM switch
Public NNI	Public ATM switch - Public ATM switch

Table 2.3; *ATM interfaces*

ATM Physical Layer

The physical layer of the ATM model comprises two sublayers, the Transmission Convergence (TC) sublayer and the Physical Medium Dependent (PMD) sublayer [Tanenbaum, p. 64].

The TC sublayer receives the cell from the ATM layer and computes a Header Error Check (HEC) computation on the first four header bytes of the ATM cell. The computation

involves the division of the 32 header bits by a predefined polynomial. The HEC provides low level security on the ATM cell, ensuring that the cell reaches the correct destination on the ATM network. Since it is computed solely on the header, it does not provide any security against payload data corruption. Payload error checks may be implemented, if required, by higher layer protocols. [Tanenbaum, p.235] notes that the HEC provides a sufficiently strong error detection and correction mechanism for ATM networks in which optical fibre is used as the transmission medium. The reason for this is that over 99% of all errors that occur on optical fibre lines are single bit errors.

After the HEC has been computed and inserted into the ATM cell, the TC sublayer converts the entire cell into a bit stream and passes it to the PMD sublayer below for transmission. The PMD sublayer interfaces directly with the transmission medium and provides the operations required for transmission and reception of data between a source and destination. These operations include the conversion of bit streams into the required signals for the transmission medium [Tanenbaum, p.64].

ATM cells may be sent individually over the network. It is more typical however, to send them in the payload of a frame appropriate for the specific transmission medium in the channel. Optical framing mechanisms like Synchronous Optical Network (SONET) or Synchronous Digital Hierarchy (SDH) are used. A single SONET frame consists of 810 bytes [Tanenbaum, p.126]. This consists of 9 rows and 90 columns [Kercheval, p.42]. The first three columns (27 bytes) are reserved for transport overhead and maintenance information. A number of ATM cells are transported in the Synchronous Payload Envelope (SPE) of such frames. By employing standard framing at the physical layer in the ATM networks allows ATM cell boundaries to be identified by the TC sublayer easily [Tanenbaum, p.126].

As described in section 2.1, transmission media may be synchronous or asynchronous. Synchronous systems have definite time slots for transmission and a master clock governs transmissions. If there is no data available for transmission from a node during its assigned time slot, non-data cells are sent. Examples of non-data cells include idle cells and Operations Administration and Maintenance (OAM) cells that are used to exchange control information between ATM switches in ATM networks. SONET and SDH networks transmit frames synchronously. On the other hand, the manner in which

ATM cells arrive to the network is asynchronous. These cells may be transmitted onto the network at any time. The asynchronous nature of ATM allows it to use the bandwidth of the transmission medium deployed in the channel more efficiently than many traditional networking technologies.

As with TCP/IP, ATM is independent of the physical medium used in the channel. SONET was developed at Bell Communications Research (now Telcorida Technologies) and was standardised by the American National Standards Institute (ANSI). It was subsequently accepted as a slightly different international standard known as the Synchronous Digital Hierarchy (SDH) by the ITU-T [Cavendish, p. 164]. SONET equipment is widely available since optical technology is ubiquitous in backbone networks. ATM speeds are based on the speeds achievable using digital telephone lines, which offer a bandwidth of 64kbps. In the United States, 24 telephone lines are multiplexed to form a single T1 line of 1.536Mbps while in the European Union, 30 telephone line are aggregated to achieve a bandwidth of approximately 2Mbps, which is called an E1 line. 32 T1 lines aggregated together or 24 E1 lines allow a throughput of 49.152Mbps. This channel combined with overhead for multiplexing, synchronisation and maintenance forms the basic ATM channel of 51.84Mbps that is called Synchronous Transport Signal (STS1). The STS level refers to the speed of the bitstream. When the bits are converted to a train of optical pulses in a fibre, they are called an Optical Carrier (OC1). Multiplexing three STS1 lines together yields a bandwidth of 155Mbps which, as an optical stream, is denoted OC-3. At STS-1 speed, a single SONET frame is sent at a time. At STS-3 speed, three SONET frames are sent at a time. The ITU developed a similar standard known as the Synchronous Transport Module. The STM1 rate is approximately the same as the STS3 rate of American National Standards Insititute (ANSI) [Kercheval, pp.41-42].

In this section, the layers of the ATM model were described. In the next section, the main operations in the transfer of IP over ATM are outlined.

2.5.4 Internet Protocol over Asynchronous Transfer Mode (IP over ATM)

[Ayanoglu, p. 400] states that

> " At this point it is unknown whether IP or ATM will be the dominant protocol in the future of integrated services networking. On the one hand, IP-Based protocols are widely deployed and are an inevitable part of Internet services. On the other hand, switching favors ATM."

The fact ATM is connection-oriented and IP is connectionless often causes confusion and debate as to the viability of the support of IP over ATM. However, a number proposals are available to provide IP support over ATM [Bray, p.67]. These include

- IP over ATM: This method was devised by the Internet Engineering Task Force (IETF) and uses an ATM Address resolution server to resolve IP and ATM addresses in an IP network. This method cannot support any other protocols other than IP and does nor take advantage of ATM's QoS offerings.
- LAN Emulation (LANE): This solution was developed by The ATM Forum and allows all network layer protocols of the OSI model (e.g. IP, IPX, NetBIOS) to be supported. However, similar to IP over ATM, it does not take advantage of the QoS benefits of ATM.
- Multi-Protocol Over ATM (MPOA): Again this solution was developed by The ATM Forum and is similar to LANE but is also capable of benefiting from ATM's QoS offerings. While the two solutions described above are limited to single IP subnetworks, this solution can route between different IP subnetworks [Ayanoglu, pp. 400-401].

Further details of the ATM networking and SONET/SDH technologies are available [Cavendish, pp.164-171][Gupta, pp.1-5][Chen and Tantiprasut, pp.82-96][Noh, pp.81-93]. In this section, the networking technology ATM was described. This is the technology of interest to this research. Another area of interest to this research is the area of wireless optical communications. In the next section, an overview of the literature on propagation through the atmosphere is presented.

2.6 Optical Transmission through the Atmosphere

Demand for optical communication is increasing due to the increase in broadband applications and demand for high speed and high security in computer networks. In this section, the main optical source and detection devices and processes are presented. These are followed by a more detailed study of wireless optical communication channels and, in particular, the effect of rain in the channel.

2.6.1 Devices and Processes

Optical Sources

An optical source is a device that generates an optical signal. Optical sources are characterised by a number of parameters including input current, modulation range, modulation bandwidth and saturation level [Gagliardi and Karp, p.10. The input current is the current required to produce an output optical signal of a particular power. The modulation range is the range over which the output power is linearly proportional to the input current. The modulation bandwidth is the rate at which information may be superimposed onto the carrier signal. In contrast to signals produced by electrical sources that cannot be modulated at more than a few hundred MHz, optical sources produce light signals that may be switched at frequencies in the GHz range. The saturation level is the maximum amount of output power that can be generated by an optical device.

Optical sources include Light Emitting Diodes (LEDs), laser diodes and lasers. LEDs are inexpensive devices fabricated from semiconductor materials. They produce light when an external current is applied. The materials used to form the semiconductor junction determine the wavelength of the light produced by the device. Gallium Arsenide (GaAs) is commonly used and produces light in the 0.8μm to 0.9μm wavelength range. Some of the main advantages of LEDs include the fact that they require low input current to generate light pulses, have a long life and are not temperature sensitive. The disadvantage of LEDs is that they produce polychromatic light that is low in power (1mW to 10mW). Consequently, LEDs are not capable of carrying signals reliably over a long distance or supporting high data rates in optical communications systems. They are however, used successfully for short-range communications in Local Area Networks [Kercheval, p. 40] [Gagliardi and Karp, p.8].

Laser diodes are also semiconductor devices but they require more current to operate. They produce coherent light pulses of higher power and narrower focus than LEDs, between 10mW and 50mW [Gagliardi and Karp, p.10]. These are used in fibre optic communications [Uiga, p.158]

The optical source that produces an output signal of the highest power and narrowest focus is the laser. The laser consists of an optical cavity filled with a light amplification

material (gas or solid). The amplification material used in the cavity determines the wavelength of the light produced by the device. A mirror surface at each end of the cavity provides a reflecting surface. Light enters the cavity through a small aperture at one end of the laser. This light is amplified by the amplification material and is continually reflected in the cavity by the reflecting mirrors. The power of the light signal increases as a result. A small aperture at the far end of the cavity enables the high power (0.1W to 1W) highly focused (monochromatic) amplified light signal to escape [Gagliardi and Karp, p.9]. The generation of such a high power monochromatic signal constitutes the main advantage offered by laser sources over the other optical sources. In order to achieve this output however, a large amount of input current is required. Lasers are also more expensive than LEDs and laser diodes, they have a lower expected lifetime and higher temperature sensitivity. Lasers are used for long-distance high-bandwidth Wide Area Network communications [Kercheval, p.40][Uiga, p.128]

Optical Source Processes

In order to transfer digital information over an optical system, the bits must be modulated onto the optical signal. Depending on the modulation type employed to achieve this, optical systems may be classified as coherent or incoherent. Coherent systems use Continuous Wave (CW) modulation to modulate the data onto the carrier signal. In this case, the light source continually emits an optical signal for the duration of the transmission. Optical systems that use Amplitude Modulation (AM), Frequency Modulation (FM) and Phase Modulation (PM) techniques are examples of coherent systems. Incoherent or direct detection systems on the other hand, use pulsed modulation, where the light source is pulsed on and off during modulation. Systems that employ Intensity Modulation (IM) techniques are examples of incoherent systems [Gagliardi and Karp, p. 4].

Destination Devices

An optical detector receives the optical signal at the destination. Two classes of optical receivers are available, power detecting or heterodyning. Power detecting receivers extract transmitted information from power variations of the incident light field. Heterodyning receivers combine the received light wave with a locally generated light wave before photodetecting the combined wave. Heterodyne receivers are used in optical

systems that use AM, PM and FM techniques to superimpose information onto the light wave. Filtering may also be implemented at the receiver [Gagliardi and Karp, pp. 4-5].

Destination Processes

There are three stages in optical detection. Firstly, a lens intercepts the light signal and focuses it onto a photodetector. The photodetector is an optical to electrical converter that produces an electrical current when light is incident upon it. The electrical signal is amplified and processed in the receiver circuitry and the original bits are recovered using decoding. The performance of the optical system depends on the amount of interference the light pulse has been subjected to, the reliability of the optical medium employed in the channel and the sensitivity of the receiver [Gagliardi and Karp, p.4]. A number of noise sources may affect the quality of an optical transmission including radiation, internal noise generated by the photodetector and thermal noise present in processing circuitry.

2.6.2 Factors Contributing to Signal Attenuation

The quality of a digital transmission medium is normally characterised by the Bit Error Rate (BER). The BER represents the number of incorrect bits received at the destination as a fraction of the total number of bits transmitted [Pratt and Bostian, p.193]. This parameter is primarily a function of signal attenuation, which is a measure of the loss in strength of the propagating signal in dB [Mazda, p.62/19]. Path length and electrical interference are the main factors in signal attenuation in electrical communication systems. In optical systems, electrical interference does not arise. Rather, impurities in the transmission fibre or deleterious interactions in the case of an atmospheric optical transmission contribute to signal attenuation [Gagliardi and Karp, p.20 and p.26].

It is specifically with the attenuation effects of rain on a wireless optical link that this research is concerned. Consequently, it is necessary to further investigate the deleterious interactions that arise between the optical signal and the particles in the atmospheric channel. The main interactions are scattering and absorption interactions that cause attenuation and distortion of the optical beam pattern [Gagliardi and Karp, p.286]. The extent of these interactions with the received signal is dependent on weather conditions. There have been numerous investigations, theoretical and experimental to quantify the effects of these interactions on electromagnetic signal propagation under different weather

conditions and at different transmission frequencies [Sekine et al., pp. 358-359][Altshuler, pp. 757-758][Wulfsberg and Altshuler, pp. 181-187][Crane (1980), pp.1717-1733]

Scattering

Scattering may result in the redirection of a portion of the propagating energy away from the original propagation path as shown in figure 2.17 [Gagliardi and Karp, p.289] [McCartney, p.20]. The random arrangement and motion of atmospheric particles causes them to scatter independently. Independent scattering predominates under all meteorological conditions. Three variations of scattering are manifested in an atmospheric channel: Rayleigh, Mie and Raman scattering. The specific type that occurs is dependent on the relationship between the size of the interacting particle and the wavelength of the propagating signal [McCartney, pp.22-23].

Rayleigh scattering occurs when the interaction particle is more than ten times smaller than the wavelength of the propagating signal. This is typically the case when an electromagnetic signal encounters gas molecules in the atmosphere. The theory assumes the scatterers to be isotropic particles that produce an equal amount of scattering in the forward and backward direction. Rayleigh scatter is proportional to the volume of the particle and inversely proportional to the fourth power of the wavelength [McCartney, p.22].

Mie scattering describes the scatter that results from the interaction between an electromagnetic signal with atmospheric particles that are greater in magnitude than Rayleigh particle. The theory applies a mathematical series over all particle sizes, the first few terms of which correlate to the Rayleigh scattering coefficients [Zavrody and Harden, pp. 422][McCartney, p.23].

Raman scattering accompanies Rayleigh scattering when the incident light is monochromatic. Scattered energy from the signal contains weak spectral lines that are not present in the original signal and are investigated using a specific Raman scattering technique [McCartney, p.23].

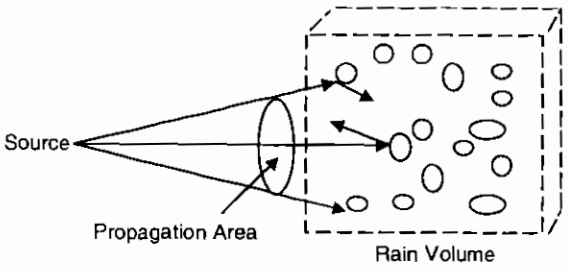

Figure 2.17; *Scattering of electromagnetic waves by atmospheric particles*

Absorption

Absorption results in the removal of flux from the propagating signal [Gagliardi and Karp, p.287]. Unlike scattering processes that do not produce a change in the internal energy states of the atmospheric particles, absorption causes the obstructing particle to receive energy from the propagating signal. The extraction of energy increases the internal energy of the particle, which is subsequently re-radiated from the particle as noise [McCartney, p.25].

Attenuation is used to quantify loss of signal strength and is equal to the difference between the strength of the received signal and the transmitted signal. Both absorption and scattering losses must be accounted for in determining the received power level. If the power of the optical signal upon transmission from the source is P and the beamwidth angle is defined by θ, the area of the beam A, at a distance x along the propagation path is given by

$$A = \frac{\pi(\theta x)^2}{4} \tag{2.3}$$

The intensity describes the power per unit area of the beam at a point along the propagation path and is expressed by $I = P/A$. When the signal experiences losses in the transmission channel, the intensity may be more accurately rewritten as $(PL)/A$, where L is the loss. This loss is typically expressed in negative exponential form [Gagliardi and Karp, pp.289-291] by

$$L = e^{-\beta_{ex} x} \tag{2.4}$$

The total extinction (loss) coefficient accounts for the extinction due to scattering and absorption which are denoted β_{sc} and β_{ab} respectively. The relationship between the total extinction coefficient and the absorption and scattering coefficients is given by

$$\beta_{ex} = \beta_{sc} + \beta_{ab} \tag{2.5}$$

For a collimated beam such as a laser beam, Brouguer's exponential law of attenuation describes the strength or irradiance at any point along the propagation path [McCartney, pp.29-31]. This law takes the form

$$E_x = E_0 \exp(-\beta_{ex} x) \tag{2.6}$$

where E_x is the irradiance of the beam at the point x on the propagation path and E_0 is the irradiance at $x = 0$. In the case of a diverging beam, Allard's Law applies. This is expressed by

$$E_x = \frac{E_0 \exp(-\beta_{ex} x)}{x^2} \tag{2.7}$$

Values of β_{ex} are available for a wide range of atmospheric conditions; clear air, cloudy and rain [Gagliardi and Karp, p.291].

In clear air conditions, there is good visibility and low attenuation of the optical signal may be expected. It is not uncommon however, for turbulence effects to arise under these conditions and cause a slight redirection of the propagating signal. Under cloudy conditions a higher number of particles are introduced into the atmosphere than those normally present in clear air conditions. The increased particle density gives rise to an increased probability of interactions with the propagating signal. Higher attenuation measurements are expected. The worst signal attenuation effects arise in rainy conditions. In this case, water droplets of varying sizes are introduced into the propagation path [Gagliardi and Karp, p.287].

The extent of signal attenuation is dependent on the relationship between the diameter of the raindrop encountered and the signal wavelength [Gagliardi and Karp, p.286]. The rate at which rain falls through the propagation path also impacts on the amount of attenuation produced. Rain rate is defined as the rate at which water would accumulate in a rain gauge situated at the ground in the region of interest and is measured in units of millimetres per hour [Pratt and Bostian, p.327]. During heavy rain a larger quantity of drops of all sizes are generated. This results in an increase in the number of interactions and signal attenuation.

2.6.3 Attenuation Models

Various authors have investigated the attenuation effects that arise in the atmospheric channel [Sander, pp. 213-220][Sweeney and Bostian, pp.275-277]. The impact of rain is of particular interest to this research since in Ireland, the predominant form of precipitation is rain [Rogers, p.87]. Consequently, the following discussion relates to the impact of rain on communication links operating at these frequencies. Several theoretical models have been developed to predict the propagation of electromagnetic radiation through rain conditions in an atmospheric channel [Crane (1980), pp.1717-1733]. Comparison between theory and experiment is key to determining the validity of these models [Sekine et al., pp. 358-359][Manabe et al. Pp. 474-477].

The level of signal attenuation is dependent on the rate at which rain falls through the propagation path. Increased rainfall rates cause increased attenuation of a signal of specific frequency and path length. Clearly, this is because there is an increased number of particles causing scattering and absorption in the channel. Several theoretical and experimental relationships between attenuation and rain rate have been reported in the literature [Marshall and Palmer, pp. 165-166][Maitra and Gibbons, pp. 657-666]. Possibly the most widely known of these is a power-law relation that is used by the ITU for prediction modelling for communication system in the frequency range 1-1000GHz [Olsen et al., p.318]. This relationship is given by

$$A = aR^bL \tag{2.8}$$

where A is the attenuation (dB/km), R is the rainfall rate (mm/hr), L is the path length (km) and a and b are constants that are dependent on signal frequency and polarisation [Pratt and Bostian, p. 334]. [Olsen et al., pp.318-328] derive this relationship in an influential paper from a more general relation using computations over all of the Mie scattering integrals for all drop diameters. The relation takes the form

$$A = a'R^{b'}\left[1 + \sum_{n=2}^{\infty} c_n f^n R^{nd}\right] \tag{2.9}$$

where a' and b' and c_n are functions of frequency, rain temperature and on the nature of a parameter known as the Drop Size Distribution (DSD), which describes the number of drops per unit size per unit volume of space, and d is a constant that is also dependent on

the DSD. In the limits where $f \to 0$ and $f \to \infty$ i.e. in the optical region, this equation is exact and a and b are independent of R.

The formula is typically used by communication system designers to obtain an estimate of the expected attenuation value of a communications link operating under specific rainfall conditions [Pratt and Bostian, p.324]. Obtaining values for a, b, L is relatively simple for frequencies 1-1000GHz. Extensive tabulations of the a and b values are available over this range [Olsen et al., p.323-324]. The value of the length L is specific to the particular link of interest while the rain rate value R, may be extracted in two ways. Either the cumulative rainfall distribution value for a particular climatic region may be used as the rain rate value or alternatively, a revised rain rate value based on a mathematical form of drop size distribution may be used [Pratt and Bostian, p.328 and 332]. These two methods are described below.

Regional Map Method

Rain exhibits spatial and temporal fluctuations and consequently, a single point rain rate measurement doe not provide an accurate measurement of the rain rate over the entire propagation path [Crane (1980), p.1718]. Instantaneous rain rate distribution measurements are required to achieve reasonable accuracy in attenuation predictions. However, practical measurements of this quantity are often contaminated by atmospheric fluctuations and turbulent effects. Averaging is thus required to suppress the statistical variability in the measured results. [Crane (1980), p.1719] notes that the optimal averaging intervals one-minute for terrestrial paths. Where instantaneous measurements are not available however, regional statistics may be employed for attenuation estimates. Regional maps containing these statistics are available from the ITU for different climatic regions throughout the world. The original regional maps were defined by [Rice and Holmberg, pp.1131-1136] who computed rain rate distribution statistics for several locations in the United States. These distributions were extracted from rainfall accumulation data [Lee, p.407]. Accumulation measurements from nearby locations were pooled together and mean statistics were computed for the entire area. These statistics may be employed in attenuation prediction calculations for a region of interest, with reasonable validity. These regions however, are not accurate in some climates where extreme conditions manifest. [Crane (1980), pp.1721] extended the regions to 8 to account for conditions in such regions.

[Manabe et al., p.474] state that empirical relationships between the rain rate and attenuation are not sufficient for describing rain attenuation at signals propagating at millimetric or sub-millimetric wavelengths. There is clear evidence throughout the literature that the number and size of raindrops in the propagation path of the signal play an increasing role in rain attenuation as signal frequency increases, with significant implications for broadband communications. Since empirical relations do not specifically account for this, they have limited value in attenuation prediction at optical frequencies, such as the one of interest to this research. It is thus necessary to investigate an alternative method of determining attenuation values in rain conditions for optical signals.

Revised Rain Rate Method

The second method involves the substitution of a drop size distribution into a mathematical expression for the rain rate. The rain rate is a vector quantity that is dependent on the speed and velocity of the falling raindrops [Ruthroff, p.123]. In mathematical terms, the rain rate is most simply expressed by the product of the rain density and the raindrop velocity. This expression takes the form

$$R = \rho v \tag{2.10}$$

where R is the rain rate (mm/hr), ρ is the rain density (g/mm^3) and v is the drop velocity (m/s). The rain density is the fraction of the volume occupied by the rain. This is expressed mathematically by

$$\rho = \frac{\pi}{6} N(D) D^3 \tag{2.11}$$

where N(D) is the number of drops of diameter D in the volume and D is the diameter of the raindrops (m). This expression of rain density (2.11) assumes that the drops are spherical in shape and have a volume described by

$$V = \frac{4}{3}\pi r^3 = \frac{\pi}{6} D^3 \tag{2.12}$$

where r is the radius (m). This assumption is often employed in theoretical derivations for simplicity. Substituting (2.11) into the first expression for rain rate (2.10) and writing as an integral over the entire drop diameter range yields

$$R = \frac{\pi}{6} \int_0^\infty D^3 N(D) v(D) dD \tag{2.13}$$

where N(D) is the number of drops of diameter D in the volume ($m^{-3}m^{-1}$) and v(D) is the velocity of the drop (m/s), which is dependent on drop diameter. Typically, raindrop diameters are measured in millimetres. They are also limited by a maximum drop diameter denoted D_{max}. Equation (2.13) is often written to account for this in a slightly different manner, given by

$$R = 6\times10^{-4}\pi\int_{0}^{D_{MAX}} v(D)D^3N(D)dD \qquad (2.14)$$

where N(D) is the drop size distribution ($m^{-3}mm^{-1}$) since drop sizes are typically measured in millimetres. This final equation (2.14) is termed the rain rate integral equation throughout this project. When the form of the drop size distribution is known, as well as the range of drop sizes and their terminal velocities, the rain rate may be calculated using this expression.

It is evident that for the estimation of attenuation at frequencies greater than 10GHz, the drop size distribution plays a vital role. [Olsen et al., pp.318-321] derive a formula for the specific attenuation due to rain based on the drop size distribution and the combined Mie scattering amplitudes of all of the drops in the scattering volume. This expression is given by

$$\gamma = 4.343\times10^{-3}\int Q(D,\lambda,m)N(D)dD \qquad (2.15)$$

where γ is the specific attenuation (dB/km), Q is the scattering coefficient (mm^2) that is dependent on the wavelength of the propagating signal, the drop diameter and the complex refractive index of the drops and N(D) is the drop distribution ($m^{-3}mm^{-1}$). The value of Q is determined using Mie scattering theory for a wave incident on a spherical absorbing particle. For optical frequencies, the magnitude of the rain drop diameter is much greater than the wavelength of the propagating signal. Thus $D>>\lambda$ and the following simplified relation applies [Maitra and Gibbons, p.658]

$$Q \approx \frac{\pi D^2}{2} \qquad (2.16)$$

It is clear that a number of parameters are required for the revised rain rate method. Firstly, in order to quantify the rain rate three parameters must be obtained: drop diameter, terminal velocity and Drop Size Distribution (DSD). For the estimation of the specific

attenuation, the DSD and scattering coefficient Q must be found. These parameters are discussed in the next section.

Diameter and Shape

Raindrops are formed by water vapour adhering to atmospheric nuclei [Rogers, p.55]. Since atmospheric nuclei vary in magnitude, raindrops of varying sizes may be produced. Aerodynamic forces and drop instability imposes a limit on the maximum drop diameter of 5-6mm [Rogers, p.92].

Traditionally, raindrops have been regarded as spherical in shape and this assumption has been employed in many of the theoretical propagation models that have been derived for rain attenuation for simplicity. The spherical assumption arises out of the fact that surface tension tends to reduce the surface area of the liquid mass to the smallest area possible, in this case a sphere. However, this assumes that the mass is not subject to any external forces. In practice however, raindrops are subject to external forces as they fall. [McDonald, p.23 and p.25] states that

> "The disturbing effects on drop shapes that appear as one considers larger and larger drops seem to be due almost entirely to aerodynamic and gravitational forces."

also

> "The gradients of internal pressure drive water from near the base and top out into the regions around the waist, thereby tending to flatten the drop and increase its horizontal diameter."

While [McDonald, p.23] states that raindrops are rarely perfectly spherical in shape beyond a diameter of 1mm, [Nousiainen and Muinonen, p.644] point out that wind tunnel experiments have indicated that only drops less than 0.3mm in diameter are practically spherical. Between 0.3mm and 1mm, raindrops are deformed and are more accurately described by oblate spheroids. Beyond this range, raindrops deviates significantly from a spherical drop shape [Nousiainen and Muinonen, p.644]. [Crane (1974), p.321] notes that vertical polarisation measurements were smaller than those predicted using a spherical drop shape, while the measurements of horizontal polarisation were larger. These findings were in agreement with the spheroidal drop shape assumption of [Oguchi, pp.31-38]. Many other researchers have noted that the oblate spheroidal drop shape more accurately

describes naturally occurring raindrops [Morrison and Chu, p. 1907][Morrison et al. P.599]. [Zarody and Harden, p.422] recorded simultaneous measurements on 36GHz and 110GHz links and found that there was better agreement between theory and experiment for the 36GHz frequencies where an oblate spheroidal drop shape was assumed. According to [Pratt and Bostian, p.341] large drops are not spherical but are of an oblate spheroid shape. They fall with their major axis almost horizontal and cause rain depolarisation which is the change in energy in transmitted signal from one polarisation to another [Pratt and Bostian, p.319].

Terminal Velocity

A raindrop reaches terminal velocity when the gravitational and resistive drag forces acting on the drop balance with one another. In a viscous fluid such as air, the drag force exerted on a sphere of radius r is expressed by

$$F_R = \frac{\pi}{2} r^2 v^2 \rho C_D \tag{2.17}$$

where F_R is the drag force (N), v is the velocity of the sphere relative to the fluid (m/s), ρ is the density of the fluid (g/cm^3) and C_D is the drag coefficient that characterises the flow [Rogers, p. 90]. The Reynolds number defines the type of fluid flow and is expressed by

$$R_e = \frac{2\rho v r}{\mu} \tag{2.18}$$

where μ is the dynamic viscosity. In terms of the Reynolds number, the drag force is rewritten as

$$F_R = \frac{\mu r v \pi}{4} C_D R_e \tag{2.19}$$

The gravitational force acting on the drop is given by

$$F_G = \frac{4}{3} \pi r^3 g \rho_L \tag{2.20}$$

where ρ_L is the density of the raindrop, using the approximation that, in this situation, the density of the water drops far exceeds the density of the surrounding air (i.e. $\rho_L >> \rho$). Equating (2.19) and (2.20) and solving for v yields

$$v = \frac{r^2 g \rho_L}{\mu (C_D R_e / 3)} \tag{2.21}$$

For the Stokes solution to the flow field around a sphere $(C_D R_e)/24 = 1$. According to [Rogers, p. 91], this solution applies to droplets up to 40 microns in radius and (2.21) may be simplified to

$$v = \frac{2}{9}\frac{r^2 g \rho_L}{\mu} \tag{2.22}$$

In terms of a function of the radius term, this may be rewritten as

$$v = k_1 r^2 \tag{2.23}$$

with $k_1 \approx 1.19 \times 10^6 \, cm^{-1} sec^{-1}$. This quadratic dependence of the fall speed on size is called Stokes' law. For particles of high Reynolds numbers such as raindrops, C_D becomes independent of R_e and takes on a value of 0.45 thus for drops greater than 40 microns in size (2.22) becomes

$$u = k_2 r^{\frac{1}{2}} \tag{2.24}$$

with $k_2 \approx 2.2 \times 10^3 (\rho_0 / \rho)^{\frac{1}{2}}$ $(cm^{1/2} sec^{-1})$. Here ρ is the air density and ρ_0 is the reference density of $1.20 \times 10^{-3} g/cm^3$, corresponding to dry air at 1013mb and 20°C.

Gunn and Kinzer used an electrical method to measure the terminal velocity of drops in the range 0.01mm to 5.8mm [Gunn and Kinzer, pp.243-248]. The results obtained are graphically presented in graph 2.1. A third order polynomial was fit to the results in order to obtain a simple expression to predict terminal velocities for drops of any size. [Gunn and Kinzer] found that the smallest drops (< 40ug) agreed with Stokes' law but that the theoretically predicted results for larger drops did not correlate well with experiment. The largest drops measured by Gunn and Kinzer had a corresponding terminal velocity of 9.17m/s [Gunn and Kinzer, p.246][Rogers, p.92].

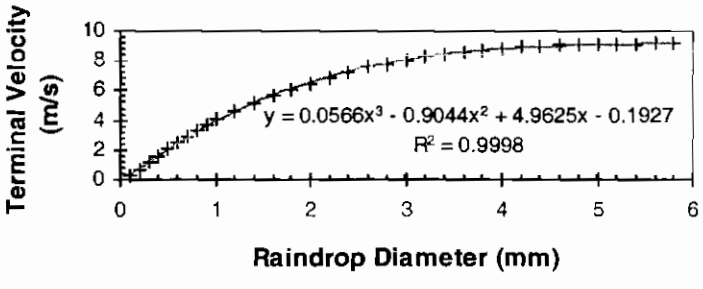

Graph 2.1 *Raindrop Diameter versus Terminal Velocity (after Gunn and Kinzer)*

Drop Size Distribution

As described, the attenuation due to rain at frequencies greater than 10GHz is depend on the size and concentration of raindrops interrupting the signal. These quantities are characterised by the Drop Size Distribution (DSD). The DSD is dependent on rainrate, with a smaller number of large raindrops than small drops occurring for a particular rainfall rate. As rainfall rate increases, so too does the number of raindrops of all sizes. The distribution of the number and size of these drops (DSD) is usually expressed mathematically.

The dynamic nature and varying structure of rain result in a spatial and temporal variation in the size and concentration of drops. Consequently, the DSD is a difficult parameter to quantify [Maitra and Gibbons, p.657]. The accuracy of rain attenuation estimates depends on the validity of the DSD in characterising the rainfall. Depending on location and weather conditions, some DSDs have been found to be more accurate than others. In general, the DSD is represented by a mathematical distribution function, derived either theoretically or from a mathematical fit to experimental data. The form of the distribution function required to adequately represent the distribution has been the subject of debate among communications researchers over the last century.

[Marshall and Palmer, p.166-167] and [Crane (1974), p.323] measured drop size distributions experimentally. Marshall and Palmer found that a negative exponential fit to experimental data achieved good correlation. [Maitra and Gibbons, p.658] note that a modified Gamma distribution fit well to experimental results obtained at infrared frequencies. The negative exponential form obtained by Marshall and Palmer is used by [Manabe et al., p.474]. The Marshall-Palmer (M-P) distribution is noted as possibly the simplest and most widely known form of the DSD is the negative exponential form proposed by Marshall and Palmer in 1948 [McCartney, p.173][Rogers, pp.136-137]. Other popular forms of the DSD include the Laws and Parsons distribution, Log Normal distribution and modified forms of the Gamma distribution [Sekine et al., p.258][Manabe et al., p.658][de Wolf and Zweisler, pp.278-279][Sander, p.214].

According to [Olsen et al., p.321], the Laws and Parsons (LP) distribution function is regarded a reasonable choice for the mean drop size distribution in continental rainfall for rates up to 35mm/hr. The validity of the Log Normal (LN) distribution function was tested

in preference to the LP function by [Sekine et al., p.358] and was found to produce a higher degree of attenuation than was measured experimentally. A new form of DSD was thus proposed by [Sekine et al., p.358] in order to achieve better correlation between theoretical estimates and experimental results. This was known as the Weibull (W) distribution that holds for drizzle and shower conditions. The W distribution was found to produce closer estimates of attenuation to the true experimental attenuation measurements for frequencies of 8.4GHz and 312.5GHz then either of the LP or of LN distributions.

Prediction models for rain attenuation based on the LN and Modified Gamma (MG) DSD forms fit to experimental data were developed for different frequencies by [Maitra and Gibbons, p.657-666]. The LN Distribution was found to provide a better fit to experimental results than the MG distribution. The reason for this was because the MG distribution overestimates the number of small drops and underestimates the number of large drops in comparison to the LN distribution and to the drop sizes that occur in nature.

Some of the most common forms of the drop size distribution discussed in the literature are presented in table 2.4.

Name	Form	Reference
Marshall-Palmer (MP)	$N(D) = N_0 \exp(-\Lambda D)$	Marshall-Palmer
	Rain	
	$N_0 = 8000, \Lambda = 4.1R^{-0.21}$	Marshall-Palmer
	$N_0 = 46000R^{-0.432}, \Lambda = 6.3R^{-0.312}$	Manabe et al.
	Drizzle (Joss et al.)	
	$N_0 = 30000, \Lambda = 5.7R^{-0.21}$	Olsen et al.
	Thunderstorm (Joss et al.)	
	$N_0 = 1400, \Lambda = 3.0R^{-0.21}$	Olsen et al.
Laws and Parsons (LP)	$N(D) = 2.53\times10^{-7} R^{0.915} e^{-\left(0.667\left(\frac{D}{D_m}\right)^3 \Big/ DD_m^3\right)}$	De Wolf et al.
	$D_m = 0.001 + 0.00039 \ln(R)$	De Wolf et al.
	$D_m = 1.238R^{1.82}$	Sekine et al.
Log Normal (LN)	$N(D) = \frac{N_T}{D\sqrt{2\pi}\ln\sigma} e^{-\left(\ln\left(\frac{D}{D_m}\right)\Big/ 2\ln\sigma\right)^2}$	Maitra and Gibbons Sekine et al.
	Rain $(5 \le R \le 50mm/hr)$	
	$N_T = 40R^{0.64}, \sigma = e^{0.29-0.001R}$	Sekine et al. Sekine et al.

	Thunderstorm ($5 \leq R \leq 50mm/hr$) $N_T = 46R^{0.55}$, $\sigma = e^{0.5-0.0035R}$ $D_m = 0.222 + 0.397 \ln R$	
Modified Gamma (MG)	$N(D) = N_0 D^n \exp(-\Lambda D)$ $n = 2$	Maitra and Gibbons
Weibull (W)	$N(D) = N_0 \frac{c}{b}\left(\frac{D}{b}\right)^{c-1} e^{-\left(\frac{D}{b}\right)^c}$ $N_0 = 1000m^{-3}$, $c = 0.95R^{0.14}$, $b = 0.26R^{0.44}$	Sekine et al.

Table 2.4; *Table of Drop Size Distributions and related parameters*

where D is the drop diameter (mm), D_m is the median drop diameter (mm), N(D) is the drop size distribution ($m^{-3}mm^{-1}$), R is the rain rate (mm/hr), N_t is the total number of drops of all sizes, μ is the mean value of ln(D), Λ is a rain rate dependent variable (mm^{-1}), N_0 is a constant intercept (m^{-3}) and σ^2 is the variance.

The importance of this parameter to attenuation estimation has been noted by a number of authors in the literature [Sekine et al., p.258][Maitra and Gibbons, p.657]. The significance of the DSD to rain attenuation becomes prevalent at higher operating frequencies.

In this section, the main processes of atmospheric transmission were outlined as well as the results of theoretical and experimental work found by a number of researchers. This concludes the literature review undertaken for this research. In the next section, a discussion of the findings of the literature review is presented.

2.7 DISCUSSION

In the light of the literature review, it is necessary to point out a number of factors and gaps that have been noted. A discussion of the findings and observations made from the literature review are presented in this section in order to provide justification for the topics covered by the research.

To begin, it is clear that the area of communications is rapidly evolving. New technologies are continually being developed and new applications are appearing. Some of these applications such as media streaming and video conferencing require low delay, high bandwidth and integrated traffic support, requirements that traditional networks may not be

able to offer. Broadband technologies such as Asynchronous Transfer Mode (ATM) and Gigabit Ethernet are addressing such needs. Although both technologies are very different, they are often compared with one another and there has been such debate about which technology will win the broadband race. The general opinion seems to be towards ATM in the backbone and Gigabit Ethernet on short distance links. However, ATM is reputed to deliver better quality of service when it comes to multimedia applications. Moreover, ATM uses cell switching and does not use a shared medium like versions of Ethernet. This means that all traffic has equal contention for available network bandwidth. Further ATM's ability to prioritise traffic implies that under congested conditions, unimportant transmissions will be discarded to free up network bandwidth and alleviate congestion. For these reasons and since it is relatively new and uses a different switching mechanism (cell switching) to traditional packet switched technologies deployed in data communications networks, it was decided that ATM would be used as the technology of interest. The fact that Gigabit Ethernet is simply a higher speed version of Ethernet, a well-known and widely deployed technology, makes its study somewhat less interesting in comparison with ATM. ATM allows different nodes e.g. Ethernet, Token Ring and ATM nodes to seamlessly communicate. ATM is hugely successful as an integrated networking technology and its study here is therefore justified. Further, this particular technology has not before been used in the particular network configuration under investigation in this research. There is another reason for its implementation here, since an ATM switch is available for testing on campus, it would seem beneficial to implement and test the technology as part of this research.

Initially in the literature review, a general study of the area of telecommunications was undertaken. This provided an introduction to the research area and allowed the author to grasp an understanding of the principal concepts and operations of the communication system. Communication systems in the form of computer networks are becoming increasingly important to everyday life. Many businesses e.g. banks and multinational corporations, rely on computer networks to conduct financial transactions and business deals with other businesses and branches around the globe. Academic institutions rely on computer networks for information dissemination and research. Individual home users rely on global computer networks for email and numerous other services. Lying at the core of

the computer network is the physical media that allows communication to take place. It is the bandwidth offered by the transmission medium that determines the number of users and types of applications that may be supported. The transmission medium determines the overall performance of the network. New applications are placing increased pressure on traditional networks and many traditional networks do not provide the delay tolerances required for applications such as voice and video. From an economic point of view, traffic integration is attractive since the maintenance costs of a single network may be much lower than the combined maintenance cost of a number of separate networks.

Different implementations have different requirements. In some cases, security may be more important than speed e.g. for financial transactions in a bank. In a military defence network, both reliability and security are an issue. Redundant infrastructure may be required to ensure that the network is operational under all conditions. If a link fails, the network traffic could be automatically rerouted through alternative links. Networks may have a number of requirements and these requirements may be prioritized. For example, an academic institution may require high speed and high capacity over high reliability, yet reliability may still be required. In this case, the network may be configured to accept instances of medium reliability rather than impose any delay on traffic. It is therefore necessary to assess the needs of a particular network so that transmission media and topology may be chosen to address the specific needs of a particular implementation.

In this research, the network configuration of interest is a dispersed college campus. While high integrity is required for some applications e.g. file transfers, for other applications, e.g. voice and video, high speed and low delay is more important. The preferred configuration is an integrated networking technology, where all traffic types, voice, video and data are combined, and where a distinction may be made between each type so that some transmissions may be prioritized over others. According to the literature, the networking technology ATM addresses these needs successfully.

The financial cost of implementing a complete optical fibre network may be excessive and unfeasible for a college campus, considering that there are digging, laying costs as well as cabling costs. Nevertheless, the capacity provided by fibre would allow the support of multimedia applications. Intercampus communication may be facilitated by either wired or wireless links. Wired links may use either copper or fibre and may be

leased or fully owned. The main problem with leased lines is the bandwidth capacity. Usually a bandwidth of only a few Mbps is offered (typically 2Mbps in Ireland). In the long run, such links may be very costly. Annual lease charges may increase while the bandwidth offered remains static. If bandwidth usage in the network increases, these links may be overwhelmed and congestion in these links may become a problem. Optical fibre, however, provides enormous bandwidth capacity and would surely support growing traffic needs. The main disadvantage of fibre is its cost. Although the cost of fibre has decreased over the last number of years, it is still regarded as a relatively expensive transmission medium. The cost of digging roads, laying the fibre combined with the cost of the actual cable itself and the required optical interfaces, is often exorbitant. Furthermore, since wired links are fixed, connectivity routes are usually constrained by local planning authorities. Links frequently need to be routed around obstacles such as buildings and houses and as a result, the required length of the cabling often far exceeds the expected length. Delays may arise in obtaining planning permission for underground cabling as well as during the actual laying and configuration processes. This often imposes unnecessary and unanticipated delay in network implementations.

Each of these factors makes wireless technologies quite attractive as quick solutions to intercampus links. The choice is then between microwave and optical systems. While microwave systems are widely deployed, they require an operating license from the telecommunications regulations office. Delays in the registration process may hinder network deployment. Further, the bandwidth capacity offered by microwave links (<34Mbps) may be lower than is required to support broadband applications and to cater for future network growth. A certain amount of redundant capacity is preferred, to be able to cope with future network expansion, without the need for new installations.

Laser systems, on the other hand, do not require licensing. They also provide support or high bandwidth applications and offer high security. These links may be leased or bought and provided the high capacity offered is sufficiently exploited, may prove a more economically sound solution over leased lines in the long-term. Such links are also relatively easily installed and maintained. Each of these reasons provides justification for the investigation of these links in this research. Another interesting point to note about laser systems is that, in comparison to microwave systems, relatively little written

information is available on the implementation of laser links in computer networks, which is another valid reason for its study here.

In a maritime climate such as Ireland, the performance and reliability of such a link under different intensities of rain is important so that the network designers may have an idea of the limits of the laser link and under what conditions the link will operate. It is thus necessary to assess the impact of rain in the channel on the link connectivity. This is a non-trivial task since the atmosphere is a dynamically varying system. Typically, prediction models are employed to simplify the task of performance estimation. Many of these are based on experimental observations and theoretical derivations for microwave frequencies. Many of the theoretical assumptions used in microwave propagation modelling are also applicable to infrared systems. However, little evidence was found of experimental work conducted at these frequencies and in particular in evaluating the impact of rain on the optical signal. It was thus decided to conduct some experimental work at the infrared wavelength of 800nm, equivalent to a frequency of 3.75×10^{14} Hz, so that results could be compared with those predicted from a theoretical model at this frequency. It is proposed that this be achieved by testing an intercampus network configured with a pair of lasers operating at 800nm. The intercampus separation distance is approximately 160m through an urban area. The link is to be continually monitored and disruptions to the link connectivity logged to allow the availability of the link on different days to be determined.

To conclude, in an age of rapidly evolving technologies and transmission media, it is crucial to understand the impact and performance of these technologies in order to achieve benefit from them. In this research, the technology that comes under investigation is ATM and the transmission medium of interest is an infrared laser link.

3 THEORETICAL MODEL DEVELOPMENT

3.1 Development Overview

In this chapter, the development of the MATLAB models is described in detail. This includes an initial description of the approach taken to develop the models and the environment in which the model was created. This is followed by an explanation of the processes of file manipulation of a TCP/IP application by the ATM protocol stack. Finally, the development of the wireless channel model aimed at predicting the attenuation of an optical wireless link subject to interference by different intensities of rainfall is presented.

3.1.1 Approach

In this section, a brief introduction to the MATLAB modelling environment and the approaches taken in the model development are outlined. A brief description of the aims and purposes of the model is firstly given.

The manipulation of an application file by the different layers of a protocol stack for transfer across a computer network comprises a number of processes. In order to obtain an understanding of some of the main physical processes, it was deemed appropriate to develop a simulation model. The protocol stack of interest was a hybrid TCP/IP-ATM stack. The TCP/IP protocol was chosen to provide the transport and network layer protocols of the model. This was primarily because of the prevalence of the TCP/IP protocol in modern computer networks.

The ATM model was chosen as the protocol stack for the datalink and physical layers due to the fact that ATM networks are becoming more widespread in local, metropolitan and wide area network implementations. As stated previously, demand for backbone and local support for a wide range of multimedia applications has required many networks to be upgraded to high-speed technologies. Many of these applications require a guaranteed Quality of Service (QOS) to deliver timely, high-quality service. ATM is a technology that meets these requirements effectively. ATM is an interesting alternative technology to traditionally packet switched technologies due to its cell switched nature. The manner in which ATM networks manipulate traffic before transmission is different to the way in which traditional networks. ATM segments all traffic, regardless of the traffic type into cells of fixed size before transmission may take place. In contrast, packet-switched networks such as Ethernet networks allow variable packet size transmissions. In this case, there is no way to prevent small packets of time-

critical traffic (e.g. voice) being caught behind large non-time critical applications (e.g. file transfers). ATM on the other hand, overcomes this problem by segmenting all traffic into 53-byte cells for transmission. Each cell thereby has equal contention for the network bandwidth and multimedia applications are supported.

Rather than develop the model in a traditional modelling environment such as C, QBasic or Pascal, a high-level programming environment (MATLAB) was selected as the platform for the simulation. This was principally to investigate the feasibility of developing a generic simulation model within the constraints of such an environment. Also, the associated learning period of a high-level programming environment such as MATLAB is significantly less than that of traditional programming environments. This fact as well as the availability of MATLAB over alternative high-level mathematical programming environments such as Mathematica or Mathcad provided sufficient incentive for the decision to use MATLAB as the environment in which to implement the model.

The approach undertaken involves the development of two theoretical models. Firstly a model to depict a basic Asynchronous Transfer Mode system was created and tested. This model simulates the process of manipulation of an application file using the TCP/IP protocol running over an ATM system. Next, a model to predict the effects of rainfall on a wireless link was developed. The development of the individual models is described in the following sections.

3.1.2 MATLAB Environment

Program Overview

MATLAB is an environment for the mathematical representation and manipulation of data. An extensive range of in-built functions contained in the various libraries in MATLAB Version 5.3 allow numerous operations to be performed within the program environment. Visual representations of data are also easily achieved in this environment. These features provided further incentive to use MATLAB as the platform for the simulation.

Program Operation

When MATLAB is run, a window is displayed on the screen. This is the Command Window shown in figure 3.1. Input values to the command window may be scalars (single numbers) or matrices (an array of numbers). MATLAB allows matrix operations to be performed on all values within the array. All variables created in the

command window are stored in the MATLAB workspace that is the program's internal buffer. It is important to note that MATLAB retains the most recent answer assigned to a variable in the workspace.

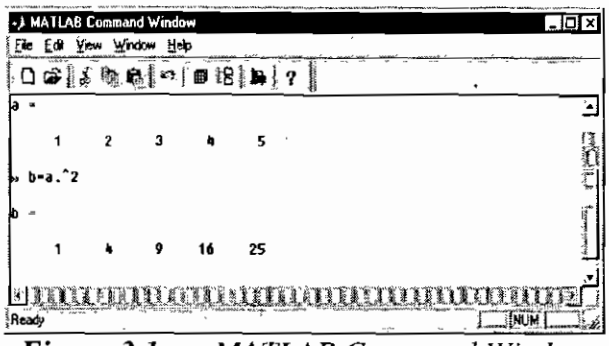

Figure 3.1; MATLAB Command Window

Typing commands at the prompt in the Command Window becomes inefficient when a large number of commands are to be executed [MATLAB Student Guide, pp.30]. Instead, the commands may be typed into an editor and a script file created to store the commands. These script files are called "M-files" and they may be run in the command window with the desired result output to the screen. An example of such a script file is shown in Figure 3.2. Commands within these script files are executed sequentially. The models developed in this project were written as script files since they contain a large number of operations.

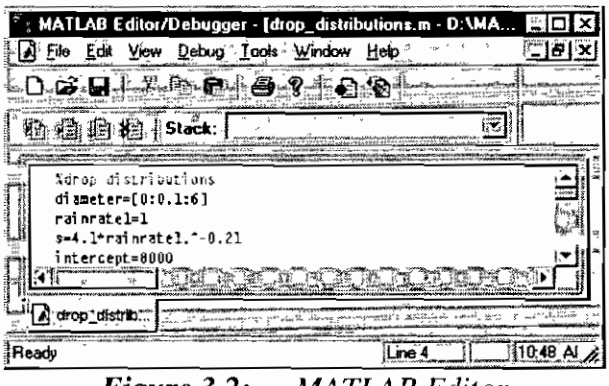

Figure 3.2; MATLAB Editor

It is appropriate here to present only a brief overview of the MATLAB programming environment in which the theoretical models were developed. Comprehensive online help is available at http://www.mathworks.com.

3.2 Basic ATM model

In this section, the first theoretical model is described. This is the hybrid TCP/IP-ATM model and is referred to as the Basic ATM model. The main stages of the model involve inputting a file for processing, determination of the number of TCP segments,

IP datagrams and ATM cells required for the transfer of the file across a network and stripping the file (where appropriate) into files of smaller size for transmission.

The basic ATM model comprises two main modules, ATM source module and ATM destination module. In practice, application data using TCP/IP over ATM is passed through the following 6 layers of the protocol stack at the ATM source module

- Application Layer
- Transmission Control Protocol Layer
- Internet Protocol Layer
- ATM Adaptation Layer
- ATM Layer
- Physical Layer

Within each layer, the data is manipulated according to the relevant protocols. At the physical layer, the data is output as a bit stream and transferred to the destination. When the bit stream is received at the destination module, it is assembled into ATM cells, IP datagrams and TCP segments. Eventually it is restored to its original form by stripping off any additional data appended by the protocols in the source module layers. It is this process of addition and stripping of data that the model seeks to simulate.

It was necessary to make a number of assumptions in the basic ATM model so that a simple model could be developed in a reasonable time period. The model objective was to simulate the stages of a data transfer across a network. Consequently, many operations that are undertaken in real ATM network are not included in the simulation model. The main operations omitted are the calculations used to obtain header information such as addressing, control information and error checking. The inclusion of these network specific operations was not deemed necessary for the adequate simulation of the ATM system processes. Furthermore, their integration into the model would have introduced an unnecessary level of complexity to the model. However, since these operations result in the addition of extra data at different stages in the data transfer across the network, they were included representatively. Consequently, byte sequences of correct length are used to simulate their existence at the different layers in the model.

In practice, error-detecting and error-correcting algorithms such as Cyclic Redundancy Checks (CRCs) and Header Error Checks (HECs) are implemented into some network protocols e.g. TCP and ATM, to ensure that data received at the

destination is valid. In the model, the availability of a matrix comparison command alleviated the need for incorporating complex error checking and detecting algorithms into the data manipulation. Error checking between layers was thus carried out using matrix comparison commands available within MATLAB. The final assumption was that the transmission medium used between the source and destination nodes is reliable and does not corrupt the transmitted bit stream. As a result, any data sent from the source physical layer is received at the destination physical layer intact.

In the MATLAB model, the data at each layer is represented in matrix form, as this is the form required for manipulation in the MATLAB environment. The layers of data processing in the basic ATM model are illustrated in figure 3.3.

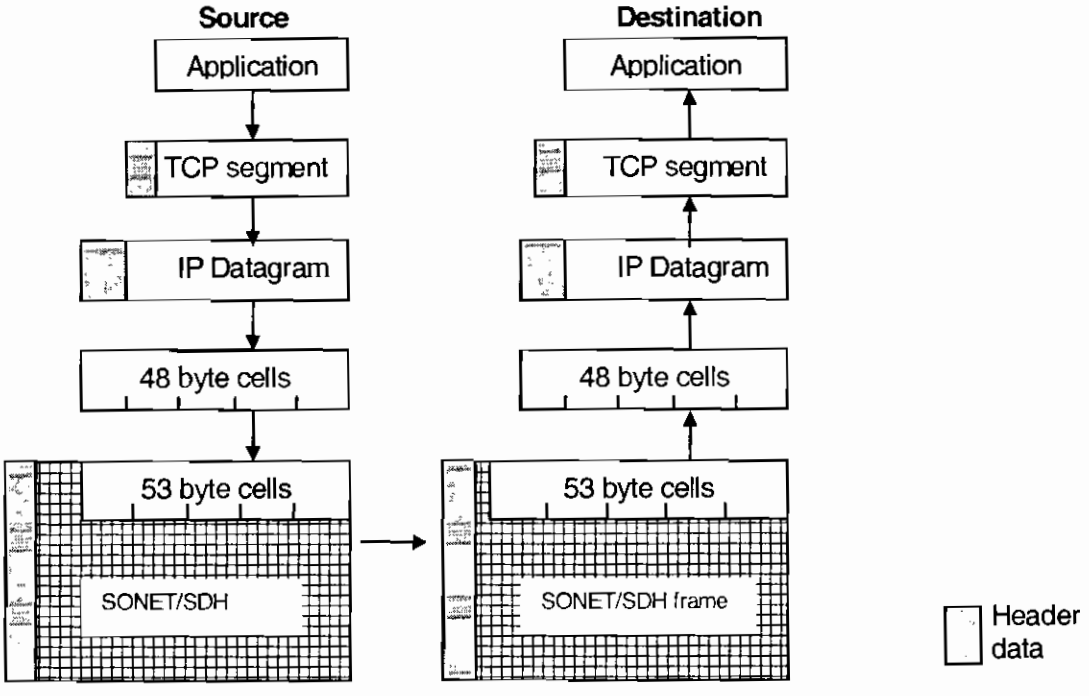

Figure 3.3; *Data processing in the basic ATM model*

It is appropriate to present the matrix notation and naming structures used to represent the parameters in the layers of the model. These are presented in table 3.1.

Network Layer	Naming Structure	Matrix Representation		Header Representation	
		Source	Destination		
Application	Message	[a]	[m]	None	[mh]
TCP	Segment	[b]	[l]	[bh]	[lh]
IP	Datagram	[c]	[k]	[ch]	[kh]
AAL5	Cell	[d]	[h]	[dh]	[hh]
ATM	Cell	[e]	[g]	[eh]	[gh]
SDH	Frame	[f]	[f]	[fh]	[fh]

Table 3.1; *Matrix Notation and Naming Structures for basic ATM model*

It has been previously stated that commands in the script files are executed sequentially. This facilitates the development of the simulation model in the order of the layers at which they occur. Thus, an overall level of consistency is maintained with the model. In the following description of the model development, the layer processes are described in their mathematical form (referred to as comment) and where appropriate, equivalent MATLAB code (referred to as code) is presented in Italics.

3.2.1 Source Module: Application Layer

In this section, the operations that are performed at the top layer of the ATM source module, the Application Layer, are presented. These include reading in a chosen file for processing and converting it into its appropriate representation in MATLAB.

In order to develop a reasonably flexible model, it was necessary to input a real file format for processing by the model. This is achieved using the file identification (*fid*) command. The next stage is to convert the application file to matrix format for processing. Within MATLAB, different commands are available to convert different file formats, for example the *imread* command is used for image files (*.bmp, *.jpg) while the *textread* command is used for text files. For this basic model the *imread* command was used. This is achieved using the following commands

```
fid=fopen('c:\example.jpg','r')
a=imread(fid)
```

where the application file ('example.jpg') is read and converted to a matrix form denoted [a] which has the following form

$$[a] = [a_1, a_2, a_3 \ldots] \tag{3.1}$$

Each element of [a] represents a pixel of the original image as its Red Green Blue (RGB) equivalent decimal number between 0-255 i.e. one byte in length. The matrix [a] is three-dimensional since different quantities of the three primary colours, red, green and blue compose each pixel of the image. The length of the entire image can only be determined in MATLAB if the matrix is converted into a single column matrix, where the entire image is represented as a one-dimensional matrix whose length is equal to the number of bytes contained in the entire image. This is achieved using the colon key syntax in MATLAB. The application matrix is then in its appropriate form for processing by the basic model and it is passed to the transmission control protocol layer for initial processing by the layers of the protocol stack.

3.2.2 Source Module: Transmission Control Protocol Layer

In this section, the processes and operations that are performed on the application layer file are described. This includes the determination of the number of TCP segments that may be created from the application file and the segmentation of the file to create units of allowable size for transmission across the network.

At the Transmission Control Protocol (TCP) layer in the MATLAB model, the application data is to be encapsulated in the payload field of a TCP segment. The TCP segment contains a variable payload size to enable applications of varying size to be encapsulated within it. Depending on the type of protocols implemented in the network and data link layers of the network protocol stack, a limit may be imposed on the maximum size of the payload in the transport and network layers. In the network layer, this amount is known as the Maximum Transmission Unit (MTU). Different types of networks specify different MTU sizes e.g. for Ethernet, an MTU of 1500 bytes is defined, whereas an ATM link using AAL5 may use an MTU of 65,538 [Kercheval, pp. 22].

The MTU defines the largest amount of data that may be transferred across the network in a single transfer. In practice, the value of the MTU for a particular transmission is relayed between the source and destination nodes to ensure optimal bandwidth usage and minimum overhead [Kercheval, pp. 28]. If the transmission unit exceeds this MTU size, the unit must be split into smaller units or *fragments* of allowable size before transmission. Fragments are transmission units that are created in the IP layer. Each fragment is preceded by a 20-byte header field that contains control information e.g. source and destination addresses, as well as a 16-bit identification field to indicate the datagram to which the fragment belongs [Washburn and Evans, pp. 209].

In the network of interest to this research, the data link layer protocol used is ATM Adaptation Layer Type 5 (AAL5). This layer allows a maximum transmission for IP datagrams of 9180 bytes to be encapsulated in the payload of the AAL5 transmission unit [RFC 1577]. This must include any headers or trailers added on at higher layers in the protocol stack. In TCP/IP, the application file is appended with a 20-byte header at the TCP layer and a further 20-byte header at the IP layer. Hence, in this scenario, the Maximum Segment Size (MSS) of a TCP segment is 9180-40 = 9140 bytes. By choosing this MSS, it is ensured that immediate fragmentation does not occur at the IP layer. [Kercheval, pp. 25] points out that this would be the case if the allowed MSS was larger than the allowed MTU of the network.

Consequently, in the model, when the application file is received at the transmission control protocol layer its size is analysed to ascertain whether it can be sent as a single TCP segment or if segmentation is required. If the file size is less than the maximum segment size set in the TCP layer, then it may be directly encapsulated into a single TCP segment for transmission. A 20-byte header is then appended to the start of the segment and the data is passed down to the IP layer. If the file size is greater than the chosen MSS however, it is necessary to sequentially segment the file into smaller units. Each of these segments is then encapsulated into a single TCP segment. The segments are then appended with 20-byte TCP headers and transmitted down to the IP layer. These two scenarios are depicted in figure 3.4.

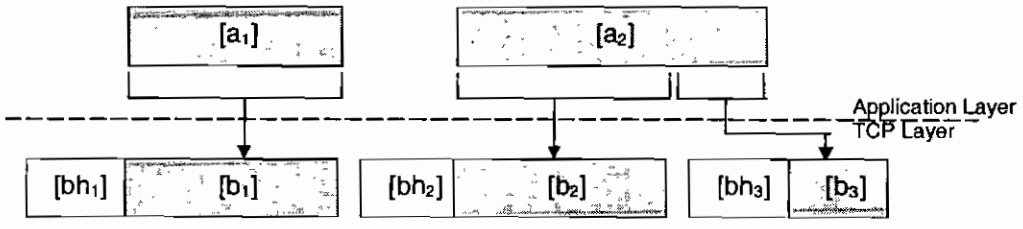

Figure 3.4; *Encapsulation of application data in TCP segment; (left) file size less than TCP MSS and (right) file size greater than TCP MSS*

In the model, this process is simulated upon examination of the length of the application file. If the length is less than or equal to the maximum segment size a new matrix for the TCP layer [b] is created by appending a TCP header [bh] onto the application matrix [a]. The code and comment for this operation are as follows

Code	***Comment***	
m = 9140 *if length(a) <= m* *[bh]=randperm(20)* *[b]=[bh , a]* *end*	[b] = [bh] + [a]	(3.2)

When the file size is greater than the maximum segment size, the application matrix must be split into smaller matrices to represent a number of segments containing application data. Hence the first stage is to calculate the number of TCP segments that are required to transfer the entire application file. This is achieved by dividing the length of the application matrix [a] by the maximum segment size denoted m. While it is possible that the division may be exact it is more likely that the division will result in a real number. Consequently the result is treated as the combination of an integer X and a remainder Y where X represents the number of complete TCP segments and the Y the number of bytes that will be in the final segment. The *fix* command in MATLAB

rounds a number down to the nearest integer value while the mod command computes the modulus (remainder) after division of an integer by another integer.

Code	***Comment***	
if length(a) > m	length[a] / m = $X_{Integer}$ + $Y_{Remainder}$	(3.3)
X = fix (length(a) / m)		
Y = mod(length(a), m)		
end		

The application matrix is then segmented based on the number of complete segments required and the amount of remainder data. This is expressed mathematically as follows

$$[a] = [a_1 \ldots a_m] + [a_{m+1} \ldots a_{2m}] \ldots + [a_{Xm+1} \ldots a_{Xm+Y}] \quad (3.4)$$

Each of these segments is then appended with a TCP header $[bh_j]$ to form individual TCP segments $[b_j]$ where j is the segment number, for example;

$$[b_1] = [bh_1] + [a_1 \ldots a_m] \qquad j = 1 \quad (3.5)$$

$$[b_2] = [bh_2] + [a_{m+1} \ldots a_{2m}] \qquad j = 2 \quad (3.6)$$

In the code this segmentation is achieved using the *for* loop command (j iterations) for the complete TCP segments. Within the *for* loop an interim matrix is created [b'_j] which is then appended with a header. The main sections of this code and comments are

Code	***Comment***	
for j = 1 : X	$1 \leq j \leq X$, inc. 1	
*b'(j) = [a(((j-1)*m)+1):a(jm)]*	$[b'_j] = [a_{(j-1)m+1} \ldots\ldots a_{jm}]$	(3.7)
b(j) = [bh , b'(j)]	$[b_j] = [bh_j] + [b'_j]$	(3.8)
end		

The final segment is created by appending a header to the segment matrix containing the remaining elements in the application matrix that do not fill a complete segment using the following code;

Code	***Comment***	
b_{end} *= [a(Xm+1):a(Xm+Y)]*	$[b_{end}] = [a_{Xm+1} \ldots a_{Xm+Y}]$	(3.9)
b_{final} *= [bh ,* b_{end} *]*		

The TCP header of each segment typically contains a number of fields such as source and destination addresses, sequence numbers and error check fields. The addresses are clearly connection specific. It was not deemed appropriate for the creation of a generic model, to include specific information relating to specific connection. Rather, in the model, representative random elements are used to represent the information contained in the 20 bytes of the header. These elements are appended to each of the segments created from the application file at the relevant layers. Once each segment has been appended with a header, it is then passed to the Internet Protocol layer for further processing.

3.2.3 Source Module: Internet Protocol Layer

At the Internet Protocol (IP) Layer, the TCP segment is encapsulated into the payload (user data field) of an IP datagram. The IP datagram is the required format for routing the data through a TCP/IP network. The IP datagram is represented by a matrix [c] containing an IP header [ch] and the TCP segment [b] received from the TCP layer. The encapsulation of a TCP segment in an IP datagram is illustrated in figure 3.5.

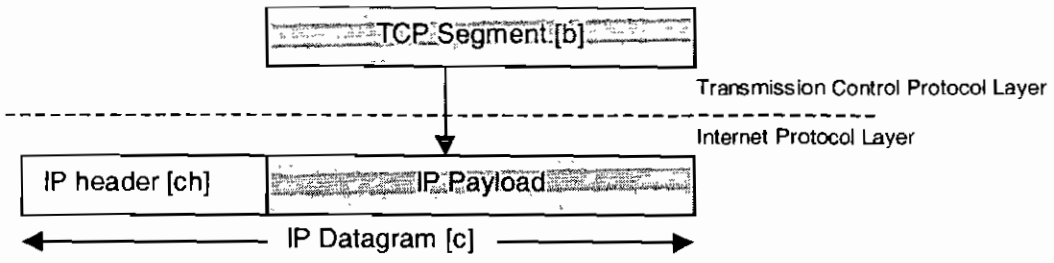

Figure 3.5; *Encapsulation of TCP segment into IP datagram*

As before, the approach taken to simulate the process of TCP encapsulation was to use generic sequences to represent the header information and append these onto the TCP segment, which represents the payload data for the IP datagram.

Code	***Comment***	
[c] = [ch,b]	[c] = [ch]+[b]	(3.10)

There was no need to implement fragmentation of TCP segments at the IP layer in the model. The segmentation process at the TCP layer sufficed to ensure that all segments are of an allowable size for the network. Hence in the IP layer of the model, only the process of adding a header to the start of the datagram is required before transmission of the datagram to the ATM Adaptation Layer. As soon as all of the datagrams have been created from the transmission, the data is transferred to the top layer of the ATM protocol stack, the ATM Adaptation Layer 5.

3.2.4 Source Module: ATM Adaptation Layer 5

In the model, the ATM Adaptation Layer chosen is type 5 due to the fact that AAL5 is the standardised type for the transfer of LAN-based protocols such as IP over ATM networks [Washburn and Evans, pp. 195]. Since the model simulates the process of a transfer of an image file over an ATM network, this is an appropriate type to use at this layer. Suppose the image is to be sent as a variable bit rate bursty transmission. The primary task of AAL5 is to segment the IP datagram received into units of 48 bytes in size. These cells represent the payload for the ATM cells that will be carried across the network. This process of segmentation in the AAL5 layer is simulated at the source module by sequentially segmenting the IP matrix into matrices 48 bytes in length. It is

thus first necessary to check if the IP datagram matrix [c] is divisible by 48. If it is, it is directly subdivided into 48 byte matrices denoted $[c_j]$. This may be expressed mathematically as

$$[c] \rightarrow [c_{1} \ldots c_{n}] + [c_{n+1} \ldots c_{n+48}] + \ldots\ldots \qquad (3.11)$$

where n = 48. If the matrix [c] is not divisible by 48 it is necessary to add padding to the payload of the last cell to ensure it reaches 48 bytes in size as shown in figure 3.6.

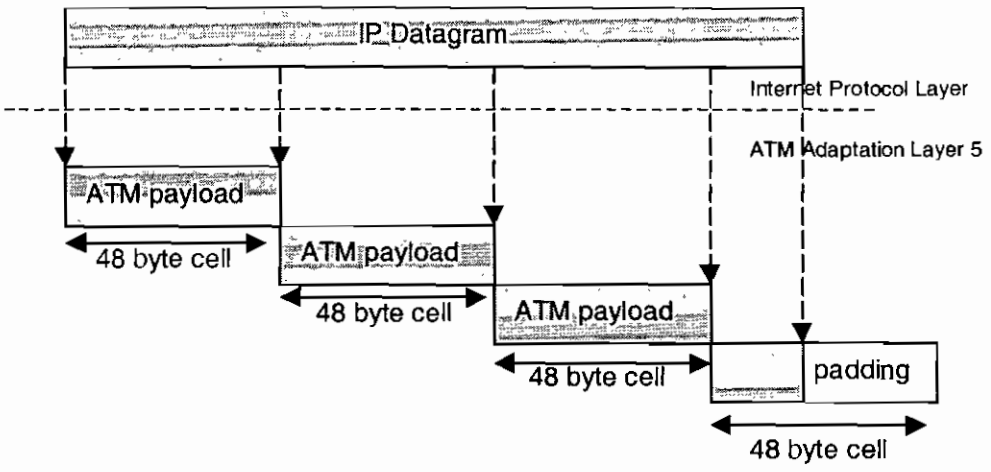

Figure 3.6; *Segmentation of IP datagram in the AAL5 Layer*

The procedure for computing the number of complete cells from the IP datagram matrix [c] is the same as that used for segmentation at the TCP layer except that in this case the datagram matrix is divided by 48. The resulting integer value indicates the number of complete cells that may be generated from the transmission. The remainder R represents the number of remaining bytes left after the division.

The remaining bytes are carried in either the second last or the last cell in the transmission depending on how many of them there are. The last 8-bytes of the final cell in an IP transmission over ATM are required to carry a trailer. This trailer contains the 16-bit length of the LAN frame and a 32-bit frame check sequence [Washburn and Evans, pp. 195]. Hence, if the remainder of the division is less than or equal to 40-bytes, the remaining bytes may be encapsulated along with the 8-byte trailer sequence in a single final cell. However if the remainder exceeds 40 bytes, the full trailer cannot be added on without the cell size increasing beyond 48 bytes. Thus a separate cell must be sent to carry the full trailer. This cell represents the final cell in such a transmission. The second last cell in this case is then used to carry the remaining bytes and is padded out, using the parameter P, to fill a 48-byte cell. The final cell is padded with 40 bytes followed by the trailer of eight bytes. This is achieved in code in the following manner

Code
R = mod (length[c],48)
P = 40 - R
If P>=0
[d] = [R , randperm(P),randperm(8)]
elseif P<0
[$d_{second\ last}$]=[R, randperm(48-R)]
[d_{last}]=[randperm(40), randperm(8)]
end

The padding and trailer bytes are generated using the *randperm* command to generate matrices of required length. As soon as all of the 48-byte cells have been created they are passed to the ATM layer for further processing.

3.2.5 Source Module: Asynchronous Transfer Mode Layer

In the ATM layer the cells are appended with a 4-byte header as illustrated in Figure 3.7. In practice, these contain the path and circuit identifiers required for routing the cells across the ATM network via intermediate ATM devices. For the reasons discussed previously, only byte sequences of the correct length are employed to represent these header bytes in the simulation.

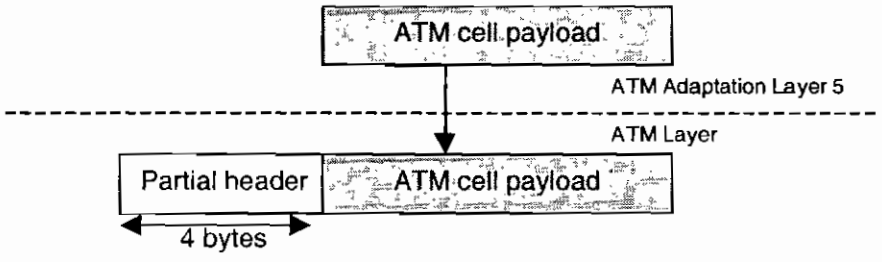

Figure 3.7; *Encapsulation of the ATM payload in the ATM cell*

The 4-bytes are contained in the matrix [eh] must then be appended to the cell matrix. In a similar manner as before, this may be expressed by

Code	***Comment***	
[e] = [eh , d]	[e] = [eh] + [d]	(3.12)

where [e] is the matrix representation of the 52 byte ATM cell. After each of the cells is affixed with a 4-byte header representation sequence, they would be passed to the physical layer of the model for final processing and transmission. It must be noted that for the purposes of efficient computation in the model, the ATM layer header bytes are actually appended along with a representative Header Error Check byte. Consequently, five representative bytes are appended to the data at one stage in the model. However, for the purposes of consistency, the processes that ordinarily are carried out at separate layers are described separately. The final layer in the ATM source module is the physical layer.

3.2.6 Source Module: Physical Layer

The Physical layer is divided into two sublayers. These are the Transmission Convergence (TC) and the Physical Medium Dependent (PMD) sublayers. The TC sublayer computes a Header Error Check (HEC) calculation on the 4-bytes appended to the ATM cell in the ATM layer as shown in figure 3.8. The result of the calculation is inserted into the ATM cell, increasing the ATM cell length to 53 bytes. This is the required cell size for transmission across the ATM network. The PMD sublayer is responsible for the physical and timing issues of outputting the ATM cells as bit sequences onto the transmission medium. In the basic ATM model, the channel medium is assumed to be reliable and does not corrupt the data in its transfer from source to destination.

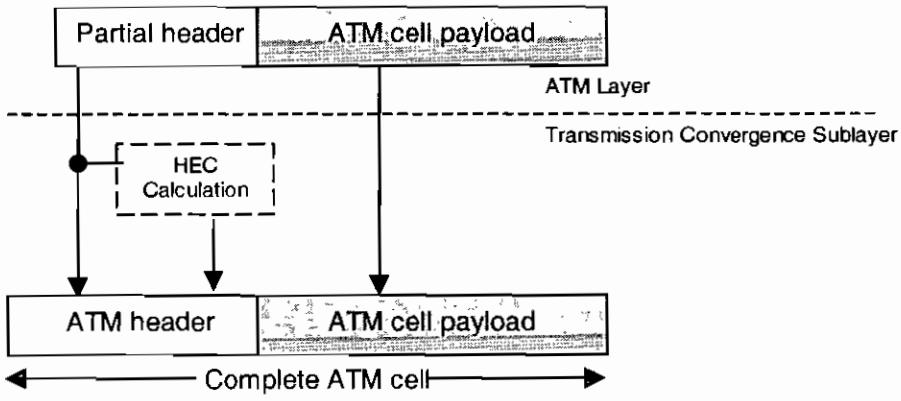

Figure 3.8; *HEC generation and encapsulation into ATM cell*

If it was not so computationally intensive in the model, this final byte, represented by a random integer denoted [fh] would have been added to the 52-byte cell matrix received from the ATM layer yielding

Code	***Comment***	
[f]=[fh,e]	[f] = [fh] + [e]	(3.13)

This matrix representation of the 53 byte cell (48 + 4 + 1) is now in appropriate format for transmission over the ATM network. As noted, in the model, the header bytes appended at the ATM layers and TC sublayer were added to the cells in one stage. Although it would have been easily achieved, the length of time for the simulation to run would have been increased.

Rather than send out individual cells over the network, standard framing systems such as Synchronous Optical NETwork (Sonet, ANSI standard) or Synchronous Digital Hierarchy (SDH, an equivalent and only slightly different ITU standard) are employed in the physical layer [Cavendish, pp.164]. These systems pack ATM cells into frames

for transmission over synchronous optical networks. The standard Sonet/SDH frame is 810 bytes in size of which 27 bytes are reserved for control information [Tanenbaum, pp.127][Kercheval, pp. 42]. This leaves 783 bytes to carry payload data in which a little over 14 ATM cells fit. The process of constructing these SDH frames from ATM cells is performed in the TC sublayer of the Physical Layer and is illustrated in Figure 3.9.

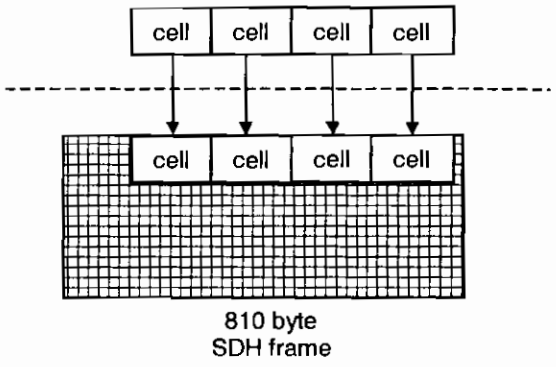

Figure 3.9; *Construction of Sonet/SDH frames from ATM cells*

In the model, this process is simulated in code by aggregating 14 cells together and encapsulating them into a new matrix representing the SDH frame. A random representation of the 27-byte header information is affixed to the start of each frame and the frame is padded to fit 810 bytes exactly.

It should be noted that, in practice, the ATM cell boundaries might not necessarily start in the fourth column of the first row. However, for the purposes of simplicity, this location is assumed to be the start of the cell sequence in the ATM simulation model. The final process at the source module is the conversion of the SDH frame into bit sequences for transmission over the physical media. This is achieved by means of the *dec2bin* command in MATLAB where the SDH matrices, which contain decimal numbers, are converted to binary sequences and transferred to the destination module.

The ATM source module description is complete. As previously noted, the hypothetical transmission medium deployed in the channel of the simulation model is assumed reliable and does not corrupt the bit stream in its transfer from source to destination. Consequently, the bit stream received at the destination physical layer is identical to that transmitted from the source physical layer. In the next section, the processes performed at the ATM destination module are described.

3.2.7 Destination Module: Physical Layer

In the destination module, reverse processes to those conducted in the source module take place. The data is stripped of its headers back into its original form. The

source module processes were described in detail. It is not necessary to describe the destination processes in such detail as they are not complex and may be easily identified from the coding of the model contained in Appendix B. However, for completeness, a brief description of the processes that occur at each layer in the destination module is given.

The physical layer at the destination module receives the binary sequence from the source. The command *bin2dec* recovers the SDH frame matrix from the binary sequence received from the source module. This frame matrix is then decomposed to 14 individual cell matrices each of length 53 bytes (48 data + 5 header). This is achieved using a *for* loop iteration sequence similar to that described in the TCP layer in the source module. In practice, at this layer, the HEC byte contained in the header is examined and the received data is only processed if this byte is valid. As explained before, in the model a different method of error checking is used, the matrix comparison command *isequal*. In the model also, recall that the HEV byte was appended as a representative byte in a single stage along with the other 4 bytes of the ATM header. Consequently, at the destination module, all 5 bytes are removed simultaneously. For consistency however, the processes are described individually.

3.2.8 Destination Module: ATM Layer

At the ATM layer, the ATM header bytes are stripped off as it is assumed that the cell has been correctly received according to the header check validation. This is implemented in MATLAB by creating a new matrix [f] containing the remaining elements of the cell matrix received after the first 4 bytes have been stripped off. The ATM layer then passes the newly constructed matrix to the AAL5 layer for further processing.

3.2.9 Destination Module: AAL5 Layer

At the AAL5 layer, the sequence of cells must be reassembled into the original IP datagram. This is simulated in the model by combining all of the received cell matrices into a single matrix representation of the IP datagram, where the first 20 bytes of the matrix represent the IP header.

3.2.10 Destination Module: IP Layer

At the destination IP layer, the 20-byte IP header is removed from the matrix and remaining data is passed to the destination TCP layer.

3.2.11 Destination Module: TCP Layer

At the TCP layer, the first 20 bytes of the matrix again represent the TCP header in which another check is contained. In the model, the contents of the received TCP segment may be checked with the transmitted TCP segment using the *isequal* command. The 20-byte header is removed and the remaining data is transmitted to the application layer of the destination module.

3.2.12 Destination Module: Application Layer

When the data is received at the application layer in the destination module, it is a matrix representation of the original data transmitted. The integrity of the received data is checked by using a matrix comparison on all of the elements of the original application matrix with those contained in the received application matrix. If each element matches correctly, the application file has been transmitted and received properly and the manipulations within the various layers of the network model had no effect on the integrity of the transmitted data.

In this section, the development of the basic ATM model was described. The objective of the model was to develop a simulation model of the processes of file manipulation in an ATM network protocol stack. A reliable channel medium was assumed and data was not corrupted in its transfer from the source to destination. The complete code for this simulation is shown in Appendix B.

The original objective of the theoretical modeling was to develop such a simulation using the reliable channel medium. It was then hoped to develop a separate model to incorporate the effects of unreliable channel medium e.g. wireless optical link subject to rain interference. In practical terms, since the basic model purely deals with the actual bits transmitted, any degradation in the channel would have to be implemented in the form of bit error corruption algorithms. In a data network, there are a number of ways of characterising degradation. Typically Bit Error Rate (BER) has been used. This defines the number of bits in error as a ratio of the total number of bits transmitted. Other ways of characterising degradation are by Severely Errored Seconds (SES) and Availability. SEC is defined as the percentage probability of one-second measurements that have a BER>10^{-3}. Availability on the other hand, is defined as a period of ten consecutive seconds or longer for which the BER exceeds 10^{-3} or for which transmission is not possible. The latter two may be regarded as more appropriate in dealing with wireless link degradation.

There is little documentation available relating to data corruption due to rain interference in an ATM network. As a result, it was necessary to conduct experimental work in this area as part of this research. These experimental tests are described in the next chapter. The tests resulted in a number of conclusions being drawn that affected the overall development of the unreliable model.

In the light of the experimental results obtained, the question was posed as to the relevance of incorporating bit error corruption algorithms into the channel section of the model. The main reason for this is that in the case of rain interfering with the wireless signal, a wireless link may be rendered inoperable for a length of time. During this time, all data is effectively obliterated and consequently the bit error rate may be regarded as irrelevant. In the context of network, it is the time for which the link is not available for transmission that is of concern. This is essentially related to the power loss (attenuation) of the wireless signal under certain rainfall conditions. In order to overcome this problem, it was decided to develop a separate theoretical model to investigate solely the effects of different rainfall intensities on a wireless optical link. This theoretical model is described in the following section.

3.3 Wireless Link Attenuation Model

It has been reported in the literature review that the extent of rain attenuation on signals operating at frequencies above 10GHz is dependent on a number of factors. These factor include the size and concentrations of rain particles, known as the Drop Size Distribution (DSD), as well as the degree of scattering of the electromagnetic signal by these particles in the propagation path.

Theoretical attenuation equations typically comprise the product of the DSD and a scattering coefficient. Two wireless models were developed and these are described in the following sections. In this project, a MATLAB model was initially developed based on existing theory as outlined in section 3.3.1. An investigation into the validity of the coefficients used in the chosen DSD was also undertaken. The findings of this investigation, as well as a proposed modification are outlined in section 3.3.2.

3.3.1 Model 1 – Existing Theory

The aim of this model is to calculate the attenuation due to rain in the propagation path of an optical signal. The model is developed in MATLAB based on the theoretical equation for attenuation that has the form

$$A = 4.343 \times 10^{-3} \int_0^6 Q(D)N(D)dD \tag{3.14}$$

where D is the drop diameter (mm), Q(D) is the scattering function (mm^2) and N(D) is the drop size distribution ($m^{-3}mm^{-1}$).

Drop Size Distribution N(D)

The initial values required are the range of drop diameters D and a rain rate value R. In this model, the range of drop diameters is set from 0 – 5.8mm in accordance with those tabulated in [Rogers, pp. 92]. The value of the rain rate R may be user defined or set. In a maritime climate such as Ireland, rainrate values in the 1 – 30 mm/hr ranges are typical. In the model, the rainrate parameter is an integer.

A number of forms of the drop size distribution N(D) are proposed in the literature. In this model it was decided to implement one of the most widely used DSD forms, the Marshall-Palmer form, due to its simplicity and widespread use. This negative exponential form is given by

$$N(D) = N_0 e^{-\Lambda D} \tag{3.15}$$

where N(D) is the drop size distribution ($m^{-3}mm^{-1}$) , D is the drop diameter (mm), N_0 is the intercept parameter ($m^{-3}mm^{-1}$) where D = 0 on the distribution curve and Λ is the exponent parameter which is dependent the rain rate R (mm/hr). Experimental work carried out by Marshall-Palmer in 1948 produced values for the intercept constant and exponent parameter as follows

$$N_0 = 8000\ mm^{-1}m^{-3} \tag{3.16}$$

$$\Lambda = 4.1R^{-0.21} \tag{3.17}$$

In order to calculate the drop size distribution over the range of drop diameters the previous formula is extended to its integral form as follows;

$$N(D) = N_0 \int_0^{5.8} e^{-\Lambda D} dD \tag{3.18}$$

Calculation of the drop size distributions based on this formula in the MATLAB model may be achieved using the trapezoidal approximation command *trapz*.

Scattering Coefficient Q(D)

In order to determine the attenuation, the DSD must be multiplied by a scattering coefficient. A simplified expression for the degree of scattering coefficient Q(D) due to rain interfering with a signal operating at optical frequencies was given by Deimendjian

[Maitra and Gibbons, pp. 658]. This is based on the Mie scattering coefficients for spherical particles and is given by;

$$Q(D) = \frac{\pi}{2} D^2 \tag{3.19}$$

In the MATLAB model, this coefficient was determined over the drop diameter range 0 – 5.8 mm.

Attenuation Calculation

Now that the drop size distribution and scattering integrals have been discussed, it is necessary to understand how the attenuation results for different rainrates were obtained using the MATLAB model. A flowchart of the model is given in figure 3.10.

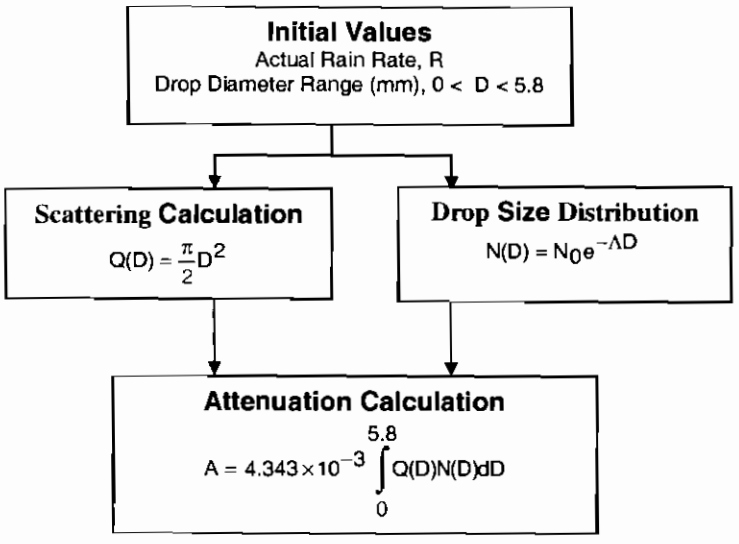

Figure 3.10; *Wireless model 1 flowchart*

The model was developed to calculate attenuation values for a range of rain rates using the *for* loop command. The following code outlines the main operations

```
D = [0:.001:5.8];
Q = (pi*D.^2)/2;
k1= 4.1;
k2 = -0.21;
k3 = 8000;
k4 = 4.343;
for R=1:100
s=k1*R.^k2;
N=k3*exp(-s.*D);
I2=N.*Q;
I3(R)=k5*10^-3*TRAPZ(D,I2);
end
```

The results obtained using the model are presented in chapter 5. The results were compared to results obtained by manually solving the equation (3.14). A deviation between the actual results and those predicted was found to exist. This deviation was less than 1% over rainrates between 1 and 100mm/hr. The manual solution to (3.14) is presented in Appendix C.

In this section, the main processes of the unmodified theoretical wireless model were described. It was noted in the literature review that the constant intercept parameter obtained by Marshall and Palmer was disputed by other researchers [Manabe et al., pp. 447]. It was decided therefore to investigate the validity of the parameter in the context of rain rate prediction. In the next section, the modified wireless model is described.

3.3.2 Model 2 – Modified Theory

In model 1, the drop size distribution used was the negative exponential form proposed by Marshall and Palmer in 1948 [Marshall and Palmer, pp.165]. This was given by $N(D) = N_0 e^{-\Lambda D}$ where $N_0 = 8000\,\mathrm{mm^{-1}m^{-3}}$ and $\Lambda = 4.1R^{-0.21}$. There has been widespread debate about the validity of the coefficients in this DSD form [Manabe et al., pp.447]. It was thus decided to evaluate the validity of this particular form using the theoretical rain rate equation [Manabe pp. 474][Rogers pp. 145],

$$R_{predict} = 6\times10^{-4}\pi\int_0^6 v(D)D^3N(D)dD \tag{3.20}$$

where D is the raindrop diameter (mm), v(D) is the drop terminal velocity (m/s) and N(D) is the DSD. The DSD used is the Marshall-Palmer distribution given in (3.15) along with the parameters given in (3.16) and (3.17). The raindrop diameter range chosen for the evaluation was 0 to 5.8mm. The terminal velocities are computed based on the results of [Gunn and Kinzer, pp. 246]. [Maitra and Gibbons, pp. 658] fit the following relation to their results

$$v = 9.65 - 10.3e^{-0.6D} + 0.65e^{-7D} \tag{3.21}$$

The MATLAB code used to achieve rain rate calculation according to (3.20) is

```
D=[0:.001:5.8];
V=9.65-10.3*exp(-0.6*D)+0.65*exp(-7*D);
Q=(pi*D.^2)/2;
k1=4.1;
k2=-0.21;
k3=8000;
k4=pi*6*10^-4;

for R=1:100
s=k1*R.^k2;
N=k3*exp(-s.*D);
I=D.^3.*N.*V;
I1(R)=k4*TRAPZ(D,I);
end
```

The resulting output *I1* indicates the rainrate in mm/hr, as predicted using the velocity relation and Marshall-Palmer DSD. When compared with the rain rate input

into the Marshall-Palmer DSD, it was found that a discrepancy existed. In all cases from 1-50mm/hr, the predicted rain rate exceeded the input rain rate. The discrepancy between the two rain rates was found to increase with increasing rain rate. The discrepancy could be attributed to a number of factors. Firstly, the rain rate integral equation (3.20) assumes a spherical drop shape. In reality, numerous authors have debated the validity of this assumption and experimental evidence has shown that in fact the spherical drop shape assumption does not hold for drops greater than 1.5mm. Consequently, any calculations based on this assumption are expected to be slightly inaccurate. Other possible sources of error are the terminal velocity relation and the DSD. The terminal velocity relation is based on the widely accepted results of [Gunn and Kinzer, pp. 246]. These results were obtained using a high degree of accuracy and based on a large number of samples. Consequently, it is not considered that this parameter would be the cause of the discrepancy.

The final parameter that may have introduced some error is the drop size distribution. As stated, the form of this distribution is widely varied and debated and therefore it is quite possible that this will have contributed to the discrepancy. The DSD was investigated further and it was found that the dominant parameter in the distribution was the intercept parameter, N_0. By modifying the N_0 value, the predicted rain rate could be optimised to produce the same rain rate value as input to the Marshall-Palmer DSD. In this manner, a table of modified N_0 coefficients could be drawn up for use in the rain rate equation. The coefficients were then incorporated into a similar model to the one described in section 3.2.1 and modified attenuation values for the rain rates could be obtained. A flowchart of the second model depicts the stages in the determination of corrected N_0 coefficients is depicted in figure 3.11.

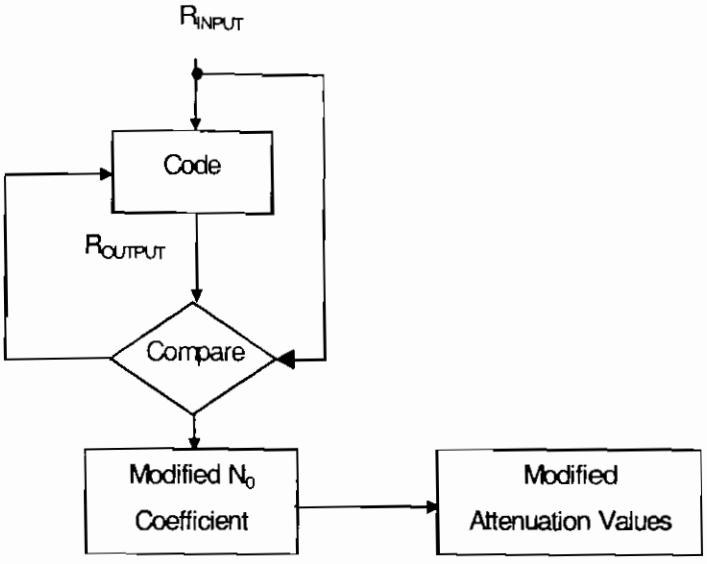

Figure 3.11; *Wireless model 2 flowchart*

To summarise, there are four stages in wireless model 2. These are outlined as follows

Step 1

The Marshall-Palmer DSD is computed for an arbitrary rain rate (Rinput) using the form

$$N(D) = N_0 e^{-\Lambda D} \tag{3.22}$$

with $N_0 = 8000\,mm^{-1}m^{-3}$, $\Lambda = 4.1R_{input}^{-0.21}$.

The arbitrary rain rate value is inserted as the R_{input} value and the DSD is computed over a range of drop diameters from 0 to 5.8 mm in increments of 0.001mm. The integral is calculated using the MATLAB trapezoidal function.

Step 2

This DSD can then be used to predict a rain rate $R_{predict}$ using the theoretical rain rate equation given in (3.20). The terminal velocities of all of the drop diameters are computed and the complete integral is evaluated using the MATLAB trapezoidal function. The result of the integration is the predicted rain rate value using the Marshall-Palmer DSD.

Step 3

The predicted rain rate is compared to the input arbitrary rain rate value and any variation between the values is compensated for by adjusting the No constant in the original MP DSD. When the difference between the rain rates is minimised, the modified N_0 coefficient is assumed optimal. This approach is based on the a number of assumptions:

- The drop diameter range D [0<D<5.8] is valid
- The Gunn and Kinzer relation for terminal velocity is valid
- The intercept constant No is the dominant coefficient over the other coefficients in the Marshall-Palmer exponential form

Step 4

The approach was used to obtain a range of modified coefficients for varying rain rates using the MP distribution. It was found that the optimal value of the N_0 coefficient varied with increasing rain rate. The results obtained for the new N_0 coefficients are presented in chapter 5.

Step 5

Calculate attenuation values based on the modified coefficients and compare to original calculated results.

In this chapter, the development of the MATLAB models was presented. This includes the basic ATM simulation model designed to simulate the stages of file manipulation in an ATM system. As explained, the main assumption in this model was the fact that the channel medium deployed was assumed reliable. It therefore did not corrupt the data in its transfer from the source to the destination module.

It was intended that a second model be developed to incorporate the effects of an unreliable channel e.g. wireless optical link, so that the results of the two models could then be compared. However, in MATLAB this would have required implementing bit corruption algorithms. Although feasible, concurrent experimental work questioned the validity and necessity of this method. Wireless links and in particular, optical wireless links are notorious for being unavailable for transmission during bouts of rainfall. When this occurs, the bit error rate is effectively irrelevant since the data is wiped out. Further, in an ATM wireless link, where data rates are of the order of 155Mbps or more, rain interference can result in the obliteration of enormous amount of data. Therefore, under such conditions the concept of Bit Error Rate is inappropriate. It is the time for which the link is unavailable for transmission that is of concern to the network designers. The Availability or percentage time for which the link is available for transmission, is therefore of more significance than the BER.

As a result of the findings, it was not appropriate to continue with the original plan for the model. The alternative direction taken involved the development of two separate models, which could in the future be incorporated into the ATM system model. These two models were based on existing theory relating to the performance of a

wireless optical link under different rainfall conditions. The first of the models estimates the attenuation caused to an optical beam under different rain rates using existing theory. This involved the incorporation of the attenuation integral equation derived by [Olsen et al., pp. 319] and used frequently throughout the literature on rain attenuation. Within this attenuation integral equation, it is necessary to choose a mathematical form for the DSD. In the particular model developed here, it was decided to avail of the Marshall-Palmer DSD due to its simplicity. The model allowed estimation of the attenuation of an optical link under varying rainfall intensities (rain rates). The results of the model depend on the validity of the Marshall-Palmer distribution. Since this was not known to a high degree of accuracy, it was decided to investigate further.

In the second wireless model developed, the Marshall-Palmer distribution came under scrutiny. It was determined that the N_0 coefficient in the distribution was the dominant parameter. Based on the optimisation of results obtained using the unmodified Marshall-Palmer DSD in the rain rate equation (3.20), modified (corrected) N_0 coefficients were found for the Marshall-Palmer DSD. The modified coefficients could then be incorporated into the wireless simulation model to yield corrected attenuation results.

The code for the models is presented in Appendix B and the results of the three models are presented in chapter 5.

4 EXPERIMENTAL PROCEDURES AND EQUIPMENT

4.1 Overview

This chapter contains an overview of the experimental work undertaken during the course of this research. This includes the network configurations adopted for the initial experimental work conducted to gain experience and understanding of the practical aspects of the network connectivity. This is followed by descriptions of the experimental setup used and procedures followed in the more specific optical link tests. The results of these experimental tests are compiled and presented in chapter 5.

4.2 ATM Network Tests

The aim of the network tests was to investigate the effect of incorporating a wireless communications link into a local area network. The main impetus for the investigation arose from the findings of the literature review. As noted previously, there has been much research conducted on the reliability of communication networks that use microwave links in the channel. Conversely, there is a deficiency in the level of information available regarding the reliability of networks using wireless optical links as transmission media in the channel. As demand for bandwidth continues to grow and optical transmission becomes more significant in computer networks, there is a need to address the issue of optical propagation. This research therefore, aims to address the issue of optical propagation by examining the reliability and performance of an optical communications link subject to different rainfall conditions. The optical link examined in the first experimental tests comprises part of a Local Area Network (LAN) containing both ATM and Ethernet nodes.

Originally, the LAN in which the research was conducted primarily comprised baseband Ethernet nodes. The availability of a state-of-the-art broadband ATM network switch however, prompted the use of ATM as the data link layer technology for this research. Incorporating the ATM technology into the network allowed the feasibility of using the ATM standard mechanism for the transfer of connectionless LAN traffic over connection-oriented ATM, LAN Emulation (LANE) to be examined.

In order to achieve the aims of the experimental work, it was necessary to first configure ATM nodes onto the network using a reliable medium (fibre) for connectivity and then to extend the network configuration to include a connection facilitated by a wireless optical link (laser). A two-stage approach was employed. Firstly, the LAN at DIT Aungier Street was configured to include an ATM node and connectivity was maintained using a reliable transmission medium in the channel (optical fibre). File transfers tests were conducted between the ATM node and an Ethernet node to test connectivity. The network was then reconfigured to include a second ATM node. The ATM node used in the initial tests was reconnected onto the network at a remote campus at a distance of approximately 160m away, with the intercampus connection provided by the wireless laser link. These network configurations and tests are outlined in more detail in the following sections.

4.2.1 ATM-Ethernet via fibre

In order to provide a basis for comparison between the reliable and unreliable channel, it was first necessary to configure the network using a reliable transmission medium in the channel. This was undertaken at the DIT Aungier Street site in a hybrid ATM-Ethernet environment.

Connecting an Ethernet node onto the local area network using 100Mbps Category 5 (CAT5) UTP cable configured the network. The ATM node was configured and connected to an ATM port on the Cisco Catalyst 5500 ATM switch via 155Mbps OC3/STM1 fibre. The ATM switch was connected to the Ethernet local area network via a LAN Emulation (LANE) module contained in the switch. The LANE module allowed the ATM and Ethernet nodes on the network to communicate. Figure 4.1 illustrates this network configuration.

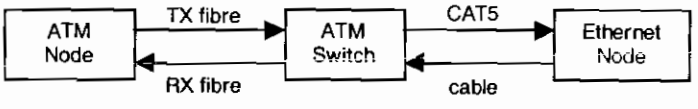

Figure 4.1; *Initial network configuration*

The network connectivity was tested initially using the Internet Control Message Protocol ping application described in RFC 2925. The ping application sends out a 32 byte message sequence to the IP address specified. If the specified node receives the message, it

sends a reply message. To achieve this in the network tests, the command *ping* was typed at a command prompt, followed by the IP address of the particular node to be contacted. Typical successful and unsuccessful ping attempts to contact nodes connected to the network are shown in Figure 4.2. In the initial network configuration, the ping attempt to contact the ATM node from the Ethernet node as well as the corresponding attempt from the Ethernet node to the ATM node was successful. The successful replies from both nodes indicated that the nodes had been correctly configured onto the network and connectivity was established.

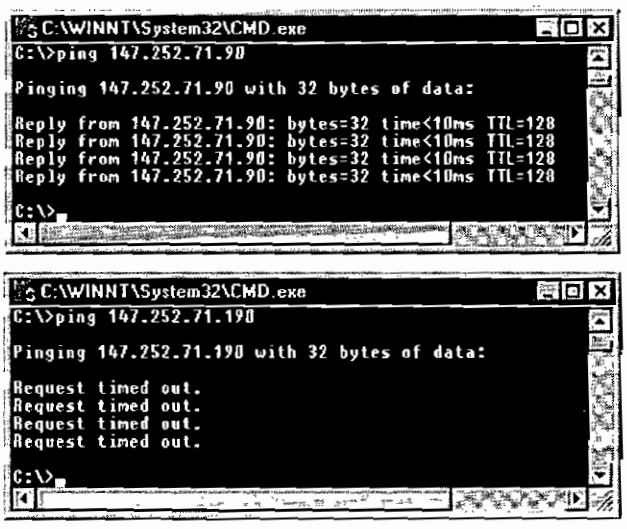

Figure 4.2; *(upper and lower) Successful and unsuccessful ping attempts*

The networking protocol TCP/IP was tested on both nodes using a variety of TCP/IP applications such as file transfers and electronic mail (e-mail). Binary files of different sizes, containing regularly and randomly generated data, were transferred successfully between the nodes by means of the file transfer program Laplink. Laplink uses the TCP/IP application File Transfer Protocol (FTP) to transfer files between nodes running the TCP/IP protocol. File transfer could be initialised at either node. A TCP/IP connection was negotiated over the network and transfers commenced on establishment of a TCP/IP connection between the nodes. File transfer statistics indicated that each file transfer between the Ethernet and ATM nodes was successful. This provided further evidence of the correct network configuration. Connectivity between the nodes and the network via the wired transmission media was 100%. This indicated that the transmission media deployed, copper cable and optical fibre allowed continual and reliable connectivity to be supported.

In this section, the network tests conducted using reliable transmission media were described. These tests involved the configuration of an ATM node onto a local area network comprised primarily of Ethernet nodes. The LAN Emulation module of the ATM switch enabled the different nodes to seamlessly communicate. It was shown that the interconnection of ATM and Ethernet nodes on a local area network could be easily achieved. The tests conducted showed that the commonly used TCP/IP protocol was fully supported on the ATM and Ethernet nodes. The next stage in the testing was to examine the effects of introducing a wireless communications link into the physical layer of the network. The configuration used and experimental procedures followed in these tests are presented in the following section.

4.2.2 ATM-ATM and Ethernet via fibre and laser

The ATM tests described in section 4.2.1 showed that the ATM node was successfully connected to the local area network (LAN) at all times using fibre and the Ethernet node was continually connected to the LAN using CAT5 cable. This shows that these wired media are reliable for maintaining network connectivity, as expected. It is of specific interest for the reasons outlined previously, to investigate the network connectivity when an unreliable transmission medium such as a wireless optical link is deployed in the channel.

In order to investigate these effects, the DIT Aungier Street LAN described in section 4.2.1 was extended to include a wireless optical link. The wireless link that provided the intercampus connection between DIT Aungier Street and DIT Kevin Street consisted of a pair of optical communication lasers operating at 800nm mounted and manually aligned on the roofs of both campuses. The laser link was implemented between the ATM node, which was relocated to DIT Kevin Street a distance of 160m away, and the DIT Aungier Street LAN. In this case, a hybrid connection of fibre and laser was used to connect the remote ATM node onto the local area network at DIT Aungier Street. One of the Ethernet nodes at the DIT Aungier Street site was upgraded to run ATM so that ATM-ATM connectivity and ATM-Ethernet local and remote connectivity could be tested. The intercampus configuration of the network is illustrated in figure 4.3 and the ATM port module of the Catalyst 5500 switch and optical laser link are shown in figure 4.4.

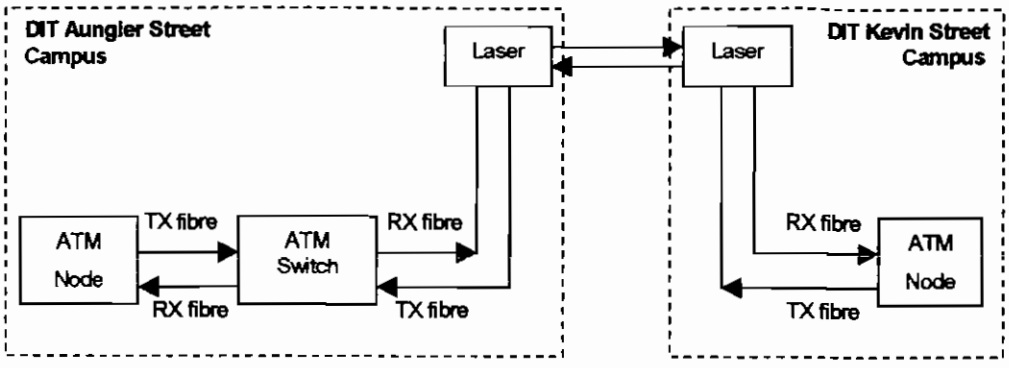

Figure 4.3; Inter campus network configuration

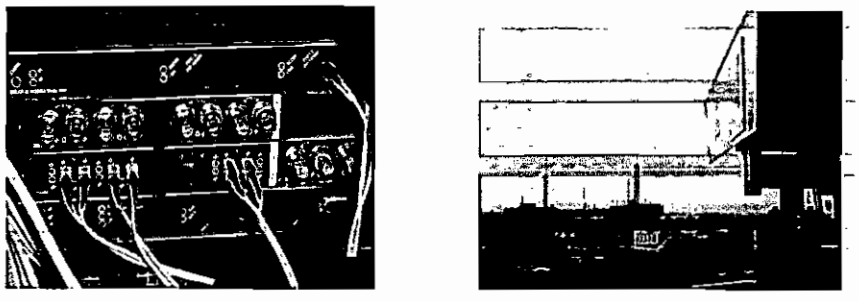

Figure 4.4; (left to right) ATM switch and laser link

Each fibre connection consisted of a separate transmit and receive fibre and it was necessary to manually configure all connections. Development was hampered by the fact that some of the newly installed fibre connections were faulty and the initial network configuration did not operate as a result. It was necessary to test each of the fibres in the configuration individually using an Optical Time Domain Reflectometer (OTDR) so that the faulty fibres could be identified and the network could be reconfigured to avoid these fibres and operate successfully. In total, four connections were required at each site (two transmit fibres and two receive fibres). Although this does not seem too laborious a task, it must be noted that at the DIT Aungier Street site alone there were four patch panels. Each fibre terminated at each patch panel, thus there was a total of 16 fibre segments. A total number of 28 fibre segments at the DIT Aungier Street site required testing. This was a considerably arduous process since the fibres ran through walls, ceilings and out to the rooftop laser. At the DIT Kevin Street site, there were fewer fibres to test. However, it was a requirement to test each of these also, for the purposes of future expansion. Once the fibres had been tested, the network was reconfigured to operate over only reliable fibres,

where the power loss was less than 2dB/m. Figure 4.5 provides a schematic of the network configuration at the DIT Aungier Street site.

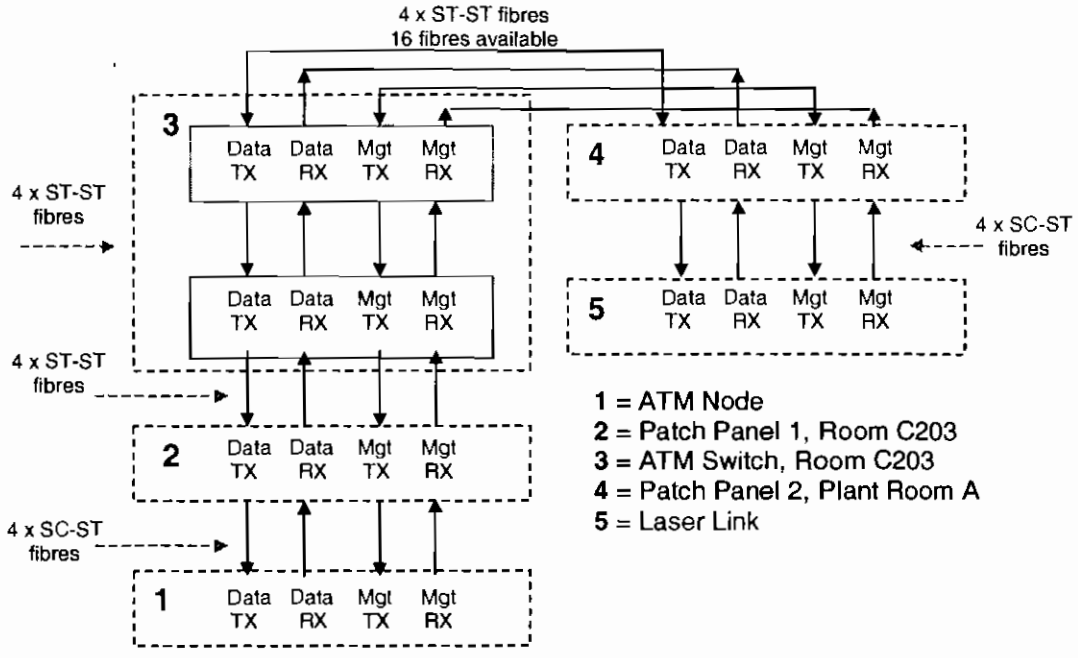

Figure 4.5; *Schematic of network configuration at the DIT Aungier Street site*

The intercampus configuration was tested in a similar manner to the initial network configuration described in section 4.2.1. Firstly, node connectivity was tested using the *ping* command. When this was found to be successful, identical file transfer tests using the same binary files described previously, were conducted. In order to examine support for high-bandwidth multimedia applications, videoconferencing software (Microsoft NetMeeting, Version 2) was installed on the local and remote ATM nodes, as well as three Ethernet nodes on the DIT Aungier Street LAN and a number of videoconferencing sessions were conducted.

The ability of the network to support voice and video simultaneously in nearly all instances showed that the hybrid ATM-Ethernet network could support constant bit rate, low delay applications. The tests also demonstrated the successful transfer of IP traffic over ATM as well as between ATM and Ethernet nodes and also demostrated Voice over IP (VoIP). A small number of instances were noted however, where glitches or delays in the video and voice transfer occurred. These instances were found to occur at peak network usage times such as early in the morning or at lunchtime, when students are logging on to

the LAN to check their email or search the World Wide Web (WWW). The increase in network traffic at these times sometimes may have caused congestion on the Ethernet sections of the network. Since Ethernet uses a shared medium, the available network bandwidth is distributed among the Ethernet nodes. Where a large number of users are logged onto the network, the bandwidth is shared among all of them. Instances of heavy network loading were evident by the delays imposed on the video and voice transmissions from these nodes during the videoconferencing sessions.

Another instance in which there was seen to be degradation in the quality of the voice and video sessions was when there was rain falling in the path of the intercampus connection. In this case, some of the data may have been lost or corrupted in the transfer of the information between the two campuses. This degradation often led to the intercampus connection to be disrupted for lengthy periods. These findings indicated that further research into the availability of the wireless link would be necessary to investigate the feasibility of the laser as a communications link between two campuses.

In order to determine the availability of the link, it was necessary to monitor the link over continual periods of time. It was decided to monitor the status of the wireless link using two types of network monitoring software, LanScout and Linkview. LanScout is an Olicom software program that monitors the status of the connection between the ATM nodes and the ATM switch. Any loss in connectivity between the ATM node and the ATM switch is logged in a status log file for future reference. Linkview is a propriety software program designed to monitor the laser system parameters and was developed by the Communication By Light (CBL) company. Linkview monitors the power levels of the laser link and records an alarm table of instances where the power level falls below the minimum detectable level. When this occurs, the link is rendered unavailable for network transmission. Using a combination of records from LanScout and Linkview allowed the following observations to be made.

It was observed that, in most instances where clear air conditions prevailed in the atmosphere, the network transmissions were uninterrupted and the status of the laser link was recorded as active over these periods in the Linkview log files. Under these conditions the laser link connection was available for network transmissions. The connectivity

between the remote ATM node and the network for the same period was logged in the LanScout status report.

A number of instances were noted in which the connectivity was interrupted. This was recorded in both the Linkview alarm table and the LanScout report. The typical causes were determined to be rain, fog, passing objects (birds flying through the beam) and sunlight. The first two causes were easily identifiable. During observed periods of rain and fog, the optical beam was scattered and absorbed as it passed through the atmospheric channel, causing the intercampus link to be unavailable for transmission. During these instances the remote node was unable to connect to the LAN at DIT Aungier Street. The length of time for which the link was interrupted and the connectivity was disrupted was dependent on the duration and intensity of the rainfall.

The third cause of interruption (birds) was indicated by periods of no longer than one or two seconds during clear air conditions, where transmission was not possible. While birds flying through the beam may not be the sole cause of these interruptions, the large number of gulls and pigeons observed in the vicinity of the link could, at times, be manually correlated to transmission interruptions to the link.

The final cause that was noted as interrupting the beam was determined to be sunlight. This conclusion was drawn after the link became unavailable for transmission during clear air conditions over the same time periods each day during the months of February and March 2000. It was noted that, at these times, the sun was positioned at a low angle in relation to previous months and was directly opposite to the laser link at the DIT Aungier Street site. This observation was made known to the manufacturer of the laser link, who promptly sent a replacement link enhanced with a "new optical feature", presumably a sunlight filter because the problem of disruption due to sunlight did not arise subsequently.

Each of these observations was significant. While the latter two causes of disruption indicate obvious causes for concern at certain times, it is not deemed to be reasonable or practical to investigate them further. Conversely, the impact of rain and fog on the availability of the optical link may be investigated with relative ease and accuracy. In a maritime climate such as Ireland, rain is the most common form of precipitation. Fog does not manifest itself in the urban area of interest to this research, except on a few occasions

each year whereas rain occurs frequently. Therefore, it would seem more beneficial and advantageous in the long-term to investigate the impact of rain on the wireless link. Further, it would not have been feasible, given the time frame of this research, to examine the effects of fog on the link availability to a great extent. Consequently, the following experimental work relates solely to the impact of rain on the availability of the link.

The prevalence of rain in a maritime climate such as Ireland prompted the investigation into the effects of particular rain intensities on the availability of the laser link in the initial tests. This was achieved by monitoring the status of the laser, determining the availability of the link using the network logs and correlating the results with rainfall statistics. The availability computation was based on the length of time that the link was interrupted and the total length of time that the link was switched on. Daily rainfall statistics obtained from Met Eireann for Dublin Airport were correlated with the daily availability values for the optical link. Although a general relationship between availability and rainfall was obtained and is shown in chapter 5 (graph 5.2), it was not convincing enough to draw any meaningful conclusions from. Consequently, it was decided to conduct further experimental tests, which may provide more convincing evidence of the relationship between link degradation and rain intensity (rain rate). These optical tests are described in the following sections.

4.3 Short - Range Optical Link Tests (Natural Rain)

During the initial tests described in section 4.1.2, specific interruptions to the optical link due to rain could not be correlated with local rain rate measurements. This was because it was not possible to simultaneously monitor the power levels of the lasers with local instantaneous rain rates along the propagation path. For an accurate rain rate measurement to be obtained, rain gauges would have had to be placed along the entire propagation path of the optical link. However, this was not feasible in the environment of this research since the propagation path extended over a 160m distance through an urban environment.

The initial tests did not provide sufficient evidence of the relationship between the degradation of the optical link and an increase in rainfall intensity on which to draw solid conclusions. As there was no method of recording local rain rates, it was decided that in order to obtain the necessary results from experimental work, a custom-built rain gauge

apparatus would have to be designed and further testing conducted. In this section a description of these further tests is presented. These tests are entitled "Optical Link Tests (Natural Rain)" since the tests were carried out on the rooftop of DIT Aungier Street where an optical link was subject to the effects of natural rain falling in the urban area.

The tests involved monitoring the operation of an optical beam operating at a similar frequency to the laser beam in place in the network. It was not possible to obtain instantaneous power level readings from the propriety laser system and this was deemed the most appropriate alternative solution. Consequently, two custom-built apparati were designed and assembled for the further tests. The optical beam apparatus consisted of an infrared emitter and detector mounted in black boxes onto an aluminium frame and separated by a distance of 1m. The custom-built rain gauge is an optical one, which uses the power levels of an optical signal to detect the amount of water that has been collected in a graduated cylinder. This gauge allowed concurrent recording of the localised rain rates alongside the optical beam power levels that could thus be correlated to extract the required relationship between the degradation in the link and the rain rate. These apparati are described in more detail in the following sections.

4.3.1 Experimental Setup

As described, the experimental setup used for further analysis of the relationship between the optical signal degradation and rain rate comprised two main sections; an optical beam and optical rain gauge. As these were custom built for this research, a great deal of time was consumed with planning and assembling of the two apparati, an illustration of which is provided in figure 4.6.

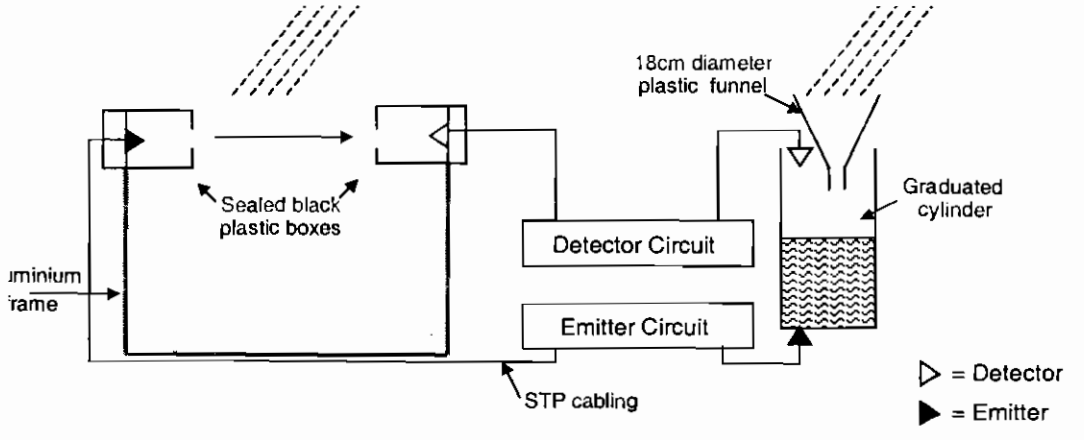

Figure 4.6; *Optical beam and optical rain gauge apparatus*

In the following sections each of these apparati is described separately. Firstly the experimental setup of the apparati is described, followed by the experimental procedure followed in the testing of the optical beam and then the optical rain gauge is outlined.

Optical Beam Experimental Setup

The initial network tests described in section 4.2.2 showed that data transmission was frequently interrupted when rain fell in the path of the propagating laser beam and that transmission recommenced when the laser link power level recovered to an acceptable level. In order to investigate the interruption effects to the laser beam caused by rain in the channel, it was necessary to determine the attenuation and availability of a similar beam operating in the optical region under varying rain rates. Since it was purely the physical effects on the power level of the optical beam caused by rain that were of interest, it was not necessary to carry actual information on the optical link.

Therefore the optical beam apparatus, which was designed and assembled specifically for this research, consists of an infrared emitter and a detector, housed in watertight black plastic boxes and mounted securely a distance of 1m apart on an aluminium frame. It was considered that a 1m-separation distance would suffice for the purposes of this research. A visible light filter was placed in front of the detector to minimise the effects of illumination outside the infrared region of interest. A small aperture at the front of each of the boxes allows the beam to propagate between the devices. The apertures were aligned with one another and the entire assembly was placed on the roof at the DIT Aungier Street.

The emitter is a hermetically sealed GaAlAs infrared emitting diode of peak wavelength 880nm that is powered by a 5V supply. The detector is a silicon photodiode. When illuminated with IR radiation, the photodetector generates a current proportional to the incident radiation intensity. The current signal is converted to a voltage signal by detector circuitry and amplified to produce a suitable voltage representation of the detected beam signal. A twisted copper cable pair provides a connection between the output of the detector circuit and the monitoring PC. The detector circuitry is described in detail in Appendix A.

An Analog-to-Digital Converter Pico ADC10 allowed the output analog voltage signal from the optical beam to be recorded on the PC. It was possible to record the detector voltages in two ways, either using Picolog and Picoscope, the vendor-specific data acquisition software appropriate to the ADC10 or using a custom written C program (listed in Appendix B). While the former method was used for initially calibrating the optical beam, the latter method was chosen for the long-term testing of the optical beam voltages due to its flexibility and efficiency.

In this section the experimental setup of the optical beam apparatus was described. In the next section, the experimental setup of the optical rain gauge is presented.

Rain Gauge Experimental Setup

In order to record localised rain rates at the test site, it was necessary to deploy a rain gauge close to the optical beam apparatus described in the previous section. Although there was found to be a number of electronic and tipping bucket rain gauges on the market, these were either too costly given the financial resources available or too elaborate for this research. .Consequently, it was decided that the only practicable solution would be to design and assemble an inexpensive yet accurate rain gauge custom-built for this research. Considering that most of the testing conducted in this research was at optical frequencies, it was decided that an optical solution would maintain consistency throughout the tests but would also provide an interesting insight into the feasibility of producing an economical optical rain gauge.

The objective of the design was to recording the instantaneous rain rate at the site, along the propagation path of the optical beam described. The rain gauge consists of a plastic transparent funnel that collects rainwater and directs it to a graduated cylinder housed in a container below. An infrared emitter and detector are mounted on opposite ends of a glass graduated cylinder. The emitter for the rain gauge is of the same type as that described for the optical beam apparatus and is mounted at the base of the graduated cylinder using an aluminium frame, directing the outgoing infrared beam up through the cylinder in which rain water is collected. The detector is a silicon photodiode that is mounted at the upper end of the cylinder on the same aluminium frame and vertically

aligned with the infrared emitter at the base of the cylinder. The rain gauge apparatus is illustrated alongside the optical beam apparatus in figure 4.6.

Similar to the way in which the optical beam output is processed, the output current signal produced at the rain gauge detector is converted to a voltage at the detector circuitry and amplified to a suitable range for monitoring at a nearby PC. The emitter and detector circuitry is described in detail in Appendix A. An analog-to-digital converter Pico ADC11 enabled the detector voltage from the rain gauge to be monitored. As in the case of the optical beam monitoring, two methods for recording the detector voltages from the ADC11 were available, either PicoLog/Picoscope, the vendor-specific software or a second custom-written C program (listed in Appendix B) may be used to monitor the output rain gauge detector voltage.

Finally, it is necessary to note that the emitter and detector circuitry of the optical beam and optical rain gauge apparati were contained together in a large sealed container. The inside of the container was lined with aluminium foil that was carefully grounded to provide screening from stray electric fields.

In this section the experimental setup of the optical beam and optical rain gauge were described. The following section is devoted to the experimental procedures followed in the experimental testing of both of the apparati.

4.3.2 Experimental Procedure

In this section the experimental procedure followed in the testing of the optical beam and optical rain gauge are outlined. Following the structure of the previous section, the experimental procedure of the optical beam is firstly discussed followed by the experimental procedure of the optical rain gauge. It was first necessary to calibrate the apparati before commencing the main testing. The first two sub-sections describe the optical beam and optical rain gauge calibration. The last sub-section describes the experimental procedure followed in the main testing of the apparati.

Optical Beam Calibration

It is necessary firstly to note that the optical beam and gauge apparati were simultaneously calibrated, under the same darkened conditions. The timestamps on the two

PCs used to monitor the detector voltages of both apparati were aligned so that the readings from the optical beam and rain gauge could be taken simultaneously and easily correlated in future analysis. In this section the calibration of the optical beam is outlined.

The experimental setup has already described the optical beam assembly. In order to calibrate the apparatus, it was necessary to ensure that the PC was capable of detecting the output voltage from the optical beam detector circuitry correctly. It was necessary to manually adjust the offset of the voltage level in the detector circuitry in order for the output detector voltage to be detectable within the allowable voltage range of the ADC 12 converter. Once this had been achieved, the amplification was adjusted to give sufficient resolution of the voltage signal within this allowed range so that the converter could detect interruptions to the optical beam.

In order to investigate the voltage thresholds of the optical beam within the ADC range, it was necessary to determine the threshold voltage levels when the optical beam was switched off, switched on (uninterrupted) and switched on (fully interrupted). This was achieved by executing the custom-written C program for the optical beam described in section 2.3.1. This allowed the average of 10,000 voltage readings taken at 10kHz at 20 second intervals each minute to be stored into a file. Initially the beam emitter was switched off and the first set of average voltage readings was recorded. These represented the background voltage detected by the optical beam detector when no infrared emitter was used. Next, the optical beam emitter was switched on and further results were taken of the detector voltage. These represented the typical uninterrupted voltage received from the optical detector. The difference between the detected voltage when the optical emitter was switched off and when it was switched on represented the voltage solely due to the optical emitter. By manually blocking the beam, the detector voltage increased significantly, due to the reverse polarity of the output signals. This indicated the expected change in the direction of the optical detector voltage due to an interruption in the propagation path. It was necessary to be aware of this fact when conducting further testing on the optical beam apparatus since future testing where rain fell in the channel of the propagation path of the optical beam could be identified by increased optical detector voltage. The results for the optical beam calibration are presented in chapter 5.

The calibration results obtained for the background radiation from the optical beam detector voltage in the darkened plant room were compared to the results recorded for the background radiation voltages detected by the optical detector under night-time conditions. In this case the optical beam apparatus was placed on the rooftop and the emitter was switched off for the entire night. The PC was setup to record the optical beam voltages over the period. A slight difference of approximately ± 0.02V was noted between the calibration background readings and the night-time readings probably due to the fact that the darkness of the plant room in which the calibration tests were conducted was not exactly the same as night time darkness.

Rain Gauge Calibration

In this section the calibration of the optical rain gauge is presented. The calibration of the rain gauge entailed recording the voltage level of the optical detector of the rain gauge apparatus when the graduated cylinder was filled with different volumes of water. The gauge apparatus was calibrated in the darkened plant room at the same time as the optical beam calibration. The second custom-written C program described in section 4.3.1 was employed to record the average of 1000 detector voltages at the ADC11 converter taken at a sampling frequency of 1kHz every 20 seconds over a one-minute interval. As with the optical beam calibration, the first stage in the optical rain gauge calibration was to determine the background voltage recorded by the optical detector in the rain gauge. This was achieved in a similar manner by leaving the infrared emitter off and recording an average background voltage level. This corresponded to the background radiation detected by the optical rain gauge detector.

The next stage was to record the optical detector voltage at the rain gauge when the optical emitter was switched on and varying volumes of water were collected in the graduated cylinder. To avoid possible complications caused by the air/glass interface at the base of the graduated cylinder, a standard volume of water (20ml) was measured into the cylinder using a pipette before any results were taken. The optical emitter was switched on and the monitoring PC was setup to record the average detector voltage from the rain gauge circuit three times per minute into a file for future analysis. A further 30ml was measured into the cylinder and the average detector voltages for 50ml were recorded in the same

manner. The procedure was repeated for each consecutive 50ml added to the cylinder up to a volume of 350ml. As the level of water in the cylinder increased, the detector voltage was observed to increase due to a reverse polarity in the output signals from the optical rain gauge circuitry. The results of the optical rain gauge calibration are presented in chapter 5.

In the last two sub-sections of the experimental procedure section 4.3.2, the calibration procedures for the optical beam and optical rain gauge apparati were outlined. In the next sub-section, the experimental procedure followed for the main testing of the optical beam and optical rain gauge are presented.

Main Test Procedure of Optical Beam and Optical Rain Gauge

In this section, the procedure followed in the main tests is outlined. The purpose of the main tests was to investigate the effects of the rain falling in the propagation path of the optical beam. This testing was conducted using the optical beam and optical rain gauge apparti over a period of 35 nights. The apparati were setup alongside one another on the rooftop of DIT Aungier Street. The monitoring PCs were setup to record the detector voltages of the optical beam and optical rain gauge concurrently over a number of days. By recording the voltages from the apparti simultaneously, they could easily be correlated for future analysis.

For the testing, the optical beam voltage was recorded three times per minute at a frequency of 10kHz whereas the optical rain gauge detector voltage was recorded only once per minute. The reason for initially sampling the rain gauge voltage less frequently than the optical beam voltage was because [Crane (1980), p. 1719] points out that a one-minute average for the rain rate is optimum to avoid contamination due to turbulence and fluctuations. In these tests a one minute average was thus chosen so that gradual increases in the water volume in the graduated cylinder could be identified, while complications that may have arisen by sampling in a shorter interval e.g. turbulent effects interfering with the results, could be avoided.

With the optical beam however, the objective was to capture specific interruptions caused by rain falling in the propagation path of the optical beam. The optical beam detector voltage was thus sampled at 10kHz and was sampled three times per minute. The

sampling frequency was determined to be sufficient to capture the smallest raindrops falling through the path of the beam.

It was decided after a number of days testing that, given the large amount of data stored even in a single night, it was becoming increasingly labour intensive to correlate the average optical beam voltages taken every twenty seconds with the minute average optical rain gauge voltage. So that correlation could be simplified, for the remainder of the testing the output from the apparati was sampled at the same time, every 20 seconds.

Two types of file were recorded for each trial period; one file of the average optical beam voltages and another of the average optical rain gauge voltages for the period. The optical beam average file recorded the average of 10,000 voltage readings from the optical beam detector taken using the ADC-12 converter. The optical rain average file recorded the average of 1,000 optical beam voltages from the optical rain gauge detector taken using the ADC-11 converter. A third file recorded the specific 10,000 voltage readings of the optical beam detector. This was initiated only when the average of all of the optical beam voltages taken at a particular instant exceeded the previous average optical beam voltage by a specified threshold. The threshold was set to 0.2V as this threshold was found to be sufficiently high to omit noise fluctuations of the beam being captured and yet ensured that significant interruptions to the beam were captured. This enabled interruptions due to raindrops falling through the propagation path of the beam to be stored for analysis. Using these individual blocks, it was also possible to identify raindrop profiles. In order that specific interruptions to the optical beam could be correlated with instantaneous rain rate results, samples stored in each of the three files were stored with timestamps and corresponding sample and block numbers. Examples of the three files stored over each test period are presented in the following tables 4.1- 4.3.

Block Number	Average Voltage (V)	Maximum Voltage (V)	Minimum Voltage (V)	Timestamp (seconds since 30 Jan 1976)
1872	1.797	1.8255	1.7815	958102420
1873	1.7952	1.8011	1.7913	958102440
1874	1.7957	1.8011	1.7913	958102460
1875	1.7861	1.8011	1.7571	958102480

Table 4.1; *Section of average rain gauge voltage file*

Block Number	Average Voltage (V)	Maximum Voltage (V)	Minimum Voltage (V)	Standard Deviation (V)	Timestamp (seconds since 30 Jan 1976)
1872	1.426	2.2332	1.4212	2.7387	958102420
1873	1.4255	1.79	1.4176	2.7387	958102440
1874	1.426	2.1893	1.4176	2.7387	958102460
1875	1.4258	1.7741	1.4212	2.7387	958102480

Table 4.2; *Section of average optical beam detector voltage file*

Sample Number	Block Number	Maximum Voltage (V)
1	1875	1.4237
2	1875	1.4249
3	1875	1.4261
4	1875	1.4261
5	1875	1.4237

Table 4.3; *Section of Optical Detector Voltage File (individual block values)*

The experimental procedure followed in the short-range optical link test has been outlined. A number of additional factors were noted throughout the course of the experimental work. These included the fact that despite the precautions taken to reduce the ingress of extraneous light at the beam detector, radiation from a number of external sources prevented detection of the infrared optical beam voltage during daylight hours by the ADC converter. The optical detector was mounted securely at the back of one of the sealed black boxes. A visible light filter was mounted in front of the optical detector. One of the main sources of this extraneous radiation was determined to be the sun. The output voltage was saturated during the daytime hours. Illumination levels from the sun may have caused the optical link detector to saturate during these periods. It was thus decided that, considering the degree of variability in daylight illumination levels each day, night-time tests would be conducted. It was determined that the background illumination levels at

night were constant over a period of approximately 8 hours each night. This was deemed to be a sufficient period over which the tests could be conducted as it would be expected that the probability of rain falling at some stage during this period, over a number of days (35 in total) is high. The overall variability of the background illumination readings taken over a sample 8-hour night test period on a night with no rainfall was determined to be less than 1%.

In the case of the optical rain gauge, similar precautions were taken to minimise the ingress of background illumination. Mounting the detector at the upper end of the aluminium frame which runs vertically outside the graduated cylinder ensures that the detector is not directly subject to ambient light entering the container via the funnel from the outside. Although this precaution reduces the amount of ambient light intercepted by the detector, the effect is not entirely eliminated. Since the funnel is transparent, light may have been introduced to the cylinder and this may have interfered with the detector readings to some extent. In order to overcome this problem as in the case of the optical beam apparatus, night-time tests were conducted to reduce the extent of the problems caused by ambient light. As stated previously, a minimum amount of water was maintained in the gauge cylinder at all times to avoid problems caused by the air/glass interface of the graduated cylinder.

In this section the short-range experimental tests were described and the procedures followed in the testing were outlined. Initial analysis of the rain gauge results were not promising, regions of unexpected behaviour of the rain gauge were identified and it was thus decided to conduct further testing on the optical beam apparatus using a different method of rain rate detection. The results and findings of the short-range optical beam tests are presented in chapter 5. In the next section, the experimental procedure for the secondary testing of the optical beam apparatus is outlined. These tests were conducted in a different location to the short-range optical link tests described in this section. Time constraints did not permit this further testing over a long period. It was necessary to conduct these tests over a single night. Further on the night in question, no rain was falling at the time the tests were to be conducted and it was thus decided to employ a method of simulating rain falling through the optical beam. This also provided a manner for the comparison of results obtained in natural rainfall and simulated rainfall.

4.4 Short - Range Optical Link Tests (Simulated Rain)

4.4.1 Experimental Setup

The discrepancies noted in the initial analysis of the optical rain gauge results prompted further testing of the optical beam apparatus using a different method of rain rate measurement. A simpler method of rainfall measurement was employed in these secondary tests. Three cylindrical measuring containers of similar diameter were used as rain gauges to measure the rain fall in the propagation path of the optical beam. In this section the experimental setup of these secondary tests is presented.

Three secondary tests were conducted, one for each of three different rain rates. The same optical beam apparatus described in section 4.3 was used for these tests. Three rain gauges were used to collect water that fell through the propagation path of the optical beam over each test period. As there was no rain falling at the time of the tests, it was necessary to employ an alternative method of generating rain. A garden hose was thus used to "simulate" rain of varying intensities for the tests. Figure 4.7 shows an illustration of the apparatus used in these tests. In the next section, the experimental procedure followed in these secondary tests is presented.

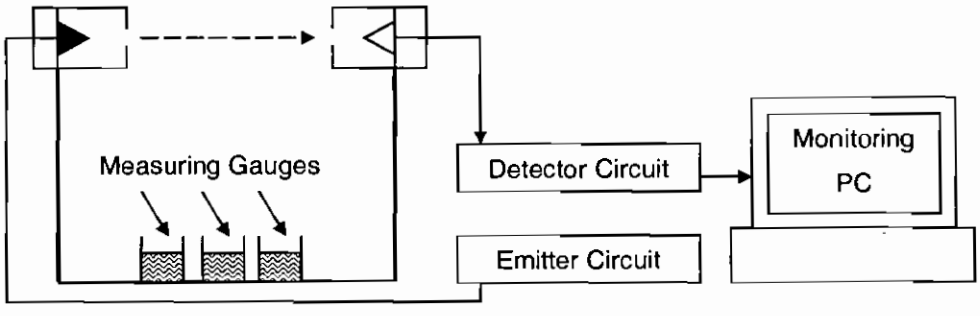

Figure 4.7; Controlled test apparatus

4.4.2 Experimental Procedure

The optical beam apparatus described in section 4.3.2 was arranged and three rain gauges were placed along the propagation path. To maintain consistency with the short-range optical link tests described in 4.3.2, the monitoring PC was setup to record the average of 10,000 detector voltages taken from the optical beam apparatus every twenty seconds during the test period. In order to capture interruptions to the optical beam due to

rain but to filter noise from the results stored, the sampling frequency was once again set to 10kHz and the threshold voltage level to 0.2 Volts.

The hose was used to produce "rain" at a height of 4m above the optical beam apparatus. This height was required to ensure that the generated drops had reached terminal velocity before they fell through the propagation path of the beam, as is the case when rain falls through the beam in the natural rain tests of section 4.3.2. A more detailed description of this requirement is presented in chapter 5. Three different rain intensities were used, one per test. The rain intensity and thus the rain rate, was adjusted by changing the tap position which controlled the volume flow rate of the water flowing through the hose. A timer ensured that each of the tests were conducted over a period of the same duration. The tests were conducted for the three rain rates over a period of two minutes. The direction of the rain falling from the hose over the beam propagation area was maintained as far as was reasonably practicable for the entire length of the test period.

Clearly, it was necessary to determine the range of drop diameters produced by the hose to ensure that a comparison between the natural and simulated test results could be carried out. For the simulated tests, the nozzle position of the hose was maintained for the duration of the three test periods. At the end of the testing a sample of drops produced by the hose nozzle were collected onto a number of plastic sheets. Given the limited number of measurement devices available for this diameter testing, it was decided to use a mass measurement to determine the drop diameters. In order to achieve this, it was necessary to select a number of random drops (55 in total) collected on the plastic sheets and to isolate them for analysis. It was easier to weigh the drops, rather than determine their diameter manually. Thus the mass of each of the collected drops was determined using a set of electronic scales. The diameter of the drops was determined using a mass to volume conversion method. The mass to volume conversion was as follows

$$\rho = \frac{m}{V} \tag{4.1}$$

where ρ is the density (kgm^{-3}), m is the mass (kg) and V is the volume (m^3). The density of water is $1000kgm^{-3}$ and using the measured drop mass, the drop volume was determined. Assuming a spherical drop shape, the radius of the drops could be determined using the following formula

$$V = \frac{4}{3}\pi r^3 \tag{4.2}$$

where V is the drop volume m^3 and r is the drop radius in m. The drop diameter could thus be determined by doubling the drop radius. It was found that the size of drop diameters produced using the hose were consistent with the range of drop sizes for raindrops described in the literature between 0 and 5.8mm [Rogers, p. 92].

When each test was finished, the rain gauges were removed and the water volume collected by each of them was measured using a plastic syringe. The gauges were then cleaned and subsequently replaced in the propagation path for the next test. This procedure was repeated for three test periods for different rain intensities. The volume of water collected over each test period allowed the rain rate to be determined for the test period. The rain rate calculation for each test period is as follows. The volume collected by the rain gauge in terms of its collecting diameter is given by the formula

$$V = \pi \frac{d^2}{4} h \tag{4.3}$$

where V is the volume collected (m^3), d is the diameter of the collecting gauge (m) and h is the height of the water in the collecting gauge (m). In the controlled tests, a plastic syringe was used to measure the volume of water in millilitres (ml) collected in each gauge. The first stage was to calculate the height of the water collected in each gauge. The standard measurement for rain rate is millimetres per hour (mm/hr) which is a height measurement. It was necessary to convert the volume measurement in ml to a height in mm. This was achieved by using the following formula

$$h = \frac{4V \times 1000}{\pi d^2} = \frac{1273V}{d^2} \tag{4.4}$$

where V is the volume (ml), d is the diameter (mm) and h is the height (mm).

An illustration of this calculation is perhaps best given by example. Suppose a water volume of 4ml is collected in a cylindrical rain gauge of diameter 70mm, the equivalent height in the gauge for the test period was given by

$$h = \frac{1273 \times 4}{(70)^2} = 1.039\text{mm} \tag{4.5}$$

The standard units for rain rate measurements are in mm/hr; it is necessary to multiply the height result by the number of test periods that occur in one hour so that the

rain rate per test may be scaled to a rain rate per hour value. Each of the test periods was 2 minutes in length. Consequently, the equivalent hourly rain rate in this example is therefore 31mm/hr. This procedure was followed for the determination of the three rain rates used in the secondary testing. Once the rain rate measurement was known they could be correlated to attenuation (power loss) measurements of the optical beam. The results of these secondary tests are presented in chapter 5.

In this chapter, the experimental work for this research was described. These included the network tests conducted in the first ATM network in DIT. This was followed by a description of the specific tests conducted to determine the rain rate attenuation relation at optical frequencies under natural rain and simulated rain conditions. The reasons for conducting the tests were outlined and some of the findings and problems of the experimental work were discussed. In the next chapter, the results of the experimental tests are presented.

5 RESULTS & DISCUSSION

5.1 ATM Network Experimental Tests

5.1.1 Results

In this section, the results of the ATM network tests are presented. The ATM network tests were carried out to illustrate the effects of rain on the performance of a laser link operating as a wireless link in a communications network. These preliminary tests were not intended to provide detailed investigation of the impact of rain effects on the laser transmission but rather to show that the effects exist. The availability of the laser link used in the ATM network was monitored using the network monitoring software Linkview over a 26-day period and the results were correlated with rainfall statistics.

A sample section of a Linkview alarm table is shown in figure 5.1. Typically wireless link performance is quantified by a parameter known as the availability. The availability is a percentage measure that is computed based on the ratio of total length of time that the link is online and available for transmissions to the total length of time that the link is switched on. The alarm tables were used to calculate the percentage availability of the laser on a daily basis. Graph 5.1 plots the daily percentage availability alongside the daily-accumulated rainfall statistics obtained over the same 26-day period by Met Eireann. The same results for the availability and rainfall are plotted directly in graph 5.2. In some instances it was noted that the same rainfall was measured on different days, in these cases the availability values given are average values. A linear fit with intercept at 100% describing the relationship between the availability and rainfall is also included.

Begin			End	
Pos.	Date	Time	Date	Time
001	31.07.2000	07:47:54	31.07.2000	07:47:56
002	01.08.2000	09:04:05	01.08.2000	09:04:12
003	01.08.2000	09:34:48	01.08.2000	09:34:48
004	01.08.2000	15:46:39	01.08.2000	15:46:42
005	01.08.2000	16:01:29	01.08.2000	16:01:30
006	02.08.2000	10:45:24	02.08.2000	10:45:24
007	02.08.2000	11:06:16	02.08.2000	11:06:16
008	04.08.2000	13:09:50	04.08.2000	13:09:52
009	05.08.2000	11:40:53	05.08.2000	11:40:54
010	05.08.2000	11:41:07	05.08.2000	11:41:12
011	05.08.2000	14:40:13	05.08.2000	14:40:16
012	05.08.2000	18:10:40	05.08.2000	18:10:40
013	05.08.2000	18:13:16	05.08.2000	18:13:18

Figure 5.1; *Sample section of a Linkview alarm table*

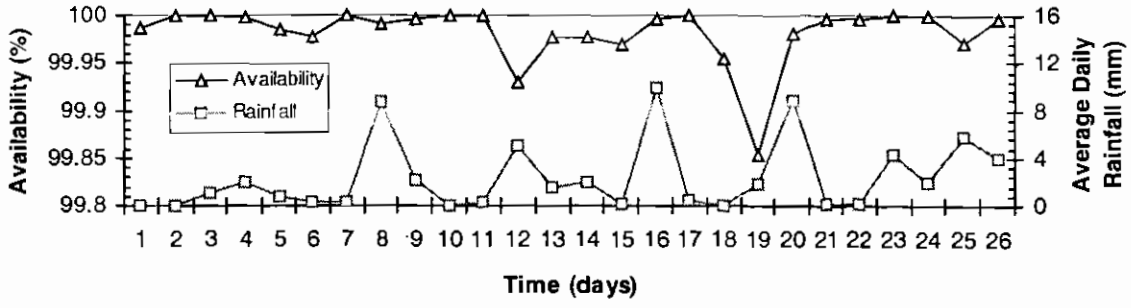

Graph 5.1; *Percentage availability of laser link and accumulated rainfall over a 26 day period*

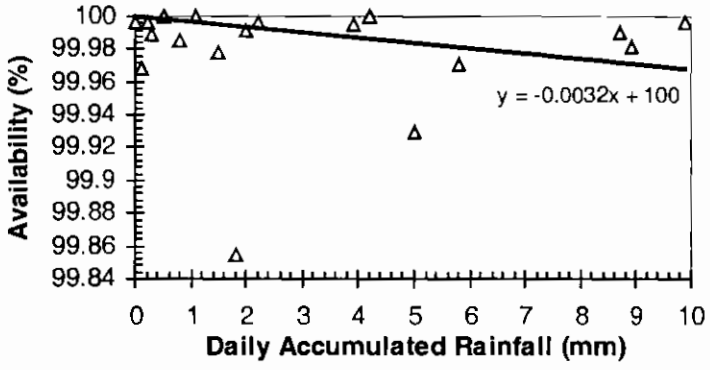

Graph 5.2; *Percentage availability versus accumulated rainfall including linear fit*

5.1.2 Discussion

With reference to graph 5.1 the following points are noted;

- It is evident that a general inverse relationship between availability and rainfall exists. This is most notable on days 12, 13, 14, 19, 20 and 25, which show reductions in availability at the higher relative rainfalls.
- Some discrepancies are also noted. Days 8 and 16 had a relatively high rainfall but no significant reduction in availability (rainfalls of 8.7 mm and 9.9mm, and availabilities of 99.97% and 99.96% respectively are noted). Other discrepancies are on days 12 and 19 days where very low availability values were accompanied by normal rainfall values (availabilities of 99.92% and 99.85%, and rainfalls of 5 mm and 1.8 mm respectively).
- Such discrepancies may be attributed to
    - Location: the rainfall values are recorded at Dublin Airport that is located approximately 7 miles from the network test site. The extent of rainfall is dependent on the rain cloud size. It is possible that

localised rain showers occurred and account for the discrepancies in the results obtained at the different locations.

- Other atmospheric effects such as temperature and humidity may have had an effect on the results obtained. These effects have not been investigated in this project due to lack of resources and time. Further, they are deemed secondary interference effects when compared with rain.
- The cause of the loss of availability of the link may have been other than rain. The location of the laser on a rooftop in an urban area makes birds most likely culprits. The presence of dust particles in the atmosphere that lead to scattering may also be a factor. The presence of such particles is likely to be wind dependent.

With reference to graph 5.2 the following points are noted;

- The linear fit indicates that the availability generally decreases with increasing rainfall, this is as expected. Based on this fit the reduction in availability is 0.0032 %/mm (i.e. for every mm increase in rainfall there is a corresponding decrease in availability of 0.0032%, in real terms this percentage equates to a interruption of 2.7 sec).
- The spread of results is however quite large. While the majority of the results are within 0.036% availability of the linear fit, two of the results deviate significantly. These results correspond to the results of days 12 and 19 that have been discussed previously.

Ultimately these tests have shown that rain has an effect on the performance of the laser link. In analysing the results however discrepancies were observed, this was most noticeable by the spread of data points in graph 5.2. While the cause of these discrepancies may be attributed to many factors, it is most likely due to the difference in location of the laser test site and the rainfall measurement site.

5.2 Short - Range Optical Link Tests (Natural Rain)

5.2.1 Equipment Testing and Calibration Graphs

In the last section, the general ATM network tests were described. In this section, the testing and calibration of the more specific optical link tests conducted to determine an experimental rain rate/attenuation relationship are outlined.

Before the optical link tests were conducted, two calibration tests were performed on the optical link and optical gauge apparatus. The purpose of the first test was to determine the effect of variations in background illumination on the voltage signal. The results of this calibration are shown in graph 5.3. The second tests involved calibration of the rain gauge. This was needed to provide a relationship between the gauge voltage measured and the volume of water collected in the gauge that could be used in analysis of the rain rate later. The rain gauge calibration curve is presented in graph 5.4.

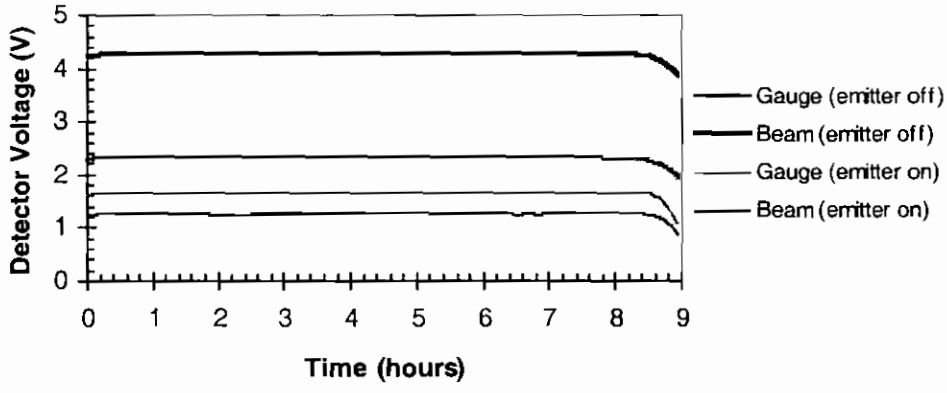

Graph 5.3; *Background illumination test results for rain gauge and beam*

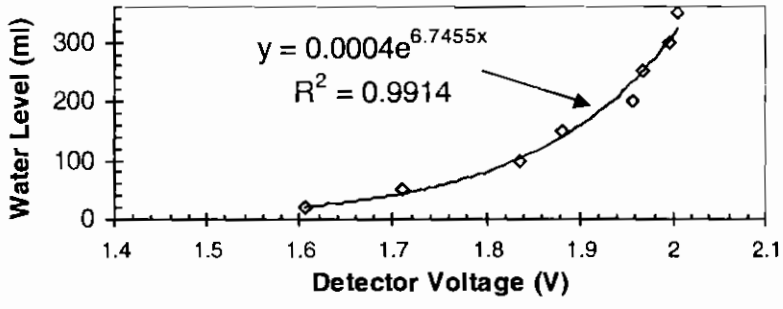

Graph 5.4; *Rain gauge calibration graph including exponential fit*

5.2.2 Results

In this section, the actual results obtained from the optical link and rain gauge tests are presented. The tests were carried out over a total of 30 nights, 8.5 hours per night. Each night the monitoring computer were setup to monitor both the rain gauge and optical link voltages. The rain gauge voltage was sampled at 1,000 Hz for a period of 1 second every minute for the duration of the test. The average of the 1,000 voltage readings measured was recorded. The beam voltage was sampled at 10,000 Hz for a period of one second every 20 seconds for the duration of the tests. The average of the

10,000 voltage readings was recorded. In some cases the complete beam data was captured (10,000 beam voltages) to allow for detailed analysis. This complete data was only captured when a sample voltage deviated from the previous block average by a voltage of 0.2 V. It was neither practical nor necessary to store the complete data for each one-second interval but rather store instances of interruption due to rain. Graph 5.5 below shows samples of the gauge and beam average voltages over two nights. Further nightly graphs are presented in Appendix C.

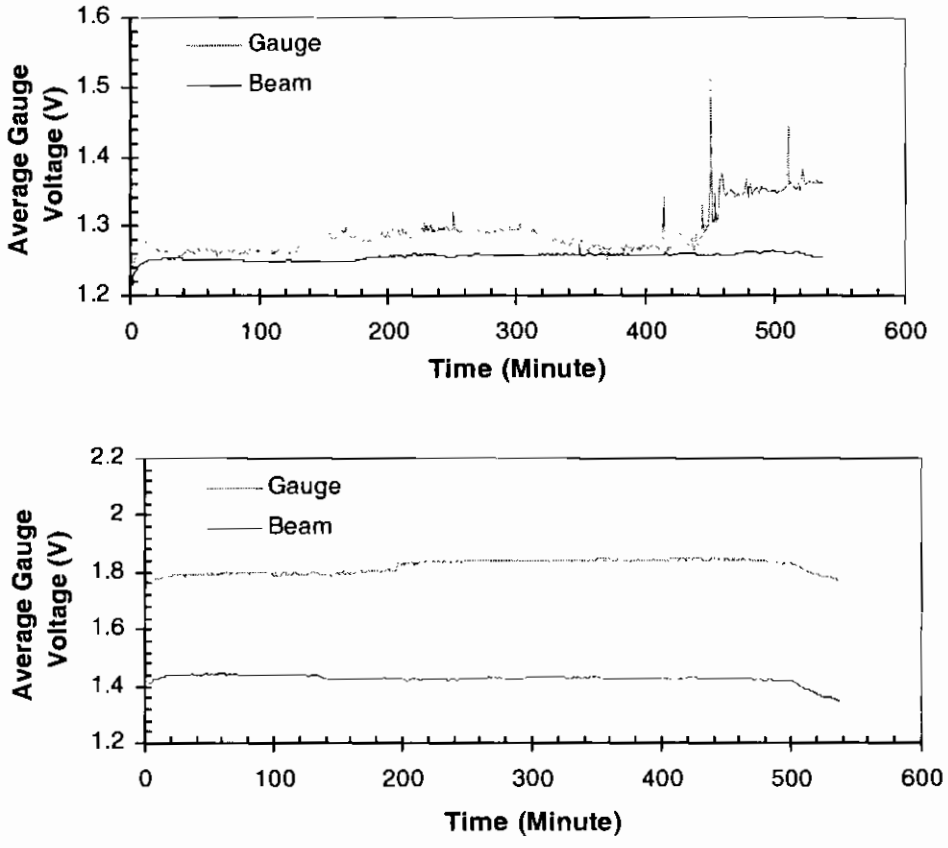

Graph 5.5; *Sample gauge and beam voltage results for two different nights*

Of the 30 nights, it was necessary to select specific areas for further analysis, it was not realistic to analyse the complete data set. Specifically 6 periods of 10 minutes each were chosen, in general these were from different nights. The periods were chosen from regions where a general increase in rain gauge voltage was observed, this was assumed to correspond to a period of rain. The reason for analysing 10 minute periods only was to limit the volume of data requiring analysis (each minute could contain a possible 3 x 10,000 voltage measurements). The minute-average gauge and beam voltage results for the six 10 minute periods are presented in Graph 5.6 and the actual results obtained are presented in tabular form in Appendix C.

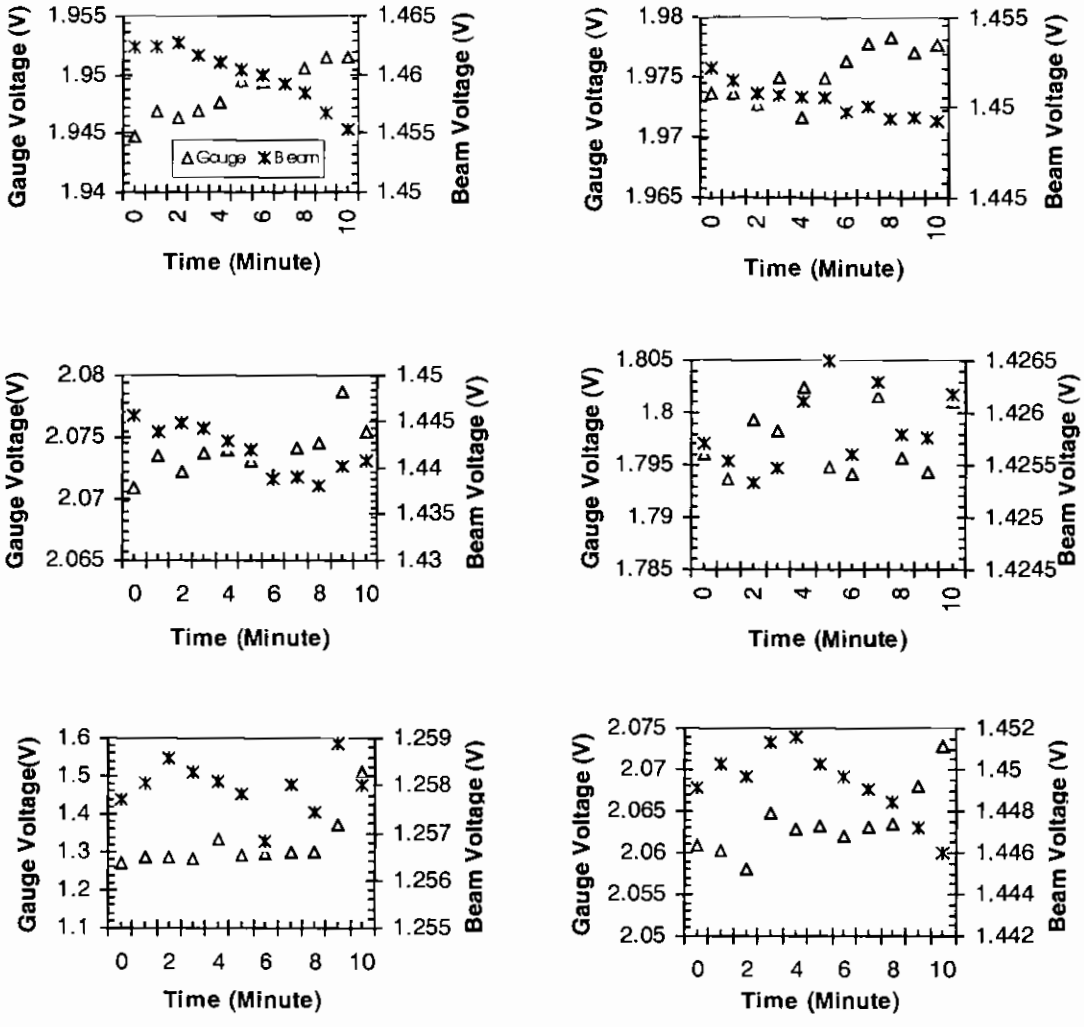

Graph 5.6; *Selected six 10 minute intervals showing minute averages for rain gauge and beam voltages (legend in first graph applies to all)*

The rain rate was calculated by taking the slope of linear fit line to the gauge voltage. This voltage was converted to a water level using the calibration curves presented in Graph 5.4 and extrapolated to give an equivalent hourly rain rate, the results are presented in tabular form in appendix B. The attenuation was calculated for every beam voltage reading in the 10 minute period (possible 10,000 readings every 20 seconds for 10 minutes yielding a maximum 300,000 attenuation calculations) using the formula

$$A = 20 \log \frac{V}{V_{avg}} \tag{5.1}$$

where V is the detector voltage and V_{avg} is the average uninterrupted detector voltage computed based on the histogram of one-second results. In total, 30 attenuation values

were obtained. These are average attenuation values for each 10,000 optical link voltages. Graph 5.7 shows the 30 average attenuation values obtained for each ten-minute period. A single attenuation value was computed by obtaining the average of each of these 30 values for each rain rate and the results are plotted in graph 5.8.

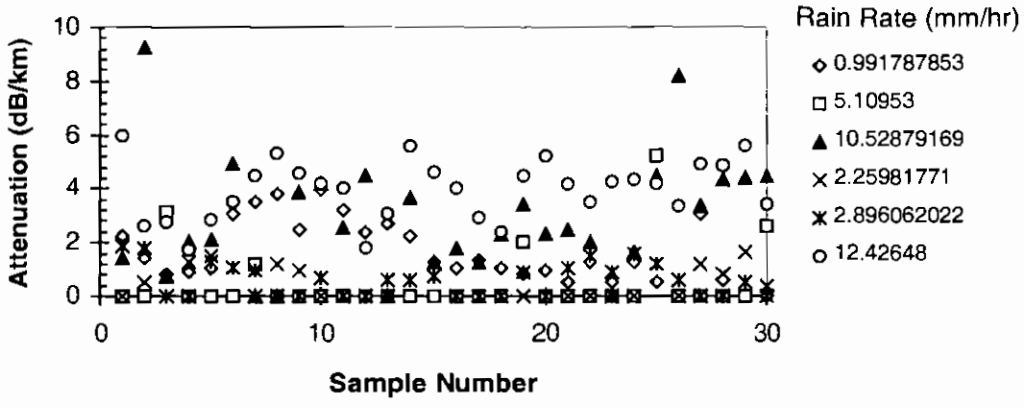

Graph 5.7; *Attenuation versus sample number for selected rain rates*

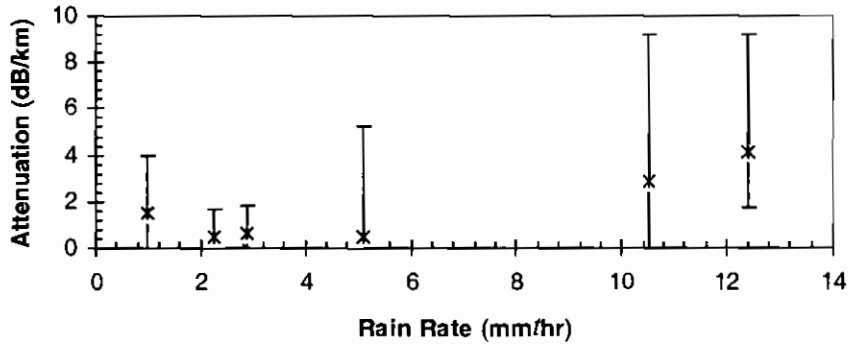

Graph 5.8; *Attenuation versus rain rate for selected periods*

It was also decided to investigate the duration of the interruptions to the optical link. This was achieved by setting fixed attenuation thresholds and determining the number of occurrences of attenuation exceeding that threshold for each rain rate. The result for one of the rain rates is given in graph 5.9. Availability figures were computed based on the number of occurrences of attenuation values exceeding a fixed threshold. Clearly, this is an alternative definition of availability from the traditional concept of availability. However, it is regarded as the most appropriate parameter for the particular experimental work conducted. In this case, the optical link is deemed unavailable when fixed attenuation thresholds shown in graph 5.9 are exceeded. The combined results for the availability of five of the six selected periods are presented in graph 5.10.

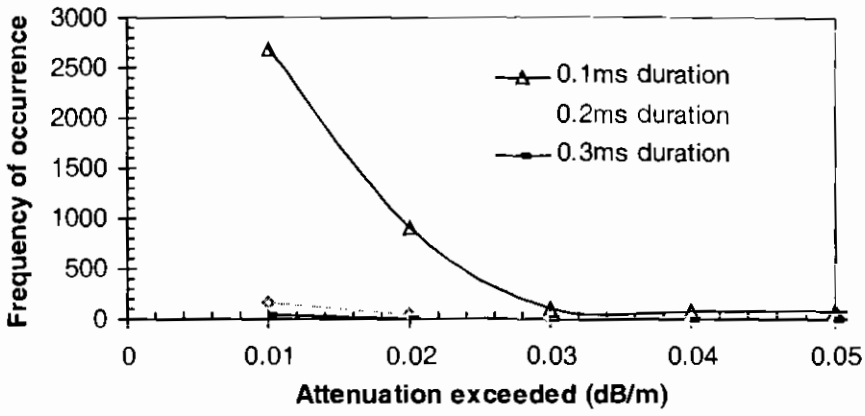

Graph 5.9; *Frequency of occurrence versus attenuation exceeded for a sample rain rate (R = 0.99 mm/hr)*

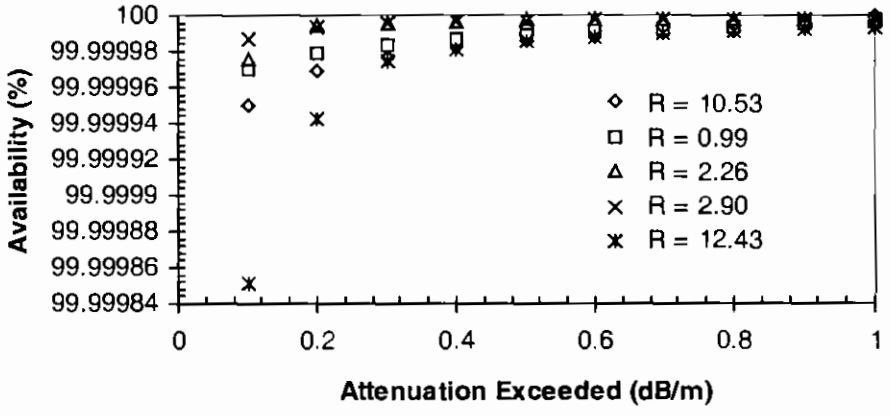

Graph 5.10; *Availability versus attenuation exceeded for 5 of the selected rain rate periods*

5.2.3 Discussion

The following points are noted from the ambient light graph 5.3 and the rain gauge calibration graph 5.4:

- The effect of background illumination changes over a night are insignificant, variations in the four signals shown in graph 5.3 over the central section only (i.e. omitting the coming on and going off sections) are in the order of 0.1% to 1.7%. The standard deviations for the gauge-off, beam-off, gauge-on, beam-on are 0.0018, 0.0003, 0.0027 and 0.0023 respectively.
- The form of the calibration graph takes an exponential form, correlation with an exponential fit is found to be in excess of 99%.

With regard to the analysis of optical test results the following points are noted;

Nightly Graphs

- Two nightly graphs were presented in the graphs 5.5. A huge amount of variation between graphs was observed, in particular the rain gauge results were found to fluctuate excessively.
- Rain Gauge Results
  - The rain gauge signal was observed to behave erratically over both long (night to night) and short (within a night) periods.
  - The form of the signal could be broadly classified as increasing, static and decreasing. The former two states would be expected to correspond to wet (rain falling) and dry periods. The latter state however does not correspond to any expected behavior. A fall in voltage can only be attributed to an increase in the amount of power received at the detector. In practical terms the most likely causes are (i) increase in the ambient lighting conditions, while attempts were made to minimise the amount of light entering the rain gauge container it is possible that light may have entered at some point and affected the readings (ii) evaporation of the collected rain from the gauge (iii) turbulence of the collected rainwater, any movement of the water in the gauge column would lead to fluctuations in the results. It should be noted that these factors might also have an effect on regions where the behavior fell within the increasing and static classifications.
  - For 6 selected nights the rain gauge signal was visually divided into regions of increasing, static and decreasing behavior (note: period of detector coming on line and going off line are not included). For illustrative purposes the division of one night's signal is presented, graph 5.11. The results for the six selected periods were compiled and are presented in pie chart form in graph 5.12. The individual classification for each period is depicted graphically in Appendix C.

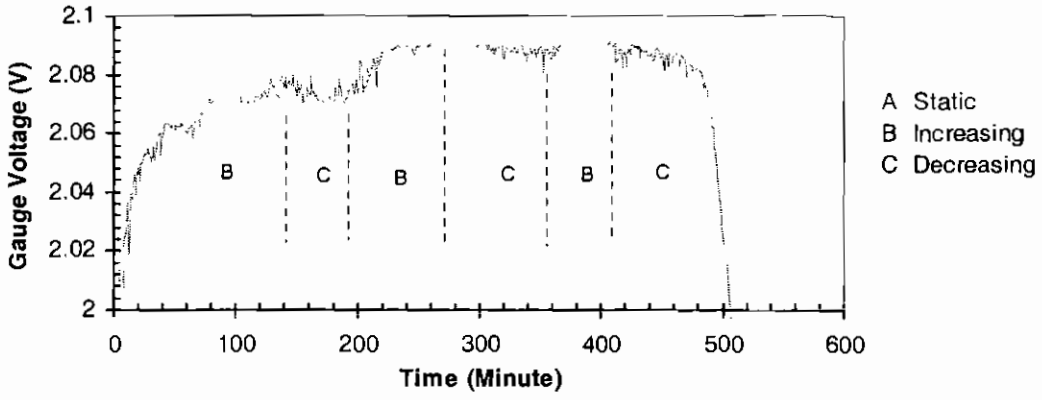

Graph 5. 11; *Classifications of gauge voltage behaviour for a selected night*

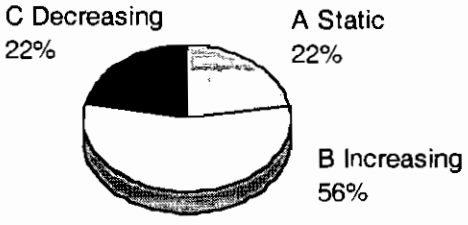

Graph 5.12; *Classification of gauge voltage behavior for 6 selected periods*

- Graph 5.10 (pie chart) shows that the rain gauge is behaving unexpectedly for 22% of its operation. This behavior reflects badly on the operation of the device and our confidence on the accuracy of the other results (increasing and static).

Selected 10 Minute Intervals

- Despite the variations in the nightly graphs and the potential problems with the rain gauge readings it was decided to proceed with an investigation of what appeared to be promising sections of the results (i.e. regions where the rain gauge voltage was observed to increase over time as would be expected with rain). These results were processed and rain rates and attenuations were calculated.

The following points are noted from Graphs 5.7 and 5.8;

- The range of calculated rain rates is between approximately 1 mm/hr and 12 mm/hr which is a typical range for a maritime climate.
- The range of attenuations is up to approximately 9 dB/km. Comparison may be made to attenuation at lower frequencies where attenuation in this range is widely documented [Pratt and Bostian, p. 324][Olsen et al., pp. 323-324].
- The degree of scatter from graph 5.7 does not indicate any immediately obvious trend. The majority of points lie in the 0 to 6 dB/km range. There are several points

where the zero attenuation has been calculated; these predominantly correspond to the lower rain rates.

- The overall averages are plotted in graph 5.8, the error bars indicate the maximum and minimum values. Within each rain rate there is significant variation in the calculated attenuation, this is most pronounced for the three highest rain rates. The scatter may be attributed to a number of factors including
  - Experimental Apparatus: There are a number of noise sources in the experimental apparatus. These include thermal and electrical noise generated in the receiver circuitry and entire assembly housing the circuitry, which may cause interference to the detector voltage. The sensitivity of the detector to other signals other than the laser signal (i.e. background illumination with infrared frequency components) may also impact.
  - Experimental Procedure: In the analysis of the raw data it is necessary for the user to set a threshold limit to eliminate noise. As this threshold limit varies for each set of data, it is possible that some results include some attenuation due to noise while other results exclude some attenuation due to rain.
  - System Complexity Issues

    Size and shape of rain particles: The diameter of rain particles may vary from a fine spray to sizable drops, typical range 0 - 5.8mm. The shape of these particles is dependent on drop diameter, small particles may be approximated by spherical particles, larger drops deviate from a spherical form, with the horizontal width of the drop exceeding the vertical width. Drops are also subject to shape deformations as they pass through a turbulent atmosphere.

    Trajectory of rain particles: The path taken by the particles through the beam is also deemed to affect the amount of attenuation caused. Drops interrupting the beam completely will cause a higher degree of attenuation than those only partially intersecting the beam will. Further, drops entering the beam path close to the emitter where the beamwidth is narrow may cause a larger amount of attenuation than those drops further away from the emitter. The velocity of the drop determines the length of time that the drop is interrupting the beam. This is dependent on drop size.
  - Finally, the problems with the rain gauge previously noted must be considered.

- The form of graph 5.8 shows a possible increase in attenuation with increasing rain rate. This trend is perhaps best described by fitting trendlines to the data. Graph 5.13 shows the attenuation versus rain rate data fitted with both a linear and logarithmic trendline.

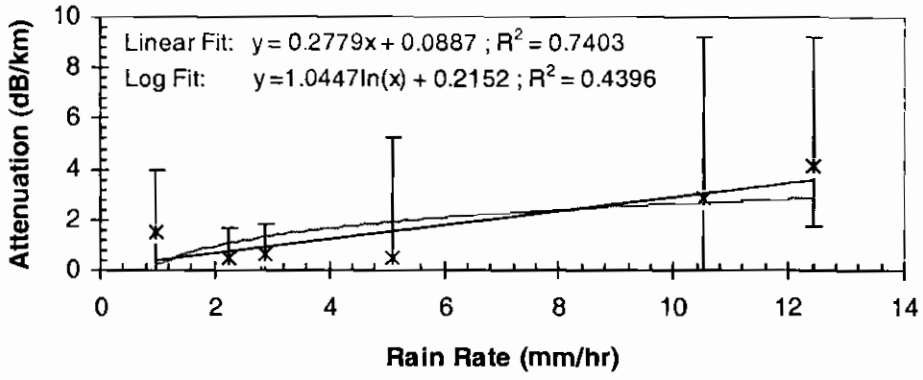

Graph 5. 13; *Attenuation versus rain rate with linear and logarithmic fits*

- It can be seem from both fits that the general trend is towards an increase in attenuation with increasing rain rates. The fits to the data are however not very well correlated. The linear fit has a correlation coefficient of 0.74 while the logarithmic fit has a correlation coefficient of only 0.44. A linear relationship between attenuation and rain rate has been documented in the literature for lower frequencies [after Pratt and Bostian, p. 324][Olsen et al., p 325].
- While a relationship between attenuation and rain rate was found, the manner in which results were selected and analysed may not be truly representative of the entire data set. In total, only six 10 minute intervals were analysed and these were for regions where the gauge behaviour was increasing. It was decided to undertake a further series of tests under more controlled conditions, in particular the duration of the test was shortened and the rain rate measured in a different manner. The results of these tests are presented in the following section.

With regard graphs 5.9 and 5.10 the following points are noted;

- The number of occurrences of attenuation values exceeding a fixed attenuation threshold decreases with increasing attenuation threshold, as expected. The larger numbers of occurrences occur at the lower attenuation thresholds and the number of occurrences fall off rapidly as attenuation threshold increases.
- The probability of an attenuation value being exceeded for more than 0.1ms is far smaller than the probability of the attenuation.

- The availability computed based on the number of occurrence of attenuation values exceeding a fixed attenuation threshold decreases as the rain rate increases.
- The availabilities determined here are in excess of 99%. This is deemed to be sufficiently reliable for an optical communications link.

In this section, the results of the experimental tests conducted on the short-range optical wireless link were presented. As the optical rain gauge did not perform properly in some instances, it was decided to conduct further experimental testing, using the same optical link apparatus but employing a different method of rain rate measurement. These further tests were also conducted using a different method of rainfall generation, using a controlled apparatus. The results of these tests are described in the following section.

5.3 Short - Range Optical Link Tests (Simulated Rain)

5.3.1 Results

The controlled tests were undertaken at three different rain rates. The rain rate was recorded mechanically using three gauges placed along the propagation path. The volume of water collected in these gauges was recorded and used to calculate an average rain rate for the test. The diameters of the gauges as well as the individual rain rates measured by them are presented in Appendix C. The main results are presented in graph 5.14.

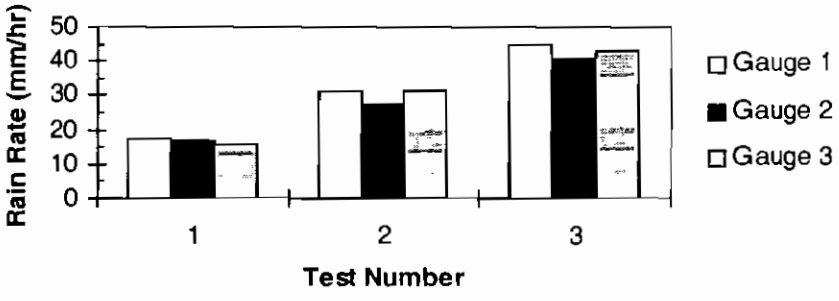

Graph 5.14; *Rain rate results for controlled tests*

The size of drops produced in the controlled tests was investigated. This was to allow comparison of the simulated drop size with naturally occurring drop sizes to ensure that the simulation was somewhat realistic. Collected drops were weighed and their diameter calculated based, for simplicity, on the assumption of spherical geometry. The actual results are tabulated in Appendix C. The range of drop diameters and their frequency of occurrence are shown in graph 5.15.

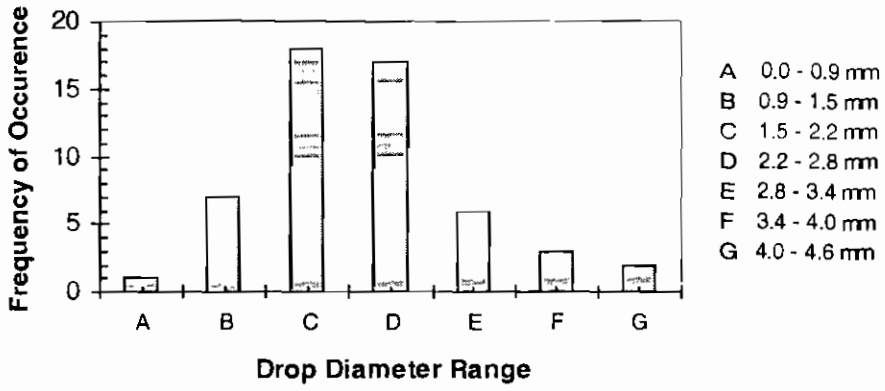

Graph 5.15; *Range of drop diameters generated and frequency of occurrence*

The terminal velocity of the drops was also investigated. Based on the results obtained by Gunn and Kinzer for the terminal velocity of raindrops the distance required for the drops to reach terminal velocity was determined using the formula

$$v^2 = u^2 + 2as \tag{5.2}$$

where v is the terminal velocity (m/s), u is the initial velocity (m/s), assumed to be equal to zero, a is the acceleration due to gravity (9.81m/s) and s is the distance (m). The distance required for drops in the 0 - 5.8mm range to fall in order to reach their terminal velocity are presented in graph 5.16. The third order polynomial expression shown was found to provide a good fit to the experimental results of Gunn and Kinzer.

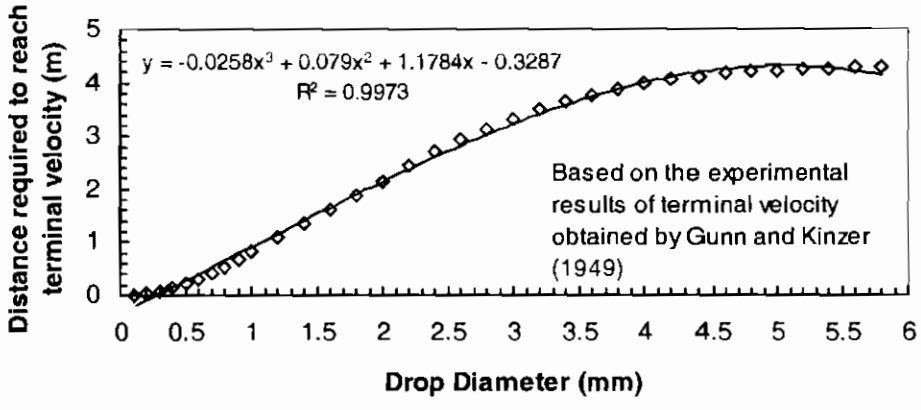

Graph 5.16; *Distance required to reach terminal velocity versus drop diameter*

During each test, the beam was monitored 6 times for a 1-second period at 10kHz (10,000-voltage recordings). The total test time was 2 minutes. Every 20 seconds, a file containing the 10,000 voltage samples taken at that second was stored. Each of these 10,000 voltage files was analysed to determine the attenuation values for each rain rate. Graph 5.17 shows a sample of 2,000 voltages stored for one of the test periods.

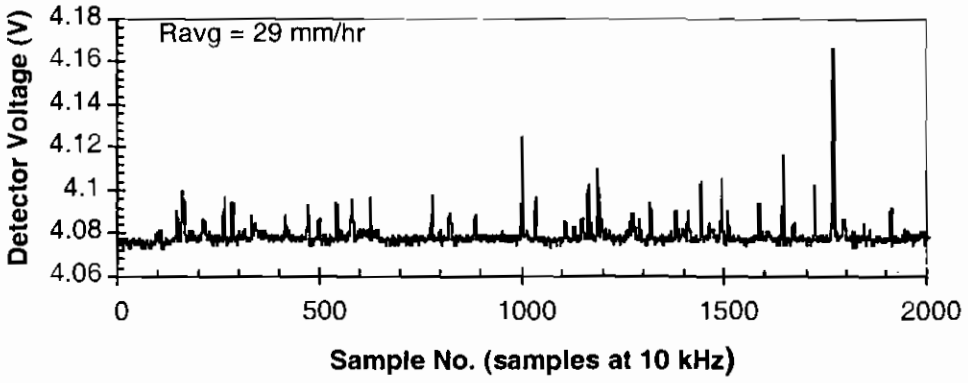

Graph 5. 17; *Typical 2,000-sample optical link voltages*

The blocks were then analysed to calculate the attenuation over the test period. The first stage involved calculation of average voltage for an uninterrupted beam to be used as a reference level. This average was obtained by using the histogram function, which allowed consideration of the voltage ranges and frequency of occurrences within these ranges. A high number of occurrences in the lower voltage ranges were assumed to be noise peaks. Other peaks assumed to be due to rain interruptions were omitted from the average calculation. The next stage was to determine a threshold voltage level to distinguish noise fluctuations from rain interruptions. The threshold voltage could be varied as required and graphically plotted against the detcctor voltages over the entire sample range. Graph 5.18 shows the average and threshold voltage levels for a 200-sample section of the previous graph 5.17.

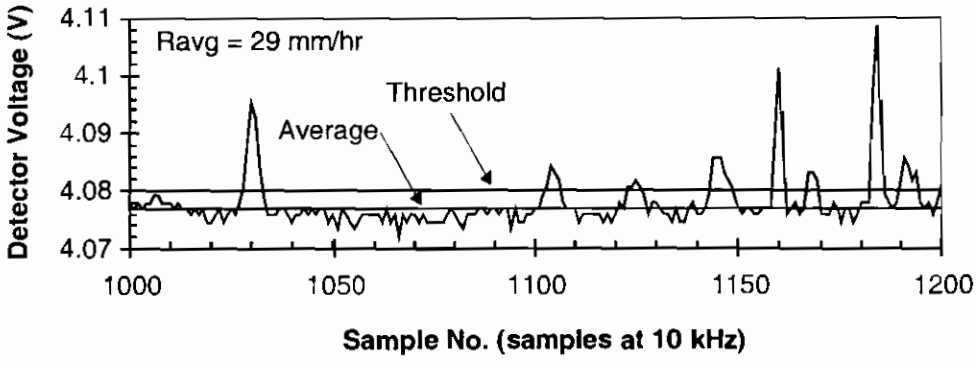

Graph 5.18; *Close-up of 200 samples of above block showing Threshold, average and actual detector voltages*

The final stage was to calculate the attenuation. This was calculated using the following formula

$$A = 20 \log \frac{V}{V_{avg}} \tag{5.3}$$

where V is the detector voltage and V_{avg} is the average uninterrupted detector voltage as described previously. For voltages that lie below the threshold (assumed noise), the detector voltage, V was set equal to the average uninterrupted detector voltage V_{avg}, yielding an attenuation of 0 dB/km. For voltages that lie above the threshold voltage, the actual detector voltage was used, giving an attenuation value.

Graph 5.19 plots the average attenuation for 50 groups of 200 voltage readings. The actual attenuation values are presented in tabular form in Appendix C. The combined average attenuation of these groups is presented in graph 5.20 for each rain rate.

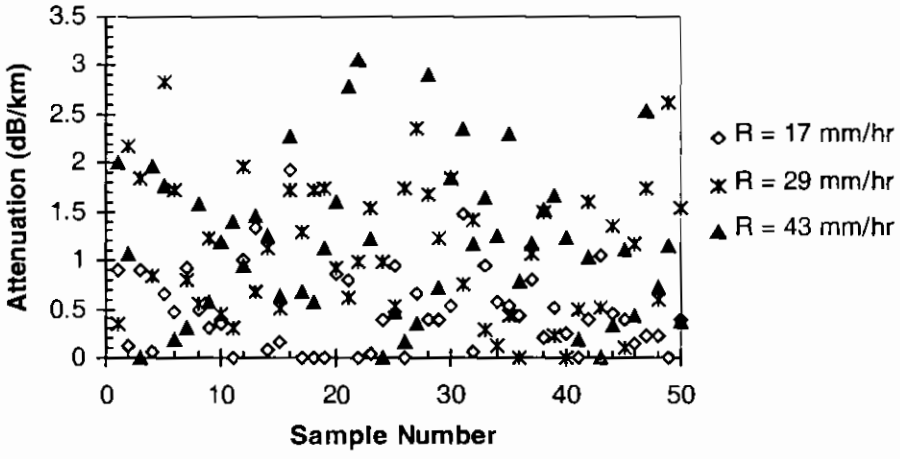

Graph 5. 19; *Attenuation against sample number for simulated rain rates*

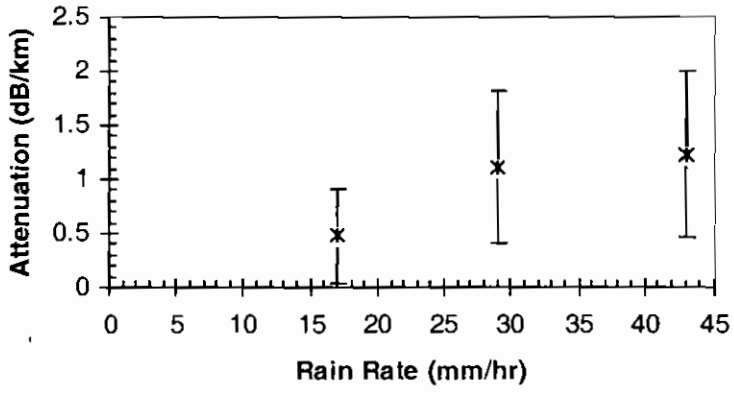

Graph 5. 20; *Attenuation versus rain rate for controlled tests*

5.3.2 Discussion

The following points are noted from the rain gauge results graph 5.12;

- The average rain rates obtained from the graph were 16.7 mm/hr, 29.4 mm/hr and 42.8 mm/hr.

- The spread (difference between maximum and minimum) of rain rates for the three tests is 1.9 mm/hr, 4.0 mm/hr and 4.1 mm/hr. This difference may be accounted for in;
    - Location of gauges: The three gauges were located at different points along the beam path and so are subject to minor variations in rain intensity which would result from the manner in which the spray was generated.
    - Problems encountered when measuring the volume of water collected: These included ensuring that all the fluid collected in the gauge was drawn into the syringe. It was noted in all cases that a small amount of water remained in the gauges (usually water which had adhered to the side walls and gradually flowed to the base of the gauge). The accuracy of the syringe was sufficient. It was possible to read the syringe graduations to approximately 0.125 ml (1/8 ml), this would result in an error only 0.03 mm for the gauges used.
- Based on the spread of results and for ease of future reference the rain rates computed for the three tests are rounded to 17 mm/hr, 29 mm/hr and 43 mm/hr. While these figures equate to medium to high rainfall rates in the Irish climate they ensure that the beam (only 1m in length) is subject to sufficient interruptions and allow attenuation values to be determined.

The following points are noted from the investigation of drop diameters graph 5.13;

- Drops in the 0 to 4.6 mm range were measured. This compares favourably with the commonly accepted range of 0 to 5.8 mm noted in the literature [Rogers, p. 92]
- The frequency of occurrences shows drops in the 1.5 – 2.8 mm ranges to be most common with fewer drops above and below this range. During the investigation it proved difficult to accurately measure small drops (in the 0 - 1.5 mm range), consequently they were not measured. This would have resulted in an inaccurate representation of drop sizes measured.
- With the exception of the smaller drop diameters, the overall form of the histogram compares well with theoretical and experimental drop size distributions. The original graph 5.13 is shown with a negative exponential fitted to the data for the drop diameter ranges C to G in graph 5.19. The negative exponential form of drop size distribution is widely accepted [Marshall and Palmer, p. 165].

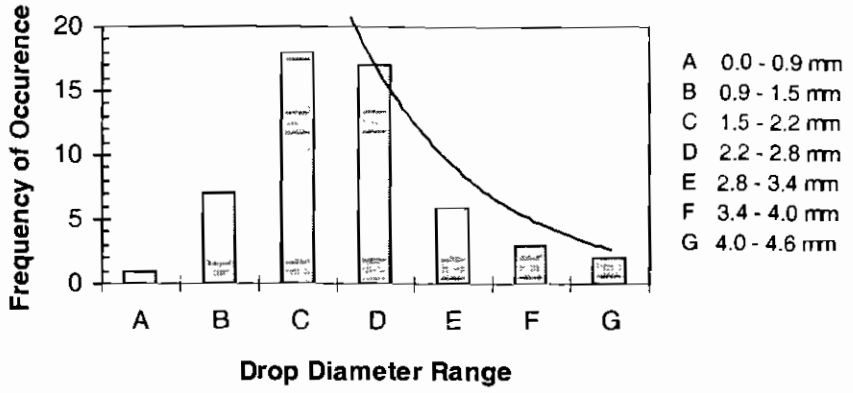

Graph 5. 21; Exponential fit to generated drop diameter histogram

- The combination of these points justifies using the simulated rain approach in the investigation of rain attenuation.

The following points are noted from the investigation of drop height to achieve terminal velocity, graph 5.14;

- Assumptions for the validity of the experimental results obtained by Gunn and Kinzer for the terminal velocities of drops of different sizes.
- For the majoity of drops produced in the simulated test (1.5 – 2.8 mm range), the fall distance required to ensure that the drops fell through the laser beam at terminal velocity was between 2m and 3m.
- According to graph 5.14, the largest drops (5.8mm) required a fall height of 4.28m in order to reach terminal velocity. The actual height from which the simulated rain fell was 4.5m. This is approximately 5% in excess of the maximum height required. Ultimately this indicates that the height used in the tests was sufficient to ensure that the drops were at terminal velocity before entering the propagation area of the beam.

With reference to graphs 5.17 and 5.18 the following points are noted;

- The attenuation range is up to approximately 3 dB/km, which is consistent with values for attenuation due to scattering by rain and dust particles noted by [Lentke].
- The degree of scatter in graph 5.17 does not indicate any obvious trend. The majority of points lie in the lower half of the overall 3 dB/km range and include some zero attenuation values. These zero attenuation values are in general results for the lowest rain rate, 17 mm/hr. Of the points lying in the upper half of the range, the majority correspond to the higher rain rates, 29 mm/hr and 43 mm/hr.

- The overall averages of the individual sample attenuations are plotted in graph 5.18. Despite the high degree of scatter, these results show an evident trend. The attenuation increases with increasing rain rate in a logarithmic fashion. The error bars on the data points represent one standard deviation. There are many possible reasons for the degree of scatter; they may be due to the experimental issues and system complexity issues (inherent).
  - Experimental Issues

    - Experimental Apparatus: There are a number of noise sources in the experimental apparatus. These include thermal and electrical noise generated in the receiver circuitry and entire assembly housing the circuitry, which may cause interference to the detector voltage. The sensitivity of the detector to other signals other than the laser signal (i.e. background illumination with infrared frequency components) may also impact.

    - Experimental Procedure: In the analysis of the raw data it is necessary for the user to set a threshold limit to eliminate noise. As this threshold limit varies for each set of data, it is possible that some results include some attenuation due to noise while other results exclude some attenuation due to rain.

  - System Complexity Issues

    - Size and shape of rain particles: The diameter of rain particles may vary from a fine spray to sizable drops, typical range 0 - 5.8mm. The shape of these drops is dependent on drop diameter, small drops (<0.3mm) in general are described as spherical in shape. Between 0.3mm and 1mm, drop shape is approximated to oblate spheroidal shapes. Above 1 mm, drop shape deviates from both of these geometries. [Nousiainen et al., p. 644].

    - Trajectory of rain particles: The path taken by the drops through the beam also effects the amount of attenuation caused. Drops that fall directly through the beam clearly must cause a higher degree of attenuation than those that only partially fall through the beam. Furthermore, the attenuation is dependent on the position along the propagation path at which the drops enter the beam. Drops intersecting the beam close to the emitter, where the beam divergence is negligible,

may cause larger attenuation than those that enter the beam further along the propagation path. Finally, the velocity of the drop, which is dependent on drop size, determines the length of time that the drop interrupts the beam.

- Finally, it should be noted that the attenuation values calculated are undersized by comparison with the experimental trend shown in graph 5.8. This is because all values below the threshold are assumed to have no effect on signal attenuation. Attenuation due to small particles is thus neglected, being filtered out as noise. Further, the attenuation caused by a large particle is not fully captured since the attenuation in the areas below the threshold (at start and end of interruption) is not accounted for. These losses have not been quantitatively investigated in this project.

In this section, the results obtained for the short-range optical link tests that were conducted under simulated rain conditions were presented. In the following sections, the results of the theoretical work are presented. Initially the results of the basic ATM model are outlined.

5.4 Basic ATM Model

5.4.1 Results

The MATLAB model described in chapter 3 was designed to read in a file that is passed through the various simulated layers of an ATM system and output at the other end. As the channel is assumed reliable the processed file is identical to the inputted file. Consequently, there are no specifically original results to be presented. However, a graphical representation of the contents of a jpeg image file at the different stages in the model is presented in figure 5.2.

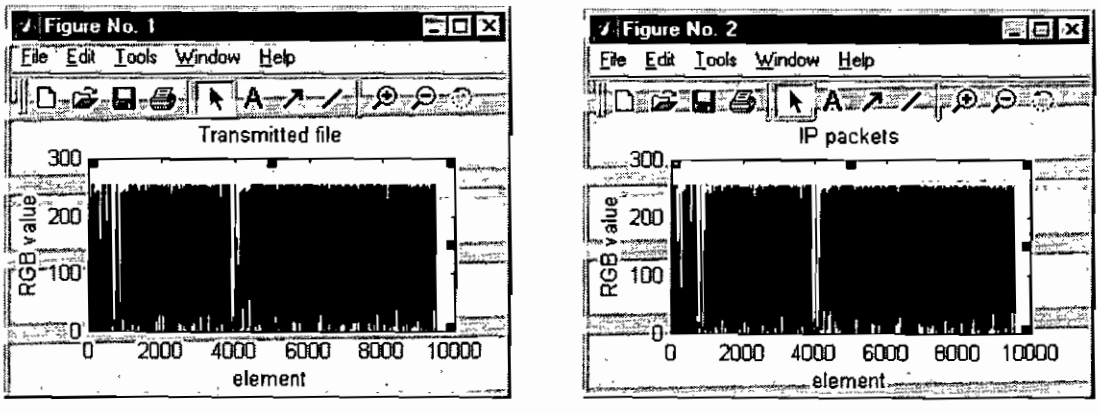

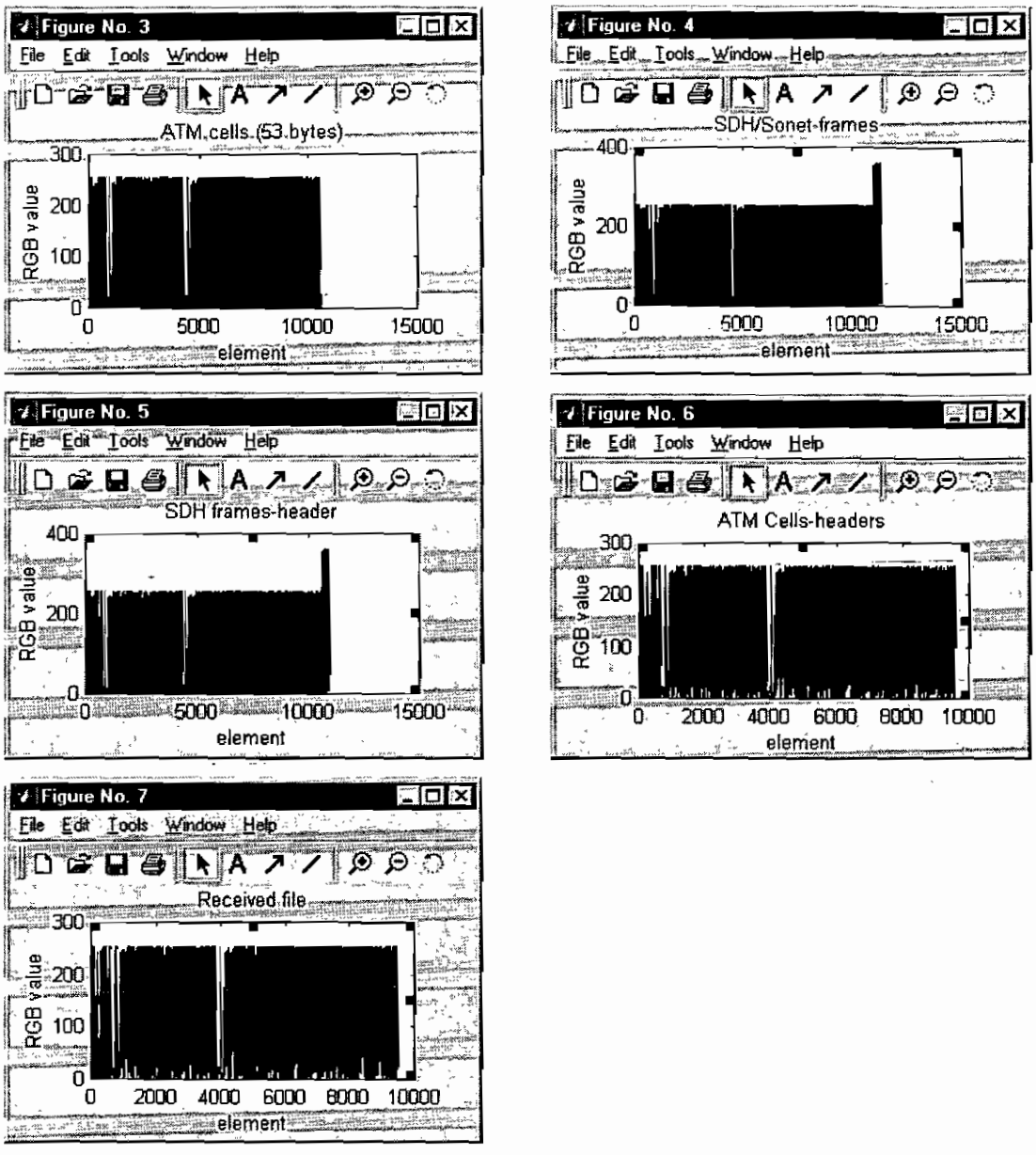

Figure 5.2; *Graphical representation of jpeg image file at the different layers in the simulation model*

5.4.2 Discussion

It may be seen from figure 5.2 that the matrix size increases as the image file is passed through the TCP, IP, ATM and physical layers of the source module due to the addition of header and trailer data. At the destination module, the received file is then stripped of these headers and the file is reverted to its original form. Comparative checks were included between equivalent layers in the source and destination stacks to ensure integrity in the data transfer.

It should be noted however that there are some limitations within the model. These include;

- File Type Limitations: Within MATLAB it is necessary to specify exactly the type of file to be imported, consequently the model was only capable of reading in a limited number of file types, jpeg image files for example. This limitation may be overcome by inclusion of more code. For the purposes of this work this was not deemed necessary.
- Layer Process: Within each layer, information is added to the application data. The specific information added in a real ATM system such as header error checks and addressing was omitted for the purposes of creating a generic ATM simulation model. Such information was represented by random data sequences. The calculation processes for the actual information could be build in to the model.

5.5 Wireless Link Attenuation Model

5.5.1 Model 1 – Existing Theory Results

In this section, the results for the existing theory model outlined in section 3.3 are presented. All results were calculated in MATLAB. The drop size distributions for 3 rain rates are presented in graph 5.22. These distributions are based on the Marshall Palmer negative exponential form. The scattering coefficient for drop diameters in the 0 to 5.8 mm range are presented in graph 5.23. These results were calculated based on the work of Deirmendjian described by [Maitra and Gibbons, p. 658][Olsen et al., p. 321]. Finally, the attenuation versus rain rate results are presented in graph 5.24.

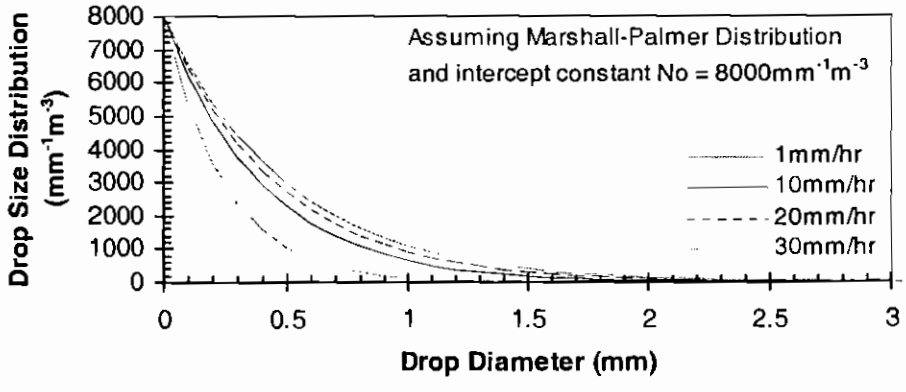

Graph 5.22; *Drop Size Distribution versus diameter for varying rain rates*

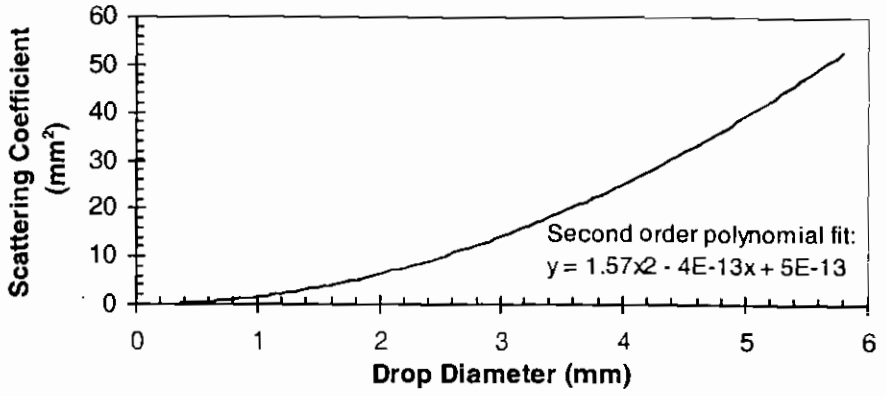

Graph 5.23; *Scattering coefficient versus drop diameter*

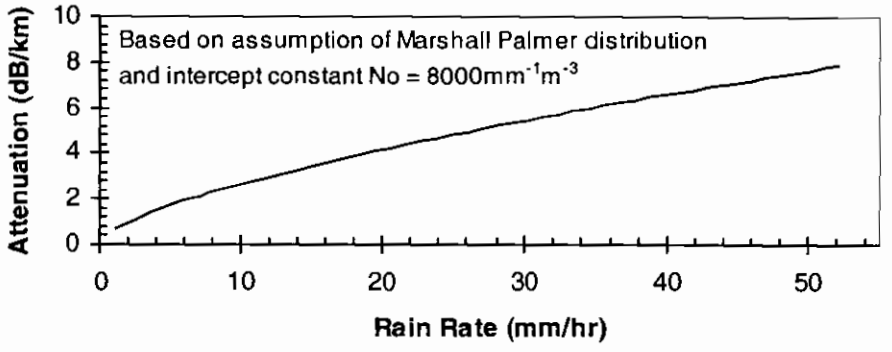

Graph 5.24; *Attenuation versus Rain Rate*

Graphs 5.25 and 5.24 assume that the coefficients N_0, α andβ used in the Marshall-Palmer DSD

$$N(D) = N_0 e^{-\Lambda D}, \ \Lambda = \alpha R^{\beta} \tag{5.3}$$

are valid and constant [Marshall and Palmer, p. 165][Rogers, pp. 137-138]. These have been debated in the literature [Manabe et al., p. 477]. It was decided therefore to analyse these coefficients further. The results of this analysis and the modified attenuation results yielded using modified coefficient values are described in the next section.

A comparison was made between the results obtained using the MATLAB model and those found by solving the attenuation integral equation using calculus. There was found to be little deviation between the results <1% difference at a rain rate of 45mm/hr. The mathematical solution and the comparison of results is presented in Appendix C.

5.5.2 Model 2 – Modified Theory Results

The aim of the modified theory model was to investigate the validity of the Marshall Palmer drop size distribution, in particular the intercept constant N_0. It has been reported in the literature that this parameter is not a constant as proposed by Marshall Palmer but is rain rate dependent [Manabe et al., p. 477].

Graph 5.25 shows a comparison of actual and predicted rain rates using the Marshall Palmer DSD (intercept constant N_0 = 8000 mm^{-1} m^{-3}). Based on the deviation between these results a modified coefficient was calculated for each rain rate. This was achieved by adjusting the coefficient to minimise the error (<1%) between actual and predicted rain rates. The modified N_0 coefficients computed for specific rain rates are presented in graph 5.26. Finally, a plot of the modified attenuation value yielded using the modified N_0 coefficient is presented in graph 5.27.

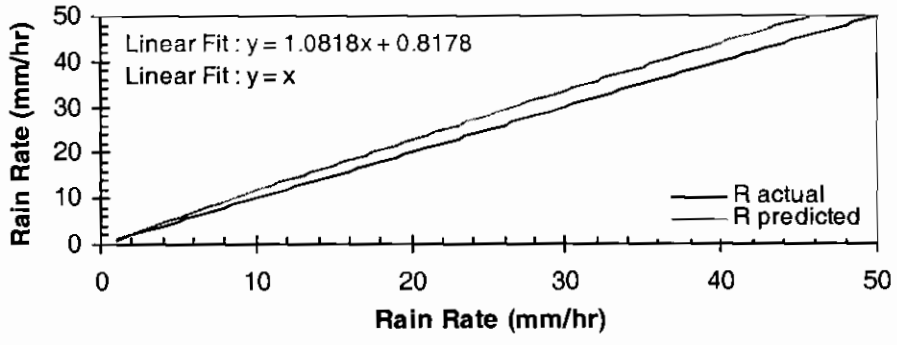

Graph 5.25; *Comparison of actual and predicted rain rates based on the Marshall Palmer DSD using intercept constant No = 8000 mm^{-1} m^{-3}*

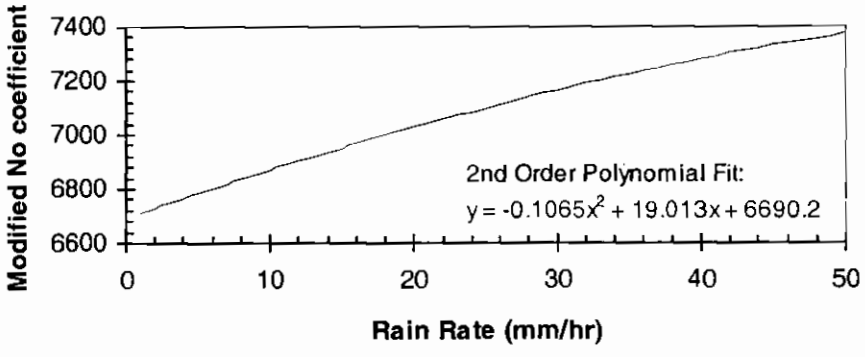

Graph 5.26; *Modified No coefficient versus rain rate*

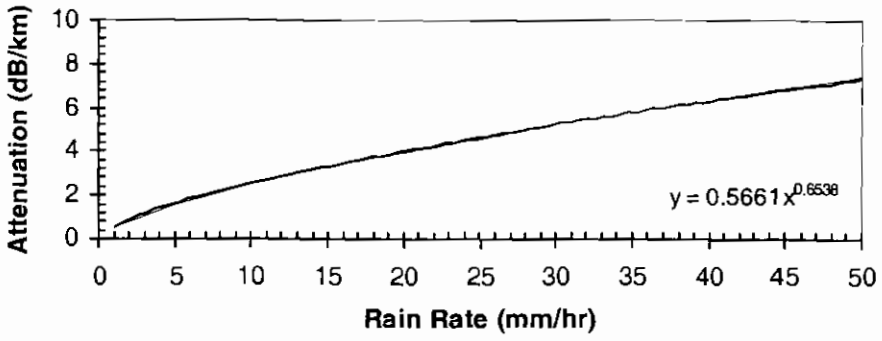

Graph 5.27; *Attenuation versus rain rate using Marshall-Palmer distribution with modified N_o coefficients*

5.5.3 Discussion

Existing Theory

The following points are noted from Graph 5.22 of the Marshall-Palmer DSD and scattering graph 5.23;

- The range of drop diameters for the DSD shown is limited to the 0 to 3 mm range. The DSD was calculated for diameters up to 5.8mm at which size very few occurrences exist.
- The DSD trends for each rain rate are of the assumed negative exponential form with a reduction in the number of occurrences with increasing drop size. As a constant intercept parameter is used all trends have 8000 occurrences per m^3 at the lowest drop diameter (mathematically 0).
- The effect of varying the rain rate is to shift the trend, an increase in the rain rate will result in an increase in the number of occurrences of drop of all sizes. This is best observed in the shifts for 1 mm/hr to 10 mm/hr where there is a 1000% increase in the rain rate. The shift for the latter 3 rain rates, 10 mm/hr, 20 mm/hr and 30 mm/hr, are less prominent where the increases are of the order 100% and 50% respectively.
- With regard Graph 5.23, as the scattering coefficient relationship used was based on a power relation the form of the graph is as expected. The degree of scattering represented by the scattering coefficient increase with increasing drop diameter. The range of the scattering coefficients is between 0 and approximately 50 mm^2.

The following points are noted with regard to the attenuation versus rain rate graph 5.24;

- The rain rate range shown is up to approximately 55 mm/hr. While this rate is not realistic on an hourly basis, the figure could be reached by extrapolating rain rate results taken during a short intense downpour.
- The attenuation range is between 0 and approximately 8 dB/km. This level of attenuation is in the same range as values documented for lower frequency devices in the literature [Lentke]

Modified Theory

The following points are noted with regard to the comparative graph 5.25 and modified coefficient graph 5.26;

- The comparative graph 5.25 plots the rain rate against itself and shows the deviation in the predicted rain rate value calculated using the theoretical rain rate equation and Marshall Palmer distribution (No = 8000 mm-1m-3) from the actual rain rate.
- The form of the deviation is divergent and of the order 8%. This illustrates that discrepancies exist in the theoretical predictions and justifies the investigation into modification of the theory. In this work one parameter was chosen for investigation based on its mathematical dominance, this was the intercept parameter No of the Marshall Palmer distribution.
- The modified No coefficients presented in graph 5.26 show that the coefficient is rain rate dependent as described by [Manabe et al., p. 477] and not constant, as the Marshall-Palmer DSD predicts. The range of coefficients is between approximately 6700 mm^{-1} m^{-3} and 7400 mm^{-1} m^{-3} for rain rates in the 0 to 50 mm/hr. This compares with the constant value of 8000 mm^{-1} m^{-3} as used by Marshall Palmer.
- The form of the modified coefficient graph is that of a 2^{nd} order polynomial.

The following points are noted with regard to the attenuation versus rain rate graph 5.27;

- The attenuation graph based on the modified coefficients is similar in form to the graph obtained using the unmodified constant intercept parameter, graph 5.24. The attenuations result obtained using the modified and unmodified No coefficients are present together in graph 5.28.

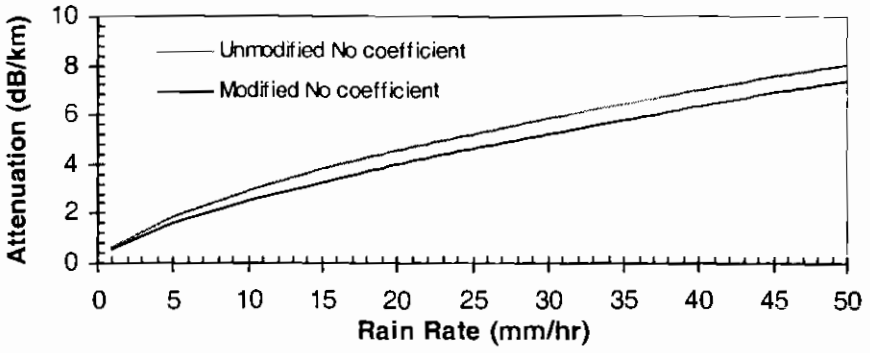

Graph 5. 28; Comparison of attenuation values using modified and unmodified N_0 coefficients

- The main point to note is the reduction in attenuation achieved using the modified N_0 coefficients. While this is a result of the reduced coefficient values presented in graph 5.26 it is in accordance with the literature which reports an overestimation of attenuation by the unmodified Marshall Palmer distribution. The reduction is in the order of 16% at the lower rain rates and drops to approximately 8% at the highest rain rates of 50 mm/hr.

In this section, the results of the unmodified and modified theoretical models developed in MATLAB were presented. In the following section, a comparison is made between the two sets of results obtained during this research, the experimental and theoretical results.

5.6 Comparison of Experimental and Theoretical Results

In this section the experimental and theoretical results are compared and discussed. The overall aim is to assess the validity of the experimental attenuation values in relation to the results predicted by the theoretical models. The combined results of the two sets of experimental attenuation results as well as the two sets of theoretical attenuation values are presented in graph 5.29.

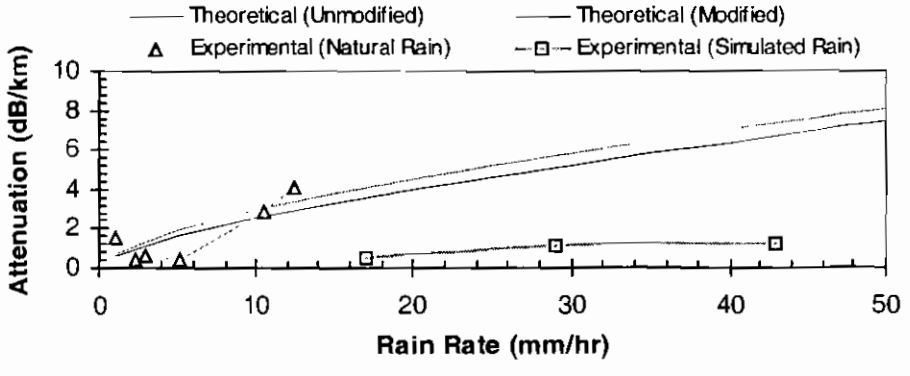

Graph 5.29; Comparison of theoretical and experimental attenuation values versus rain rate

In the following paragraphs, the individual experimental results are compared with the theoretical predictions.

Experimental (Natural Rain)

The results for the natural rain tests are best compared to the theoretical results by plotting the 0 – 15 mm/hr range as shown in graph 5.30 below.

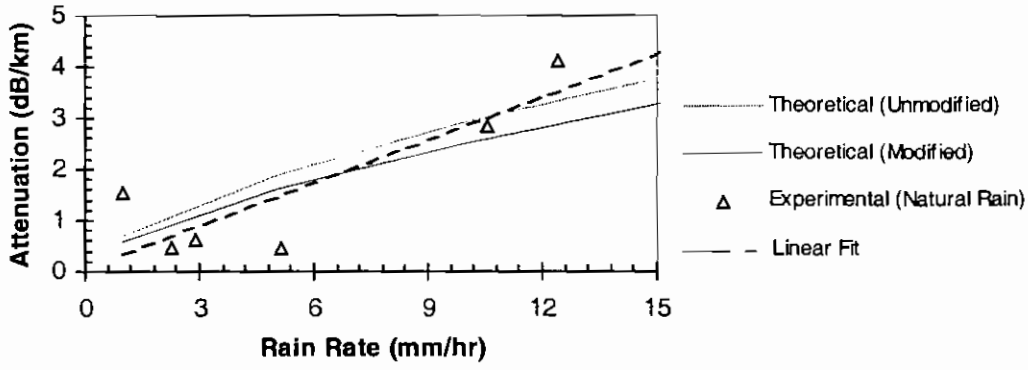

Graph 5.30; *Comparison of experimental (natural rain) results with theoretical attenuation*

Despite the scatter of the averaged experimental results, the general trend reflects the theoretical predictions. The error bars on the experimental data have been omitted for clarity. The linear fit to the experimental data has a correlation coefficient of 0.74. This fit shows reasonable correlation visually with theoretical results in the 0-15 mm/hr range, in terms of both form and magnitude. The modified form shows better correlation with the linear fit in the approximate range 0 – 8 mm/hr after which the unmodified form provides closer correlation. The results do not provide any indication that modification of the intercept parameter improves the accuracy of the model. Recall however that it has been reported that the Marshall Palmer distribution with intercept parameter No = 8000 mm-1 m-3 overestimates the attenuation and that the modified form predicts lower attenuation values.

Experimental (Simulated Rain)

Graph 5.31 plots the experimental results obtained from the short-range optical link tests conducted in simulated rainfall conditions.

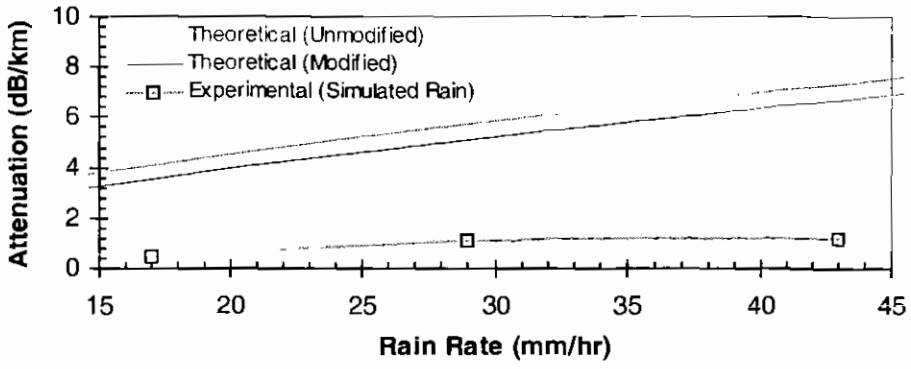

Graph 5.31; *Comparison of attenuation results (simulated rain) with theoretical results*

Clearly, the attenuation results obtained from the simulated tests are far below those obtained from the predictions. Specifically the results are in the order of approximately 6 times lower than theoretically predicted. This level of difference prompts the question, which of the results is correct? Unfortunately, no published data has been found, experimental or theoretical, for the attenuation of links operating in the 10^{14} Hz range. Thus, we cannot conclude that either the theoretical or the experimental results are correct. As a result, it is only possible to discuss limitations of the experimental work and theoretical models that may be lead to inaccurate results and ultimately account for the 6-fold difference in results obtained.

Experimental Work: The setting of the threshold in the analysis of raw data would impact on the attenuation results obtained. While the objective of thresholding is to eliminate noise, it is possible that a large amount of minor attenuations may have also been eliminated. These would correspond to attenuations due to large amounts of small drops.

Theoretical Model: Any theoretical model is developed based on assumptions. In the development of the rain attenuation model the following assumptions that may impact on the validity of the results were made

(i) Assumption of a spherical drop shape: In reality drops tends to flatten out as the drop size increase covering a larger area than their spherical counterparts. This leads to larger drops interrupting the optical beam for shorter periods of time that may results in inaccuracies in the attenuation calculated

(ii) Drop diameter range is assumed to be 0 – 5.8 mm in line with the literature, in reality drop instability occurs when drop reach 3 mm diameter [Rogers, p. 138]. Thus

the theoretical model accounts for attenuation due to drops that may not occur in reality, this would lead to an overestimation of attenuation.

Overall Comments

The results of the natural rain test are promising. The magnitudes of the attenuation compare favorably with the theoretical results. Since the amount of scatter in graph 5.19 is excessive, it is not possible to confidently fit a trendline to the data the experimental results. However, by plotting the overall averages and maximum and minimum threshold, some degree of validation of the theoretical results in the 0 – 15 mm/hr range. The results of the controlled tests conducted using simulated rain are disappointing. It was thought that the tests would provide more accurate results as the test period was shorter and the rain rate measurement more reliable. This was not found to be the case. These results do not provide any validation of the theoretical model in the 15 – 45 mm/hr ranges.

In summary, it should be noted that the natural rain tests undertaken have provided a degree of validation of the theoretical models in the 0 – 15 mm/hr range. Rain rates in this range are typical for the Irish climate. The development of the model is justified and, based on the limited experimental results obtained, may be used to provide an approximate prediction of the rain attenuation at optical frequencies. No experimental evidence has been obtained to support the modified theory over the original form. However, it is noted that the modified form provides lower attenuation values, which concurs with the opinion that the original theory overestimates the attenuation.

In this section, a comparison of the experimental and theoretical results was presented. It was found that the experimental results obtained for the optical link tests conducted under natural rain were in the correct range, as estimated by the MATLAB theoretical model. The results of the optical link tests conducted in the simulated rain environment were not found to agree well with the theoretical predictions.

6 CONCLUSIONS AND RECOMMENDATIONS

In this section, the overall conclusions drawn from this research are presented. Recommendations for future work are also included.

6.1 Conclusions

- The theoretical model developed was based on a modification of existing theory. The attenuation values predicted by this model were found to be lower than those predicted by the unmodified theory. This modification provides results in accordance with the literature that reports an overestimation of attenuation using the existing theory.
- The ATM network tests showed that while rain has an effect on the availability of an optical communications link, it is very difficult to correlate availability results with meteorological rainfall data to a high degree of accuracy.
- In the short-range optical link tests (natural rain), the rain rate was recorded locally over a series of nights. While the rain gauge apparatus proved unreliable in some instances, it was possible to analyse sections of the recorded data and to correlate the rain rate values to corresponding attenuation results. Comparison with theoretically predicted results showed that, despite a degree of scatter, the results were within the correct range. Attenuations of between 0 and 5dB/km were found for rain rates in the 0 -15mm/hr range.
- The short-range optical link tests highlighted the complexity of the system being investigated. This complexity is a result of (i) the variability in the rain rate and attenuation values measured and (ii) the large amount of generated data requiring analysis. These tests indicated that where project limitations such as time, resources etc. exist, simplification of the system by reducing the number of possible variables is necessary.
- The attenuation results obtained for the optical link tests conducted in the simulated rain tests were far below the expected theoretical values. The undersized results may be attributed to the fact that attenuation due to small raindrops was neglected as well as attenuation values that fell below the fixed threshold value.
- Finally, it has also been shown that it is possible to develop a model of a generic ATM network in MATLAB.

6.2 Recommendations

- In terms of experimental work, the manufacture of an apparatus capable of generating repeatable rain rates would remove some of the variability that was experienced in the current work.
- There is also scope to develop algorithms to extract relevant results from the large amount of data captured. This would reduce data analysis time and potentially allow a greater number of experimental tests to be conducted. Ultimately, this would provide results that are more reliable.
- The combination of the points noted above would be beneficial in terms of validating and improving existing theoretical models. Within these models, there are many assumptions that could be re-addressed if more accurate results were available. For example, the drop size distributions and scattering coefficients.
- Finally, a wireless unreliable module could be incorporated into the ATM model. Such a model would provide useful quantitative information (e.g. network downtime) that would allow network managers to foresee network failures and to prepare alternative network solutions (e.g. leased lines, fibres).

REFERENCES

1. D.Y. Al-Salameh, M. T. Fatehi, W. J. Gartner, S. Lumish, B. L. Nelson and K. K. Raychaudhuri, "Optical Networking," Bell Labs Technical Journal, pp. 39-55, January-March 1998.
2. E.E Altshuler, "A Simple Expression for Estimating Attenuation by Fog at Millimeter Wavelengths," *IEEE Transactions on Antennas and Propagation*, vol. AP-32, no.7,pp. 757-758, July 1984.
3. E. Ayanoglu, "Wireless broadband and ATM systems," *Computer Networks*, vol. 31, Elsevier Science B.V., pp. 395-409, 1999.
4. A. Bray, "IP over ATM: A Switch for the better? ", *Telecomunications*, vol. 32, no.10, pp.67-71, October 1998.
5. D. Cavendish, "Evolution of Optical Transport Technologies: From SONET/SDH to WDM," *IEEE Communications Magazine*, pp. 164-171, June 2000.
6. Chen and D. T. Tantiprasut, "Evolution of ATM Internetworking," Bell Labs Technical Journal, pp. 82-96, Spring 1997.
7. R.K. Crane, "The Rain Range Experiment-Propagation through a Simulated Rain Environment," *IEEE Transactions on Antennas and Propagation*, vol. AP-22, no. 2, pp. 321-328, March 1974.
8. R.K. Crane, "Prediction of Attenuation by Rain," *IEEE Transactions on Communication*, vol. Com-28, no.9, pp.1717-1733, Sept 1980.
9. J. Derfler, Jr., *Guide to Connectivity*, California, Ziff-Davis Press, 1991.
10. D.A. de Wolf and A.J. Zweisler, "Rayleigh-Mie Approximation for Line-of-Sight Propagation through Rain at 5-90GHz", *IEEE Transactions on Antennas and Propagation*, vol. 44, no.3, pp. 273-279, March 1996.
11. R. M. Gagliardi and S. Karp, *Optical Communications*, 2nd edition, New York, John Wiley & Sons, 1995.
12. R. Gupta, "The "Glue" of Networks: Looking at IP over ATM," *53 bytes The ATM Forum newsletter*, volume 7, no. 1, February1999.
13. R. Gunn and G.D. Kinzer, "The Terminal Velocity of Fall for Water Droplets in stagnant air," *Journal of Meteorology*, vol.6, pp. 243-248, 1949.
14. S. Haykin, *Digital Communications*, Singapore, John Wiley & Sons, 1988.
15. T. H. Noh, "ATM Scenarios for SDH/SONET Networks", *Bell Labs Technical Journal*, pp. 81-93, January – March 1998.

16. B. Kercheval, *TCP/IP over ATM*, New Jersey, Prentice-Hall, 1998.
17. A. Kapoor and J. Ryan, "Reassessing Networks for an IP Architecture," *Telecommunications*, vol. 32, No. 10, pp. 48-56, October 1998.
18. W.C.Y. Lee, "An Approximate Method for obtaining Rain Rate statistics for use in Signal Attenuation Estimating," *IEEE Transactions on Antennas and Propagation*, vol. AP-27, no.3, pp. 407-413, May 1979.
19. H. Lentke, "Connection of data networks (LAN) directly through the atmosphere using infrared light", CBL GmbH, June 1994
20. Maitra, C.J. Gibbins, "Modeling of raindrop size distributions from multi-wavelength rain attenuation measurements," *Radio Science*, vol. 34, pp.657-666, May/June 1999.
21. T.Manabe, T. Ihara and Yoji Furuhama, "Inference of Raindrop Size Distribution from Attenuation and Rain Rate Measurements," *IEEE Transactions on Antennas and Propagation*, vol. Ap-32, no.5, pp.474, May 1984.
22. J.S. Marshall and W. Palmer, "The Distribution of Raindrops with Size", *Journal of Meteorology*, vol.5, pp. 165-166, Aug 1948.
23. F. Mazda, *Telecommunications Engineers Reference Book*, Oxford, Butterworth-Heinemann, 1993.
24. E.J. McCartney, *Optics of the Atmosphere*, New York, John Wiley & Sons, 1976.
25. J. E. McDonald, "The Shape of Raindrops", *Scientific American "The Physics of Everyday Phenomena"*, W.H. Freeman and Co., pp.23-27, 1979.
26. M. Mead, "Propagation impairment at 28GHz", *LMDS Supplement*, June 1998

Web reference: http://www.americasnetwork.com

27. J. A. Morrison and T.S. Chu, "Perturbation Calculations of Rain-induced Differential Attenuation and Differential Phase Shift at Microwave Frequencies", *The Bell System Technical Journal*, pp.1907-1913, December 1973.
28. J. A. Morrison, M. J. Cross and T.S. Chu, "Rain-induced Differential Attenuation and Differential Phase Shift at Microwave Frequencies", *The Bell System Technical Journal*, pp.599-604, April 1973.
29. D. Niedermiller-Chaffins and D. Heywood, *NetWare Training Guide: Networking Technologies*, USA, New Riders Publishing, 1993.
30. T. Nousiainen, K. Muinonen, "Light scattering by Gaussian, randomly oscillating raindrops," *Journal of Quantitative Spectroscopy & Radiative Transfer 63,* pp. 643-666, 1999.

31. T. Oguchi, "Attenuation and phase rotation of radio waves due to rain: Calculations at 19.3 and 34.8GHz", *Radio Science*, vol. 8, pp. 31-38, 1973.

32. R.L. Olsen, D.V. Rogers and D.B. Hodge, "The aR^b Relation in the Calculation of Rain Attenuation," *IEEE Transactions on Antennas and Propagation*, vol. AP-26, pp.318-328, 1978.

33. A. D. Olver, *Microwave and Optical Transmission*, England, John Wiley & Sons Ltd., 1992.

34. T.Pratt and C.W.Bostian, *Satellite Communications*, New York, John Wiley & Sons, 1986.

35. P. L. Rice and N. R. Holmberg, "Cumulative time statistics of surface-point rainfall-rates," *IEEE Transactions on Communications*, vol. COM-21, pp. 1131-1136, 1973.

36. R.R. Rogers, *A Short Course in Cloud Physics*, 2nd Edition, Pergamon Press, U.K., 1979.

37. C.L. Ruthroff, "Rain Attenuation and Radio Path Design," *Bell Systems Technical Journal*, vol. 49, pp. 121-126, Jan 1970.

38. J. Sander, "Rain Attenuation of Millimeter waves at 5.77,3.3 and 2mm," *IEEE Transactions on Antennas and Propagation*, vol. AP-23, pp.213-220, 1975.

39. S. Schatt, *Understanding Local Area Networks*, Howard W. Sams & Co., 1987

40. M. Sekine, C. Chen, T. Musha, "Rain Attenuation from Log-Normal and Weibull Raindrop-Size Distributions," *IEEE Transactions on Antennas and Propagation*, vol. AP-35, No.3, pp.358-359, March 1987.

41. A. Shtainhart, R. Segal, A. Tsherniak, "WDM: Wavelength Division Multiplexing" web reference: http://www.rad.com/networks/1999/wdm/wdm.html

42. S. D. Smith, *Optoelectronic Devices*, Prentice-Hall International, UK, 1995

43. D.G. Sweeney and C.W. Bostian, "The Dynamics of Rain-Induced Fades," *IEEE Transactions on Antennas and Propagation*, vol. 40, no. 3, pp. 275-278, March 1992.

44. A. S. Tanenbaum, *Computer Networks*, 3rd edition, Prentice-Hall International, 1996, NewJersey

45. Tangney and D. O'Mahony, *Local Area Networks and their applications*, Prentice-Hall, 1988, UK

46. E. Uiga, *Optoelectronics*, Prentice-Hall, Inc., New Jersey, 1995

47. K. Washburn and J. Evans, *TCP/IP, running a successful network*, 2nd edition, Addison-Wesley, 1996, UK

48. K. N. Wulfsberg and E.E Altshuler, "Rain attenuation at 15 and 35GHz", *IEEE Transactions on Antennas and Propagation*, vol. AP-20, no. 2, pp. 181-187, March 1972

49. C. Zacker, *TCP/IP Administration*, IDG Books Worldwide Inc., 1998, California

50. A.M. Zavody and B.N. Harden, "Attenuation/ rain-rate Relationships at 36GHz and 110GHz," *Electronics Letters*, vol. 12, no. 17, August 1976.

Bibliography

1. M. Allon, "Opting for the Hybrid," *Telecommunications*, vol. 33, no. 5, pp. 57-60, May 1999.
2. S. Arora and A. Nagpaul, "Broadband Wireless Solutions for Global Business," *Telecommunications*, vol. 32, no. 9, pp. 83-86, September 1998.
3. W.F. Bodtmann and C.L Ruthroff, "Rain Attenuation and Short radio Paths-Theory, Experiment and Design," *Bell Systems Technical Journal*, vol. 53, no.7, pp. 1329-1350, Sept 1974.
4. J. Cunliffe, " Networking at the speed of light," *Telecommunications*, vol. 33, vo. 6, pp. 56-58, June 1999.
5. K. Gibson, "Towards a Photonic Future," *Telecommunications*, vol. 33, no. 3, pp. 63-72, March 1999.
6. J. Goldhirsh, "Rain Cell Size Statistics as a Function of rain rate for Attenuation Modeling," *IEEE Transactions on Antennas and Propagation*, vol. AP-31, no. 5,pp. 799-801, Sept 1983.
7. Hac and H. Lin, "Congestion Control for ABR traffic in ATM network," *International Journal of Network Management 9*, John Wiley and Sons, Ltd. 1999
8. D.B. Hodge, "Frequency Scaling of Rain Attenuation," *IEEE Transactions on Antennas and Propagation*, pp. 446-447, May 1977.
9. E. Lewis, *Communication Services via Satellite*, 2nd edition, Butterworth-Heinemann, 1992.
10. P. J. Lombardi, "Solving the Gigabit Challenge," *Telecommunications*, vol. 33, no. 4, pp. 41-44, April 1999.
11. S.N. Livieratos, G. Ginis and P.G. Cottis, "Availability and performance of satellite links suffering from interference by an adjacent satellite and rain fades," *IEEE Proceedings in Communication*, vol. 146, no. 1, pp. 61-67, February 1999.

12. B. McClure, "Europe gets Backbone," *Telecommunications*, vol. 33, no. 6, pp. 23-24, June 1999.
13. W.L. Nowland, R.L. Olsen and I. P. Shkarofsky, "Theoretical relationship between rain depolarisation and attenuation," *Electronics Letters*, vol. 13, no. 22, pp.676-678, 27th October 1977.
14. Moupfouma, "Improvement of a Rain Attenuation Prediction Method for Terrestrial Microwave Links," *IEEE Transactions on Antennas and Propagation*, vol. AP-32, no.12, pp. 1368-1372, Dec 1984.
15. G. Partridge, *Gigabit Networking*, Addison-Wesley, 1994
16. R.R. Persinger, W. L. Stutzman, P.E. Castle, Jr., and C.W. Bostian, "Millimeter Wave Attenuation Prediction Using a Piecewise Uniform Rain Rate Model," *IEEE Transactions on Antennas and Propagation*, vol. AP-28, no.2, pp. 149-153, March 1980.
17. J. Walrand and P. Varaiya, *High Performance Communication Networks*, San Francisco, Morgan Kaufmann Publishers, Inc., 1996.
18. RFC 1483 Multiprotocol Encapsulation over ATM Adaptation Layer 5 (07/93) replaced by RFC 2684
51. RFC 1577/2225 Classical IP and ARP over ATM
52. RFC 1626/2225 Default IP MTU for use over ATM AAL5
53. RFC 1755 ATM Signaling Support for IP over ATM
54. RFC 2022 Support for Multicast over UNI 3.0/3.1 based ATM Networks
55. RFC 2226 IP Broadcast over ATM Networks
56. M. Richharia, *Satellite Communication Systems Design Principles*, MacMillan, 1999.
57. D. Roddy, *Satellite Communications*, 2nd Edition, Mc-Graw Hill, 1996.
58. R. E. Skerjanec and C. A. Samson, "Rain Attenuation Measurements in Mississippi at 10GHz and 14.43GHz," *IEEE Transactions on Antennas and Propagation*, pp. 575-578, July 1971.
59. W. Stallings, *Data and Computer Communications*, Prentice-Hall International Inc., 1997.
60. V. Tandon, "DWDM: Optimising City Networks," *Telecommunications*, vol. 33, no. 5, pp. 40-46, May 1999.
61. T. Tazaki, H. Tabuchi, K. Ikeda and S. Ito, "Laboratory measurements of polarimetric radar signatures of randomly distributed spherical and spheroidal

scatterers at 30GHz," *IEEE Procedures on Microwaves and Antennas Propagation*, vol. 147, no. 1, pp. 8-12, February 2000.

62. J.Troughton and B.G. Evans, "Rain-induced deflection of microwave and millimetre-wave radiowaves," *Electronics Letters*, 5th February, vol. 12, no. 13, pp. 68-70, 1976.
63. P. A. Watson and A. W. Dissanayake, "Calculation of forward scatter and crosspolarisation from ice spheroids," *Electronics Letters*, vol. 13, no. 19, pp. 555-556, 15th September 1977.
64. P.B. Ulrich and J. Wallace, "Propagation characteristics of collimated, pulsed laser beams through and absorbing atmosphere," *Journal of the Optical Society of America*, vol. 63, no. 1, pp.8-12, January 1973.

APPENDIX A

EQUIPMENT AND DATA SHEETS

List of Test Equipment

ATM-Ethernet via Fibre Test

Monitoring PCs:	2× Gateway G6-400 PCs
Network Cards:	1× 3Com Fast Etherlink XL network interface card (Ethernet)
	1× Olicom RapidFire 6162 network interface card (ATM)
Cabling:	Hiperlink Category 5 UTP cabling
	OC3/STM1 155Mbps optical fibre cabling (SC Type connectors)
Network switch:	Cisco Catalyst 5500 switch
Software:	Travelling Software Laplink file transfer program
	Olicom LanScout v1.16 network management program

ATM-ATM via Fibre and Laser Test

Monitoring PCs:	2× Gateway G6-400 PCs
Network Cards:	2× Olicom RapidFire 6162 network interface card (ATM)
Cabling:	OC3/STM1 155Mbps optical fibre cabling (SC and ST type connectors)
Wireless Link:	2× FDDI/ATM 800nm laser links from Communication By Light
Network switch:	Cisco Catalyst 5500 switch
Software:	Travelling Software Laplink file transfer program
	Olicom LanScout v1.16 network management program
	Linkview 2.1 proprietary software to CBL Lasers

Short – Range Optical Link Tests (Natural Rain)

Optical Link

Emitter:	Siemens SFH480, hermetically sealed GaAlAs IR emitting diode of peak wavelength 880nm.
Detector:	Siemens BPW21 Silicon photodiode
PC connector:	25-way male D-type connector
Data Acquisition module:	Analog-to-digital converter Pico ADC12
Data Acquisition Software:	Picolog and Picoscope software, C program 1 (listed in appendix B)

Rain Gauge

Apparatus:	Plastic funnel (Internal diameter 18cm)
	500ml glass graduated cylinder
Emitter:	Siemens SFH480, hermetically sealed GaAlAs IR emitting diode of peak wavelength 880nm.
Detector:	Siemens BPX43 Silicon photodide, hermetically sealed
PC connector:	25-way female D-type connector
Data Acquisition module:	ADC11
Data Acquisition Software:	Picolog and Picoscope software, C program 2 (listed in appendix B)

Short – Range Optical Link Tests (Simulated Rain)

Optical Link

Emitter:	Siemens SFH480, hermetically sealed GaAlAs IR emitting diode of peak wavelength 880nm.
Detector:	Siemens BPW21 Silicon photodide, hermetically sealed
PC connector:	25-way male D-type connector
Data Acquisition module:	ADC12
Data Acquisition Software:	Picolog and Picoscope software, C program 1 (listed in appendix B)

Rain Gauge

Apparatus:	Three measuring jars of diameter 70mm, 75mm and 70mm
Measuring device:	5ml capacity Plastipak syringe

Other:	Garden Hose

Catalyst 5500 Switching System

THE AWARD-WINNING CISCO CATALYST® 5500 IS THE MOST FLEXIBLE, FEATURE-RICH SWITCH IN THE INDUSTRY. WITH A GIGABIT ARCHITECTURE THAT SCALES THROUGHPUT TO MILLIONS OF PACKETS PER SECOND, THE CATALYST 5500 SUPPORTS UP TO 528 USER PORTS AND IS IDEAL FOR HIGH-DENSITY WIRING CLOSETS. ADVANCED MULTILAYER FEATURES PROVIDE THE INTELLIGENCE NEEDED TO SUPPORT MISSION-CRITICAL APPLICATIONS BY DELIVERING END-TO-END QUALITY OF SERVICE (QOS) AND MULTICAST SUPPORT.

Building the Intranet Infrastructure

The Cisco Catalyst 5500 is the company's modular switching platform for high-density wiring closets or distribution points. As a wiring closet solution, the Catalyst 5500 supports high-density, dedicated Token Ring or 10/100/1000 Ethernet switching. The Catalyst 5500 also supports all advanced Cisco wiring closet features such as automatic protocol broadcast filtering to conserve valuable bandwidth, intelligent multicast forwarding to handle multimedia traffic, and load balancing over redundant links.

The flexible architecture of the Catalyst 5500 supports interface modules from these Cisco campus backbone devices: Catalyst 8510, LightStream® 1010, and 7500 Series routers. This capability means the Catalyst 5500 can support high-performance multilayer switching, Asynchronous Transfer Mode (ATM) switching, and Wide Area Network (WAN) connectivity. With Catalyst 5500, users can deploy the Catalyst 8510 modules for nonblocking, high-performance IP and IPX® multilayer switching. Users can also deploy LightStream 1010 interface modules for native ATM switching. Finally, along with the route switch module in a Catalyst 5500, users can deploy interface modules from the Cisco 7500 series routers for WAN connectivity.

The Catalyst 5500 is a 13-slot chassis with two dedicated slots—slots 1 and 13. Slot 1 is dedicated for the Supervisor Engine that monitors all system components and is responsible for all frame-switching and forwarding functions in the switch. Supervisor Engine II or Supervisor III is required for operation of the Catalyst 5500. A Supervisor II is a 1.2Ghps switch fabric. A Supervisor III is a 3.6Gbps crossbar switching fabric. Slot 13 is the second dedicated slot and is reserved for the LS1010 ATM Switch Processor (ASP) module or Catalyst 8510 Switch Route Processor (SRP). The ASP or SRP modules are 10Gbps switching fabrics and are required if interface modules from the LightStream 1010 or Catalyst 8510 are to be used in the Catalyst 5500.

The Catalyst 5500 architecture is based on a combination of two high-capacity switching fabrics integrated into a single platform. This architecture ensures optimal performance whether the Catalyst 5500 is used as a high-density cell or a frame switch. All Catalyst 5000 Family interface modules can be used in slots 2 to 12, whereas LightStream 1010 or Catalyst 8510 modules can be used in slots 9 to 12. Slot 2 is a dual-purpose slot that can be used for either a redundant Supervisor Engine or any Catalyst 5000 family interface module.

With its support for hot-swappable modules, power supplies, and fans, the Catalyst 5500 chassis delivers high availability for production networks. Dual redundant switching engines, power supplies, and a passive backplane design ensure full system redundancy for mission-critical environments. The Catalyst 5500 chassis fits into a standard 19-inch rack, and all system components are accessible from the same side of the chassis. Only one power supply is required to run a fully configured system.

Figure 1 The Catalyst 5500 Delivers the Best Technologies from Cisco on a Single Platform.

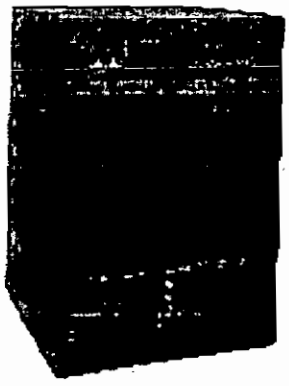

The media-independent architecture of the Catalyst 5500 supports all LAN and ATM switching technologies through a wide range of 10/100/1000 Ethernet, Fiber Distributed Data Interface (FDDI), Token Ring, and ATM switch modules shown in Table 1.

Table 1 Catalyst 5500 Interface Support

Catalyst 5000 Family Switching Modules	Number of Interfaces Supported per Slot	Maximum Interfaces per Chassis
Group-Switched 10BaseT Ethernet	48	528
Switched 10BaseT Ethernet (RJ-21)	48	528
Switched 10BaseT Ethernet (RJ-45)	24	264
Switched 10BaseFL Ethernet	12	132
Group-Switched 100BaseTX Ethernet	24	264
Switched 10/100BaseTX Fast Ethernet	24	264
Switched 100BaseFX Fast Ethernet	12	134
ATM LAN Emulation (OC-3 or OC-12)	1 (dual PHY)	7 (dual PHY)
CDDI/FDDI	1	11
ATM OC-3, 155-Mbps Multimode Fiber	4	32
ATM OC-3, 155-Mbps Single-Mode Fiber	4	32
ATM OC-3, 155-Mbps Unshielded Twisted-Pair (UTP), Category 5 (UTP-5)	4	32
ATM OC-12, 622-Mbps Single-Mode Fiber	1	8
DS3	2	16
E3	2	16
T1/E1 ATM Trunk	4	32
T1/E1 Circuit Emulation	4	32
25-Mbps ATM	12	96

Delivering a Comprehensive Suite of Intranet Services

The Catalyst 5500 is ideally suited for building large campus Intranets by delivering a full set of Intranet services. These services enable efficient and reliable delivery of application traffic.

- Efficient Intranet multimedia and multicast support through PIM, IGMP Snooping, and the Cisco Group Management Protocol (CGMP) delivers end-to-end, scalable bandwidth for multimedia and multicast applications. By utilizing these advanced multicast features, the Catalyst 5500 is an intelligent multicast device that forwards multicast streams only to the appropriate user end stations.
- The Catalyst 5500 is part of the CiscoAssure end-to-end QoS solution. Deployed in a wiring closet, the Catalyst 5500 can identify user applications and classify traffic with the appropriate priority level. It enables admission control at the network edge to prevent unauthorized applications from being allowed on the network. The Catalyst 5500 switch is a QoS edge device that is "application aware."
- Network resilience is achieved through a combination of device, link, and network service redundancy supported on the Catalyst 5500. Device redundancy is provided with support for redundant switch engines, power supplies, and route switch modules. Link redundancy is implemented on Cisco dual PHY ATM modules, integrated in Fast EtherChannel® or Gigabit EtherChannel, and supported on all VLAN trunk links. Network service redundancy is achieved through ATM Simple Server Redundancy Protocol (SSRP), HSRP, and support for Spanning-Tree Protocol on a per VLAN basis.
- Security on the intranet is supported with secure port filtering, enabling individual ports to allow access only to certain workstations. Terminal Access Controller Access Control System+ (TACACS+) prevents unauthorized access to the switch in secure environments.
- Mobility or moves, adds, and changes in the intranet is supported using DHCP and DNS, along with dynamic VLAN services and distributed NetFlow switching for optimal scalable performance, regardless of location.

Intranet Management

The Catalyst 5500 delivers a comprehensive set of management tools to provide the required visibility and control in the network. Managed with CiscoWorks for Switched Internetworks (CWSI), the Catalyst 5500 switch can be configured and managed to deliver end-to-end device, VLAN, traffic, ATM and policy management.

Policy management is achieved through a combination of intelligent embedded agents on the switches and CWSI, a powerful network management application. CWSI will provide policy management for all Cisco network services including: class of service (CoS), multicast, security, network resiliency, and mobility of users. Policy management is implemented using Cisco Virtual Membership Policy Server (VMPS). VMPS is present on all Catalyst 5000 Family switches and delivers the database information required to implement policies for all Cisco network services.

Intelligent embedded agents on all Catalyst 5000 Family switches include support for Cisco discovery protocol (CDP) delivering network topology discovery and mapping, Cisco VLAN trunking protocol (VTP) supporting dynamic VLANs and dynamic trunk configuration across all switches. Embedded intelligent Remote Monitoring (RMON) agents on every port deliver powerful traffic monitoring and control. RMON groups supported includes statistics, history, events, and alarms groups.

Enhanced Switched Port Analyzer (SPAN) functionality enables the user to mirror traffic on any port or VLAN to another Ethernet or Fast Ethernet port for analysis by a sniffer or RMON SwitchProbe® product.

The Catalyst 5500 supports local, out-of-band management through a terminal or modem attached to the EIA/TIA-232 interface; remote in-band management through Simple Network Management Protocol (SNMP), Telnet client, BOOTP, and Trivial File Transfer Protocol (TFTP).

Summary

The Catalyst 5500 brings the highest level of scalability, flexibility, and functionality to the Catalyst 5500 Family. The 5500 design is based upon proven Cisco switching technology that is being used in the largest campus networks in the world. With support for comprehensive array of advanced multilayer switching features and a wide range of interface modules, the Catalyst 5500 effectively meets all requirements of the evolving corporate intranet.

Technical Specifications

Standard Network Protocols

- Ethernet: IEEE 802.3, 10BaseT, and 10BaseFL
- Fast Ethernet: IEEE 802.3u, 100BaseTX, 100BaseFX
- Gigabit Ethernet: 803.3z, 1000BaseSX, 1000BaseLX, 1000BaseEX
- FDDI: ISO 9314-1 FDD PHY standard; ISO 9314-3 FDDI physical medium dependent (PMD) standard; CDDI TP-PMD standard; ANSI FDDI X3T9.5 SMT 7.3
- ATM: ATM Forum—3.1 UNI specification, Q.2931 signaling protocols, LAN Emulation

Signaling and Routing

- UNI 3.1
- Interim Local Management Interface (ILMI)
- Private Network-to-Network Interface (PNNI) Phase 1, Internet Interswitch Signaling Protocol (IISP)
- Soft permanent virtual path (PVC)/permanent virtual path (PVP) support
- ATM access lists and firewalls
- Crankback
- Plug-and-play mode with PNNI image
- Redundant link support with load balancing or best-fit selection

Network Management

- CWSI graphical user interface (GUI) management, including:
  - CiscoView
  - VlanDirector™
  - TrafficDirector™
  - AtmDirector™
  - NETSYS tools
- Cisco Discovery Protocol
- VLAN Trunk Protocol
- SNMP agent V.1 (RFCs 1155-1157)
- Cisco WorkGroup MIB
- Ethernet MIB (RFC 1643)
- Ethernet repeater MIB (RFC 1516)
- SNMP MIB II (RFC 1213)
- RMON (RFC 1757)
- Interface table (RFC 1573)
- Bridge MIB (RFC 1493)
- ILMI MIB
- FDDI MIB (RFC 1512)
- AToM MIB (RFC 1695)
- ATM RMON
- LEC MIB (ATM Forum LANE v. 1.0)
- Cisco LECS, LES/BUS MIB
- PNNI MIB
- LAN Emulation Configuration Server (LECS), LAN Emulation Server (LES), broadcast and unknown server (BUS) MIB
- SMT 7.3 (RFC 1285)
- Enhanced SPAN
- Port snooping and connection steering
- Text-based command-line interface based on familiar router interface
- Standard Cisco IOS® security capabilities: passwords and TACACS+
- Telnet, TFTP, BOOTP, LAN Emulation client, RFC 1577 classical IP over ATM client, for management access

Traffic Management

- Single, dual-mode leaky bucket traffic policing
- Per-port traffic pacing
- Multiple, configurable per connection, port, and switch thresholds
- Multiple priority classes
- All ATM connection types and ATM adaption layers (AALs)
- Connection admission control
- Cell loss priority (CLP) tagging and discard
- Intelligent packet discard
- Available bit rate support: explicit forward congestion indication (EFCI) marking mode and relative rate marking mode

Physical Specifications

- Dimensions (H x W x D): 25.25 x 17.3 x 18.25 in. (64.14 x 43.9 x 46.36 cm)
- Minimum weight: 70 lb (31.7 kg)
- Maximum weight: 160 lb (72.5 kg)
- Mounting: 19-in. rack-compatible (rack and cable guide hardware included)

Power Requirements (one power supply)

8.0A @ 230 VAC 50 Hz

16A @ 115 VAC 60 Hz

KVA rating: 1.84 KVA

Power consumption: 1100W

Environmental Conditions

Operating temperature: 32 to 104 F (0 to 40 C)

Storage temperature: –40 to 167 F (–40 to 75 C)

Relative humidity: 10% to 90%, noncondensing

Operating altitude: –60 to 4000 m

Mean time between failures (MTBF): Seven years for system configuration

Regulatory Compliance

Safety Certifications

- UL 1950
- EN 60950
- CSA-C22.2 no. 950
- IEC 950

Electromagnetic Emissions Certifications

- FCC 15J Class A
- VCCI CE II
- CE Mark
- EN 55022 Class B
- CISPR 22 Class B

CISCO SYSTEMS

orporate Headquarters
isco Systems, Inc.
70 West Tasman Drive
an Jose, CA 95134-1706
SA
ttp://www.cisco.com
el: 408 526-4000
800 553-NETS (6387)
ax: 408 526-4100

European Headquarters
Cisco Systems Europe s.a.r.l.
Parc Evolic, Batiment L1/L2
16 Avenue du Quebec
Villebon, BP 706
91961 Courtaboeuf Cedex
France
http://www-europe.cisco.com
Tel: 33 1 69 18 61 00
Fax: 33 1 69 28 83 26

Americas Headquarters
Cisco Systems, Inc.
170 West Tasman Drive
San Jose, CA 95134-1706
USA
http://www.cisco.com
Tel: 408 526-7660
Fax: 408 527-0883

Asia Headquarters
Nihon Cisco Systems K.K.
Fuji Building, 9th Floor
3-2-3 Marunouchi
Chiyoda-ku, Tokyo 100
Japan
http://www.cisco.com
Tel: 81 3 5219 6250
Fax: 81 3 5219 6001

Cisco Systems has more than 200 offices in the following countries. Addresses, phone numbers, and fax numbers are listed on the Cisco Connection Online Web site at http://www.cisco.com/offices.

rgentina • Australia • Austria • Belgium • Brazil • Canada • Chile • China • Colombia • Costa Rica • Croatia • Czech Republic • Denmark • Dubai, UAE Finland • France Germany • Greece • Hong Kong • Hungary • India • Indonesia • Ireland • Israel • Italy • Japan • Korea • Luxembourg • Malaysia Mexico • The Netherlands • New ealand • Norway • Peru • Philippines • Poland • Portugal • Puerto Rico • Romania • Russia • Saudi Arabia • Singapore Slovakia • Slovenia • South Africa • Spain • weden • Switzerland • Taiwan • Thailand • Turkey • Ukraine • United Kingdom • United States • Venezuela

1699LW

Catalyst 5500 ATM Fabric Integration Module

DEPLOYABLE IN A CATALYST® 5500, THE CISCO ASYNCHRONOUS TRANSFER MODE (ATM) FABRIC INTEGRATION MODULE DELIVERS HIGH-SPEED CONNECTIVITY BETWEEN ATM AND ETHERNET. THE ATM FABRIC INTEGRATION MODULE INTERNALLY CONNECTS THE CATALYST 5500 ATM CELL BACKPLANE TO THE FRAME BACKPLANE BY UTILIZING ATM FORUM STANDARD LAN EMULATION (LANE), MULTIPROTOCOL OVER ATM (MPOA), OR PERMANENT VIRTUAL CIRCUIT (PVC) TO VIRTUAL LAN (VLAN) MAPPINGS. THIS MODULE ALSO SUPPORTS AN EXTERNAL MULTIMODE FIBER ATM OC-12 NETWORK-TO-NETWORK INTERFACE (NNI).

The Catalyst 5500 ATM Fabric Integration Module Delivers Leading Edge Performance for Today's Campus Networks Requiring Support for Both Ethernet and ATM.

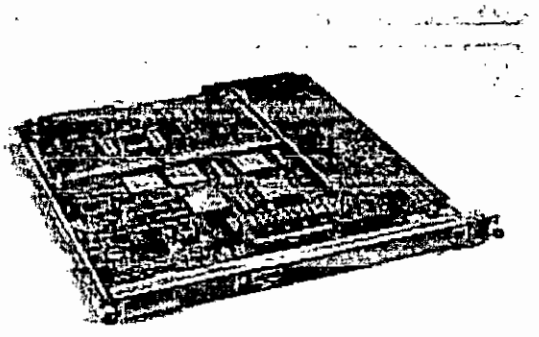

Accelerating Today's ATM Networks

The ATM Fabric Integration module provides a seamless connection between ATM and Ethernet by internally connecting the Catalyst 5500 frame and ATM cell backplanes. Each ATM Fabric Integration module delivers ATM to Ethernet connectivity utilizing LANE v1.0 or LUNI v2.0 connectivity and services and has the necessary hardware scalability for MPOA client, quality of service (QoS), and traffic shaping. Cisco extends the Catalyst 5500's leading-edge performance for today's ATM and Ethernet networks and sets the stage for future technologies.

MPOA

As an integral part of the Cisco Layer 3 switching strategy, MPOA provides a standards-based Layer 3 switching solution for ATM networks. An MPOA network comprises the following: an MPOA server (MPS) and an MPOA client (MPC). Routers, such as the Cisco 7000 series or the Catalyst 5000 route switch module, support the MPS function that supplies all the Layer 3 forwarding information used by MPCs. The Catalyst 5500 ATM Fabric Integration module supports MPC through dedicated onboard hardware. With a hardware implementation of MPOA, Cisco provides unmatched performance for MPOA and delivers distributed, high-speed Layer 3 switching through the ATM backbone.

QoS

With the convergence of mission-critical business and multimedia applications on the common Intranet, there is an increasing need for QoS and support for multicast-intensive applications. A new set of Intranet services is required to ensure the reliability and availability of these applications. Future IOS software upgrades enable mapping between IP Precedence, RSVP, 802.1p, and ATM QoS. Used with the Cisco end-to-end QoS strategy, customers can deploy the Catalyst 5500 ATM Fabric Integration module and prioritize traffic into different ATM service classes, such as the Cisco unspecified bit rate plus minimum cell rate (UBR+MCR), as well as the ATM Forum's constant bit rate (CBR), variable bit rate (VBR), UBR, and available bit rate (ABR).

External ATM OC-12 Interface

Aside from an internal ATM-to-Ethernet connection, the Catalyst 5500 ATM Fabric Integration Module also provides an external OC-12 Network-to-Network Interface (NNI). With this interface, users can connect the Catalyst 5500 directly into the high-speed ATM backbone.

Fault-Tolerant ATM Connectivity

LAN Emulation Server Redundancy

The Catalyst 5500 Fabric Integration module delivers redundant LANE services using the Cisco LANE Simple Server Redundancy Protocol (SSRP). LAN Emulation SSRP provides redundancy for all of the server components in LAN Emulation—the LAN Emulation Configuration Server (LECS), the LAN Emulation Server (LES) and the Broadcast and Unknown Server (BUS). Cisco SSRP allows for the enterprise-wide deployment of ATM by removing LANE servers as a single point of failure.

Scalable, Distributed LANE Servers

Unique among ATM edge devices, the Catalyst 5500 enhances ATM LANE network performance by delivering support for the entire range of LANE servers. By using this feature, network administrators can easily distribute LANE services using the Catalyst 5500 ATM Fabric Integration module. For example, this feature allows scalable distribution of bandwidth-intensive LANE BUS services for multimedia applications. Operating as a standalone LANE v1.0 BUS, the Catalyst 5500 ATM Fabric Integration module can forward more than 500,000 pps.

Flexible Architecture

The LANE protocols and signaling run on onboard processors, permitting software upgrades to meet evolving ATM standards. Future upgrades will provide ABR and Token Ring LANE.

VLAN/ATM Integration

By using the industry-leading Cisco Internetwork Operating System (Cisco IOS®) software, the Catalyst 5500 ATM Fabric Integration module extends virtual LAN (VLAN) capabilities throughout the network, spanning switched LANs and ATM-based services, such as ATM servers, by mapping VLANS to ATM LAN Emulated LANs (ELANs). The Catalyst 5500 ATM Fabric Integration maps RFC 1483 PVCs to VLANs.

ATM Traffic Shaping

Besides supporting PVC to VLAN mappings, the Catalyst 5500 ATM Fabric Integration Module supports PVC traffic shaping. Customers can create and enforce bandwidth contracts using traffic shaping. This capability is a hardware-based implementation that provides wirespeed performance. Therefore, customers will not experience performance degradation when using this advanced functionality. The traffic shaping features supported are Peak Cell Rate (PCR), Sustained Cell Rate (SCR), and burst size. Customers create a bandwidth contract by setting a maximum transmission rate on PVC using PCR, and an average transmission rate using SCR and burst size. The ATM Fabric Integration Module enforces this bandwidth contract with dedicated on-board hardware for unmatched industry performance.

Catalyst 5500 Fabric Integration Module Specifications

- Physical Specifications
- Occupies one slot in the Catalyst 5500 platform (should be deployed in slots 9-12)
- Dimensions (H x W x D): 1.2 x 14.4 x 16 in. (3 x 35.6 x 40.6 cm)
- Weight: 3 lb./0.65 kg
- Environmental Conditions
- Operating Temperature: 32 to 104 F (0 to 40 C)
- Storage Temperature: -40 to 167 F (-40 to 75 C)
- Relative Humidity: 10 to 90%, noncondensing

Safety Certifications

- UL 1950
- CSA 950
- EN60950
- CE Marking
- TUV GS
- IEC 950
- AS/NZS 3260

Electromagnetic Emissions Certifications

- FCC Part 15 (CFR 47) Class A
- VCCI Class B
- EN55022 Class B
- CISPR 22 Class B
- CE Marking
- AS/NZS 3548 Class B

Processors

- ATM Control Processor: Motorola 68EC030
- SAR: Two Maker 100-MHz processors (Transmit/Receive)

Frame-to-Cell Conversion

- AAL5
- 4096 virtual circuits
- 255 concurrent reassembly

ATM Standards

- RFC 1483 LLC SNAP bridging encapsulation (PVC)
- PVC traffic shaping (GCRA) (future software upgrade)
- ATM Forum LANE v1.0 LEC, LECS, LES, BUS
- ATM Forum LUNI v2.0
- ATM Forum MPOA v1.0 MultiProtocol Client (MPC)
- UNI 3.0/3.1, Q.2931 signaling protocols
- ILMI

Network Management

- Cisco Discovery Protocol
- Definitions of Managed Objects for Bridges (RFC 1493)
- Evolution of Interfaces Group of MIB-II (RFC 1573)
- SNMP MIB II (RFC 1213)
- AToM MIB (RFC 1695)
- LEC MIB (ATM Forum LANE V1.0)
- Cisco Workgroup Stack MIB
- Cisco VLAN Trunk Protocol (VTP) MIB
- Cisco LECS, LES/BUS MIB
- ILMI MIB

Indicators

- Module Status: green (operational)/red (faulty)
- Carrier Detect (OC-12 NNI port): green (operational)
- RX (OC-12 NNI port): green flashing (receive activity)
- TX (OC-12 NNI port): green flashing (transmit activity)

Interfaces

- ATM OC-12 Network-to-Network Interface (NNI) Multimode fiber (SC)
- Diag Port: RJ-45

Optical Specifications

Multimode Fiber (OC-12)

- Transmitter output power: -19 to -14 dBm
- Receiver sensitivity: -26 to -14 dBm
- Wavelength: 1300 nm
- Optical source: LED
- Maximum span: 500m

Corporate Headquarters
Cisco Systems, Inc.
170 West Tasman Drive
San Jose, CA 95134-1706
USA
http://www.cisco.com
Tel: 408 526-4000
800 553-NETS (6387)
Fax: 408 526-4100

European Headquarters
Cisco Systems Europe s.a.r.l.
Parc Evolic, Batiment L1/L2
16 Avenue du Quebec
Villebon, BP 706
91961 Courtaboeuf Cedex
France
http://www-europe.cisco.com
Tel: 33 1 69 18 61 00
Fax: 33 1 69 28 83 26

Americas Headquarters
Cisco Systems, Inc.
170 West Tasman Drive
San Jose, CA 95134-1706
USA
http://www.cisco.com
Tel: 408 526-7660
Fax: 408 527-0883

Asia Headquarters
Nihon Cisco Systems K.K.
Fuji Building, 9th Floor
3-2-3 Marunouchi
Chiyoda-ku, Tokyo 100
Japan
http://www.cisco.com
Tel: 81 3 5219 6250
Fax: 81 3 5219 6001

Cisco Systems has more than 200 offices in the following countries. Addresses, phone numbers, and fax numbers are listed on the Cisco Connection Online Web site at http://www.cisco.com/offices.

Argentina • Australia • Austria • Belgium • Brazil • Canada • Chile • China • Colombia • Costa Rica • Croatia • Czech Republic • Denmark • Dubai, UAE Finland • France • Germany • Greece • Hong Kong • Hungary • India • Indonesia • Ireland • Israel • Italy • Japan • Korea • Luxembourg • Malaysia Mexico • The Netherlands • New Zealand • Norway • Peru • Philippines • Poland • Portugal • Puerto Rico • Romania • Russia • Saudi Arabia • Singapore Slovakia • Slovenia • South Africa • Spain • Sweden • Switzerland • Taiwan • Thailand • Turkey • Ukraine • United Kingdom • United States • Venezuela

RapidFire 6161 and 6162

olicom

ATM 155 PCI Adapters

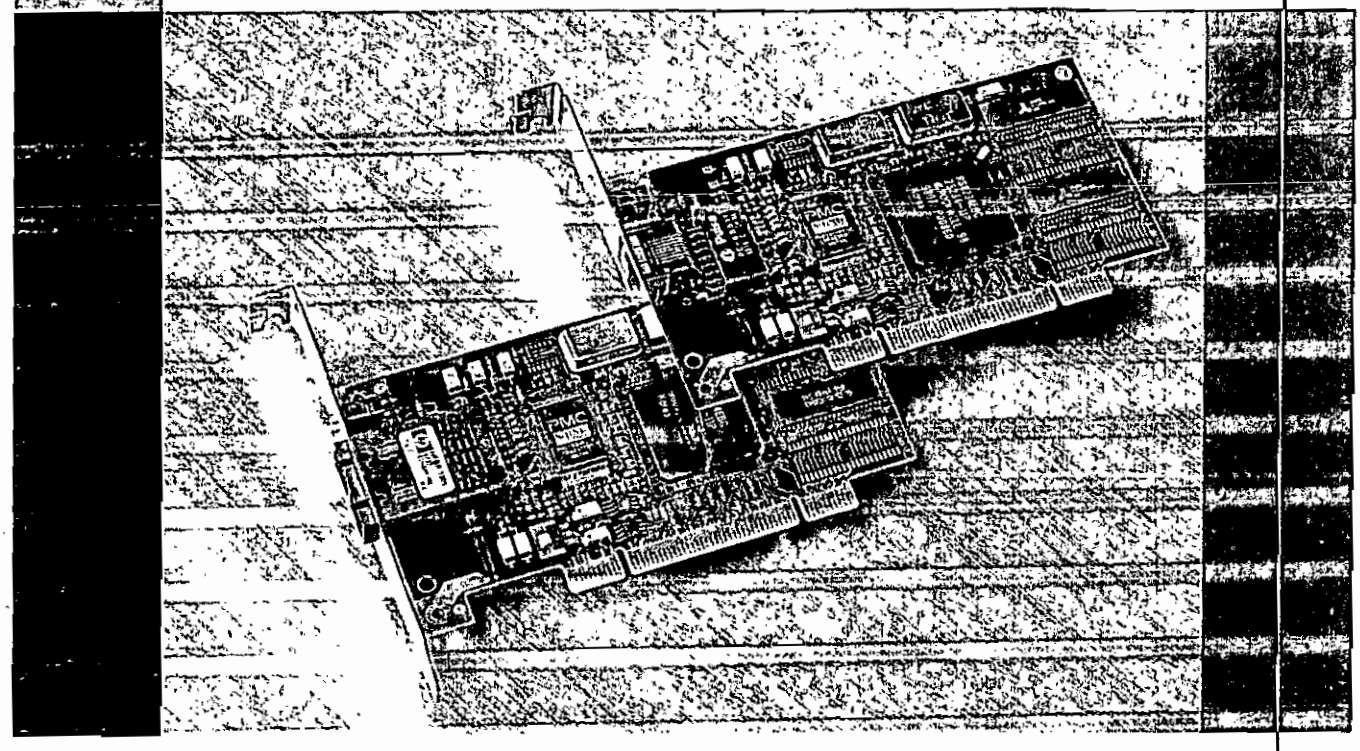

Olicom's RapidFire™ 6161 and 6162 ATM 155 PCI adapters are among the industry's first to fully support the Available Bit Rate (ABR) traffic class. ABR is a key technology for preventing congestion and making effective use of "extra" bandwidth while maintaining QoS guarantees for time-sensitive multimedia data.

The RapidFire 6161 is a UTP Cat. 5 version while the RapidFire 6162 is a multi-mode fiber version with SC connectors. Both support OC-3/STS-3 data rates and full-duplex 155.52 Mbps communication.

They also feature Olicom's advanced CellDriver™ ATM software technology, which includes LAN Emulation Client and Classical IP drivers for Microsoft Windows, Novell NetWare, and IBM OS/2 environments.

True ABR Support

Both adapters support true ABR in hardware for full compliance with current and future networks using Explicit Rate, Relative Rate and EFCI ABR flow control. This ensures optimal utilization of available network bandwidth without the risk of excessively retransmitted frames due to network or buffer congestion.

Key Features and Benefits

- On-chip support for all traffic classes, including ABR, reduces CPU load and minimizes cell delay variation
- Up to 32 different ABR traffic profiles improve bandwidth allocation and reduce congestion
- Unlimited CBR, VBR and UBR traffic profiles allow high granularity in bandwidth allocation
- Support for 4096 simultaneous virtual connections
- Optional ClearServer™/ATM support allows load-sharing and active redundancy, ensuring high availability and sub three-second recovery times
- RapidConfig software provides simple and flexible configuration of LAN Emulation drivers to control parameters for both the ATM adapter and emulated LANs
- Segmentation and Reassembly (SAR) is done directly from/to host memory
- Interrupt pacing minimizes CPU load
- Two LEDs (loss of signal and lock detect) indicate adapter status
- PC97/PC98/Server 98 compliant
- Includes LANscout™ and RapidMon adapter management applications

Software Features

- Full ATM LAN Emulation Services compliant with the ATM Forum LAN Emulation over ATM version 1.0 specification
- Token-Ring and Ethernet LAN Emulation Clients are included for Windows 95/98, Windows NT, IBM OS/2 Warp and Novell NetWare 4.1x/5.0
- Unique persistent DD-Vcc feature maintains LAN Emulation connections even when switching from a primary to backup LAN Emulation Server
- LAN Emulation drivers support up to 32 LAN Emulation Clients
- Supports WinSock 2 interface, allowing native ATM access from applications developed for WinSock 2
- Support for 4.5 KB, 9 KB and 18 KB Token-Ring frame sizes

No problem.

ClearServer/ATM Support

Support for optional ClearServer functionality – an element of Olicom's ClearSession™ technology – provides active redundancy and transparent load-sharing between multiple physical adapters installed in the same server. This ensures fail-safe protection for maximum network availability. (Purchased separately)

Effective Management Utilities

Both ATM adapters are supplied with Olicom's LANscout Desktop Management System for Windows, and RapidMon Management NLM for NetWare. LANscout allows remote monitoring of a comprehensive range of network traffic and adapter diagnostics data.

Specifications

Form factor: Single-slot PCI bus card
Size: 137.7 mm x 60 mm
ATM adaptation layer support: AAL5 using special-purpose, single-chip processor for ATM cell segmentation and re-assembly, traffic policing, and HEC and CRC calculations.
Physical layer interface: OC-3 155.52 Mbps, SONET or SDH framing, software configurable.
SAR memory: 1 MB
Connectors: RapidFire 6161: RJ45 8-pin shielded female connector for UTP5 cables. RapidFire 6162: SC multi-mode fiber connector.
Power: 5V or 3.3V (auto detect)
MTBF:

- RapidFire 6161: 1,780,000 POH
- RapidFire 6162: 740,000 POH

Warranty: Limited lifetime

Software

All drivers support:

- SVC operation
- LAN Emulation Client for simultaneous Ethernet and Token-Ring emulation
- Classical IP (RFC 1577)
- RFC 1483, bridged and routed

Operating systems supported:

- **Windows 95 & NT 3.51/4.0:** NDIS 3.0 FullNIC driver, LANscout, WinSock 2, and optional ClearServer/ATM support
- **Windows 98/NT5.0:** NDIS 3.0 and NDIS 5.0. Note that NDIS 5.0 does not allow LANscout, classical IP, or ClearServer, though NDIS 3.0 does
- **Novell NetWare 4.1x/5.0:** Native ODI spec 3.31 server driver for NetWare 5.0 with LANscout, classical IP and optional ClearServer support. Also supports ATMODI (thin driver) spec 1.0.
- **OS/2 Warp 3.0:** NDIS 2.02

Other software

- RapidConfig: adapter and driver configuration program for Windows NT/95/98
- LANscout Desktop Management System for Windows NT/95/98
- RapidMon Management NLM for NetWare

Compliancy

Physical layer: OC-3, SDH or SONET
ATM cell structure: Conforms to ITU recommendation I.363
ATM AAL layer: AAL5
ATM rate pacing: ATM CBR, VBR UBR, and ABR pacing types supported
ATM signaling: Conforms to ITU recommendation Q.2931 and Q.2130, ATM Forum UNI 3.0, UNI 3.1, Signaling 4.0 (UNI 4.0)
Traffic management: Conforms to ATM Forum Traffic Management 4.0 (UNI 4.0)
LAN Emulation: Conforms to ATM Forum LAN Emulation over ATM v.1.0
PCI: Local Bus Specification rev. 2.1, 5V and 3.3V operation
Network management: Supports ATM Forum OAM cell flows F4, F5. Supports ILMI as per UNI 3.1

Model Numbers

6161 0010: RapidFire 6161 with RJ45 UTP5 connector
6162 0010: RapidFire 6162 with multi-mode fiber connector

(Both adapters are supplied with software kit, drivers and manual. ClearServer/ATM software is ordered separately.)

Customer Support

Hotline Support

- USA: (+1) 800-OLICOM-1 or 972-516-4638, 24 hours a day, incl. holidays
- International: (+45) 45 27 01 02, between 8 a.m. and 6 p.m. CET Monday to Friday

See our Web site for more details about Olicom's extensive customer support.

olicom

Olicom on the Web: For further information on Olicom solutions and services, visit our Web site at **http://www.olicom.com**

Olicom Head Office: Olicom A/S · Nybrovej 114 · 2800 Lyngby · Denmark · Tel.: (+45) 45 27 00 00 / Fax: (+45) 45 27 01 01
Olicom, Inc. · 1680 N. Prospect Drive · Richardson, TX 75081 · USA Tel.: (+1) 972 907 4600 / Fax: (+1) 972 671 7525
Additional offices: Olicom Africa · Tel.: (+27) 11 432-3295 · Olicom Australia · Tel.: (+61) 2 9955 1755 · Olicom Benelux · Tel.: (+31) 73 6 49 15 46 · Olicom Canada · Tel.: (+1) 416 977 2400
Olicom France · Tel · (+33) 1 4191 1717 · Olicom GmbH · Tel · (+49) 6105 2992 0 · Olicom The Networking Company Ibérica S.L. · Tel.: (+34) 91 372 9814 · Olicom Japan K.K. · Tel.: (+81) 3 5276 ...
Olicom Nordic · Tel.: (+45) 45 27 00 00 · Olicom Poland Sp. z o.o. · Tel.: (+48) 58 346 12 75 · Olicom Sweden · Tel.: (+46) 8 594 704 94 · Olicom UK Limited · Tel.: (+44) 1494 556600

Publication 3198 1195 01/99

Detection Circuitry for short-range optical link tests

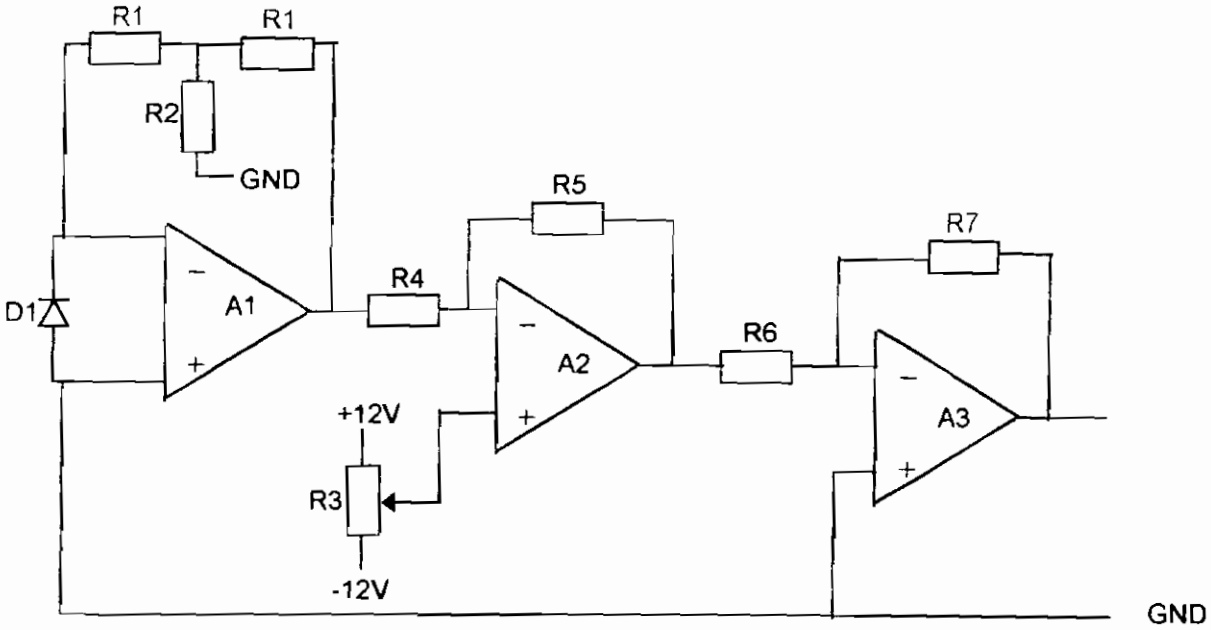

Figure 1; *Detector Circuit*

Detector Circuit Design

Figure 1 shows the detector circuit used in the short – range optical link tests. The infrared (IR) test link and rain gauge both consist of a narrow beamwidth 880nm IR emitting diode, operated at a quiescent current of 100mA, as well as a diode connected photo transistor. The detection circuitry is based upon the use of a quad JFET operational amplifier that provides the necessary high input impedance and low input bias currents required in the input detection stage. Radiation-induced current, produced by the diode-connected photo transistor (D1), is converted to a voltage signal by the transimpedence A1 amplifier stage. The gain at this stage is approximately $R1^2/R2$ and is varied by adjustment of R2. A suitable (negative) offset is added to the signal at this stage in the A2 stage. A final stage of amplification provided in A3 to produce a signal that is within the conversion range of the Picolog data acquisition module that interfaces with a monitoring PC.

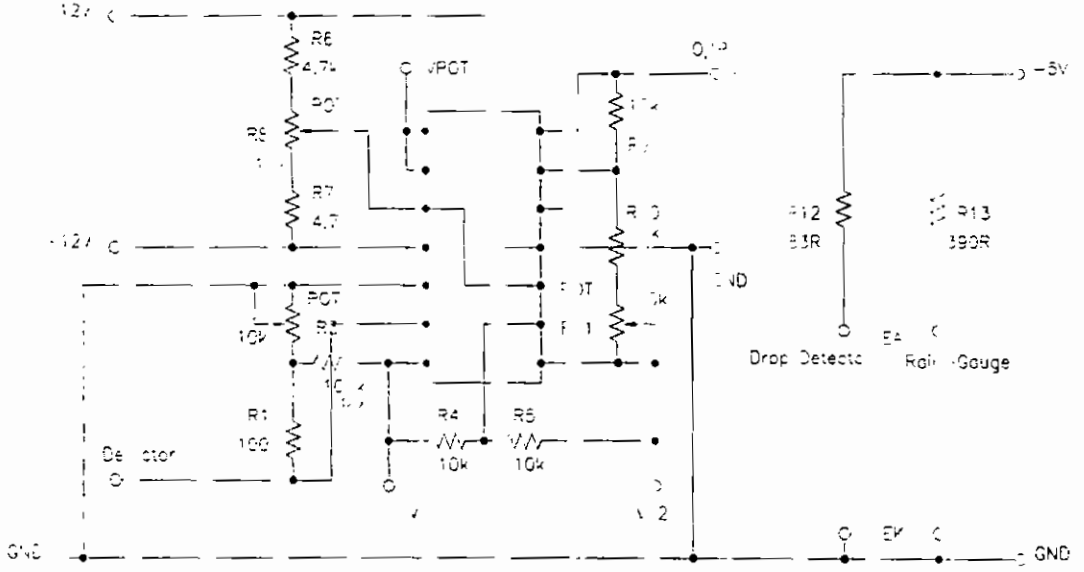

R8 Offse

R3 Emitter C n

R11 Output Gain

14-pin DIL device pin-out

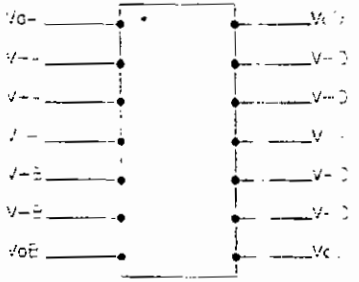

Quad FET Input Op-Amp

Texas Instruments TL084

691

Karen Dunne
Dublin Institute of Technology
Emitter-Detector Module #4

Page Size: A

Revision: 1.5 April 14th, 2003 Page 1 of 1

Laser Integrated Detector IC

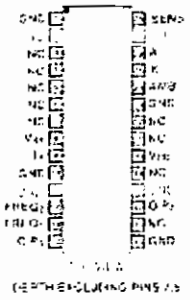

Supplied to RS by Vector Technology

The LiD3010 is a multi-function hybrid laser integrated detector consisting of an input amplifier, high pass filter, ambient compensator, tone decoders and modulation circuitry all housed in an industry standard 28 d.i.l. plastic package.
The module may be configured as a simple light intensity detector or as a modulated detector. A tone decoder is also included which may be tuned to lock onto a particular modulating frequency, this facility is needed where high noise levels exist. The detector can also drive both the **RS** modulating laser diode modules allowing a simple and easy method of developing a synchronous (closed loop) detection system. For suitable PIN diodes, refer to this section.

Other features include:

- d.c. to 6MHz bandwidth
- Ambient light compensated
- 100Hz flicker filter (fluorescent lights)
- Asynchronous/synchronous detection
- 5kHz - 500kHz tunable tone decoder
- Reverse polarity protection
- Hybrid reliability

Typical applications include: intensity stability checking, security beam break monitoring, fog/particle detection, alignment, data transmission and audio/video communications.

technical specification	
Overall characteristics	
Supply voltage	
V_{CC}	10V to 14V
V_{SS}	-10V to -14V
Supply current	
I_{CC} (typ.)	30mA
I_{SS} (typ.)	20mA
Input amplifier	
Bandwidth	d.c. to 6MHz
Noise voltage (typ.)	10µV p to p
Slew rate (typ.)	12V/µs
Input bias current (max.)	100pA
Input offset current (max.)	50pA
High pass filter	
Bandwidth (3dB)	1kHz to 1MHz
Ambient compensator	
Output offset voltage (typ.)	2mV
Tone decoder	
Centre frequency	27kHz
Frequency stability	50 ±200ppm/°C
Detection bandwidth	10% of fo
Modulator	
Output voltage (typ.)	±400mV
Output impedance	50Ω
Outputs	
Output voltage swing	
OP1/2 (typ.)	10V p to p
OP3	0V to 5V

SLOS081E – FEBRUARY 1977 – REVISED FEBRUARY 1999

- Low Power Consumption
- Wide Common-Mode and Differential Voltage Ranges
- Low Input Bias and Offset Currents
- Output Short-Circuit Protection
- Low Total Harmonic Distortion . . . 0.003% Typ
- High Input Impedance . . . JFET-Input Stage
- Latch-Up-Free Operation
- High Slew Rate . . . 13 V/μs Typ
- Common-Mode Input Voltage Range Includes V_{CC+}

description

The TL08x JFET-input operational amplifier family is designed to offer a wider selection than any previously developed operational amplifier family. Each of these JFET-input operational amplifiers incorporates well-matched, high-voltage JFET and bipolar transistors in a monolithic integrated circuit. The devices feature high slew rates, low input bias and offset currents, and low offset voltage temperature coefficient. Offset adjustment and external compensation options are available within the TL08x family.

The C-suffix devices are characterized for operation from 0°C to 70°C. The I-suffix devices are characterized for operation from −40°C to 85°C. The Q-suffix devices are characterized for operation from −40°C to 125°C. The M-suffix devices are characterized for operation over the full military temperature range of −55°C to 125°C.

symbols

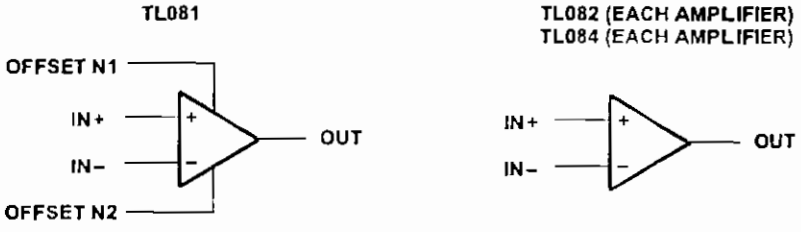

AVAILABLE OPTIONS

T_A	V_{IO}max AT 25°C	PACKAGED DEVICES										CHIP FORM (Y)
		SMALL OUTLINE (D008)	SMALL OUTLINE (D014)	CHIP CARRIER (FK)	CERAMIC DIP (J)	CERAMIC DIP (JG)	PLASTIC DIP (N)	PLASTIC DIP (P)	TSSOP (PW)	FLAT PACK (U)	FLAT PACK (W)	
0°C to 70°C	15 mV	TL081CD	—	—	—	—	—	TL081CP	TL081CPW	—	—	—
	6 mV	TL081ACD						TL081ACP				
	3 mV	TL081BCD						TL081BCP				
	15 mV	TL082CD	—	—	—	—	—	TL082CP	TL082CPW	—	—	TL082Y
	6 mV	TL082ACD						TL082ACP				
	3 mV	TL082BCD						TL082BCP				
	15 mV	—	TL084CD	—	—	—	TL084CN	—	TL084CPW	—	—	TL084Y
	6 mV		TL084ACD				TL084ACN					
	3 mV		TL084BCD				TL084BCN					
−40°C to 85°C	6 mV	TL081ID	—	—	—	—	—	TL081IP	—	—	—	—
	6 mV	TL082ID						TL082IP				
	6 mV	TL084ID	TL084ID				TL084IN					
−40°C to 125°C	9 mV	—	TL084QD	—	—	—	—	—	—	—	—	—
−55°C to 125°C	6 mV	—	—	TL081MFK	TL084MJ	TL081MJG	—	—	—	TL081MU	TL084MW	—
	6 mV			TL082MFK		TL082MJG				TL082MU		
	9 mV			TL084MFK								

The D package is available taped and reeled. Add R suffix to the device type (e.g., TL081CDR).

TL082Y chip information

These chips, when properly assembled, display characteristics similar to the TL082. Thermal compression or ultrasonic bonding may be used on the doped-aluminum bonding pads. Chips may be mounted with conductive epoxy or a gold-silicon preform.

BONDING PAD ASSIGNMENTS

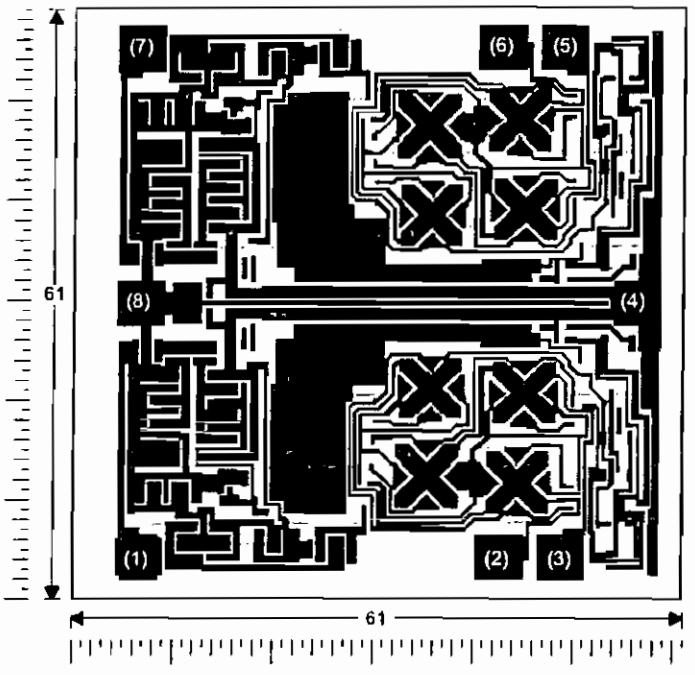

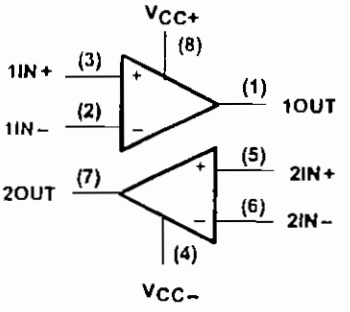

CHIP THICKNESS: 15 TYPICAL

BONDING PADS: 4 × 4 MINIMUM

$T_{J}max$ = 150°C

TOLERANCES ARE ±10%.

ALL DIMENSIONS ARE IN MILS.

PIN (4) IS INTERNALLY CONNECTED TO BACKSIDE OF CHIP.

absolute maximum ratings over operating free-air temperature range (unless otherwise noted)†

		TL08_C TL08_AC TL08_BC	TL08_I	TL084Q	TL08_M	UNIT
Supply voltage, V_{CC+} (see Note 1)		18	18	18	18	V
Supply voltage V_{CC-} (see Note 1)		−18	−18	−18	−18	V
Differential input voltage, V_{ID} (see Note 2)		±30	±30	±30	±30	V
Input voltage, V_I (see Notes 1 and 3)		±15	±15	±15	±15	V
Duration of output short circuit (see Note 4)		unlimited	unlimited	unlimited	unlimited	
Continuous total power dissipation		See Dissipation Rating Table				
Operating free-air temperature range, T_A		0 to 70	−40 to 85	−40 to 125	−55 to 125	°C
Storage temperature range, T_{stg}		−65 to 150	−65 to 150	−65 to 150	−65 to 150	°C
Case temperature for 60 seconds, T_C	FK package				260	°C
Lead temperature 1,6 mm (1/16 inch) from case for 60 seconds	J or JG package				300	°C
Lead temperature 1,6 mm (1/16 inch) from case for 10 seconds	D, N, P, or PW package	260	260	260		°C

† Stresses beyond those listed under "absolute maximum ratings" may cause permanent damage to the device. These are stress ratings only, and functional operation of the device at these or any other conditions beyond those indicated under "recommended operating conditions" is not implied. Exposure to absolute-maximum-rated conditions for extended periods may affect device reliability.

NOTES: 1. All voltage values, except differential voltages, are with respect to the midpoint between V_{CC+} and V_{CC-}.
2. Differential voltages are at IN+ with respect to IN−.
3. The magnitude of the input voltage must never exceed the magnitude of the supply voltage or 15 V, whichever is less.
4. The output may be shorted to ground or to either supply. Temperature and/or supply voltages must be limited to ensure that the dissipation rating is not exceeded.

DISSIPATION RATING TABLE

PACKAGE	$T_A \le 25°C$ POWER RATING	DERATING FACTOR	DERATE ABOVE T_A	$T_A = 70°C$ POWER RATING	$T_A = 85°C$ POWER RATING	$T_A = 125°C$ POWER RATING
D (8 pin)	680 mW	5.8 mW/°C	32°C	460 mW	373 mW	N/A
D (14 pin)	680 mW	7.6 mW/°C	60°C	604 mW	490 mW	186 mW
FK	680 mW	11.0 mW/°C	88°C	680 mW	680 mW	273 mW
J	680 mW	11.0 mW/°C	88°C	680 mW	680 mW	273 mW
JG	680 mW	8.4 mW/°C	69°C	672 mW	546 mW	210 mW
N	680 mW	9.2 mW/°C	76°C	680 mW	597 mW	N/A
P	680 mW	8.0 mW/°C	65°C	640 mW	520 mW	N/A
PW (8 pin)	525 mW	4.2 mW/°C	25°C	336 mW	N/A	N/A
PW (14 pin)	700 mW	5.6 mW/°C	25°C	448 mW	N/A	N/A
U	675 mW	5.4 mW/°C	25°C	432 mW	351 mW	135 mW
W	680 mW	8.0 mW/°C	65°C	640 mW	520 mW	200 mW

electrical characteristics, $V_{CC\pm}$ = ±15 V (unless otherwise noted)

PARAMETER		TEST CONDITIONS†	T_A	TL081M, TL082M			TL084Q, TL084M			UNIT
				MIN	TYP	MAX	MIN	TYP	MAX	
V_{IO}	Input offset voltage	V_O = 0, R_S = 50 Ω	25°C		3	6		3	9	mV
			Full range			9			15	
α_{VIO}	Temperature coefficient of input offset voltage	V_O = 0 R_S = 50 Ω	Full range		18			18		µV/°C
I_{IO}	Input offset current‡	V_O = 0	25°C		5	100		5	100	pA
			125°C			20			20	nA
I_{IB}	Input bias current‡	V_O = 0	25°C		30	200		30	200	pA
			125°C			50			50	nA
V_{ICR}	Common-mode input voltage range		25°C	±11	±12 to 15		±11	±12 to 15		V
V_{OM}	Maximum peak output voltage swing	R_L = 10 kΩ	25°C	±12	±13.5		±12	±13.5		V
		R_L ≥ 10 kΩ	Full range	±12			±12			
		R_L ≥ 2 kΩ		±10	±12		±10	±12		
A_{VD}	Large-signal differential voltage amplification	V_O = ±10 V, R_L ≥ 2 kΩ	25°C	25	200		25	200		V/mV
		V_O = ±10 V, R_L ≥ 2 kΩ	Full range	15			15			
B_1	Unity-gain bandwidth		25°C		3			3		MHz
r_i	Input resistance		25°C		10^{12}			10^{12}		Ω
CMRR	Common-mode rejection ratio	V_{IC} = V_{ICR}min, V_O = 0, R_S = 50 Ω	25°C	80	86		80	86		dB
k_{SVR}	Supply voltage rejection ratio ($\Delta V_{CC\pm}/\Delta V_{IO}$)	V_{CC} = ±15 V to ±9 V, V_O = 0, R_S = 50 Ω	25°C	80	86		80	86		dB
I_{CC}	Supply current (per amplifier)	V_O = 0 No load	25°C		1.4	2.8		1.4	2.8	mA
V_{O1}/V_{O2}	Crosstalk attenuation	A_{VD} = 100	25°C		120			120		dB

† All characteristics are measured under open-loop conditions with zero common-mode input voltage unless otherwise specified.
‡ Input bias currents of a FET-input operational amplifier are normal junction reverse currents, which are temperature sensitive as shown in Figure 17. Pulse techniques must be used that maintain the junction temperatures as close to the ambient temperature as is possible.

operating characteristics, $V_{CC\pm}$ = ±15 V, T_A = 25°C (unless otherwise noted)

PARAMETER		TEST CONDITIONS				MIN	TYP	MAX	UNIT
SR	Slew rate at unity gain	V_I = 10 V,	R_L = 2 kΩ,	C_L = 100 pF,	See Figure 1	8*	13		V/µs
		V_I = 10 V, T_A = – 55°C to 125°C,	R_L = 2 kΩ, See Figure 1	C_L = 100 pF,		5*			
t_r	Rise time	V_I = 20 mV,	R_L = 2 kΩ,	C_L = 100 pF,	See Figure 1		0.05		µs
	Overshoot factor						20%		
V_n	Equivalent input noise voltage	R_S = 20 Ω	f = 1 kHz				18		nV/√Hz
			f = 10 Hz to 10 kHz				4		µV
I_n	Equivalent input noise current	R_S = 20 Ω,	f = 1 kHz				0.01		pA/√Hz
THD	Total harmonic distortion	$V_I$rms = 6 V, f = 1 kHz	A_{VD} = 1,	R_S ≤ 1 kΩ,	R_L ≥ 2 kΩ,		0.003%		

* On products compliant to MIL-PRF-38535, this parameter is not production tested.

PARAMETER MEASUREMENT INFORMATION

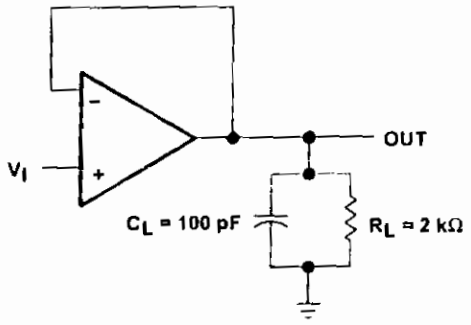

Figure 1

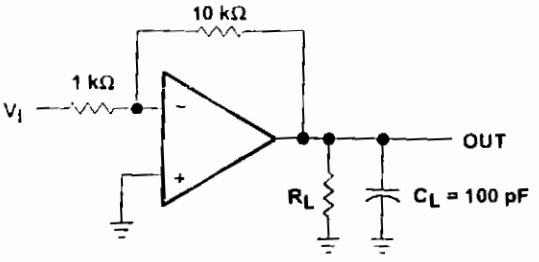

Figure 2

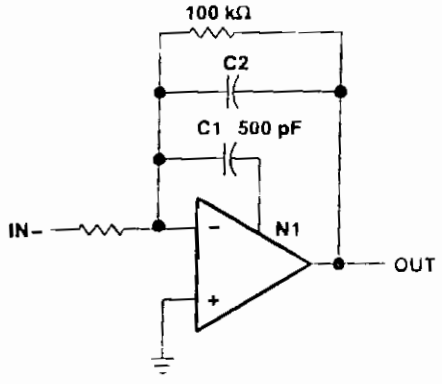

Figure 3

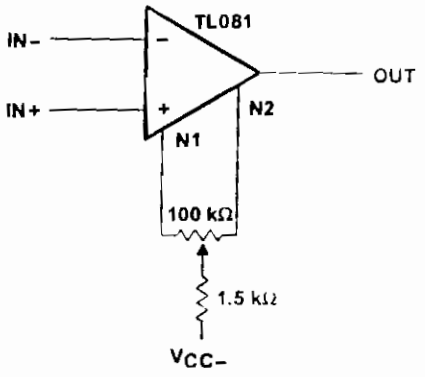

Figure 4

TYPICAL CHARACTERISTICS†

MAXIMUM PEAK OUTPUT VOLTAGE
vs
FREQUENCY

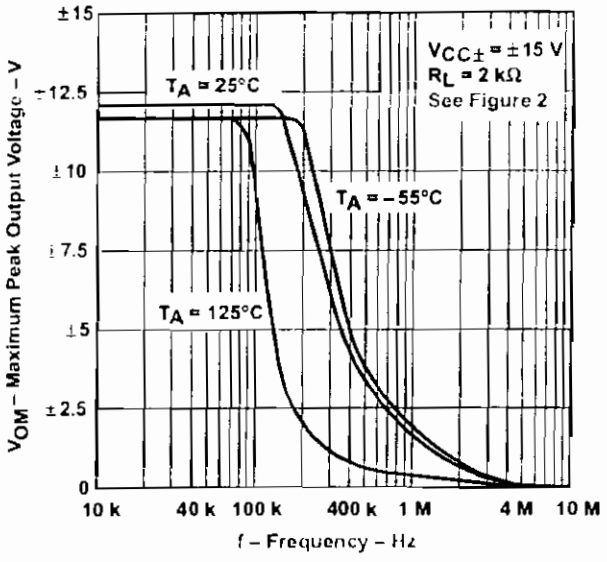

Figure 7

MAXIMUM PEAK OUTPUT VOLTAGE
vs
FREE-AIR TEMPERATURE

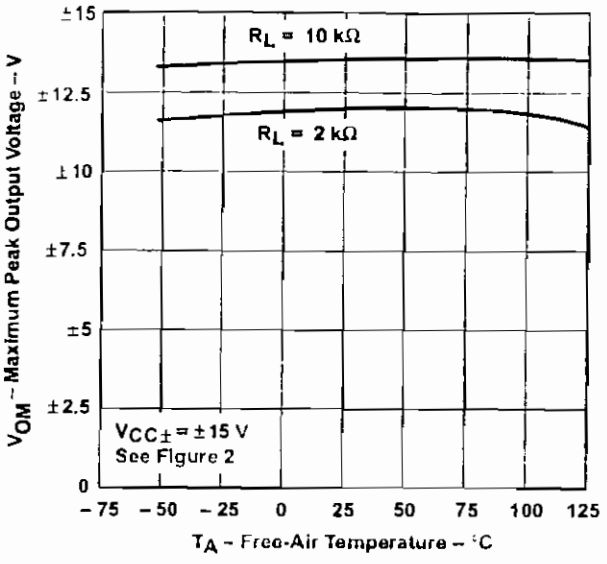

Figure 8

MAXIMUM PEAK OUTPUT VOLTAGE
vs
LOAD RESISTANCE

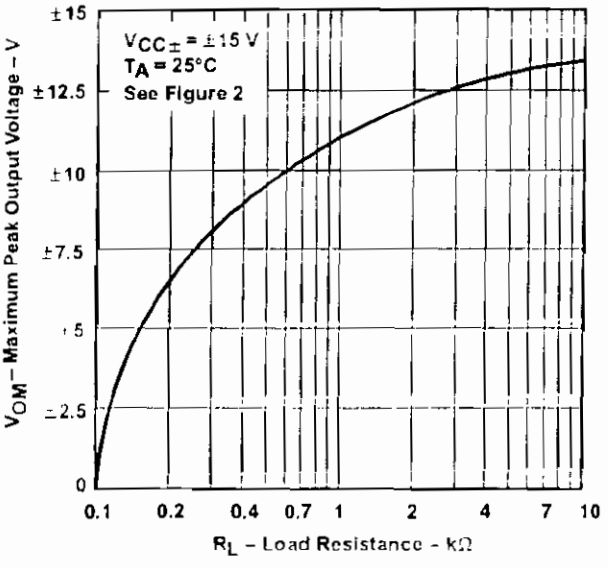

Figure 9

MAXIMUM PEAK OUTPUT VOLTAGE
vs
SUPPLY VOLTAGE

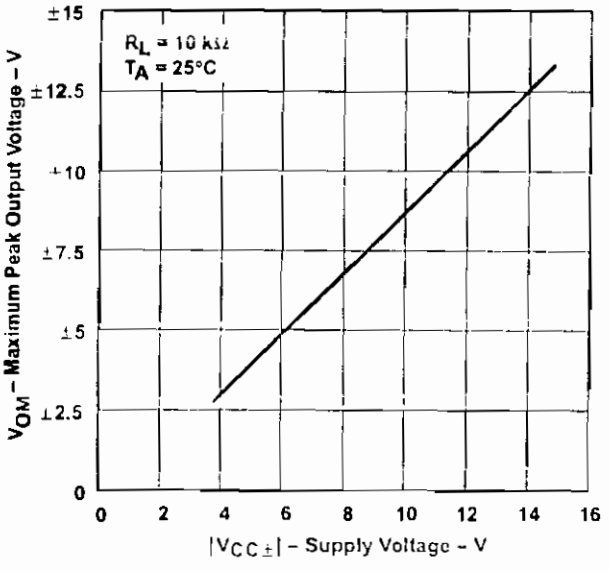

Figure 10

† Data at high and low temperatures are applicable only within the rated operating free-air temperature ranges of the various devices

TYPICAL CHARACTERISTICS†

DIFFERENTIAL VOLTAGE AMPLIFICATION
vs
FREQUENCY WITH FEED-FORWARD COMPENSATION

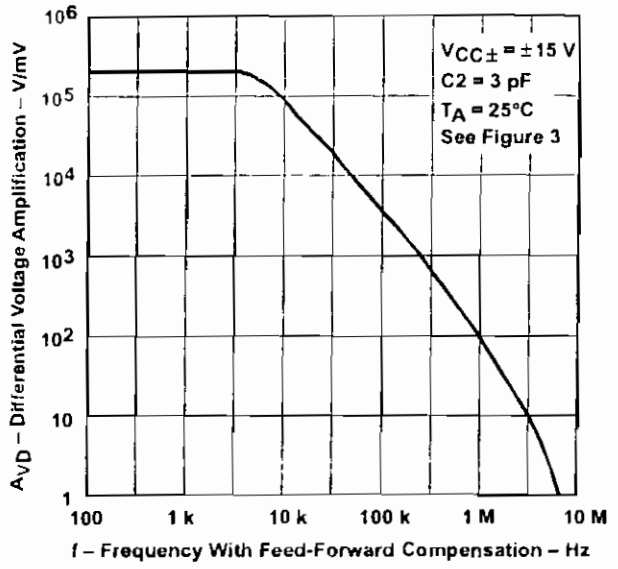

Figure 13

TOTAL POWER DISSIPATION
vs
FREE-AIR TEMPERATURE

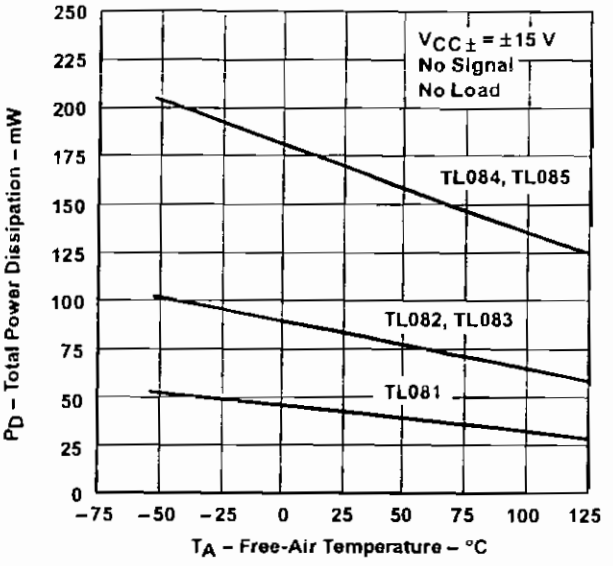

Figure 14

SUPPLY CURRENT PER AMPLIFIER
vs
FREE-AIR TEMPERATURE

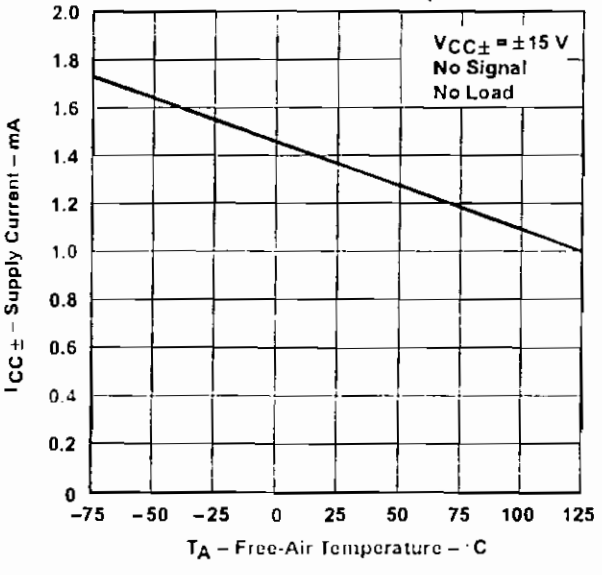

Figure 15

SUPPLY CURRENT
vs
SUPPLY VOLTAGE

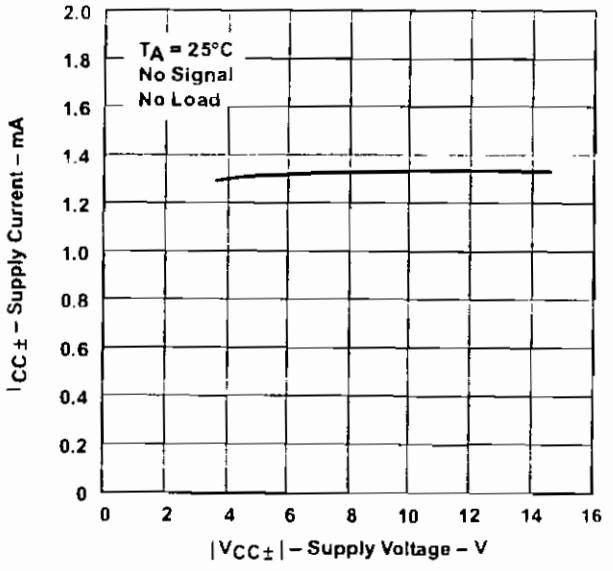

Figure 16

† Data at high and low temperatures are applicable only within the rated operating free-air temperature ranges of the various devices

TYPICAL CHARACTERISTICS†

EQUIVALENT INPUT NOISE VOLTAGE
vs
FREQUENCY

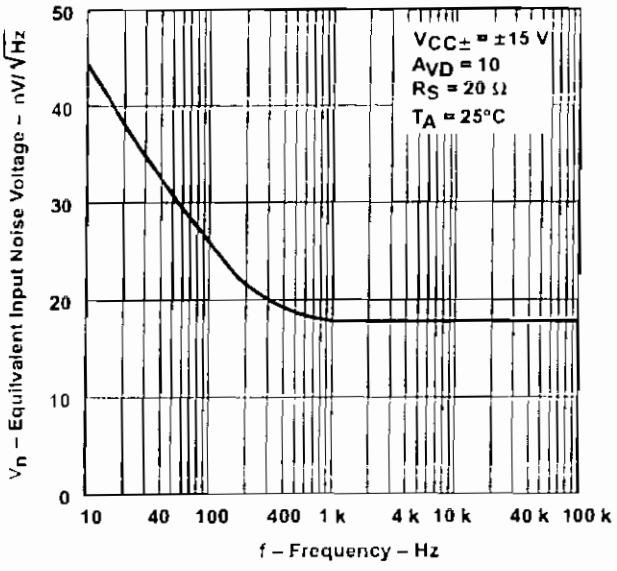

Figure 21

TOTAL HARMONIC DISTORTION
vs
FREQUENCY

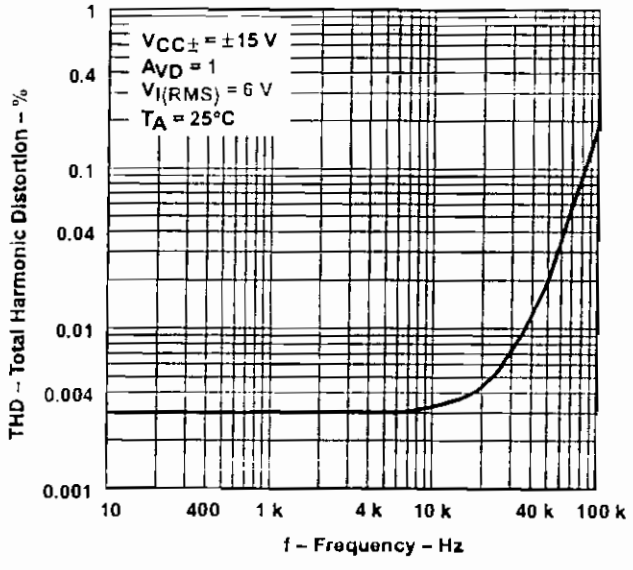

Figure 22

† Data at high and low temperatures are applicable only within the rated operating free-air temperature ranges of the various devices.

APPLICATION INFORMATION

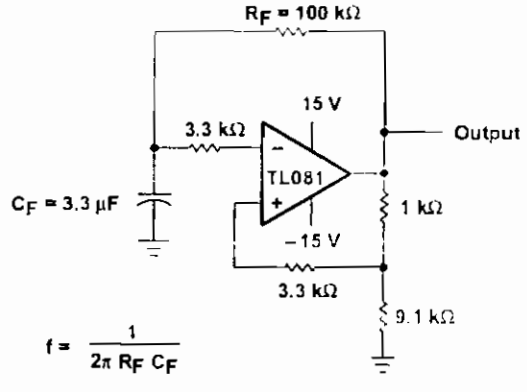

Figure 23

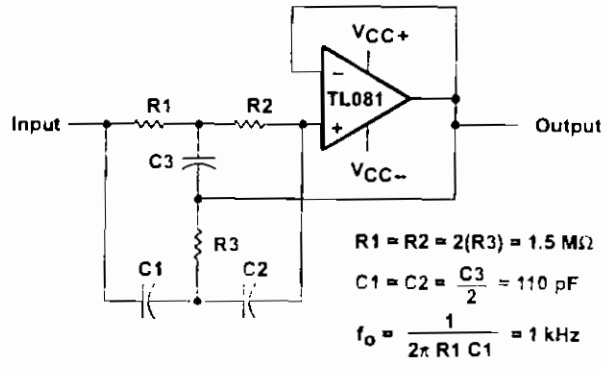

Figure 24

APPLICATION INFORMATION

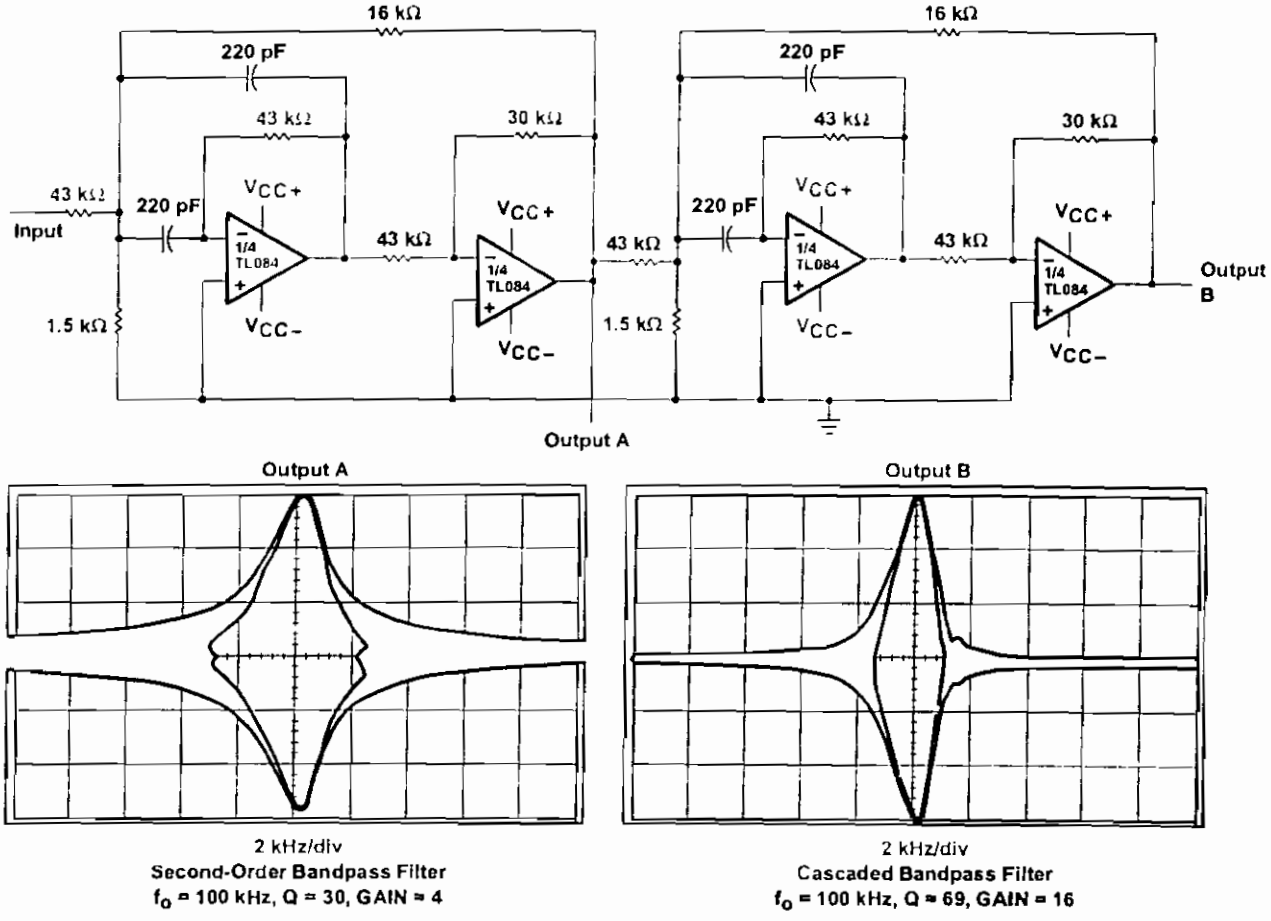

Figure 27. Positive-Feedback Bandpass Filter

MECHANICAL DATA

FK (S-CQCC-N)** **LEADLESS CERAMIC CHIP CARRIER**

28 TERMINAL SHOWN

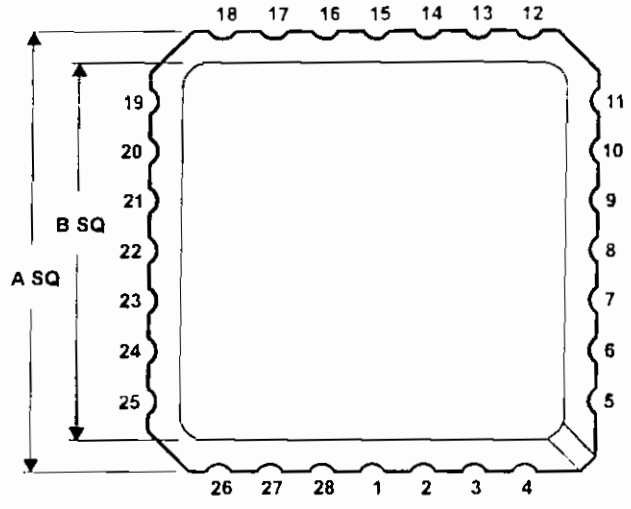

NO. OF TERMINALS **	A		B	
	MIN	MAX	MIN	MAX
20	0.342 (8,69)	0.358 (9,09)	0.307 (7,80)	0.358 (9,09)
28	0.442 (11,23)	0.458 (11,63)	0.406 (10,31)	0.458 (11,63)
44	0.640 (16,26)	0.660 (16,76)	0.495 (12,58)	0.560 (14,22)
52	0.739 (18,78)	0.761 (19,32)	0.495 (12,58)	0.560 (14,22)
68	0.938 (23,83)	0.962 (24,43)	0.850 (21,6)	0.858 (21,8)
84	1.141 (28,99)	1.165 (29,59)	1.047 (26,6)	1.063 (27,0)

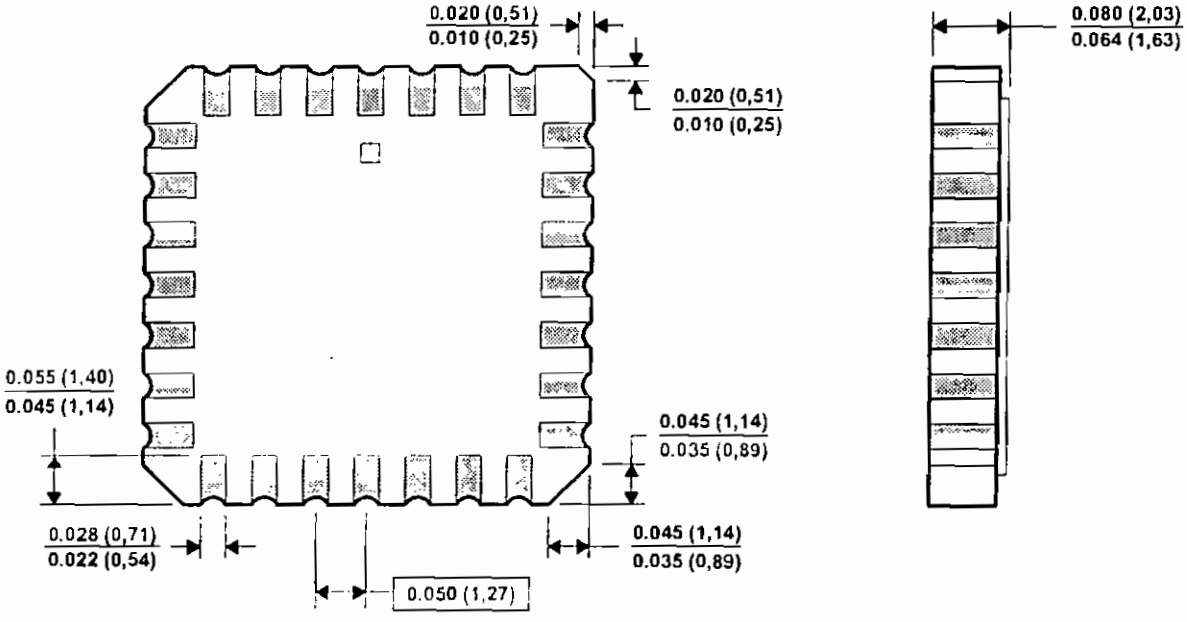

4040140/D 10/96

NOTES: A. All linear dimensions are in inches (millimeters).
B. This drawing is subject to change without notice.
C. This package can be hermetically sealed with a metal lid.
D. The terminals are gold plated.
E. Falls within JEDEC MS-004

MECHANICAL DATA

JG (R-GDIP-T8) **CERAMIC DUAL-IN-LINE PACKAGE**

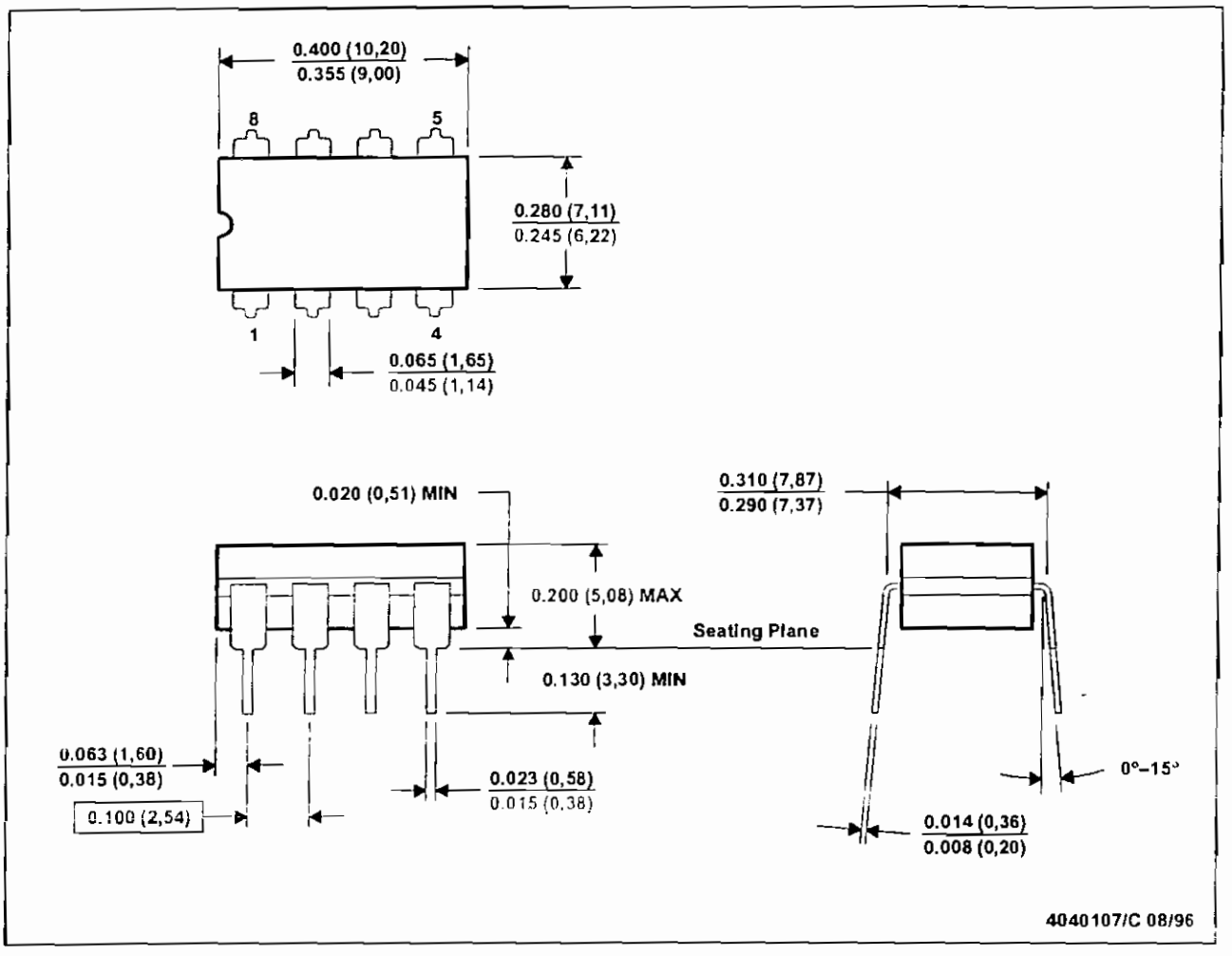

NOTES: A. All linear dimensions are in inches (millimeters).
B. This drawing is subject to change without notice.
C. This package can be hermetically sealed with a ceramic lid using glass frit.
D. Index point is provided on cap for terminal identification only on press ceramic glass frit seal only.
E. Falls within MIL-STD-1835 GDIP1-T8

MECHANICAL DATA

P (R-PDIP-T8) PLASTIC DUAL-IN-LINE PACKAGE

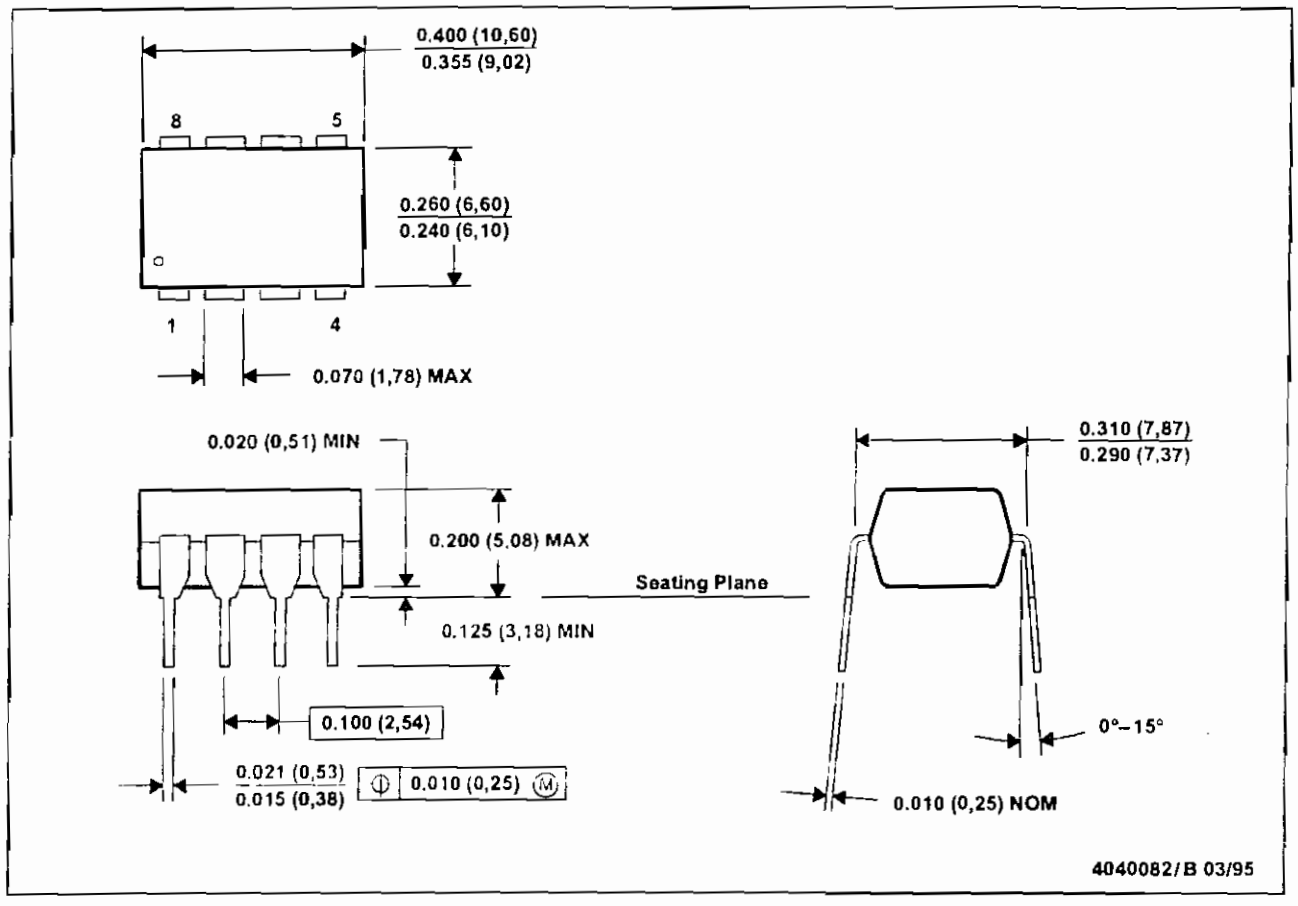

NOTES: A. All linear dimensions are in inches (millimeters).
B. This drawing is subject to change without notice.
C. Falls within JEDEC MS-001

MECHANICAL DATA

U (S-GDFP-F10) **CERAMIC DUAL FLATPACK**

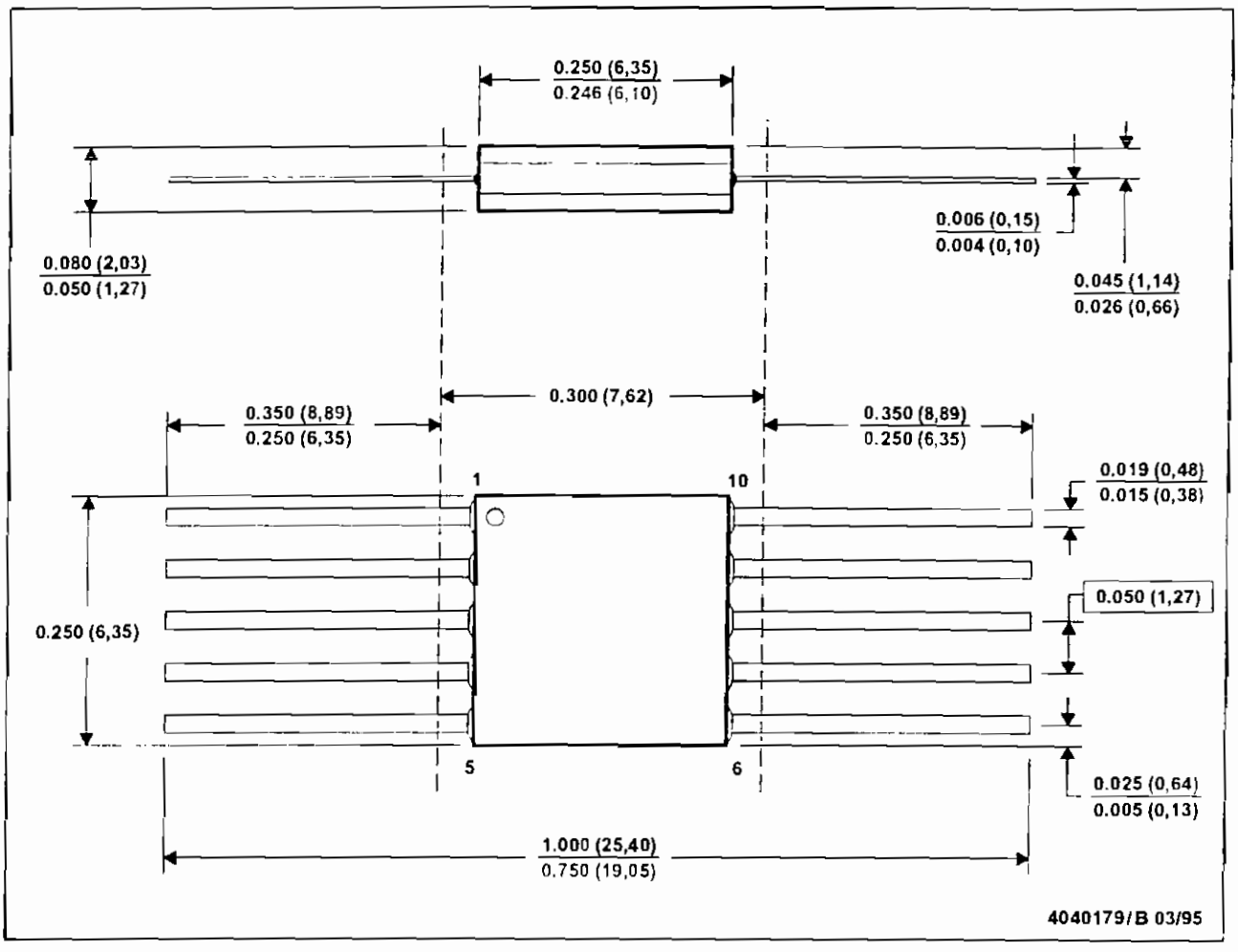

NOTES: A. All linear dimensions are in inches (millimeters).
B. This drawing is subject to change without notice.
C. This package can be hermetically sealed with a ceramic lid using glass frit.
D. Index point is provided on cap for terminal identification only.
E. Falls within MIL STD 1835 GDFP1-F10 and JEDEC MO-092AA

IMPORTANT NOTICE

Texas Instruments and its subsidiaries (TI) reserve the right to make changes to their products or to discontinue any product or service without notice, and advise customers to obtain the latest version of relevant information to verify, before placing orders, that information being relied on is current and complete. All products are sold subject to the terms and conditions of sale supplied at the time of order acknowledgement, including those pertaining to warranty, patent infringement, and limitation of liability.

TI warrants performance of its semiconductor products to the specifications applicable at the time of sale in accordance with TI's standard warranty. Testing and other quality control techniques are utilized to the extent TI deems necessary to support this warranty. Specific testing of all parameters of each device is not necessarily performed, except those mandated by government requirements.

CERTAIN APPLICATIONS USING SEMICONDUCTOR PRODUCTS MAY INVOLVE POTENTIAL RISKS OF DEATH, PERSONAL INJURY, OR SEVERE PROPERTY OR ENVIRONMENTAL DAMAGE ("CRITICAL APPLICATIONS"). TI SEMICONDUCTOR PRODUCTS ARE NOT DESIGNED, AUTHORIZED, OR WARRANTED TO BE SUITABLE FOR USE IN LIFE-SUPPORT DEVICES OR SYSTEMS OR OTHER CRITICAL APPLICATIONS. INCLUSION OF TI PRODUCTS IN SUCH APPLICATIONS IS UNDERSTOOD TO BE FULLY AT THE CUSTOMER'S RISK.

In order to minimize risks associated with the customer's applications, adequate design and operating safeguards must be provided by the customer to minimize inherent or procedural hazards.

TI assumes no liability for applications assistance or customer product design. TI does not warrant or represent that any license, either express or implied, is granted under any patent right, copyright, mask work right, or other intellectual property right of TI covering or relating to any combination, machine, or process in which such semiconductor products or services might be or are used. TI's publication of information regarding any third party's products or services does not constitute TI's approval, warranty or endorsement thereof.

GaAlAs-IR-Lumineszenzdioden (880 nm)
GaAlAs Infrared Emitters (880 nm)

SFH 480
SFH 481
SFH 482

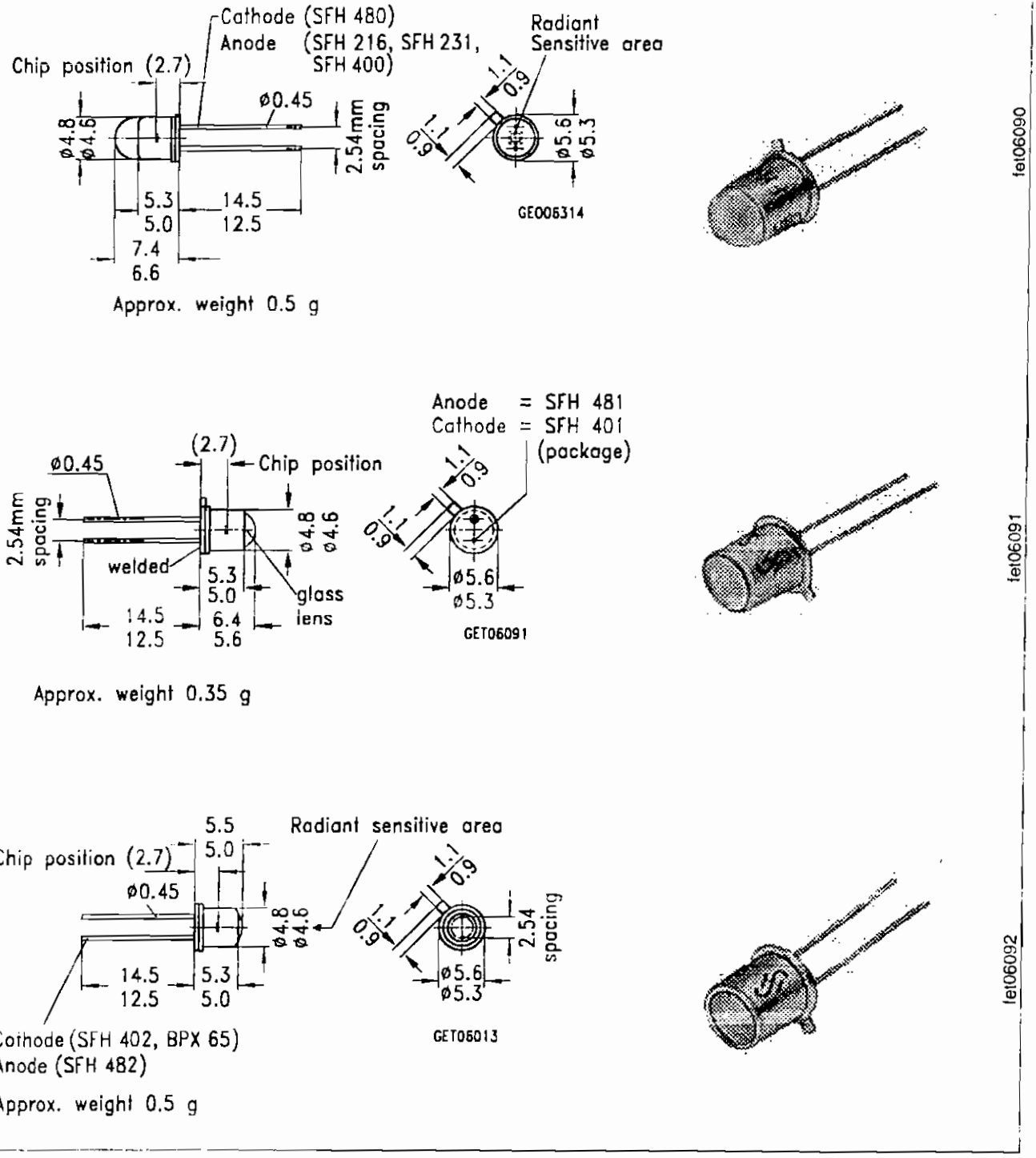

Maße in mm, wenn nicht anders angegeben/Dimensions in mm, unless otherwise specified.

Wesentliche Merkmale

- Hergestellt im Schmezepitaxieverfahren
- Anode galvanisch mit dem Gehäuseboden verbunden
- Hohe Zuverlässigkeit
- Gute spektrale Anpassung an Si-Fotoempfänger
- Hermetisch dichtes Metallgehäuse
- SFH 480: Gehäusegleich mit SFH 216
- SFH 481: Gehäusegleich mit BPX 43, BPY 63
- SFH 482: Gehäusegleich mit BPX 38, BPX 65

Anwendungen

- Lichtschranken für Gleich- und Wechsellichtbetrieb
- IR-Geräteferns teuerungen

Features

- GaAlAs infrared emitting diode, fabricated in a liquid phase epitaxy process
- Anode is electrically connected to the case
- High reliability
- Matches all Si-Photodetectors
- Hermetically sealed package
- SFH 480: Same package as SFH 216
- SFH 481: Same package as BPX 43, BPY 63
- SFH 482: Same package as BPX 38, BPX 65

Applications

- Photointerrupters
- IR remote control of various equipmet

Typ Type	Bestellnummer Ordering Code	Gehäuse Package
SFH 480-2	Q62703-Q1662	18 A3 DIN 41876 (TO-18), Anschlüsse im 2.54-mm-Raster ($^1/_{10}$"), Kathodenkennzeichnung: Nase am Gehäuseboden 18 A3 DIN 41876 (TO-18), lead spacing 2.54 mm ($^1/_{10}$"), cathode marking: projection at package
SFH 480-3	Q62703-Q1663	
SFH 481	Q62703-Q1088	
SFH 481-1	Q62703-Q1664	
SFH 481-2	Q62703-Q1665	
SFH 482	Q62703-Q1089	
SFH 482-1	Q62703-Q1667	
SFH 482-2	Q62703-Q1668	
SFH 482-3	Q62703-Q1669	
SFH 482-M E7800	Q62703-Q2186	

Grenzwerte (T_C = 25 °C)
Maximum Ratings

Bezeichnung Description	Symbol Symbol	Wert Value	Einheit Unit
Betriebs- und Lagertemperatur Operating and storage temperature range	T_{op}; T_{stg}	– 55 ... + 100	°C
Sperrschichttemperatur Junction temperature	T_j	100	°C
Sperrspannung Reverse voltage	V_R	5	V
Durchlaßstrom Forward current	I_F	200	mA
Stoßstrom, t_p = 10 µs, D = 0 Surge current	I_{FSM}	2.5	A
Verlustleistung Power dissipation	P_{tot}	470	mW
Wärmewiderstand Thermal resistance	R_{thJA} R_{thJC}	450 160	K/W K/W

Kennwerte (T_A = 25 °C)
Characteristics

Bezeichnung Description	Symbol Symbol	Wert Value	Einheit Unit
Wellenlänge der Strahlung Wavelength at peak emission I_F = 100 mA	λ_{peak}	880	nm
Spektrale Bandbreite bei 50 % von I_{max} Spectral bandwidth at 50 % of I_{max} I_F = 100 mA	$\Delta\lambda$	80	nm
Abstrahlwinkel Half angle SFH 480 SFH 481 SFH 482	 φ φ φ	 ± 6 ± 15 ± 30	 Grad deg.
Aktive Chipfläche Active chip area	A	0.16	mm^2
Abmessungen der aktive Chipfläche Dimension of the active chip area	$L \times B$ $L \times W$	0.4 × 0.4	mm

Kennwerte (T_A = 25 °C)
Characteristics

Bezeichnung **Description**	**Symbol** **Symbol**	**Wert** **Value**	**Einheit** **Unit**
Abstand Chipoberfläche bis Linsenscheitel Distance chip front to lens top			
SFH 480	H	4.0 ... 4.8	mm
SFH 481	H	2.8 ... 3.7	mm
SFH 482	H	2.1 ... 2.7	mm
Schaltzeiten, I_e von 10 % auf 90 % und von 90 % auf 10 %, bei I_F = 100 mA, R_L = 50 Ω Switching times, I_e from 10 % to 90 % and from 90 % to10 %, I_F = 100 mA, R_L = 50 Ω	t_r, t_f	0.6/0.5	µs
Kapazität Capacitance V_R = 0 V, f = 1 MHz	C_o	25	pF
Durchlaßspannung Forward voltage			
I_F = 100 mA, t_p = 20 ms	V_F	1.50 (≤ 1.8)	V
I_F = 1 A, t_p = 100 µs	V_F	3.00 (≤ 3.8)	V
Sperrstrom Reverse current V_R = 5 V	I_R	0.01 (≤ 1)	µA
Gesamtstrahlungsfluß Total radiant flux I_F = 100 mA, t_p = 20 ms	Φ_e	12	mW
Temperaturkoeffizient von I_e bzw. Φ_e, I_F = 100 mA Temperature coefficient of I_e or Φ_e, I_F = 100 mA	TC_I	– 0.5	%/K
Temperaturkoeffizient von V_F, I_F = 100 mA Temperature coefficient of V_F, I_F = 100 mA	TC_V	– 2	mV/K
Temperaturkoeffizient von λ, I_F = 100 mA Temperature coefficient of λ, I_F = 100 mA	TC_λ	+ 0.25	nm/K

Gruppierung der Strahlstärke I_e in Achsrichtung
gemessen bei einem Raumwinkel $\Omega = 0.01$ sr
Grouping of radiant intensity I_e in axial direction
at a steradian of $\Omega = 0.01$ sr

Bezeichnung Description	Symbol Symbol	Wert Value					Einheit Unit
		SFH 480-2	SFH 480-3	SFH 481	SFH 481-1	SFH 481-2	
Strahlstärke Radiant intensity $I_F = 100$ mA, $t_p = 20$ ms	$I_{e\,min}$ $I_{e\,max}$	40 –	63 –	≥ 10	10 20	16 –	mW/sr mW/sr
Strahlstärke Radiant intensity $I_F = 1$ A, $t_p = 100$ µs	$I_{e\,typ.}$	540	630	220	130	220	mW/sr

Bezeichnung Description	Symbol Symbol	Wert Value					Einheit Unit
		SFH 482	SFH 482-1	SFH 482-2	SFH 482-3	SFH 482-M E 7800[1)]	
Strahlstärke Radiant intensity $I_F = 100$ mA, $t_p = 20$ ms	$I_{e\,min}$ $I_{e\,max}$	≥ 3.15 –	3.15 6.3	5 10	8 –	1.6 ... 3.2 –	mW/sr mW/sr
Strahlstärke Radiant intensity $I_F = 1$ A, $t_p = 100$ µs	$I_{e\,typ.}$	–	40	65	80	–	mW/sr

[1)] Die Messung der Strahlstärke und des Halbwinkels erfolgt mit einer Lochblende vor dem Bauteil (Durchmesser der Lochblende: 2.0 mm; Abstand Lochblende zu Gehäuserückseite: 5.4 mm). Dadurch wird sichergestellt, daß bei der Strahlstärkemessung nur diejenige Strahlung in Achsrichtung bewertet wird, die direkt von der Chipoberfläche austritt. Von der Bodenplatte reflektierte Strahlung (vagabundierende Strahlung) wird dagegen nicht bewertet. Diese Reflexionen sind besonders bei Abbildungen der Chipoberfläche über Zusatzoptiken störend (z.B. Lichtschranken großer Reichweite). In der Anwendung werden im allgemeinen diese Reflexionen ebenfalls durch Blenden unterdrückt. Durch dieses, der Anwendung entsprechende Meßverfahren ergibt sich für den Anwender eine besser verwertbare Größe. Diese Lochblendenmessung ist gekennzeichnet durch den Eintrag "E 7800", der an die Typenbezeichnung angehängt ist.

[1)] An aperture is used in front of the component for measurement of the radiant intensity and the half angle (diameter of the aperture: 1.1 mm; distance of aperture to case back side: 4 mm). This ensures that solely the radiation in axial direction emitting directly from the chip surface will be evaluated during measurement of the radiant intensity. Radiation reflected by the bottom plate (stray radiation) will not be evaluated. These reflections impair the projection of the chip surface by additional optics (e.g. long-range light reflection switches). In respect of the application of the component, these reflections are generally suppressed by apertures as well. This measuring procedure corresponding with the application provides more useful values. This aperture measurement is denoted by "E 7800" added to the type designation.

Radiation characteristics, SFH 480 $I_{rel} = f(\varphi)$

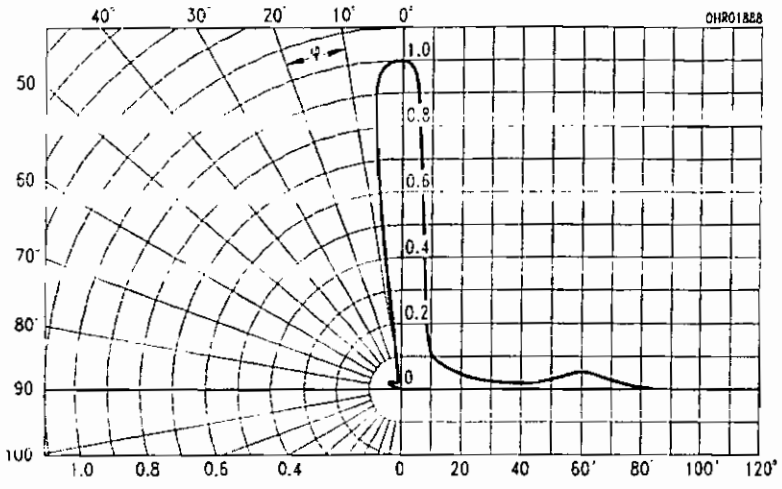

Radiation characteristics, SFH 481 $I_{rel} = f(\varphi)$

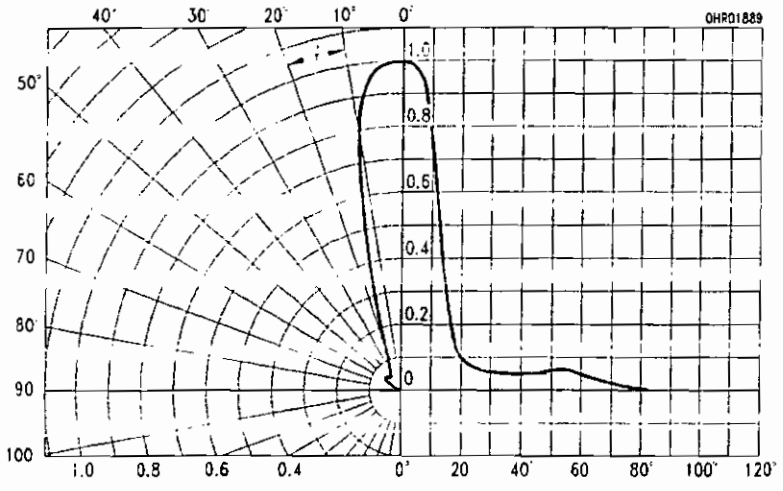

Radiation characteristics, SFH 482 $I_{rel} = f(\varphi)$

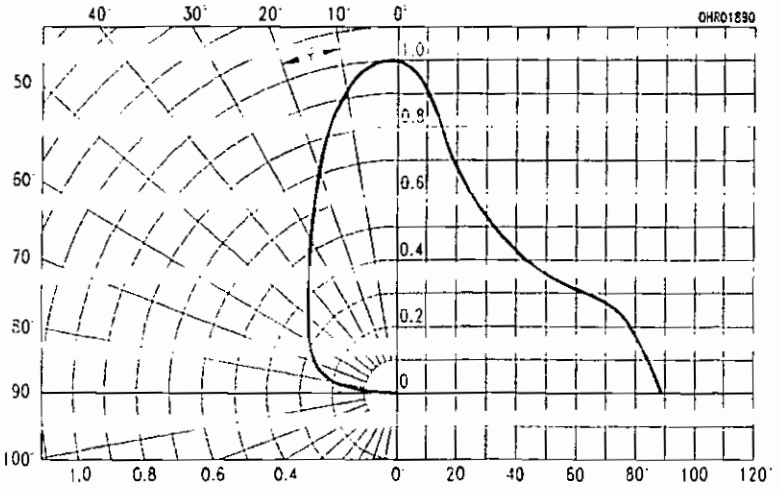

Relative spectral emission
$I_{rel} = f(\lambda)$

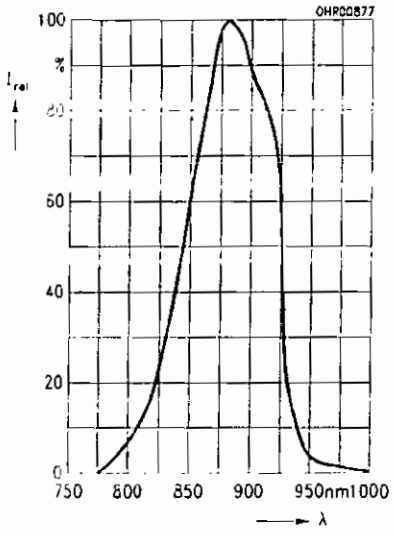

Radiant intensity $\frac{I_e}{I_e\ 100\ mA} = f(I_F)$

Single pulse, $t_p = 20\ \mu s$

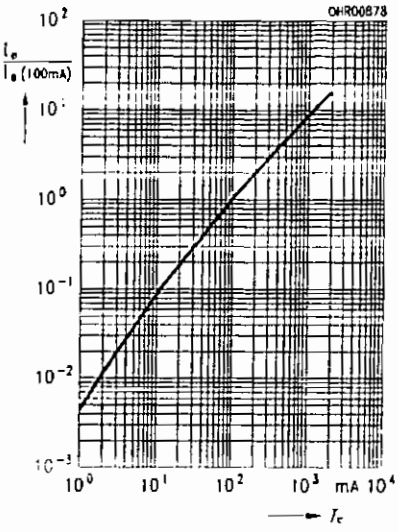

Max. permissible forward current
$I_F = f(T_A, T_C)$

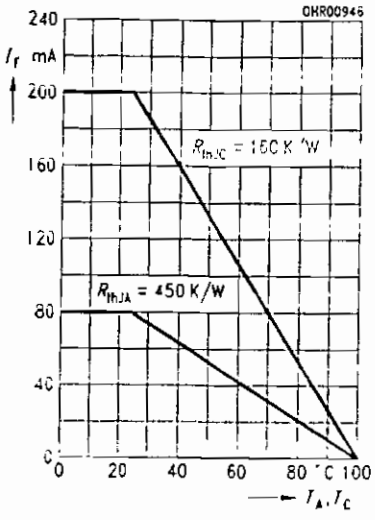

Forward current, $I_F = f(V_F)$
Single pulse, $t_p = 20\ \mu s$

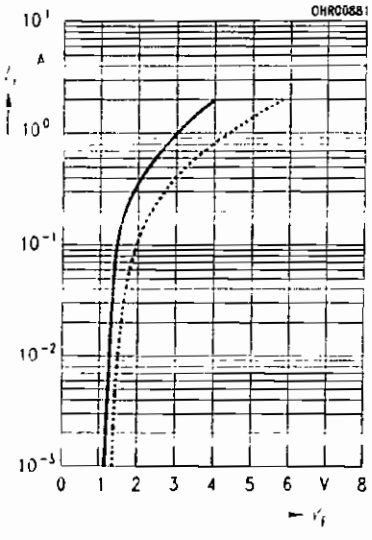

Permissible pulse handling capability
$I_F = f(\tau)$, $T_C = 25$ °C,
duty cycle D = parameter

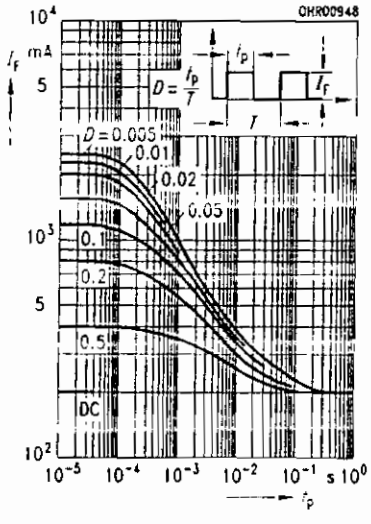

SIEMENS

Silizium-Fotodiode für den sichtbaren Spektralbereich — BPW 21
Silicon Photodiode for the visible spectral range

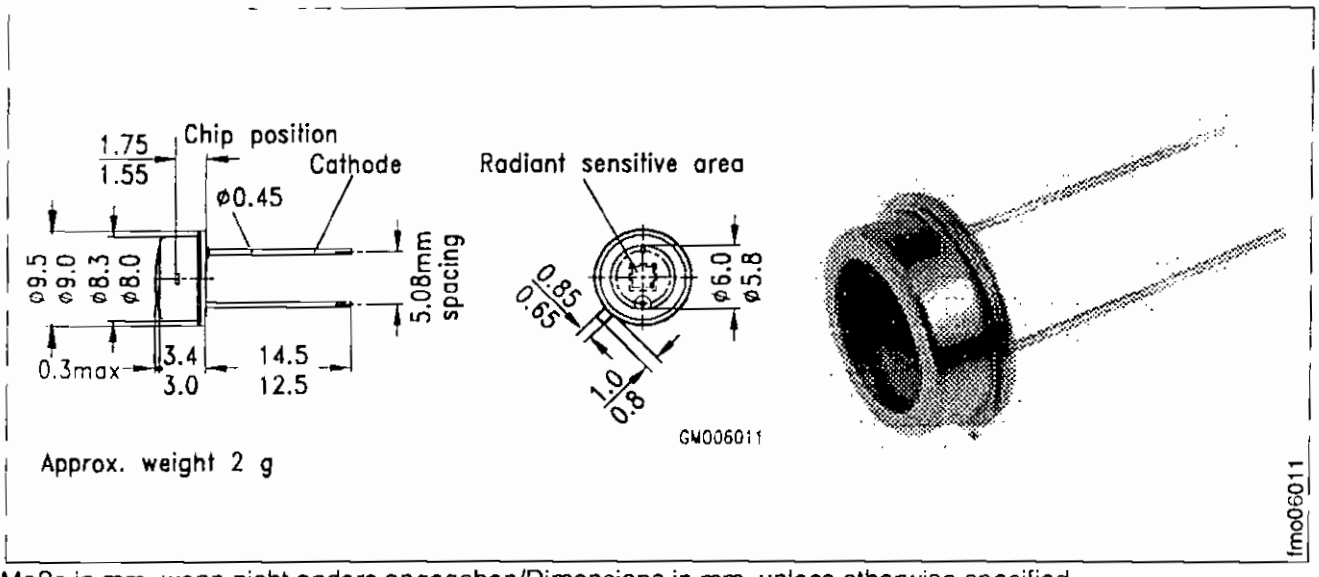

Maße in mm, wenn nicht anders angegeben/Dimensions in mm, unless otherwise specified.

Wesentliche Merkmale

- Speziell geeignet für Anwendungen im Bereich von 350 nm bis 820 nm
- Angepaßt an die Augenempfindlichkeit (V_λ)
- Hermetisch dichte Metallbauform (ähnlich TO-5)

Anwendungen

- Belichtungsmesser für Tageslicht
- Für Kunstlicht mit hoher Farbtemperatur in der Fotografie und Farbanalyse

Features

- Especially suitable for applications from 350 nm to 820 nm
- Adapted to human eye sensitivity (V_λ)
- Hermetically sealed metal package (similar to TO-5)

Applications

- Exposure meter for daylight
- For artificial light of high color temperature in photographic fields and color analysis

Typ Type	Bestellnummer Ordering Code
BPW 21	Q62702-P885

Grenzwerte
Maximum Ratings

Bezeichnung Description	Symbol Symbol	Wert Value	Einheit Unit
Betriebs- und Lagertemperatur Operating and storage temperature range	T_{op}; T_{stg}	– 40 ... + 80	°C
Löttemperatur (Lötstelle 2 mm vom Gehäuse entfernt bei Lötzeit $t \leq 3$ s) Soldering temperature in 2 mm distance from case bottom ($t \leq 3$ s)	T_S	235	°C
Sperrspannung Reverse voltage	V_R	10	V
Verlustleistung, $T_A = 25$ °C Total power dissipation	P_{tot}	250	mW

Kennwerte ($T_A = 25$ °C, Normlicht A, $T = 2856$ K)
Characteristics ($T_A = 25$ °C, standard light A, $T = 2856$ K)

Bezeichnung Description	Symbol Symbol	Wert Value	Einheit Unit
Fotoempfindlichkeit, $V_R = 5$ V Spectral sensitivity	S	10 (≥ 5.5)	nA/lx
Wellenlänge der max. Fotoempfindlichkeit Wavelength of max. sensitivity	$\lambda_{S\,max}$	550	nm
Spektraler Bereich der Fotoempfindlichkeit $S = 10$ % von S_{max} Spectral range of sensitivity $S = 10$ % of S_{max}	λ	350 ... 820	nm
Bestrahlungsempfindliche Fläche Radiant sensitive area	A	7.34	mm^2
Abmessung der bestrahlungsempfindlichen Fläche Dimensions of radiant sensitive area	$L \times B$ $L \times W$	2.73 × 2.73	mm × mm
Abstand Chipoberfläche zu Gehäuseoberfläche Distance chip front to case surface	H	1.9 ... 2.3	mm
Halbwinkel Half angle	φ	± 55	Grad deg.

Kennwerte (T_A = 25 °C, Normlicht A, T = 2856 K)
Characteristics (T_A = 25 °C, standard light A, T = 2856 K) (cont'd)

Bezeichnung Description	Symbol Symbol	Wert Value	Einheit Unit
Dunkelstrom Dark current			
V_R = 5 V V_R = 10 mV	I_R I_R	2 (≤ 30) 8 (≤ 200)	nA pA
Spektrale Fotoempfindlichkeit, λ = 550 nm Spectral sensitivity	S_λ	0.34	A/W
Quantenausbeute, λ = 550 nm Quantum yield	η	0.80	Electrons / Photon
Leerlaufspannung, E_v = 1000 lx Open-circuit voltage	V_O	400 (≥ 320)	mV
Kurzschlußstrom, E_v = 1000 lx Short-circuit current	I_{SC}	10	µA
Anstiegs- und Abfallzeit des Fotostromes Rise and fall time of the photocurrent R_L = 1 kΩ; V_R = 5 V; λ = 550 nm; I_p = 10 µA	t_r, t_f	1.5	µs
Durchlaßspannung, I_F = 100 mA, E = 0 Forward voltage	V_F	1.2	V
Kapazität, V_R = 0 V, f = 1 MHz, E = 0 Capacitance	C_0	580	pF
Temperaturkoeffizient von V_O Temperature coefficient of V_O	TC_V	− 2.6	mV/K
Temperaturkoeffizient von I_{SC} Temperature coefficient of I_{SC}	TC_I	− 0.05	%/K
Rauschäquivalente Strahlungsleistung Noise equivalent power V_R = 5 V, λ = 550 nm	NEP	7.2×10^{-14}	$\frac{W}{\sqrt{Hz}}$
Nachweisgrenze, V_R = 5 V, λ = 550 nm Detection limit	D*	1×10^{12}	$\frac{cm \cdot \sqrt{Hz}}{W}$

Relative spectral sensitivity
$S_{rel} = f(\lambda)$

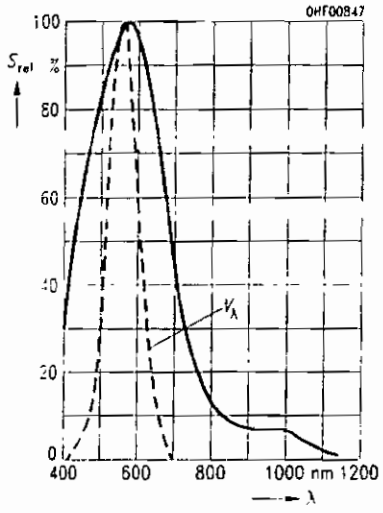

Photocurrent $I_P = f(E_v)$, $V_R = 5$ V
Open-circuit voltage $V_O = f(E_v)$

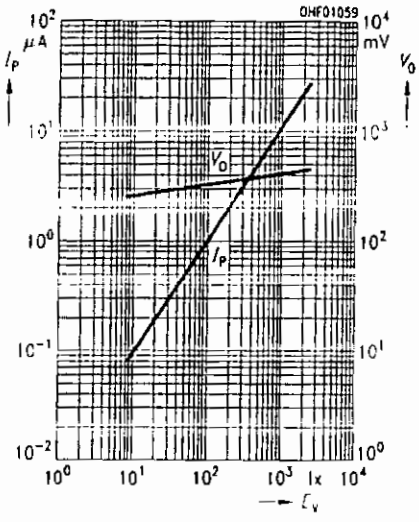

Total power dissipation
$P_{tot} = f(T_A)$

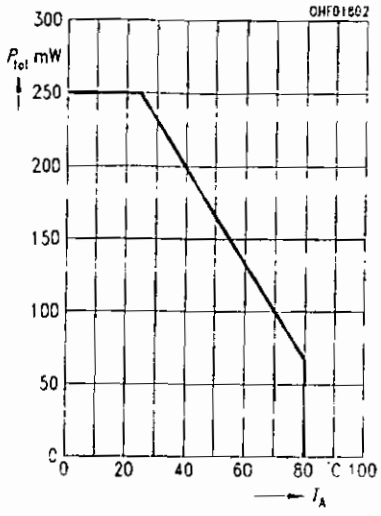

Dark current
$I_R = f(V_R)$

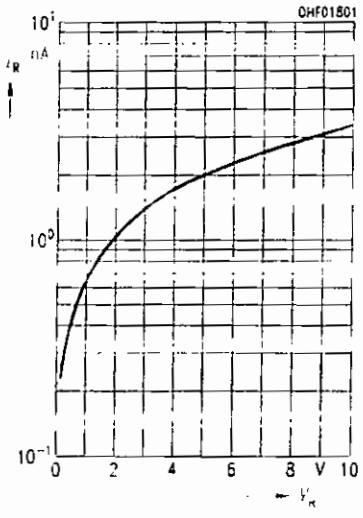

Capacitance
$C = f(V_R)$, $f = 1$ MHz, $E = 0$

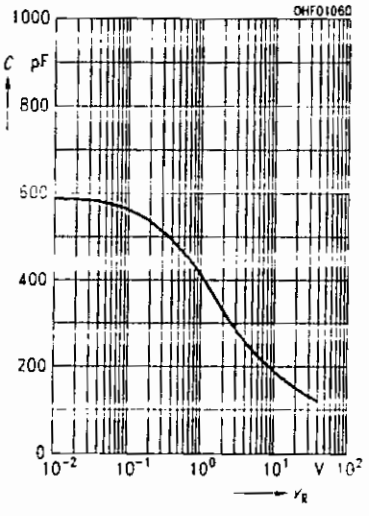

Dark current
$I_R = f(T_A)$, $V_R = 5$ V

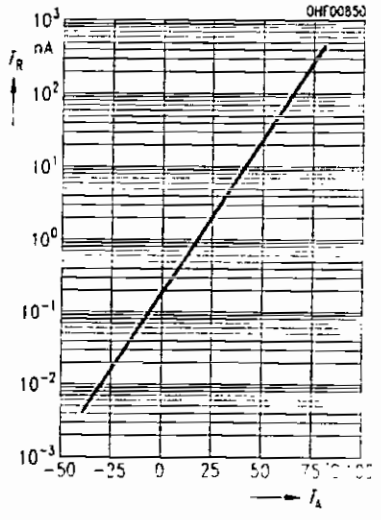

Directional characteristics $S_{rel} = f(\varphi)$

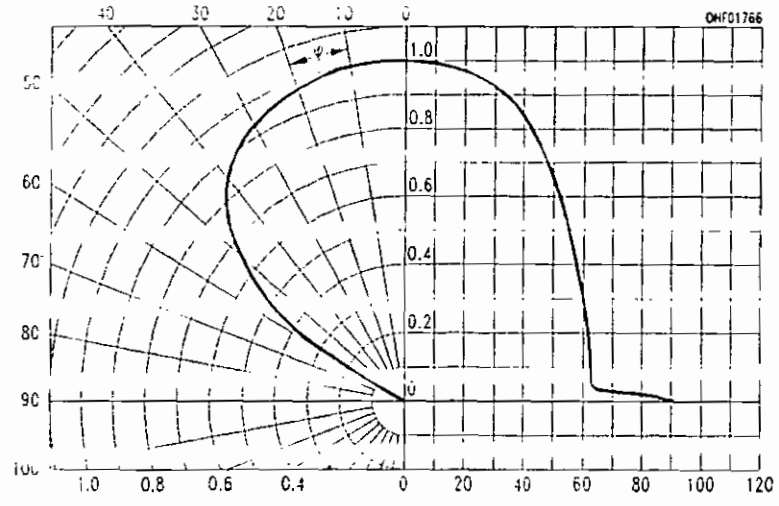

Silicon NPN Phototransistor

Description

BPX43 is a very high sensitive silicon NPN epitaxial planar phototransistor in a standard TO–18 hermetically sealed metal case with a glass lens.
A superior linearity of photocurrent vs. irradiation makes it ideal for linear applications. A base terminal is available to enable biasing and sensitivity control.

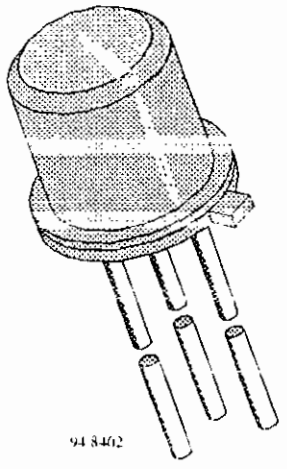

Features

- Hermetically sealed TO–18 case
- Lens window
- Angle of half sensitivity $\varphi = \pm 15°$
- Exact central chip alignment
- Base terminal available
- Very high photo sensitivity
- High linearity
- Suitable for visible and near infrared radiation
- Selected into sensitivity groups

Applications

Detector for analogue and digital applications in industrial electronics, measuring and control, e.g. long range light barriers with additional optics, optical switches, alarm systems.

Absolute Maximum Ratings

$T_{amb} = 25°C$

Parameter	Test Conditions	Symbol	Value	Unit
Collector Base Voltage		V_{CBO}	80	V
Collector Emitter Voltage		V_{CEO}	70	V
Emitter Base Voltage		V_{EBO}	7	V
Collector Current		I_C	50	mA
Peak Collector Current	$t_p \leqq 10$ µs	I_{CM}	200	mA
Total Power Dissipation	$T_{amb} \leqq 25$ °C	P_{tot}	250	mW
Junction Temperature		T_j	125	°C
Operating Temperature Range		T_{op}	–55...+125	°C
Storage Temperature Range		T_{stg}	–55...+125	°C
Soldering Temperature	t ≦ 5 s, distance from touching border ≧ 2 mm	T_{sd}	260	°C
Thermal Resistance Junction/Ambient		R_{thJA}	400	K/W
Thermal Resistance Junction/Case		R_{thJC}	150	K/W

Basic Characteristics

T_{amb} = 25°C

Parameter	Test Conditions	Symbol	Min	Typ	Max	Unit
Collector Emitter Breakdown Voltage	I_C = 1 mA	$V_{(BR)CE}$	70			V
Collector Dark Current	V_{CE} = 25 V, E = 0	I_{CEO}		10	200	nA
Collector Emitter Capacitance	V_{CE} = 0 V, f = 1 MHz, E = 0	C_{CEO}		23		pF
Emitter Base Capacitance	V_{EB} = 0 V, f = 1 MHz, E = 0	C_{EBO}		47		pF
Collector Base Capacitance	V_{CB} = 0 V, f = 1 MHz, E = 0	C_{CBO}		41		pF
Collector Light Current	E_e = 0.5 mW/cm², λ = 950 nm, V_{CE} = 5 V	I_{ca}	0.8			mA
Temp. Coefficient of I_{ca}	λ = 950 nm	TK_{Ica}		1		%/K
Base Light Current	E_e = 0.5 mW/cm², λ = 950 nm, V_{CB} = 5 V	I_{ba}		10		µA
Angle of Half Sensitivity		φ		±15		deg
Wavelength of Peak Sensitivity		λ_p		920		nm
Range of Spectral Bandwidth		$\lambda_{0.5}$		630...1040		nm
Collector Emitter Saturation Voltage	E_e = 0.5 mW/cm², λ = 950 nm, I_C = 0.1 mA	V_{CEsat}		0.15	0.3	V

Type Dedicated Characteristics

T_{amb} = 25°C

Parameter	Test Conditions	Type	Symbol	Min	Typ	Max	Unit
Current Gain	V_{CE}= 5 V, I_C = 1 mA	BPX38-4	B		330		
		BPX38-5	B		520		
		BPX38-6	B		650		
Collector Light Current	E_e=0.5 mW/cm², λ=950nm, V_{CE}=5V	BPX38-4	I_{ca}	0.5	0.7	1.0	mA
		BPX38-5	I_{ca}	0.8	1.25	1.6	mA
		BPX38-6	I_{ca}	1.25	2		mA
Rise Time/ Fall Time	V_{CE}=5V, I_C=1mA, R_L=1kΩ λ=820nm	BPX38-4	t_r, t_f		15		µs
		BPX38-5	t_r, t_f		20		µs
		BPX38-6	t_r, t_f		25		µs

Typical Characteristics (T_{amb} = 25°C unless otherwise specified)

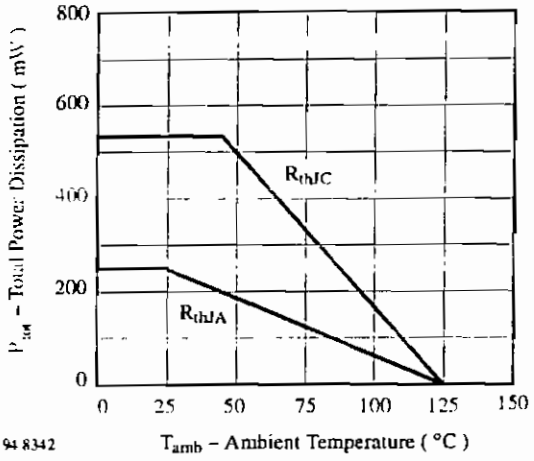

Figure 1. Total Power Dissipation vs. Ambient Temperature

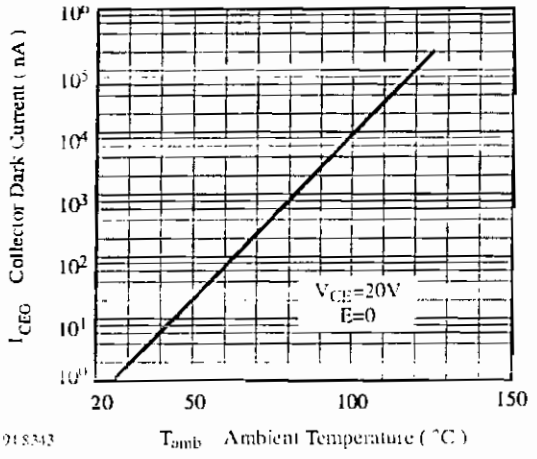

Figure 2. Collector Dark Current vs. Ambient Temperature

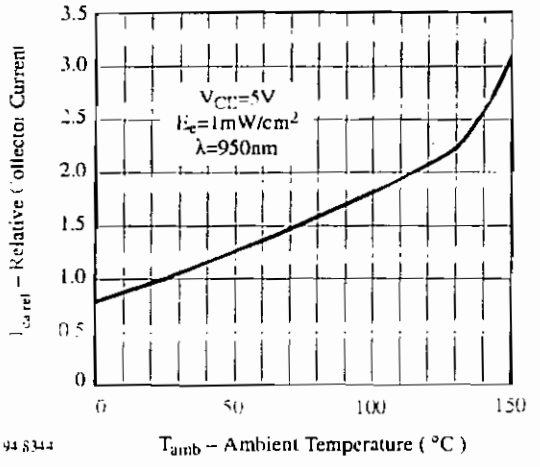

Figure 3. Relative Collector Current vs. Ambient Temperature

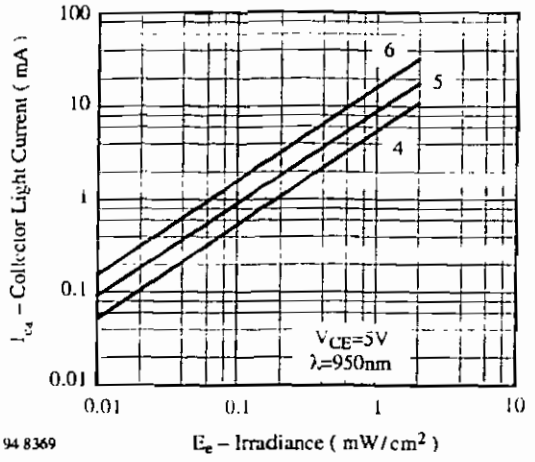

Figure 4. Collector Light Current vs. Irradiance

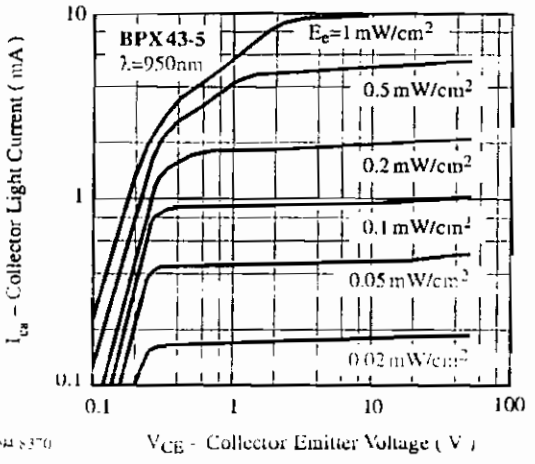

Figure 5. Collector Light Current vs. Collector Emitter Voltage

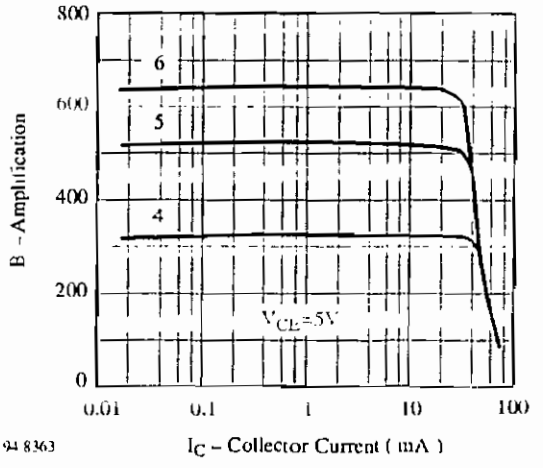

Figure 6. Amplification vs. Collector Current

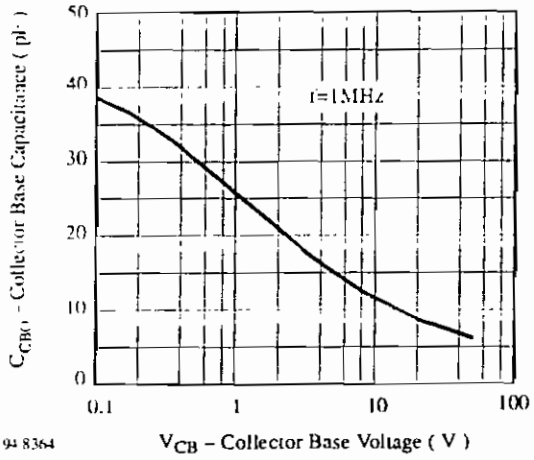

Figure 7. Collector Base Capacitance vs. Collector Base Voltage

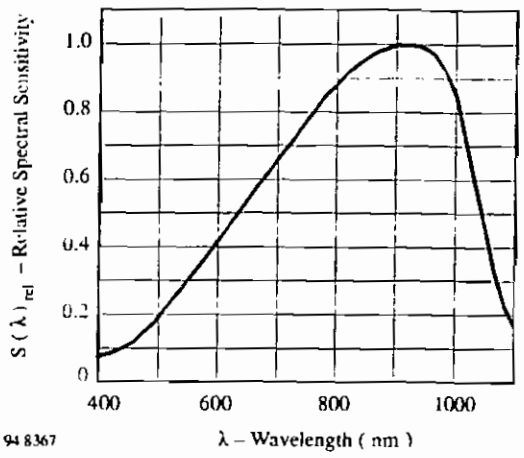

Figure 10. Relative Spectral Sensitivity vs. Wavelength

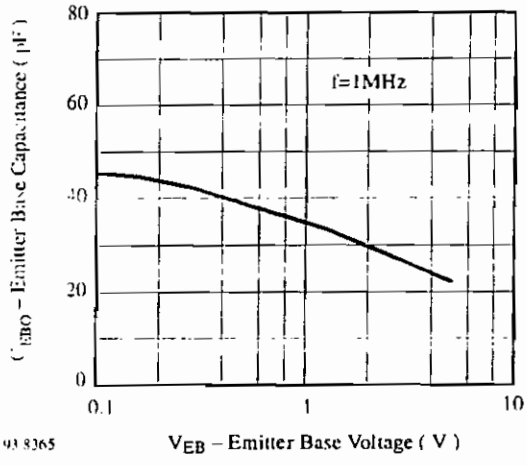

Figure 8. Emitter Base Capacitance vs. Emitter Base Voltage

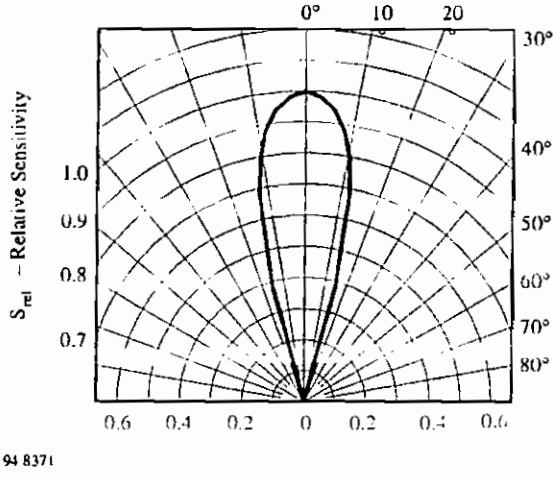

Figure 11. Relative Radiant Sensitivity vs. Angular Displacement

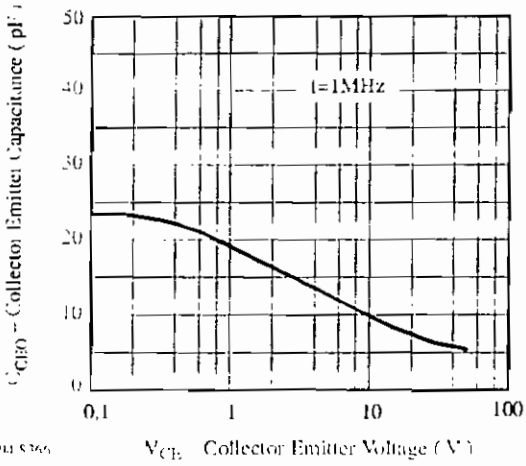

Figure 9. Collector Emitter Capacitance vs. Collector Emitter Voltage

Dimensions in mm

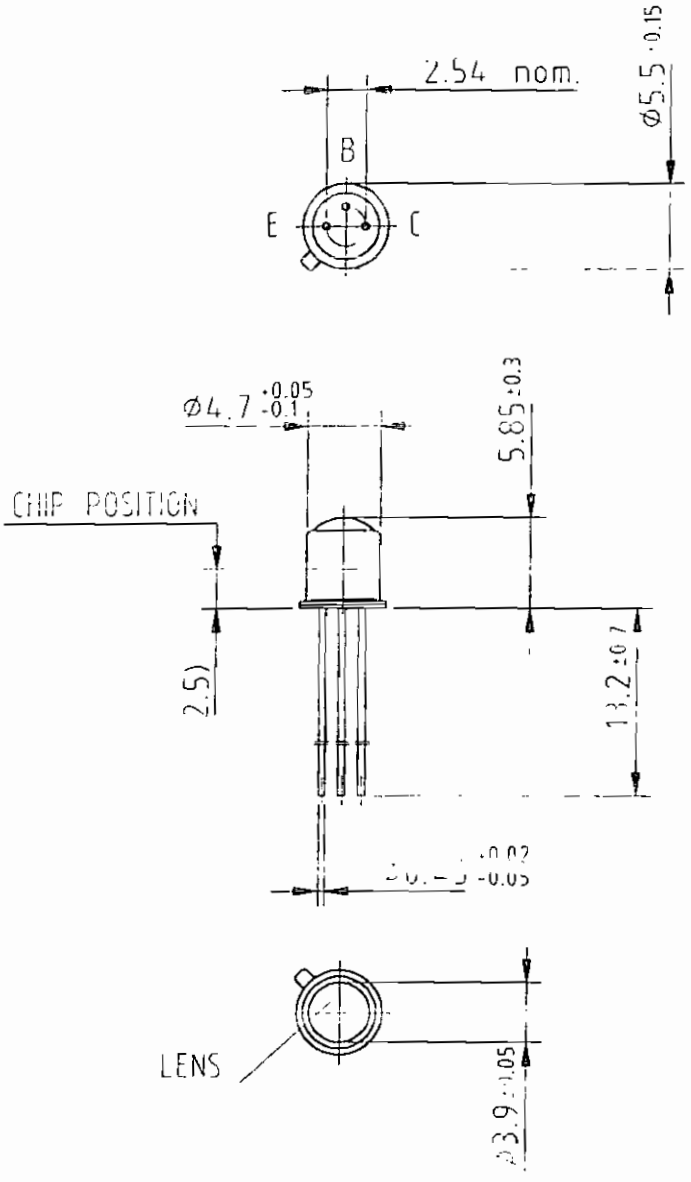

technical drawings
according to DIN
specifications

Vishay Telefunken

Ozone Depleting Substances Policy Statement

It is the policy of **Vishay Semiconductor GmbH** to

1. Meet all present and future national and international statutory requirements.

2. Regularly and continuously improve the performance of our products, processes, distribution and operating systems with respect to their impact on the health and safety of our employees and the public, as well as their impact on the environment.

It is particular concern to control or eliminate releases of those substances into the atmosphere which are known as ozone depleting substances (ODSs).

The Montreal Protocol (1987) and its London Amendments (1990) intend to severely restrict the use of ODSs and forbid their use within the next ten years. Various national and international initiatives are pressing for an earlier ban on these substances.

Vishay Semiconductor GmbH has been able to use its policy of continuous improvements to eliminate the use of ODSs listed in the following documents.

1. Annex A, B and list of transitional substances of the Montreal Protocol and the London Amendments respectively

2. Class I and II ozone depleting substances in the Clean Air Act Amendments of 1990 by the Environmental Protection Agency (EPA) in the USA

3. Council Decision 88/540/EEC and 91/690/EEC Annex A, B and C (transitional substances) respectively.

Vishay Semiconductor GmbH can certify that our semiconductors are not manufactured with ozone depleting substances and do not contain such substances.

Vishay Semiconductor GmbH, P.O.B. 3535, D-74025 Heilbronn, Germany
Telephone: 49 (0)7131 67 2831, Fax number: 49 (0)7131 67 2423

ADC-11 and ADC-16

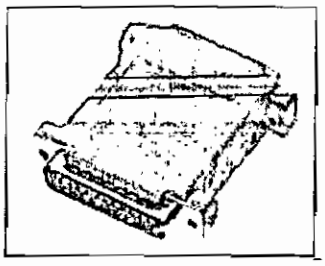

ADC-11

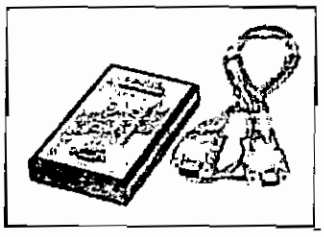

ADC-16

Two devices with supplied software (see ADC-10/12 for details) which will turn a PC into a powerful multichannel datalogger. They plug directly into the PC and require no external power, making them suitable for use with portable PCs.
ADC-11, 10 bit; an 11 channel, high speed, medium resolution device suitable for use as a general datalogging unit for temperature, pressure, humidity etc. Can also be used as a virtual instrument with the PicoScope software.

- Parallel port connection
- Digital output for control/alarm functions
- Software supports English, French, German, Spanish and Swedish

ADC-16, 8-16 bit; an 8 channel, high resolution device capable of detecting small signal changes (40μV). If more than 8 channels are required the PicoLog software can support up to 4 ADC-16 devices running off separate serial ports.

- Serial port connection
- 5V reference outputs
- Pairs of inputs can be used differentially to reject noise
- Software supports English, French, German, Spanish and Swedish

technical specification

	ADC-11	*ADC-16*
Input range	0 to +2·5V	±2.5V
Resolution	2·0mV/lsb (approx.)	40μV/lsb (approx.)
Sampling rate	15kHz (max.)	200Hz at 8 bit
		2Hz at 16 bit
Accuracy	1%	0·1%
Input impedance	>1MOhm	>1MOhm
Overload protection	30V	30V
Input connector	D25	D25

Typical Application	*ADC-10*	*ADC-11*	*ADC-12*	*ADC-16*
Oscilloscope	•	•	•	
Voltmeter	•	•	•	•
Spectrum analyser	•	•	•	
Freq. meter	•	•	•	
Audio sampling	•	•	•	
Chart recorder		•		•
Temp. measurement	•	•	•	•
Pressure measurement	•	•	•	•
Automotive monitoring		•		•
Medical research		•		•
Education	•	•	•	•

S.S.M. = 1

type	stock no.	price each 1-4	5-9
ADC-11 + PicoScope+ PicoLog	830-053	£ 110·20	£ 107·50
ADC-16 + PicoLog	206-4258	£ 146·40	£ 142·70

Parallel/Serial Port Plug-Ins

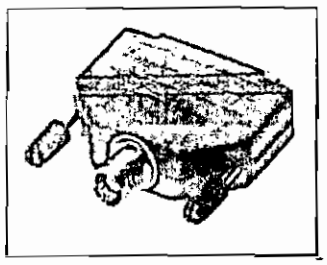

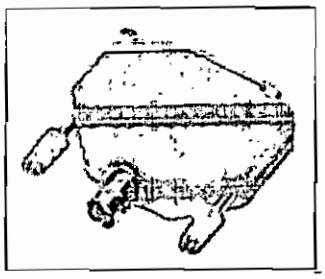

ADC-10, 8-bit device ADC-12, 12 bit device; Data acquisition devices for use with IBM® compatible PCs. These units plug directly into the PC parallel port and require no external power, making them ideal for use with portable PCs. BNC sockets allow standard (x1) oscilloscope probes to be used.
Each device is supplied with instruction manual and software (on 3.5in disk). For users who wish to write their own programs, C Pascal and Basic software drivers are included. The software supports English, French, German, Spanish and Swedish.
PicoScope software; provides a PC with a digital oscilloscope, voltmeter, spectrum analyser, frequency meter, voltmeter and dB meter. It is easy to use, has a full file and printer support and on line help is available.

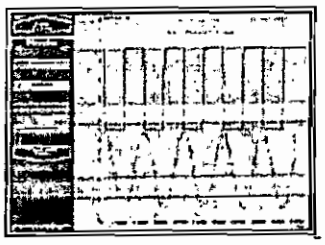

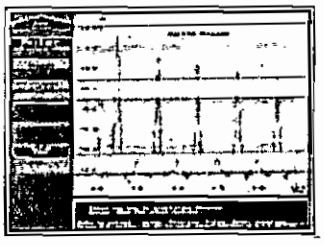

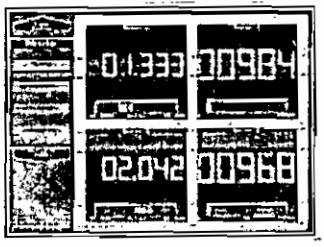

- 1ms to 5s/div timebase
- Trigger-auto single/repeat with pre/post options
- Real time display of amplitude and frequency
- Moveable ruler for event timing
- Zoom on both axis
- Signal averaging to reduce noise
- Displays volts, frequency or dB
- Max/min selectable display frequencies
- 7 window types and up to 12 meters on screen
- Digital and bargraph displays
- Linear or log scales

Picolog software; a powerful and flexible data logging package for collecting, analysing and displaying data.

- Collect, store, display and print data (1 sample/ms to 1/day)
- Record max/min/average or scaled values
- Display reports during and after data collection
- Monitor with max/min alarms
- Y-T graphs, X-Y graphs, tabulation

technical specification

Input range	0 to +5V
ADC-10 resolution	20mV/lsb (app.)
ADC-12 resoltuion	1.2mV/lsb
Sampling rate	20kHz (max)
Accuracy	1%
Input impedance	200kOhm
Overload protection	30V

S.S.M. = 1

	stock no.	price each 1-4	5-9
ADC-10 + PicoScope+ PicoLog	830-031	£ 68·47	£ 66·76
ADC-12 + PicoScope+ PicoLog	830-075	£ 110·20	£ 107·50

APPENDIX B

COMPUTER PROGRAMS

MATLAB Simulation Programs:

Program 1: Basic ATM Network Simulation

```
%                    MATLAB Version 5.3
%          Simulation of packet segmentation and reassembly in ATM network
%                Author: Karen Dunne, DIT Aungier Street

%This code simulates the processes of segmentation and reassembly of an image file (JPEG
%format). In this M-file, a maximum transmission unit of 9140 at the top layer is used. The
%image matrix is split into smaller sequences of allowable size. Each of these is appended with
%a 5 byte representative header and is transferred to the next layer, where further header
%information is added to the TCP segments, IP datagrams, ATM cells and SONET frames.
%Specific header and trailer information is not included, although such information could be
%readily introduced to the simulation if required. The purpose of this simulation is to create a
%generic simulation of the operations and manipulations that are performed to an application
%file in the ATM system. Connection specific details are deliberately omitted therefore.

v1=fopen('c:\dmc.jpg')   % Opens the file c:\dmc.jpg
a1=fread(v1)             % Reads contents of file to a matrix
u=length(a1)             % Determines the length of the image matrix
m=9140;
% Sets the Maximum Transmission Unit (MTU) size to avoid fragmentation at the IP layer

x=fix(u/m)
% Determines the number of full TCP segments that can be created from the image

y=mod(u,m)
% Computes the number of remaining elements of the image matrix after complete TCP
%segments have been created

for i=1:x
  c{i}=a1((i-1)*m+1:i*m);
end
% Sequentially segments the image matrix into matrices of size 9140.
% These matrices are representative of the payload for the TCP segments

s=cat(1,c{:})
s1=rot90(s)
x1=fix(length(s1)/m)

%The aim is to simulate the processes at each layer in the ATM system, however for
%computational reasons in MATLAB, it was found to be more efficient to perform the
%segmentations, append the headers and then combine all of the data into a single matrix for
% MATLAB to perform simulation processes at the next layer. This is achieved using the code
%above


% The following for loop segments the composed matrix back into the payload TCP segments.
%The TCP and IP headers (20 bytes each) are added onto each payload using a single loop
%expression for simulation simplicity and efficiency.

for j=1:x1
  d{j}=s1((j-1)*m+1:j*m)
  s5{j}=[randperm(40),d{j}]
end


s6=cat(1,s5{:})
```

```
s7=rot90(s6);
s8=flipud(s7);
s9=s8(:);
s10=rot90(s9)
v=length(s10)

% Algorithm for creating final datagram matrix from image matrix. The datagram is then
%appended to the sequence of datagrams already created, yielding a matrix containing all of
%the datagrams that were created from the original image matrix, plus the representative TCP
%and IP headers.

if y>0
   last_frame=a1((x1*m)+1:end);
   flip_frame=rot90(last_frame);
   last_tcp_frame=[randperm(40),flip_frame];
   complete_transmission=[s10,last_tcp_frame]
elseif y<=0
   complete_transmission=[s10]
end

% In the following code, the physical processes of the Segmentation and Reassembly (SAR)
%sublayer of the ATM Adaptation Layer Type 5,are simulated. Here, the IP datagrams are split
%into 48-byte payload for the ATM cells. Since the entire sequence of datagrams are contained
%in the matrix "complete_transmission", the cells may be created from this matrix, rather than
%from a series of matrices which, for a large input file, may have been extremely
%computationally intensive

x2=fix(length(complete_transmission)/48)
y1=mod(length(complete_transmission),48)
%The number of complete cell payloads (48-bytes) that may be created is computed and the
%number of elements remaining is determined

for l=1:x2
  h{l}=complete_transmission((l-1)*48+1:l*48);
  h1{l}=[randperm(5),h{l}];
end
h3=cat(1,h1{:})
h4=rot90(h3);
h5=flipud(h4);
h6=h5(:);
h7=rot90(h6)
%The complete 48-byte payloads are created
%To each 48-byte payload, a 5-byte representative header is added

%The final cell is to contain an 8-byte trailer. Thus if the number of remaining elements is
%greater than 40, two final cells must be sent. On the other hand, if less than 40 elements
%remain, only one final cell is sent, with the trailer and padding bytes to fill the fixed 48-byte
%payload field of the ATM cell. The following algorithm implements this process

      if y1<40
      padding1=40-y1
      z=complete_transmission((x2*48)+1:end);
      z1=[randperm(5),z,randperm(padding1),randperm(8)];
      z2=[h7,z1];
      z5=z2(:)
    elseif y1>=40
      z=complete_transmission((x1*48)+1:end);
      z1=[randperm(5),z,randperm(48-y1)];
      z2=[randperm(53)];
      z4=[h7,z1,z2];
```

```
  z5=z4(:)
end
```

%Where standard optical framing mechanisms such as Synchronous Optical NETwork %(SONET) or Synchronous Digital Hierarchy are to be used at the physical layer, the ATM cells %are packed into frames of 810 bytes in size for transmission SONET and SDH are equivalent %framing standards. The SONET frames which are 810 bytes in size include a 27-byte header %field which leaves 783 bytes for payload data (or ATM cells). This allows for a little more than %14 cells to be carried in a SONET frame. In the simulation, the sequence of ATM cells created %from the original image file are contained in a single matrix. It is therefore relatively easy to %determine the number of SONET/SDH frames that need to be created from the transmission %data. The process of determining the number of complete and incomplete SONET frames %from the transmission data is conducted using the following algorithm

```
z6=rot90(z5)
k1=fix(length(z5)/783)
k=mod(length(z5),783)

for n=1:k1
  r(n)=z6((n-1)*783+1:n*783);
  r16(n)=[randperm(27),r(n)];
end
r1=cat(1,r16(:))
r12=rot90(r1);
r13=flipud(r12);
r14=r13(:)  ;
r15=rot90(r14)
```

%The final SONET frame is created using the following code

```
if k~=0
  if k<783
  padding2=783-k
  r2=z6(k1*783+1:end);
  sonet=[randperm(27),r2,randperm(padding2)];
  r3=[r15,sonet]
  r4=r3(:)
  else
  r4=r15(:)
  end
end
```

%For completeness, the entire transmission sequence of SONET frames is converted into %binary digit form as this is the required format for transmission over a digital medium. A %reliable medium is assumed. Consequently, all of transmitted data is received without %corruption at the destination.

```
bit_strings=dec2bin(r4)
```

%When the bit strings reach the destination, they are reconverted to their decimal %representation. Rather than perform this conversion on each SONET frame separately, the %conversion is carried out on the entire sequence of frames in one single operation. This %ensures that the simulation is not unneccessarily complicated.

```
rx_values=bin2dec(bit_strings)
```

%The rx_values matrix is a matrix of the entire SONET frames that have been transmitted from %the source. At the destination, the reverse operations that took place at the source are %conducted. This entails stripping the received information of the headers and trailers that %have been added on to the data as it passed through the layers of the source protocol stack. %The following code relates to these processes.

```
rx_file=rot90(rx_values)
f1=fix(length(rx_file)/810)
f2=mod(length(rx_file),810)
```

%In order to be able to strip the data of the headers and trailers, the data must be converted %from a line vector into a matrix. This is achieved using the rot90 command. The number of %complete SONET frames that can be created from the received data is computed. The %number of remaining elements after complete SONET frames have been created from the %received data is computed

```
if f2>0
    disp('Invalid SONET frames received')
  else
```

%Since the received data should contain only complete SONET frames, if any remaining %elements are remaining elements are detected, the received data is invalid and an error %message is displayed. If only complete SONET frames are received, the data may be %processed further. Each SONET frame is identified and stripped of its 27-byte header using %the following for loop.

```
    for q3=1:f1
      q4{q3}=rx_file((q3-1)*810+28:q3*810)
    end
    q5=cat(1,q4{:})
    q6=rot90(q5)
    q7=flipud(q6)
    q8=q7(:)
    q9=rot90(q8)
    last_frame=rx_file(f1*810:28:end)
    all_frames=[q9,last_frame]
    p1=all_frames(1:end-padding2)
    p2=fix(length(p1)/53)
    p3=mod(length(p1),53)
```

%The final SONET frame is stripped of its header. For consistency, all of the SONET frames %are combined into a single matrix and any padding added on at the source to fill the frames %completely, is removed. The complete number of cells that may be created from the SONET %frames is determined. The number of remaining elements in the combination matrix after the %ATM cells have been created is determined. The ATM cells are identified and are stripped of %their 5-byte headers using the following code.

```
    for p4=1:p2
      p5{p4}=p1((p4-1)*53+6:p4*53)
    end
    p6=cat(1,p5{:})
    p7=rot90(p6)
    p8=flipud(p7)
    p9=p8(:)
    p10=rot90(p9)
```

%The IP datagrams are identified and are stripped of their IP headers as well as their TCP headers in a single stage

```
    f5=fix(length(p10)/9180)
    g5=mod(length(p10),9180)
    for m1=1:f5
      m2{m1}=p10((m1-1)*9180+41:m1*9180)
    end
    k2=cat(1,m2{:})
    k3=rot90(k2)
```

```
    k4=flipud(k3)
    k5=k4(:)
    k6=rot90(k5)
    k7=p10((m1*9180)+41:end-8-padding1)

    end_file=[k6,k7]
    k8=end_file(:)
    ans=isequal(k8,a1)
  end
```

%The last cell is stripped of its trailer and is appended to the sequence of TCP payload
%segments. The file received at the application layer is compared with the image file
%transmitted from the source. If ans is equal to one, this means that each element
%of the received matrix is identical to the corresponding element in the transmitted
%image file from the source.

%The following code plots the transmission at a number of stages in the transfer of the data from the source to the destination.

```
  figure(1)
  plot(a1)
  title('Transmitted file')
  xlabel('element')
  ylabel('RGB value')
  figure(2)
  plot(complete_transmission)
  title('IP packets')
  xlabel('element')
  ylabel('RGB value')
  figure(3)
  plot(z6)
  title('ATM cells (53 bytes)')
  xlabel('element')
  ylabel('RGB value')
  figure(4)
  plot(r4)
  title('SDH/Sonet frames')
  xlabel('element')
  ylabel('RGB value')
  figure(5)
  plot(all_frames)
  title('SDH frames-header')
  xlabel('element')
  ylabel('RGB value')
  figure(6)
  plot(p10)
  title('ATM Cells-headers')
  xlabel('element')
  ylabel('RGB value')
  figure(7)
  plot(k8)
  title('Received file')
  xlabel('element')
  ylabel('RGB value')
```

Program 2: Scattering Coefficient and Drop Diameter Program

```
%                    MATLAB Version 5.3
%     Determination of scattering coefficient for optical frequencies
%                Author: Karen Dunne, DIT Aungier Street, Dublin 2

% In the determination of attenuation using the formula A=4.343*10^-3*integral(N*Q), The
%scattering coefficient Q is computed using the formula Q=(pi*D.^2)/2. Clearly, the value of this
%coefficient depends on drop diameter. This M-file plots the value of this scattering coefficient
%against drop diameter

D=[0:0.001:5.8];
% The range of drop diameters from 0 to 5.8mm in increments of 0.001 is defined
Q=0.5*pi.*(D).^2;
% The formula for the scattering coefficient is defined and Q is calculated over the range of
defined drop diameters

% The following code plots the scattering coefficient values against the range of drop diameters
figure(1)
plot(D,Q,'k')
title('Scattering Coefficient versus Drop Diameter at optical frequencies')
xlabel('Drop Diameter (mm)')
ylabel('Scattering Coefficient mm^2')
```

Program 3: Unmodified Theoretical Attenuation Model

```
%                    MATLAB Version 5.3
%   Determination of attenuation values for rain rates from 1 to 100mm/hr
%              using Marshall-Palmer Drop Size Distribution
%                Author: Karen Dunne, DIT Aungier Street, Dublin 2


% This following file generates the drop size distributions as predicted by Marshall-Palmer and
%plots the results of predicted rain rate against actual rain rate, determines the ratio between
%them and generates a plot of the attenuation versus rain rate curves

format long                    % Defines a scaled fixed point format with 15 digits
D=[0:.001:5.8];
% Matrix of the range of raindrop diameters from 0-5.8mm in increments of .001mm

V=.0566*D.^3-.9044*D.^2+4.9625*D-.1927;
% Corresponding terminal velocities of raindrops using Maitra and Gibbons relation

Q=(pi*D.^2)/2;
% Scattering coefficient for optical frequency transmission

k1=4.1;
k2=-0.21;
k3=8000;

% Definition of coefficients for Marshall-Palmer Drop Size Distribution (DSD) computation where
%N (below) is the distribution value and N=k3*exp((-k1*R^k2)*D). In this simulation, k1, k2 and
%k3 are the constants found by Marshall and Palmer [1948]
```

```
% The rain rate integral equation is given by R=6*10^-4*pi*integral(D^3*v*N). The multiplier is
%defined as a constant k4.

k4=pi*6*10^-4;

% The attenuation equation is given by 4.343*10^-3*integral(N*Q) where Q is the scattering
%coefficient. The multiplier is defined as k5.

k4=4.343*10^-3;

% The routine below calculates the Marshall-Palmer integral for different rain rates and
%determines the ratio of the actual rain rate inserted into the RHS of the equation to the rain
%rate predicted by the rain rate integral equation. This ratio shows the deviation between the
%two results and is used later for modification of the k3 (No in theory) coefficient of the M-P
%DSD.

For R=1:100
s=k1*R.^k2;              %determines the exponent for the calculation of N(D)
N=k3*exp(-s.*D);         %Computes N(D) for each rain rate
I=D.^3.*N.*V;            %Defines the integrand for calculation of the rain rate
I1=k4*TRAPZ(D,I);  %Calculates the rain rate in terms of the drops size distribution
I2=N.*Q;             %Defines the integrand for calculation of the attenuation due to drops
I3=k5*TRAPZ(D,I2);
%Computes the aggregated attenuation due to these drops at a particular rain rate
end

R=1:100;
int=I1(:)
ratio=R./I1          %Computes the ratio of the actual rain rate to the M-P predicted rain rate
ratio1=ratio(:)
I3(:)

% The following codes plot the predicted rain rate against the actual rain rate inserted into the
%rain rate integral equation as well as the ratio between the two rain rates. Finally, a graph of
%the rain rate and predicted attenuation values is plotted.

Figure(1)
plot(R,I1,'k',R,R,'k:')
title('Predicted Rain Rate (M-P DSD) and Actual Rain Rate')
xlabel('Sample Rain rate mm/hr')
ylabel('Rain Rate (mm/hr)')
text(45,25,'solid line = M-P Predicted Rain Rate')
text(45,15,'dashed line = Actual Rain Rate')

figure(2)
plot(R,ratio1,'k:')
title('Ratio of Actual rain rate to predicted rain rate using M-P DSD')
xlabel('Rain Rate (mm/hr)')
ylabel('Ratio')

figure(3)
plot(I1,I3,'k:')
title('Predicted attenuation in dB/km versus Rain Rate using M-P DSD')
xlabel('Rain Rate (mm/hr)')
ylabel('Predicted Attenuation (dB/km)')
```

Program 4: Modified Theoretical Attenuation Model

```
%                    MATLAB Version 5.3
%          Simulation of packet segmentation and reassembly
%          Author: Karen Dunne, DIT Aungier Street, Dublin 2

% In this simulation, the Marshall-Palmer Drop Size Distribution (DSD) is employed, where N
%(below) is the distribution value and N=k3*exp((-k1*R^k2)*D). Here the values for k1 and k2
%are the constants found by Marshall and Palmer [1948]. The k3 coefficient however, has
%been modified from a constant to a rain rate dependent variable. The expression used for the
%computation of k3 was found by optimisation of the rain rate integral equation with the M-P
%DSD. It was found that, of the three coefficients k1, k2 and k3, the dominant coefficient was k3
%and this could be easily modified to yield a better correlation between the rain rate value as
%predicted by the rain rate integral equation and the rain rate value inserted into the rain rate
%integral equation.

format long
D=[0:.001:5.8];
Q=(pi*D.^2)/2;
k1=4.1;
k2=-0.21;
k4=4.343*10^-3;

% The routine below calculates the Marshall-Palmer DSD for rain rates between 1 and
%100mm/hr using a modified rain rate dependent value of k3 and then computes the
%attenuation due to rain for each rain rateto the rain rate predicted by the equation

for R=1:100
  s=k1*R.^k2;
  k3=-0.1065*R^2+19.013*R+6690.2;
% Polynomial expression to determine k3 over the range of rain rates
  N=k3*exp(-s.*D);
  I2=N.*Q;
  I3(R)=k4*TRAPZ(D,I2);
end

% The following code plots the attenuation versus rain rate determined using the modified k3
%coefficient of the M-P DSD

I3(:)
figure(1)
plot(I1,I3,'k:')
title('Attenuation in dB/km versus Rain Rate using M-P DSD and modified No coefficient')
xlabel('Rain Rate (mm/hr)')
ylabel('Predicted Attenuation (dB/km)')
```

Data Acquisition C Programs:

Program 1: Optical Link Data Acquisition Program

```
/ ***************************************************************************/
 *       Infra-Red Link Monitor
 *       Product:        PICO ADC-12
 *       Version:        1-E.5T
 *       Date:           April 14th, 2000
 *
 * 05/04/2000 :  Block average of previous sample group used to determine
 *               threshold for event recording of current block.
 * 07/04/2000 :  Time-stamped averages recorded in File1.
 *               Events recorded of data values above oldav(1 + thld2) and
 *               below oldav(1 - thld2) in File2 as volts.
 * 10/04/2000 :  Block max, min and variance determined and stored in File1.
 *               Events in File2 are sample and block-stamped for each sample stored.
 * 12/04/2000 :  Optional Statistics printout added.
 * 14/04/2000 :  If (blockmax - blockmin) > vthld then a block is stored.
 *               Variance is not computed. Negates decision effect of
 *               05/04/2000 and 07/04/2000.
 ***************************************************************************/

#include <stdio.h>
#include <conio.h>
#include <dos.h>
#include <time.h>
#include "adc12.h"

#define TRUE   1
#define FALSE  0
#define ABORT  0

FILE  *fptr1;
FILE  *fptr2;

        int c_break(void)
        {
                printf("\n****Programme Manually Terminated****\n");
                fclose(fptr1);
                fclose(fptr2);
                return(ABORT);
        }

void main (void)
 {
 int   buffer [20000];
 char  av_file [80];
 char  ev_file [80];
 int   end_prog;
 long  actual;
 unsigned long  microsec;
 unsigned long  secs_now;
 unsigned long  st_time;
 unsigned long  end_time;
 unsigned long  timetogo;
```

```
unsigned long  duration;
unsigned long  interval;
unsigned long  sfreq;
int  i;
int  rflag = 0;
int  nsamp;
int  port;
int  value;
float volts;
float xyz;
float convert = 5.0 / 4095.0;
float average = 0.0;
float oldav = 100.0;
float blockmax;
float blockmin;
float gmax = -100.0;
float gmin = 100.0;
float vthld;
float var = 0.0;
float block = -1.0;
char  yesno1 = 'x';
char  yesno2 = 'x';

ctrlbrk(c_break);

clrscr ();
printf ("ADC-12 C Infra-Red Link Data Acquisition System\n");
printf ("Excel Version 1-E.5T : 14th April, 2000\n");

 do
 {
    printf ("Enter Printer Port (1..4): ");
    port = getchar () - '0';
 } while ((port < 1) || (port > 4));
 adc12_driver_open (port);

 do
 {
        printf("\Enter the required sampling frequency (Hz) <20000 : ");
        scanf("%lu", &sfreq);
        printf("Enter the number of samples in each set of readings <20000 : ");
        scanf("%d", &nsamp);
 } while ((sfreq > 20000) || (nsamp > 20000));

 do
 {
        printf("Enter the interval (secs) between the start-points of each set of readings : ");
        scanf("%lu", &interval);
 } while ((float)interval < ((float)nsamp / (float)sfreq));

  printf("\r%5d samples in %3e seconds every %5lu seconds\n", nsamp, (float)nsamp /
(float)sfreq, interval);
  printf("\rEnter the total duration of the data acquisition (secs) : ");
  scanf("%lu", &duration);
  printf("\rEnter the voltage range detection threshold : ");
  scanf("%f", &vthld);

  printf("Enter the name of the output average file : ");
  scanf("%s", &av_file);
  printf("Enter the name of the output event file : ");
```

```
  scanf("%s", &ev_file);

  do
  {
        printf("Do you want to display statistical values ? (y/n) ");
        scanf("%c", &yesno1);
        printf("\r");
  } while ((yesno1 != 'y') && (yesno1 != 'n'));

  time(&secs_now);
  printf("\rThe clock time is currently %lu\n", secs_now);
  printf("Enter the time at which acquisition is to start : ");
  scanf("%lu", &st_time);

  do
  {
        printf("\rAre these settings correct ? (y/n) ");
        scanf("%c", &yesno2);
        printf("\r");
        if (yesno2 == 'n')
        exit ();
  } while ((yesno2 != 'y') && (yesno2 != 'n'));

  fptr1 = fopen(av_file, "w");
  fptr2 = fopen(ev_file, "w");

  end_time = st_time + duration;

  xyz = 1e6 * (float)nsamp / (float)sfreq;
  microsec = (unsigned long)xyz;
  actual = adc12_set_interval (microsec, nsamp);

  clrscr ();

  do
  {
        time(&secs_now);
        timetogo = st_time - secs_now;
        printf("Acquisition begins in %lu seconds  \r", timetogo);
  } while (secs_now < st_time);

  printf("\n");
  fprintf(fptr1,"%lu\t%lu\t%lu\t%d\t%lu\n", st_time, end_time, sfreq, nsamp, interval);
  fprintf(fptr2,"%lu\t%lu\t%lu\t%d\t%lu\n", st_time, end_time, sfreq, nsamp, interval);
/*
  printf("Start Time %lu\tEnd Time %lu\tDuration %lu\n", st_time, end_time, (end_time -
st_time));
*/
  timetogo = st_time + interval;

  do
  {
        time(&secs_now);
        adc12_get_values (buffer, nsamp);
        average = 0;
        blockmax = -4095.0;
        blockmin = 4095.0;
        block = block + 1;

        for (i = 0; i < nsamp; i++)
```

```
        {
                average = average + (float)buffer[i];
                if ((float)buffer[i] > blockmax)
                blockmax = (float)buffer[i];
                if ((float)buffer[i] < blockmin)
                blockmin = (float)buffer[i];
        }
        average = convert * (average / (float)nsamp);
        blockmax = convert * blockmax;
        blockmin = convert * blockmin;
        if (gmax < blockmax)
                gmax = blockmax;
        if (gmin > blockmin)
                gmin = blockmin;
/*
        var = 0.0;
        for (i = 0; i < nsamp; i++)
        {
                xyz = (convert * (float)buffer[i]) - average;
                var = var + (xyz * xyz);
        }
        var = var / (float)nsamp;
*/
        fprintf(fptr1, "%.0f\t%.4f\t%.4f\t%.4f\t%.4f\t%.4f\t%.4f\t%lu\n", block, average, var,
blockmax, blockmin, gmax, gmin, secs_now);

        rflag = 0;

        for (i=0; i < nsamp; i++)
        {
        if ((block > 0.0) && ((blockmax - blockmin) > vthld))
                rflag = 1;
        }
        if (rflag == 1)
                printf("Drop(s) detected in block %.0f at start-time %lu\n", block, secs_now);

        for (i=0; i < nsamp; i++)
        {
        if ((rflag == 1) && ((blockmax - blockmin) > vthld))
                fprintf(fptr2, "%d\t%.0f\t%.4f\n", i, block, (convert * (float)buffer[i]));
        }
/*
        oldav = average;
*/
        if (yesno1 == 'y')
                printf("%.0f %.4f %.4f %.4f %.4f %.4f %.4f %lu %lu\n", block, average, var,
blockmax, blockmin, gmax, gmin, secs_now, (end_time - timetogo));

        do
        {
                time(&secs_now);
        } while (secs_now < timetogo);
        timetogo = timetogo + interval;
  } while (secs_now < end_time);

  fclose(fptr1);
  fclose(fptr2);
  }
```

Program 2: Rain-Rate Acquisition Program

```
/ ***************************************************************************/
 *       Rain-Rate Monitor
 *       Product:        PICO ADC-11
 *       Version:        1-E.2
 *       Date:           April 10th, 2000
 *
  ***************************************************************************/

#include <stdio.h>
#include <conio.h>
#include <dos.h>
#include <time.h>
#include "adc11.h"

#define TRUE 1
#define FALSE 0
#define ABORT 0

FILE *fptr1;

        int c_break(void)
        {
                printf("\n****Program Manually Terminated****\n");
                fclose(fptr1);
                return(ABORT);
        }
void main (void)
{
int buffer [20000];
char out_file [80];
int end_prog;
long actual;
unsigned long microsec;
unsigned long secs_now;
unsigned long st_time;
unsigned long end_time;
unsigned long timetogo;
unsigned long duration;
unsigned long interval;
unsigned long sfreq;
int i;
int nsamp;
int port;
int value;
int do_value;
float volts;
float xyz;
float convert = 2.5 / 1023.0;
float average = 0.0;
float bmax = 0.0;
float bmin = 0.0;
float bvar = 0.0;
float block = 0.0;
char yesno = 'x';
```

```
char channels [11];
COMBINATION_METHOD modes [11];
int     no_of_readings [11];
long    readings [11];

ctrlbrk(c_break);

clrscr ( );
printf ("ADC-11 C Rain-Rate Data Acquisition System\n");
printf ("Excel Version 1-E.2: 10th April, 2000\n");

        do
        {
                printf ("Enter Printer Port (1...4): ");
                port = getchar () – '0' ;
                } while ((port<1) || (port>4));
                  adc11_driver_open (port);
                do
                {
                        printf("\Enter the  required sampling frequency (Hz) <20000: ");
                        scanf("%lu",$sfreq);
                        printf("Enter the number of samples in each set of readings <20000: ");
                        scanf("%d",&nsamp);
                } while ((sfreq > 20000) || (nsamp > 20000));
  do
  {
        printf("Enter the interval (secs) between the start-points of each set of readings : ");
        scanf("%lu", &interval);
  } while ((float)interval < ((float)nsamp / (float)sfreq));

        printf("\rEnter the total duration of the data acquisition (secs) : ");
        scanf("%lu", &duration);

        printf("\r%5d samples in %3e seconds every %5lu seconds\n", nsamp, (float)nsamp /
        (float)sfreq, interval);
        printf("Enter the name of the output file : ");
        scanf("%s", &out_file);

        time(%secs_now);
        printf("\n The clock time is currently %lu\n";secs_now);
        printf("Enter the time at which the acquisition is to start: ")
        scanf("%lu",&st_time);

yesno = 'x';
do
{
printf("\r Are these settings correct (y/n)?");
scanf("%c",&yesno);
printf("\r");
if (yesno=='n')
exit();
} while ((yesno != 'y')&&(yesno !='n'));
fptr1=fopen(out_file,'w');

end_time = st_time+duration;
xyz=1e6 * (float)nsamp / (float)sfreq;
microsec = (unsigned long)xyz;
actual = adc11_set_interval(microsec,nsamp);
adc11_set_channels(3,0);
```

```
yesno = 'x';
do
{
        printf("Do you want to display statistical values (y/n)?");
        scanf("%c",%yesno);
        printf("\r");
} while ((yesno != 'y' )&&(yesno != 'n'));

clrscr ();

do
{
        time(&secs_now);
        timetogo = st_time-secs_now;
        printf("Acquisition begins in %lu seconds \r",timetogo);
        } while (secs_now<st_time);
        printf("\n");
        fprintf(fptr1,"%lu\t%lu\n",st_time,end_time);
        printf("Start Time %lu\tEndTime %lu\tDuration %lu\n", st_time, end_time, (end_time-
        st_time));
        timetogo = st_time+interval;

        do
        {
                time(&secs_now);
                adc11_get_values(buffer,nsamp);
                average = 0.0;
                bmax = -100.0;
                bmin = 100.0;
                bvar = 0.0;
                block = block+1.0;
                for (i=0;i<nsamp;i++)
                average = average+(float)buffer[i];
                average = convert * (average/(float)nsamp);
                for (i=0;i<nsamp;i++)
                {
                if((convert * (float)buffer[i] > bmax)
                bmax=convert * (float)buffer[i];
                if ((convert * (float)buffer[i] < bmin)
                bmin = convert * (float)buffer[i];
                xyz=((convert * (float)buffer[i] – average);
                bvar =bvar +(xyz * xyz);
        }
bvar = bvar / (float)nsamp;
fprintf(fptr,"%.0f\t%.4f\t%.4f\t%.4f\t%.4f\t%lu\n",block,average,bmax,bmin,bvar,secs_now);
if(yesno ==0)
printf("%.0f %.4f %.4f %.4f %.4f %lu %lu
\n",block,average,bmax,bmin,bvar,secs_now,(end_time-secs_now));
do
{
        time(%secs_now);
} while (secs_now<timetogo);
        timetogo=timetogo+interval;
} while (secs_now<end_time);
        fclose(fptr1);
}
```

Data Analysis UNIX GREP Commands

The UNIX Get Regular Expression (*GREP*) command was used in the analysis of the large data files stored during the optical link testing. A number of small batch files were created using variations of the GREP command to extract the relevant information from the files. Among the GREP expressions used were

```
>>cat %1 | tr . x |  grep -w %2 | tr x . > %3
>>cut %1  -f2-3 | tr . x  |  grep -w -f %2 | tr x . > %3
```

The first command strips out relevant pattern stored in file %2 from file %1 and creates a new file %3 containing only the relevant pattern. The second command initially cuts column 2 and 3 from file %1, replaces any decimal points with an x to ensure that only the correct pattern (block number) is matched and not data which may have the same digits. This command strips out the relevant pattern %2 from file %1 to a new file %3, which can then be analysed.

E.g. Suppose it is necessary to analyse a large data file containing all of the 10,000 block samples recorded over a period of rain (ev1105.xls). It is not possible to open this file fully in Excel. Instead the relevant information is stripped from the file before manual analysis of the data occurs. The command line

```
>>d:\event_files\stripevent ev1105.xls pat1105.txt ev1105_stripped.txt
```

strips out any elements containing the pattern defined in pat1105.txt and outputs the stripped file to a new text file ev1105_stripped.txt. In this manner, specific blocks were extracted from the data and were in a suitable form for analysis in Excel. This allowed the relevant interruption blocks over each of the six rain rate periods to be found easily.

APPENDIX C

ADDITIONAL RESULTS

Optical Link Tests (Natural Rain) –Table of Optical Link and Gauge Voltages

The following table shows the average gauge and optical link voltages per minute for each of the six rain rate periods examined from the short-range optical link test (natural rain).

Date	22/5/00	22/5/00	22/5/00	22/5/00	16/5/00	16/5/00	28/4/00	28/4/00	11/5/00	11/5/00	24/5/00	24/5/00
Time	R (V)	B (V)	R (V)	B (V)	R (V)	B (V)	R (V)	B (V)	R (V)	B (V)	R (V)	B (V)
0	1.945	1.462	1.974	1.452	2.071	1.446	1.272	1.258	1.796	1.4257	2.061	1.449
1	1.947	1.462	1.974	1.452	2.074	1.444	1.284	1.258	1.7937	1.4255	2.06	1.45
2	1.946	1.463	1.973	1.451	2.072	1.445	1.285	1.259	1.7993	1.4253	2.058	1.45
3	1.947	1.462	1.975	1.451	2.074	1.444	1.283	1.258	1.7983	1.4255	2.065	1.451
4	1.948	1.461	1.972	1.451	2.074	1.443	1.333	1.258	1.8024	1.4261	2.063	1.452
5	1.95	1.46	1.975	1.451	2.073	1.442	1.29	1.258	1.7949	1.4265	2.063	1.45
6	1.949	1.46	1.976	1.45	2.072	1.439	1.296	1.257	1.7941	1.4256	2.062	1.45
7	1.949	1.459	1.978	1.45	2.074	1.439	1.299	1.258	1.8015	1.4263	2.063	1.449
8	1.951	1.458	1.978	1.449	2.075	1.438	1.301	1.257	1.7957	1.4258	2.064	1.448
9	1.951	1.457	1.977	1.449	2.079	1.44	1.372	1.259	1.7943	1.4258	2.068	1.447
10	1.951	1.455	1.978	1.449	2.075	1.441	1.511	1.258	1.801	1.4262	2.073	1.446

Optical Link Tests (Natural Rain) – Nightly Graphs

The following 23 graphs (not labelled individually but date shown) plot the gauge and optical link voltages over the same time period each night for 23 of the nights where the short-range optical link tests were conducted.

Optical Beam Voltage
Rain Gauge Voltage

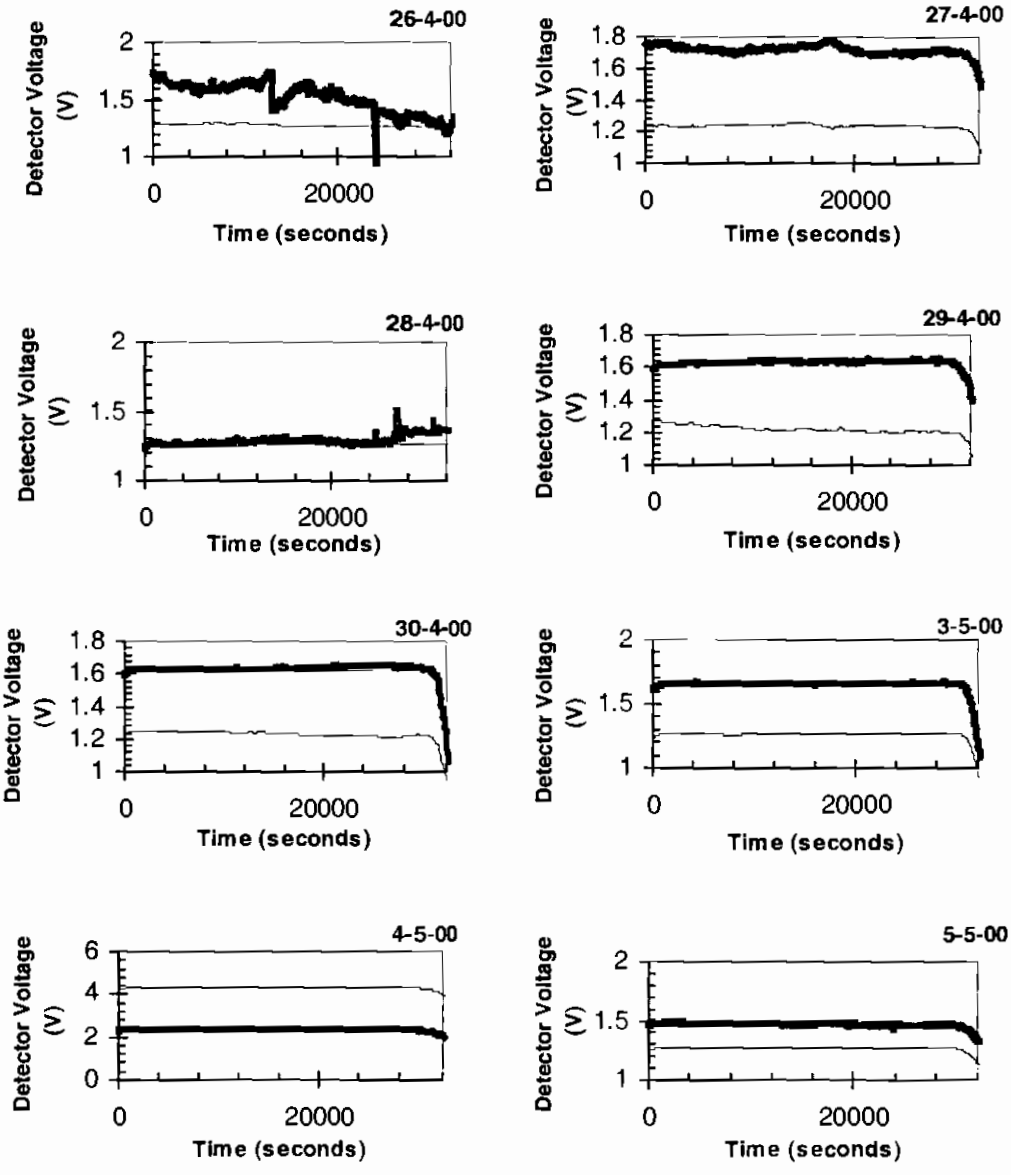

Optical Link Tests (Natural Rain) – Nightly Graphs (continued)

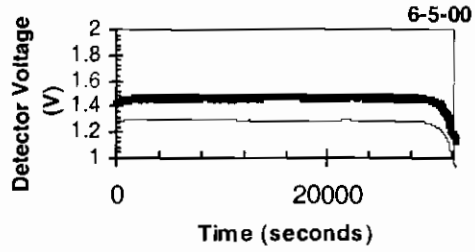

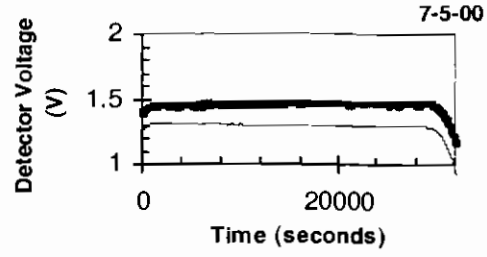

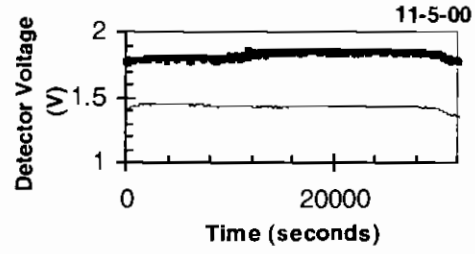

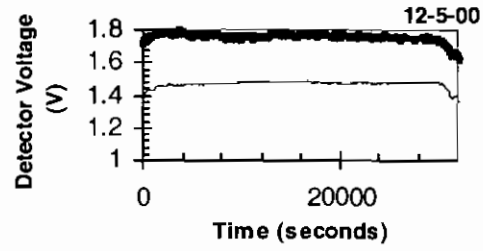

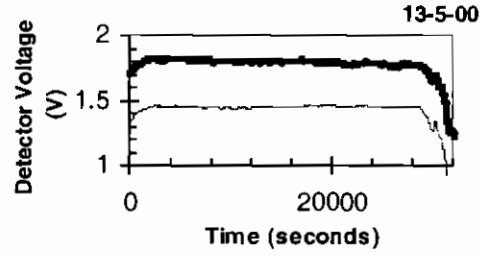

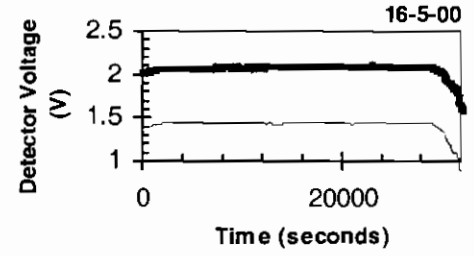

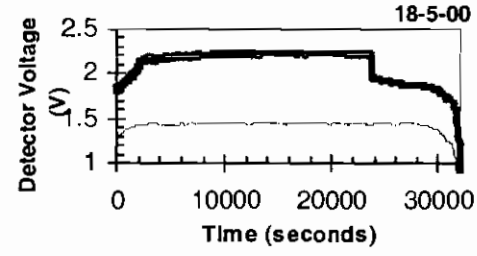

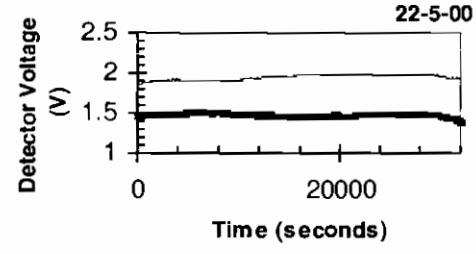

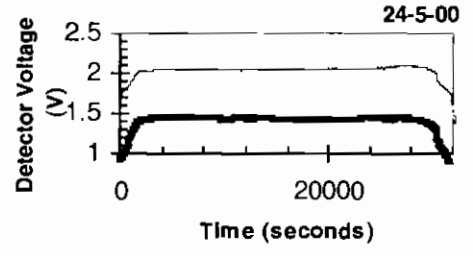

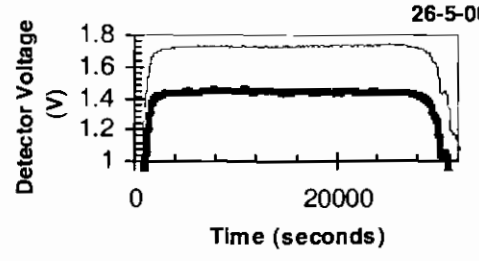

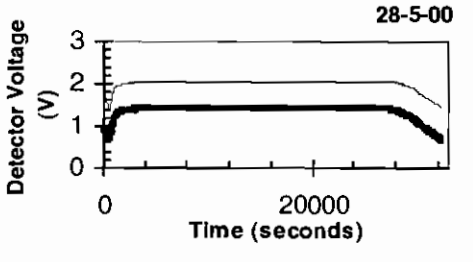

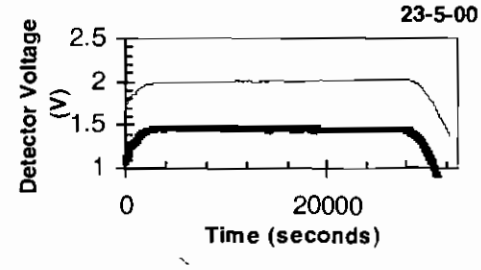

Optical Link Tests (Natural Rain) - Classification of Rain Gauge Behaviour

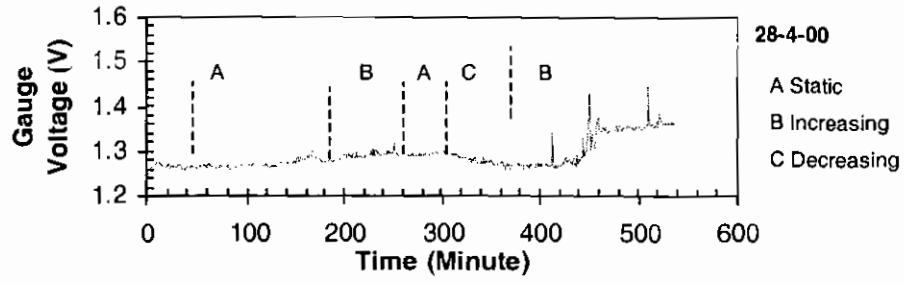

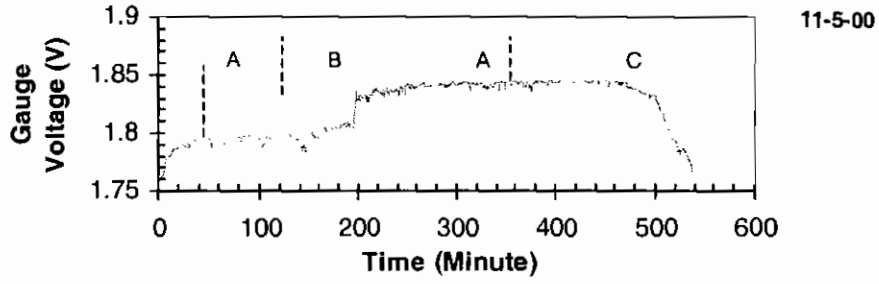

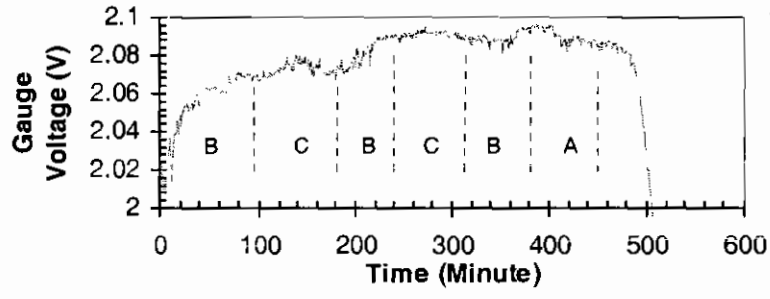

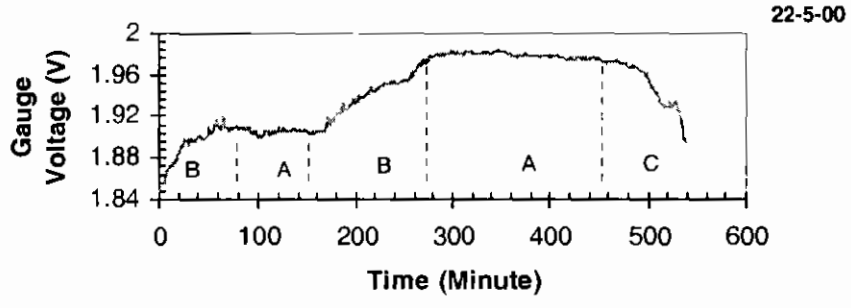

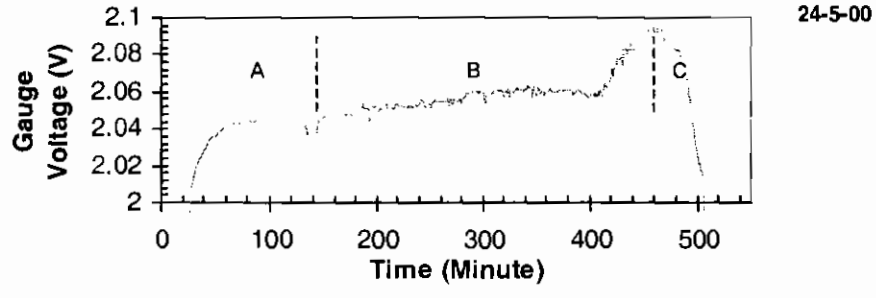

Optical Link Tests (Natural Rain) – Sample Beam Interruptions

The following graphs were generated by analysis of the individual 10,000 sample blocks stored on a night where rain fell. It can be seen that the high frequency sampling allowed profiles of interruptions to the optical signal to be stored.

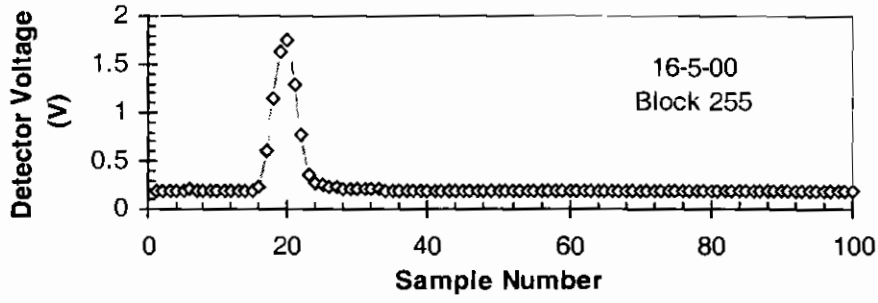

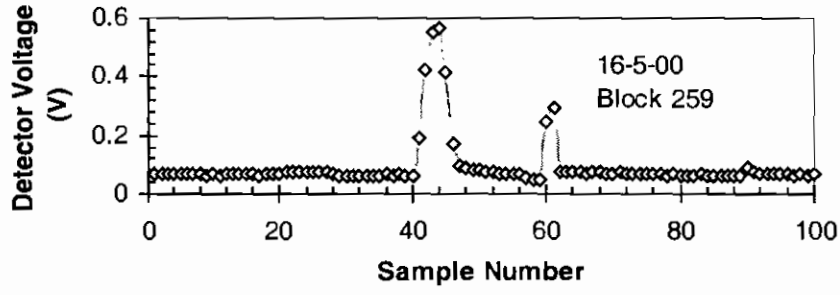

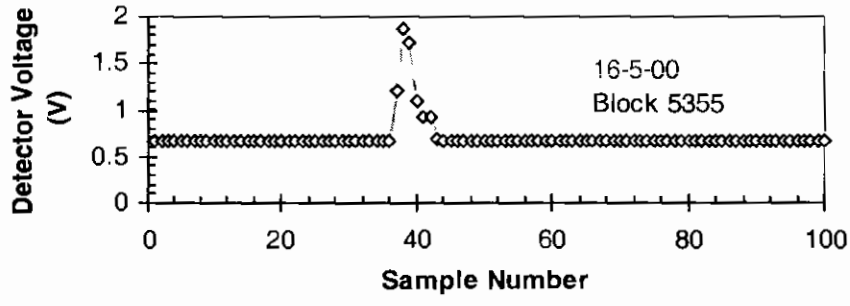

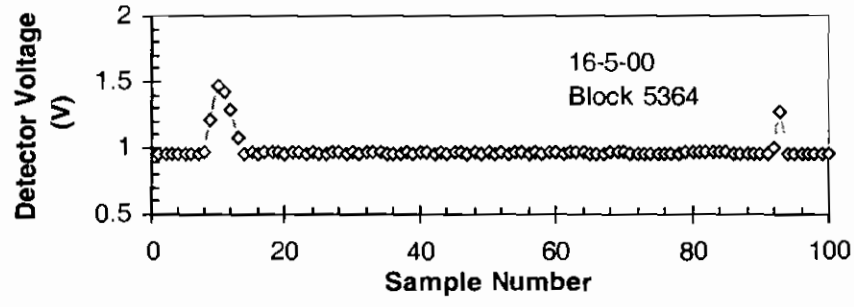

Optical Link Tests (Simulated Rain) - Measurement of Drop Diameters

In the simulated tests, the drop diameters of a number of selected drops were computed based on their mass and an assumption of a spherical drop shape. A tabulation of the results is shown below.

Drop number	Radius (mm)	Diameter (mm)	Mass (g)
1	1.031778311	2.063556621	0.0046
2	2.035115531	4.070231063	0.0353
3	0.894763282	1.789526565	0.003
4	0.959550877	1.919101755	0.0037
5	1.230357214	2.460714428	0.0078
6	0.710175729	1.420351457	0.0015
7	1.008842492	2.017684985	0.0043
8	0.874420866	1.748841733	0.0028
9	0.83062527	1.66125054	0.0024
10	1.358508485	2.717016969	0.0105
11	0.894763282	1.789526565	0.003
12	0.710175729	1.420351457	0.0015
13	1.358508485	2.717016969	0.0105
14	1.09510162	2.19020324	0.0055
15	1.127328489	2.254656979	0.006
16	0.457113432	0.914226864	0.0004
17	0.677095712	1.354191425	0.0013
18	0.941940624	1.883881247	0.0035
19	0.677095712	1.354191425	0.0013
20	0.932883031	1.865766063	0.0034
21	1.000960667	2.001921334	0.0042
22	1.121030496	2.242060992	0.0059
23	1.332123242	2.664246483	0.0099
24	1.275966519	2.551933037	0.0087
25	0.740431463	1.480862927	0.0017
26	1.261128501	2.522257001	0.0084
27	0.768398067	1.536796135	0.0019
28	1.008842492	2.017684985	0.0043
29	1.09510162	2.19020324	0.0055
30	1.197964551	2.395929103	0.0072
31	1.505835348	3.011670696	0.0143
32	0.874420866	1.748841733	0.0028
33	0.754673865	1.50934773	0.0018
34	0.640422748	1.280845496	0.0011
35	0.884709011	1.769418022	0.0029
36	0.923646051	1.847292102	0.0033
37	0.81892488	1.63784976	0.0023
38	0.984813477	1.969626953	0.004
39	1.192392598	2.384785197	0.0071
40	1.396263613	2.792527225	0.0114
41	0.941940624	1.883881247	0.0035
42	1.275966519	2.551933037	0.0087
43	1.658349936	3.316699873	0.0191
44	1.428188884	2.856377768	0.0122

45	1.722408457	3.444816914	0.0214
46	1.73307369	3.466147379	0.0218
47	1.553454571	3.106909142	0.0157
48	2.240460983	4.480921965	0.0471
49	2.60107134	5.202142681	0.0737
50	1.799401081	3.598802161	0.0244
51	1.498782222	2.997564444	0.0141
52	1.114660931	2.229321862	0.0058
53	1.230357214	2.460714428	0.0078
54	1.318529334	2.637058668	0.0096
55	1.375544677	2.751089354	0.0109

Optical Link Tests (Simulated Rain) – Table of Gauge Diameters

Three measuring gauges were employed for the rain rate measurements in the simulated tests. The diameters of the gauges are presented below.

Gauge	Diameter (mm)
1	70
2	75
3	70

Optical Link Tests (Simulated Rain) – Table of Rain Rate Measurements from Gauges

Three tests of different rain intensities were conducted in the simulated rain environment. Since three separate rain gauges were used, three rain rates were computed for each test, based on the volume of water collected in each of the three gauges. The following table presents the different rain rates obtained for each test using the different gauges, as well as the average, maximum and minimum values.

	Test 1	Test 2	Test 3
Gauge	Rain Rate (mm/hr)	Rain Rate (mm/hr)	Rain Rate (mm/hr)
Gauge 1	17.54842	31.19719	44.84596
Gauge 2	16.98514	27.17622	40.76433
Gauge 3	15.5986	31.19719	42.89614
Average RR	16.71072	29.85687	42.83548
Max	0.837702	1.340324	2.010486
Min	1.112122	2.680648	2.071147

Optical Link Tests (Simulated Rain) – Table of Attenuation Measurements

In the optical link tests, attenuation values were determined from the event data files stored every 20 seconds. The results of the attenuation values obtained for the simulated testing are presented in the following table.

	R = 17 mm/hr	R = 29 mm/hr	R = 43 mm/hr
Sample	Attenuation (dB/km)	Attenuation (dB/km)	Attenuation (dB/km)
1	0.891975973	0.338756181	2.008047762
2	0.131069174	2.176248332	1.068164239
3	0.895409568	1.845551754	
4	0.065534587	0.849392575	1.970772896
5	0.65546395	2.82946521	1.766887217
6	0.470470936	1.716289988	0.176208727
7	0.913429677	0.790366904	0.313131617
8	0.491534342	0.550102371	1.581413213
9	0.302334434	1.226766209	0.578878368
10	0.357218857	0.453523612	1.195669919
11	0	0.31034704	1.381717332
12	1.007242	1.968380311	0.932020098
13	1.332735	0.6721901	1.458290668
14	0.088771	1.116615267	1.250636179
15	0.165947	0.510828115	0.640818723
16	1.93224	1.728431429	2.270774438
17	0	1.298003259	0.667370507
18	0	1.723827764	0.568347081
19	0	1.733019169	1.122896647
20	0.86106	0.922398148	1.588571625
21	0.794366	0.614342831	2.783180884
22	0	0.986306419	3.055259786
23	0.045412	1.526504995	1.235469851
24	0.388757	0.981940292	
25	0.934951	0.530233396	0.476802958
26	0	1.74341768	0.170089088
27	0.651783	2.36391343	0.349004286
28	0.394086	1.686711913	2.907988088
29	0.394013	1.219251952	0.719047753
30	0.537596	1.836061693	1.834060247
31	1.482523386	0.754293076	2.347984502
32	0.063833525	1.416234128	1.159520305
33	0.942882282	0.287083611	1.637336898
34	0.579431305	0.130026041	1.256353449
35	0.532700144	0.427645369	2.288387035
36	0.433342725	0	0.778192882
37	0.800000903	1.0645606	1.169046988
38	0.214594298	1.50402168	1.511263727
39	0.508664774	0.221490297	1.656311081
40	0.238866407	0	1.226564609
41	0	0.494481157	0.17732244
42	0.391908	1.600762723	1.015566318

43	1.039288	0.520916853	0
44	0.458372	1.355861374	0.327237487
45	0.387607	0.111949517	1.104165122
46	0.141541	1.169866108	0.435944101
47	0.226972	1.729907543	2.528638983
48	0.224997	0.59373206	0.717853509
49	0	2.616398373	1.142381493
50	0.394003	1.53819169	0.369717233
average	**0.475298565**	**1.115732211**	**1.227527258**
stdev	**0.429161339**	**0.702259016**	**0.771083335**

Mathematical Solution of Attenuation Integral equation and comparison with MATLAB model results

The specific attenuation is expression mathematically in terms of the drop size distribution and a scattering coefficient as

$$A = 4.343\times10^{-3}\int_{0}^{5.8} N(D)Q(D)dD \qquad (1)$$

where N(D) is the Drop Size Distribution (DSD) ($m^{-3}mm^{-1}$) and Q(D) is the scattering coefficient (mm^2). In the theoretical model developed in MATLAB, the form of the DSD used was the negative exponential form proposed by Marshall and Palmer. Also, since the attenuation of interest is that of an optical signal, a simplified expression for the scattering coefficient as derived by Deirmendjian [Olsen et al., p.321]. In this analysis, the results predicted by the MATLAB are compared with results obtained from a mathematical solution obtained using calculus and numerically tested in Excel.

The Marshall-Palmer drop size distribution is a negative exponential form and is expressed mathematically by

$$N(D) = N_0 e^{-\Lambda D} \qquad (2)$$

where N_0 is a constant describing the number of drops at the intercept D = 0 and is given by $N_0 = 8000mm^{-1}m^{-3}$ and Λ is a rain rate dependent variable that is given by $\Lambda = 4.1R^{-0.21}$. Assuming a spherical drop shape, the scattering coefficient Q(D) for optical frequencies is expressed as a function of the drop diameter by

$$Q(D) = \frac{\pi D^2}{2} \qquad (3)$$

where D is the diameter (mm). Substituting the expressions for the DSD and scattering coefficient into the attenuation integral equation yields

$$A = 54.548 \int_0^{5.8} e^{-\Lambda D} D^2 dD \qquad (4)$$

There are finite limits for the integration because there are limitations in the maximum drop size that occurs in nature. In order to solve the integral equation it is necessary to employ the integration by parts formula, which is given by

$$\int_0^{\infty} u dv = uv - \int_0^{\infty} v du \qquad (5)$$

Letting

$u = D^2 \Rightarrow du = 2DdD$

$dv = e^{-\Lambda D} \Rightarrow v = -\frac{e^{-\Lambda D}}{\Lambda}$

The integral in ( ) thus becomes

$$\left[-\frac{D^2 e^{-\Lambda D}}{\Lambda}\right]_0^{5.8} + \frac{2}{\Lambda}\int_0^{5.8} De^{-\Lambda D} dD \qquad (6)$$

Using a second integration by parts where

$u = D \Rightarrow du = dD$

$dv = e^{-\Lambda D} \Rightarrow v = -\frac{e^{-\Lambda D}}{\Lambda}$

gives

$$\left[-\frac{D^2 e^{-\Lambda D}}{\Lambda}\right]_0^{5.8} - \frac{2}{\Lambda}\left[\frac{De^{-\Lambda D}}{\Lambda}\right]_0^{5.8} + \frac{2}{\Lambda^2}\int_0^{5.8} e^{-\Lambda D} dD \qquad (7)$$

Finally, the last integral is evaluated as

$$\int_0^{5.8} e^{-\Lambda D} dD = \frac{e^{-\Lambda D}}{\Lambda} \qquad (8)$$

Substituting (8) into (7) yields a final expression for the integral equation

$$\left[-\frac{D^2 e^{-\Lambda D}}{\Lambda}\right]_0^{5.8} - \left[\frac{2De^{-\Lambda D}}{\Lambda^2}\right]_0^{5.8} - \left[\frac{2e^{-\Lambda D}}{\Lambda^3}\right]_0^{5.8} \qquad (9)$$

Each of these bracketed terms may be evaluated between the limits 0 and 5.8 as

$$\left[-\frac{(5.8)^2 e^{-\Lambda(5.8)}}{\Lambda} + \frac{(0)^2 e^{-\Lambda(0)}}{\Lambda}\right] - \left[\frac{2(5.8)e^{-\Lambda(5.8)}}{\Lambda^2} - \frac{2(0)e^{-\Lambda(0)}}{\Lambda^2}\right] - \left[\frac{2e^{-\Lambda(5.8)}}{\Lambda^3} - \frac{2e^{-\Lambda(0)}}{\Lambda^3}\right] \qquad (10)$$

All that remains is to evaluate Λ. As noted previously, the value of Λ is given by $\Lambda = 4.1R^{-0.21}$. In the model, this value for the multiplier and exponent are used. The value of Λ is thus solely dependent on the rain rate R. Using a spreadsheet, equation

(10) was used to determine the specific attenuation (dB/km) over a range of rain rates. The results obtained from the spreadsheet analysis are tabulated in table I below. In Table 2, the spreadsheet results are tabulated alongside the results obtained from the MATLAB model. It can be seen that there is and error of less than 1% between the two values up to a rain rate of 45mm/hr. This provides good confidence in the MATLAB model results.

THEORETICAL ANALYSIS RESULTS									
D	D^2	2D	R	Λ	Λ^2	Λ^3	$e^{-\Lambda(0)}$	$e^{-\Lambda(5.8)}$	A (dB/km)
0	0	0	1	4.1	16.81	68.92	1	5E-11	1.5837
5.8	33.64	11.6	5	2.924	8.551	25	1	4E-08	4.3654
			10	2.528	6.391	16.16	1	4E-07	6.7555
			15	2.322	5.39	12.51	1	1E-06	8.7209
			20	2.186	4.777	10.44	1	3E-06	10.453
			25	2.086	4.349	9.071	1	6E-06	12.029
			30	2.007	4.029	8.087	1	9E-06	13.491
			35	1.943	3.776	7.338	1	1E-05	14.864
			40	1.89	3.57	6.746	1	2E-05	16.166
			45	1.843	3.398	6.264	1	2E-05	17.407
			50	1.803	3.251	5.861	1	3E-05	18.598

SPREADSHEET RESULTS		MODEL RESULTS		DIFFERENCE
R	A (dB/km)	R	A (dB/km)	
1	1.5837	1	1.5837	-2.169E-05
5	4.3654	5	4.3654	-5.342E-05
10	6.7555	10	6.7555	-7.615E-06
15	8.7209	15	8.7207	0.00021377
20	10.453	20	10.452	0.00068489
25	12.029	25	12.027	0.00146002
30	13.491	30	13.488	0.00257823
35	14.864	35	14.86	0.0040676
40	16.166	40	16.16	0.00594822
45	17.407	45	17.399	0.00823432
50	18.598	50	18.587	0.01093576

APPENDIX D

CUBOID DROP MODEL HYPOTHESIS

CUBOID DROP MODEL HYPOTHESIS

The work presented in this report provides a good basis for further investigation of a novel statistical channel model based upon a cuboid drop model.

It was noted in the report that, in the estimation of the attenuation due to rain in the channel of a wireless optical link, theoretical models are employed. However, the validity of these remains questionable. In particular, it is the assumption of a spherical raindrop shape used in many of these models that is invalid. The hypothesis presented here describes a method of adjusting the raindrop shape to a cuboid in shape, for simplified analysis.

The attenuation of a signal operating at optical frequencies due to rain is dependent on the number and size of drops interrupting the beam, as well as the extent of scattering caused by these drops. The modified theoretical model developed provided a means of computing an attenuation value based on a correction of the No coefficient in the MP drop size distribution. The modified DSD is dependent on rain rate and drop diameter. This modified DSD could be used to simulate the attenuation characteristics due to rain of an optical wireless signal and could be incorporated as a wireless channel module into the ATM network model.

If the beam diameter is known, the interacting volume is known. If a specific rain rate is to be simulated, the drop size distribution could be used to determine the number and size of drops required to be generated per unit time in order to accurately simulate the rain in the channel. These drops could be generated at the correct times using a suitable algorithm. A hypothetical generation plane that is termed the cloud base provides a standard area for the drops to be produced from. Each drop may be assigned a random position in the cloud base from which to fall. The drops vary in size and thus in terminal velocity. Consequently, when they are generated, the time for the drops to reach the optical beam area is variable. Further, depending on the location in the cloud base at which they were generated, they may or may not interact with the optical beam. Those drops that interact with the beam may interact completely or only partially with the beam. Therefore the amount of attenuation drops caused is dependent on the position at which they enter the beam area.

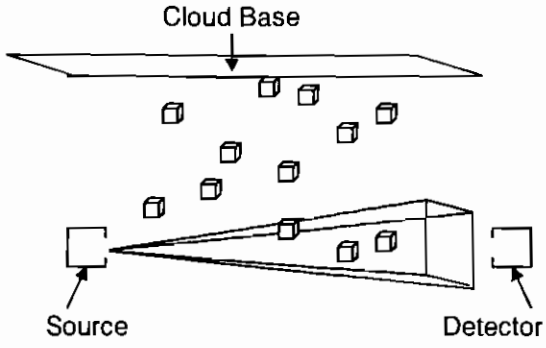

Each drop is assigned an x and y coordinate in the cloud base from which it is to fall. A time variable z could be introduced to ensure that the drops fall at the relevant times. If the dimensions of the optical beam are known, it may be determined whether the drop will fall through or will miss the beam when it reaches it. Based on the interruptions calculated as well as the dimensions of the drops that cause the interruptions, the attenuation caused to the beam as a result of the rain drops may be computed. For simplicity, the beam area may be regarded as pyramidal in shape and the drops are considered cuboidal in geometry. This alleviates the complexity of computing the attenuation due to spherical or oblate spheroidal drop shapes falling though a cone shaped beam. By projecting the width of the drops onto the detector, the effective area of the interruption on the detector may be determined. The attenuation caused by resulting water layer may then be determined using an attenuation coefficient of water. This result may then be compared with those results predicted by the theoretical model and with those results obtained in the experimental work.

Either a deterministic or probabilistic approach could be taken in incorporating this model into the ATM network model. A deterministic approach would involve incorporating an expression to depict the attenuation characteristics of the channel into the physical layer of the ATM network model. On the other hand, a probabilistic approach would involve incorporating a statistical model into the physical layer of the ATM network model, which would simulate the characteristics of the rain in the channel. However, in order to determine the effects of the channel interruptions on the ATM network, it would be necessary to understand and model the nature of the network traffic, perhaps using a network traffic profile. By linking such a network traffic profile into the physical layer as well as the wireless channel module described, the overall performance of the network under different rainfall conditions could be ascertained. This would be of use to network designers and administrators from the

point of view that they would appreciate the conditions under which the network may degrade and could implement contingency plans for situation where the network performance was severely critical.

Although the development of a corresponding model in MATLAB commenced during the course of this research, the results, at the time of print, were found to be inconclusive. However, there is great scope for investigation into the validity of such a model and its application to rain attenuation prediction at optical frequencies